THE UNIVERSITY OF QUEENSLAND
School of Earth Sciences

Evaluating the Geochemistry of Uranium Mineralisation at the Headwaters Project

Arnhem Land, Northern Territory, Australia

By

Helen T. Wood, B.Sc

A thesis submitted in partial fulfillment of the requirements for the degree of Master of Mineral Resources in the field of exploration.

Supervisors: Professor Paulo Vasconcelos
Dr Gideon Rosenbaum

11th June 2010

Declaration

The information contained in this thesis is the result of investigations conducted by the author, unless otherwise acknowledged, and has not been in part or otherwise submitted to any other degree or qualification.

Helen T Wood

11th June 2010

Acknowledgements

I would like to thank Vale and Uranium Equities for giving me the opportunity to work on this project. I would also like to thank Peter Walker from Vale's Perth office for his valuable guidance and input for this project. Thank you also to Grant Williamson from Uranium Equities in Adelaide not only for his guidance and input, but also for his help with collecting samples in Darwin.

Thank you to my supervisor Paulo Vasconcelos for getting me this project in the first place as well as helping to steer the project in the right direction.

Gideon Rosenbaum's desk top structural study of the project area was very helpful in working out different possible mineralisation events within the Headwaters tenements.

Thanks also have to go to many other staff and postgraduate students at the University of Queensland. Grant Dawson and Nathan Siddle were very generous in taking time to creation of thin sections. Grant was also very helpful in performing SEM analysis for a sample of interest.

The principal component analysis and factor analysis for this thesis would have been almost impossible without the help of Marietjie Mostert. Marietjie not only helped me analyze the very large dataset I was given but also took the time to explain the different multivariate analysis techniques. Thank you also to Sue Golding who was happy to point me in the right direction when I was having difficulty interpreting some of the results.

Thank you to David Theady, Ben Cohen, Grant Dawson and Sarah Collins for proof reading my thesis and giving me good suggestions on how to improve it.

Finally a huge thanks to my family and fellow postgraduates for helping through the last few weeks of my thesis.

Table of Contents

List of Figures

List of Tables

Abstract

The McArthur Basin in the Northern Territory hosts many world-class uranium deposits. Deposit types include unconformity-type in the northern part of the basin and sandstone-hosted deposits in the south.

The Headwaters project is situated in the northern part of the basin and contains numerous uranium anomalies in several prospects throughout the tenements. The anomalies are thought to be surface expressions of a uranium source at depth, although, the type of source is currently unknown. The main anomalies appear to be related to structures that occur throughout the tenements.

Analysis of geochemical data from samples previously collected within the project has shown similarities between the Headwaters anomalies and uranium mineralisation for both unconformity-type and sandstone-hosted deposits. Alteration assemblages of chlorite, illite, sericite, kaolinite and hematite generally accompany precipitation of uranium, arsenic, gold, platinum and occasionally lead.

Transects through mineralised fault zones and multivariate analysis have determined the possibility of two ore-forming processes, or else two mineralisation events, within the project area. Two separate mineral assemblages and two separate factors were observed for rare earth elements and trace elements which correspond to mineralised and unmineralised areas in Headwaters. Mineralised areas are mostly associated with heavy rare earth elements along with uranium, gold, arsenic, platinum and palladium. Unmineralised areas are generally associated with light rare earth elements along with copper, cobalt, molybdenum and beryllium although some of these elements were associated with the highest uranium levels. This suggests that there may be both hypogene and supergene processes responsible for mineralisation.

In order to determine if the uranium anomalies are a surface expression of a deeper uranium source and whether or not more than one process is involved in the formation of the anomalies further sampling and geochemical analysis will be required.

1. Introduction

The Paleo- to Mesoproterozoic McArthur Basin in the Northern Territory of Australia is host to a number of different styles of uranium mineralisation. The northern part of the basin contains the Alligator Rivers uranium field which contains a number of unconformity-type uranium deposits including Nabarlek, Jabiluka, Ranger, Koongarra and Rum Jungle. The majority of these deposits involve mineralisation near an unconformity between metamorphosed basement rock and the Kombolgie Subgroup of the Katherine River group (Foster et al., 1990; Hein, 2002; Isobe et al., 1992; Komninou and Sverjensky, 1996; Ludwig et al., 1987; Polito et al., 2005b; Sullivan and Matheson, 1952; Wilde and Wall, 1987).

The South Alligator River uranium district, also in the northern part of the McArthur Basin, contains several high grade deposits hosted in carbonaceous siltstones and sandstones of Lower Proterozoic age. The mineralisation is structurally controlled and is generally formed in veins and stringers within shears associated with a major reverse fault (Rich et al., 1980).

In the southern part of the McArthur Basin, sandstone-hosted deposits including Redtree, Junnagunna and Huarabagoo, together with forty seven other deposits, form the Westmoreland uranium field. Mineralisation in the Westmoreland area is due to transport and deposition of uranium by basinal brines (Polito et al., 2005a; Rheinberger et al., 1998).

The Headwaters tenements are situated in the northern part of the McArthur basin but fall between the three types of uranium deposits mentioned previously (Figure 1). The purpose of this study is to determine if the uranium anomalies discovered in the Headwaters tenements have similar characteristics to other types of uranium deposits in the Northern Territory. This may indicate a particular type of mineralisation or may indicate that uranium anomalies are formed by a different process altogether.

This study will be conducted by analysing geochemical data collected during previous exploration. Different aspects of uranium mineralisation will be investigated including, host lithology, alteration assemblages and elemental associations. These results will then be compared with aspects of mineralisation from the different deposit types.

Geochemical data will also be examined for transects that cross four mineralised zones. These zones appear to be related to structures the Headwaters area. Concentrations of trace elements will be graphed to determine if they increase towards fault zones. This will also enable mineralisation assemblages to be determined for each zone. Hand samples, and a small

selection of thin sections, will be examined for each transect to determine if alteration changes in relation to faults or other structures in the area.

Multivariate analysis will also be conducted to determine if anomalies in the Headwaters area are related to a particular type of mineralisation and/or alteration process. This will help to establish if some of the anomalies are related to leaching of uranium from volcanic units as opposed to ore-forming processes seen in other parts of the McArthur Basin.

Determining the process or processes responsible for the formation of uranium anomalies discovered in the Headwaters tenements will hopefully aid in defining drilling or mining targets in the area.

2. Background

2.1 Location, Access and Climate

The Headwaters project area is located within the northern part of the McArthur Basin in the Northern Territory. The south-western extent of the tenements is approximately 95 kilometres north-east of Katherine and the north-western extent is approximately 280 kilometers east of Darwin (Figure 2). The tenements cover an area of approximately 5,300 square kilometres.

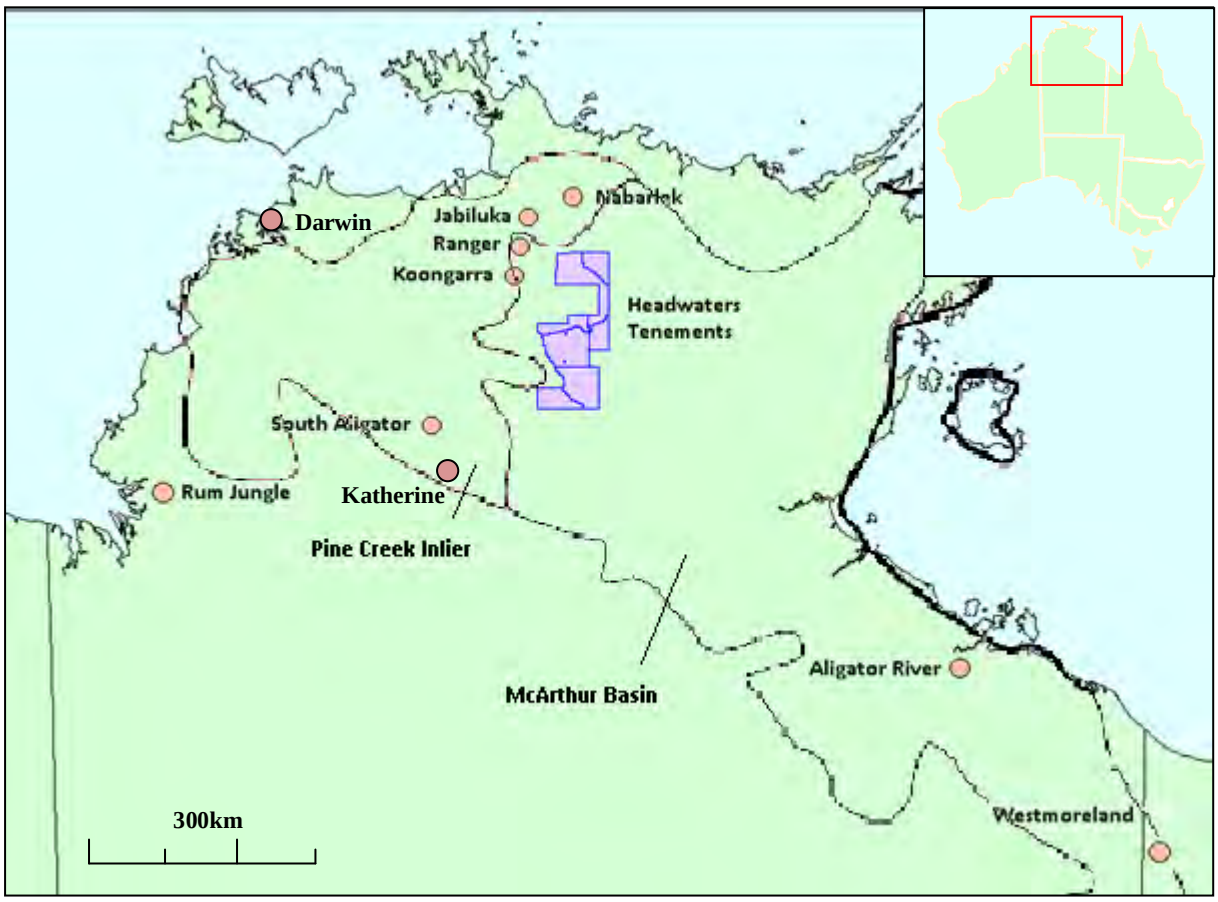

Figure 1: Location of unconformity-type and sandstone-hosted uranium deposits in the Northern Territory along with the location of the Headwaters tenements (blue lines) and the outline of the McArthur Basin.

Most of the tenements are located outside the south-east margin of Kakadu National Park (Drever et al., 1998). Access to the central tenements (24711, 24712, 27514 and part of 27513) has previously been by sealed roads and formed gravel tracks from Katherine to the Manyallaluk Aboriginal community. A dirt road leads to a helicopter base previously constructed by Cameco Australia PTY LTD (Drever et al., 1998). A track, named Bat Guyanggayang by traditional owners, was established in later years to provide access to another campsite (Drever et al., 1999).

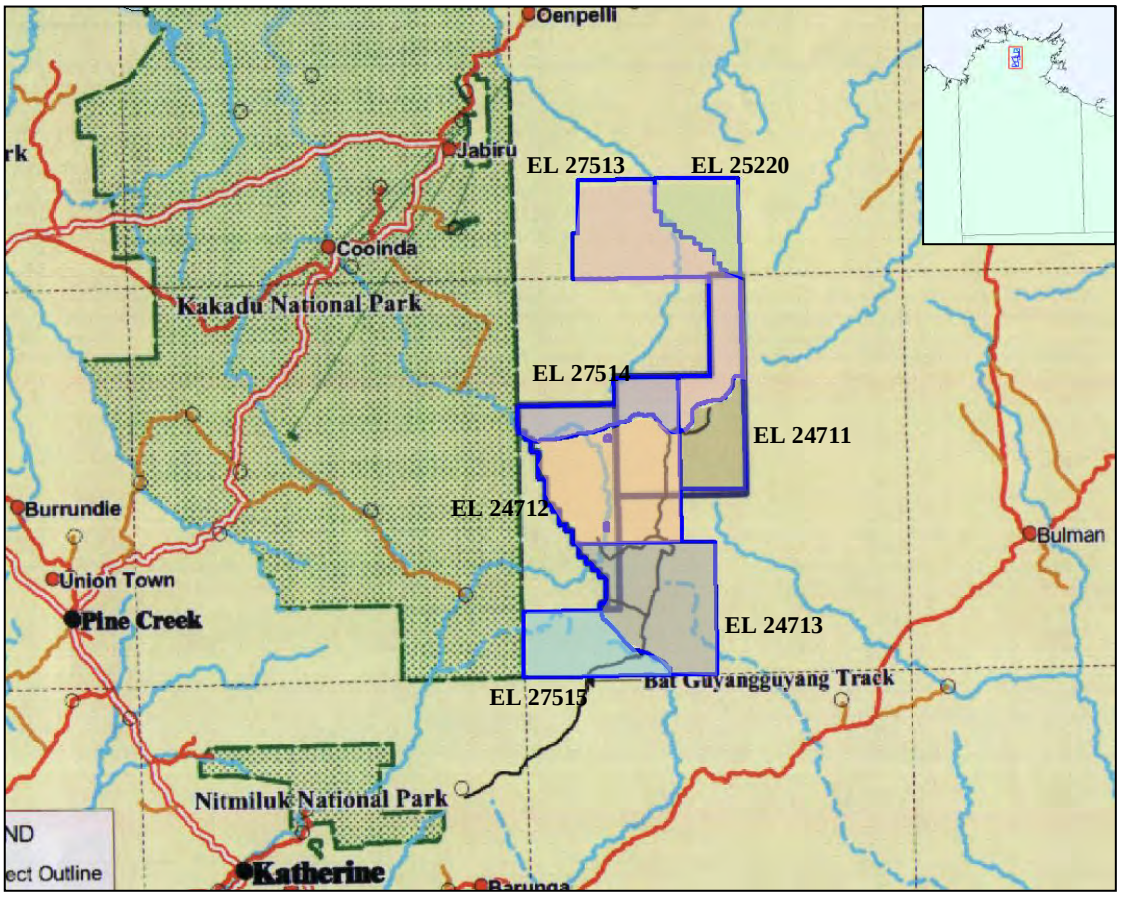

Figure 2: Location of Headwater project (with labled tenements) in Northern Territory, Australia (from Drever and Marlatt, 2000).

Exploration licenses (EL) 27515 and 24713 are located within the Arnhem Land Reserve on Aboriginal freehold land (Price, 1996). Access to these tenements is via the Stuart Highway south of Katherine then along the partially sealed Central Arnhem Road. Access can also be attained by the Bat Guyangguyang Track. Limited access within the tenements is by unsealed tracks (Price, 1996).

EL 25220 and most of EL 27513 are located in the northern part of the project area. There is no access by vehicle to or within these tenements (Carter and Beckitt, 2003). As vehicular access is either poor or non-existent within the Headwaters tenements, access is restricted to helicopters.

The Arnhem region in the Northern Territory has a tropical climate which is characterised by hot, wet monsoonal summers and mild, dry winters. The monsoon season generally lasts from October to May with temperatures averaging around 33˚C. Temperatures during the dry season averaged around 20˚C (Woinarski, 2009).

2.2 Regional Geology

The Headwaters tenements are located the northern part of the McArthur Basin on the Arnhem Shelf in the Northern Territory (Figure 3).

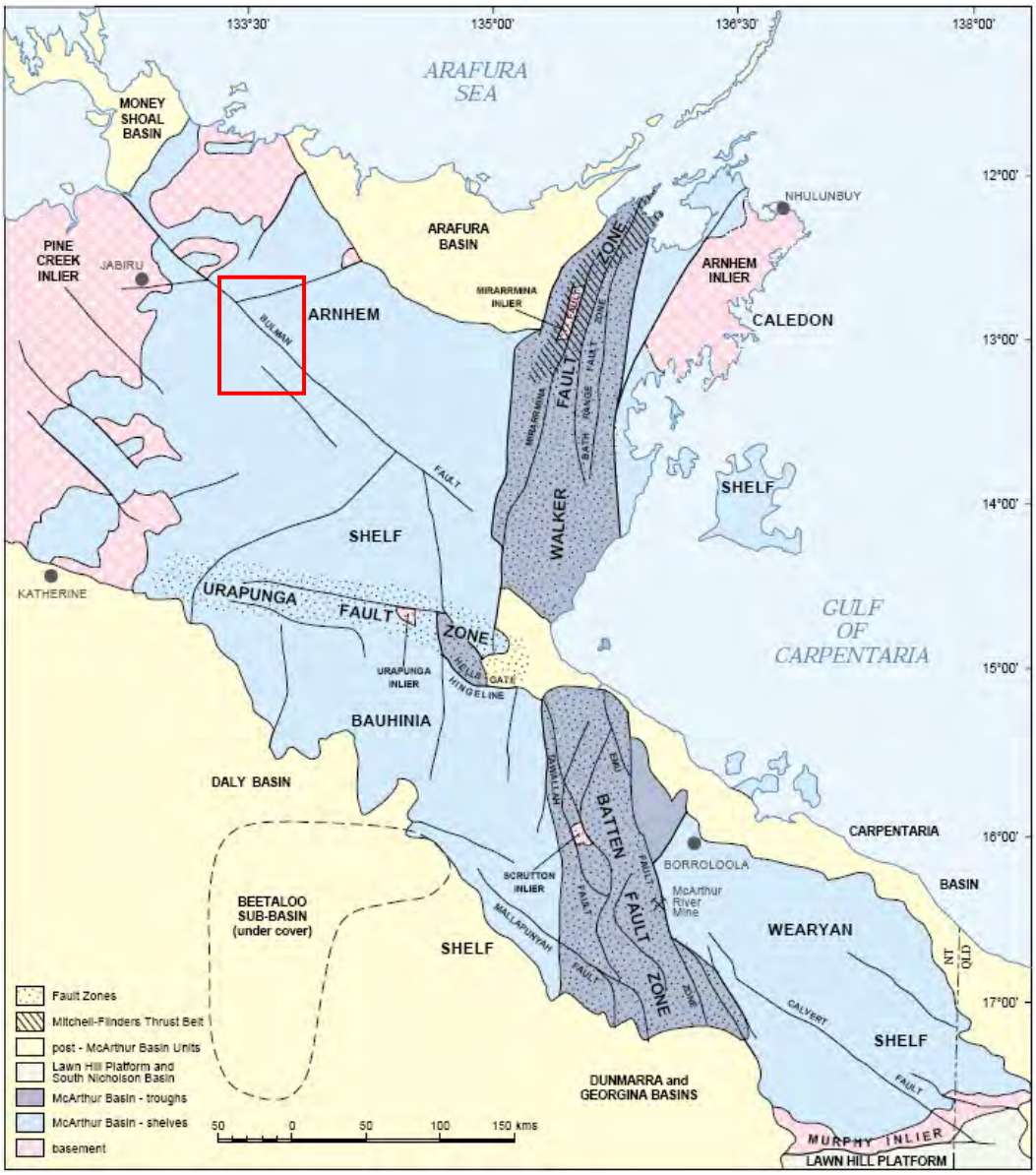

Figure 3: Regional tectonic elements and geological divisions of the McArthur Basin, northern Australia (From Rawlings, 2001).

The McArthur Basin is composed of a group of mid-Proterozoic basins which unconformably overlie the Paleoproterozoic North Australian Orogenic Province. These basins are the principal element of the North Australian Platform Cover (Price, 1996; Warren, 1997).

The basin covers an area of approximately 200,000km^2 and contains a sequence of relatively undeformed and unmetamorphosed sedimentary rocks up to 12km thick. These rocks are divided into groups, shown in Figure 3, which are separated by regional unconformities (Price, 1996; Warren, 1997).

The lowest group is the Katherine River Group (Tawallah Group in the south) that comprises sandstones with minor volcanics, clastics and carbonates. It is up to 4.5km thick with an age of approximately 1700 to 1800 Ma (Price, 1996; Warren, 1997). These platform fluviatile and shallow marine sediments unconformably overlie the sedimentary successions of the Pine Creek Basin which are strongly deformed and metamorphosed. They are known to host the major unconformity-related U deposits of the Alligator Rivers region (Drever et al., 1998).

Overlying the Katherine River Group is the Habgood-Parson Range Group (McArthur Group in the south) and the Mt Riggs-Nathan group. These groups are primarily comprised of evaporitic and stromatolitic cherty dolostones interbedded with sandstone and shale. The groups are approximately 5.5km thick in total and around 1600 to 1700 Ma old (Price, 1996; Warren, 1997).

The uppermost group is the Roper group which, with an approximate age of 1450 Ma, is significantly younger than the lower groups. It consists of alternating sandstones, mudstones and siltstones up to 5km thick (Price, 1996; Warren, 1997).

The McArthur Basin overlies and is bounded by basement to the north-west, north-east and south-west. Basement rocks consist of the Pine Creek Basin succession mentioned above, the Nanambu Complex, the metamorphic Kakadu Group and the Cahill Formation (Carter and Beckitt, 2003; Drever et al., 1998). The Cahill Formation is known to host uranium ore bodies in the area including the Nabarlek uranium deposit (Carter and Beckitt, 2003).

The Oenpelli Dolerite (1710-1720 Ma), the youngest Precambrian rock outcropping within the tenements, intruded early Palaeoproterozoic metamorphosed sediments and the Kombolgie Formation. This resulted in the formation of large lopolithic bodies. Later post-orogenic Proterozoic granites (1780-1750 Ma), such as the Tin Camp Creek and Nabarlek Granites, have intruded the metamorphosed sediments in the eastern and southern parts of the region (Carter and Beckitt, 2003).

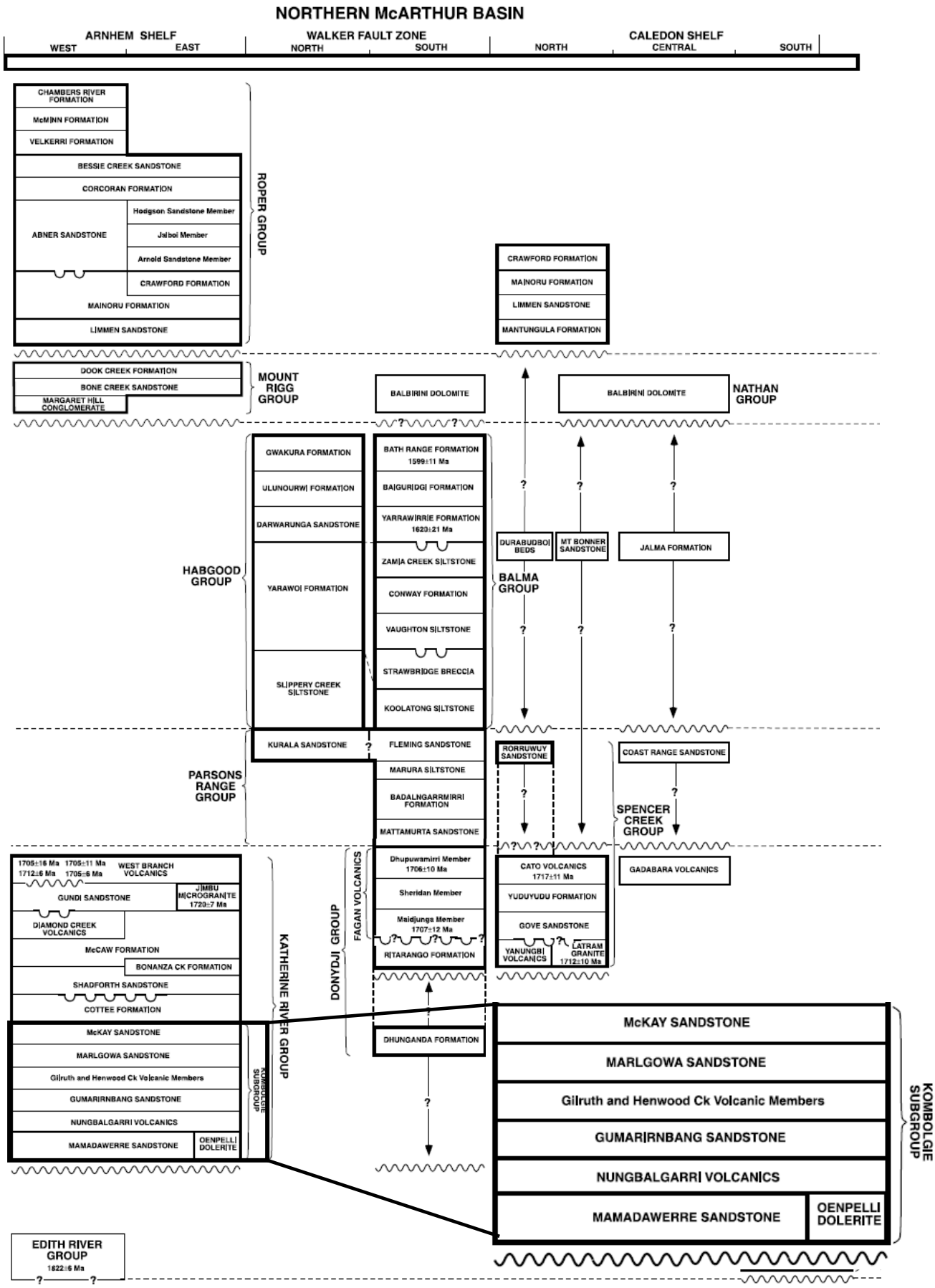

Figure 4: Stratigraphic column for the Northern McArthur Basin, Northern Territory, Australia (Rawlings, 1999). Stratigraphy found within the Headwaters tenements is enlarged.

2.3 Regional Structure

Major structural elements have been identified in the Arnhem shelf. These structural elements have been attributed to a rift model in which shelves and an adjacent north-south trough are dissected by several features. These features include a west-north-west trending basement rise, known as the Uranpunga Tectonic Ridge, and north-west trending faults which include the Mallapunyah and Bulman faults shown in Figure 5 (Price, 1996; Warren, 1997).

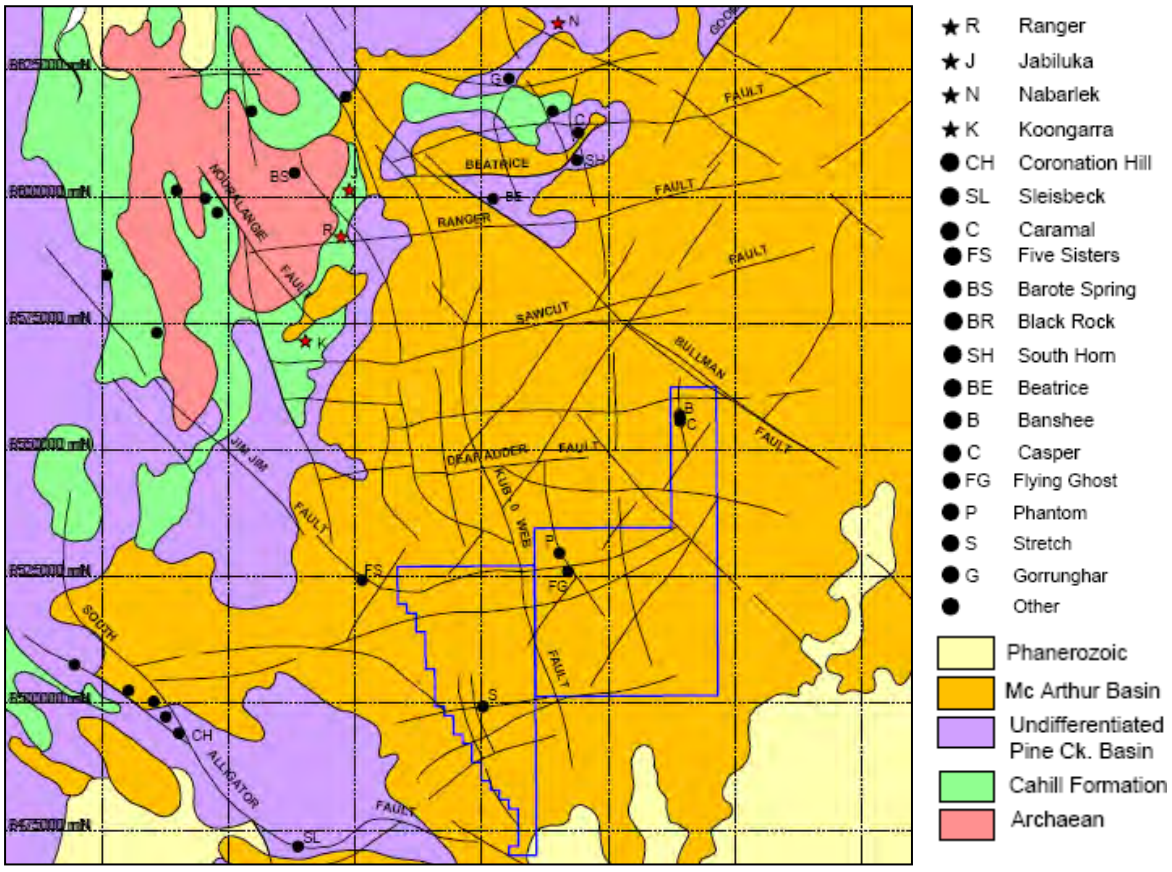

Figure 5: Regional structure map with known uranium occurrences in the McArthur Basin, Northern Territory (Modified from Drever et al., 1998). Blue lines represent the outline of two tenements within the Headwaters area.

Extensional basin tectonics was responsible for the formation of the Kombolgie Subgroup of the McArthur Basin and the Barramundian sequences of the Pine Creek Basin. A compressional phase, the Barramundi Top-End Orogeny, occurred between the two extensional phases resulting in metamorphism and multiple deformations of the Barramundian sequences and late tectonic related granite intrusions (Drever et al., 1999).

The key mineralising structures in Arnhem Land are thought to be second order reverse faults which formed dilational zones in concurrence with strike slip fault systems in compressional domains (Drever et al., 1999). However, similar dilation zones may also be associated with normal faults in extensional domains (Drever et al., 1999).

2.4 Local Geology

The Headwaters tenements are predominantly comprised of the gently south-east dipping platform sequences of the Kombolgie Subgroup (Figure 6). The lowermost units, the Mamadawerre Sandstone and the Nungbalgarri Volcanics, outcrop in the northern parts of the tenements. The Mamadawerre Sandstone unconformably overlies basement rocks of the Nimbuwah Complex These basement rocks do not outcrop in any of the tenements (Zaluski, 2003), but are known to exist in the tenement areas from stratigraphic drill cores.

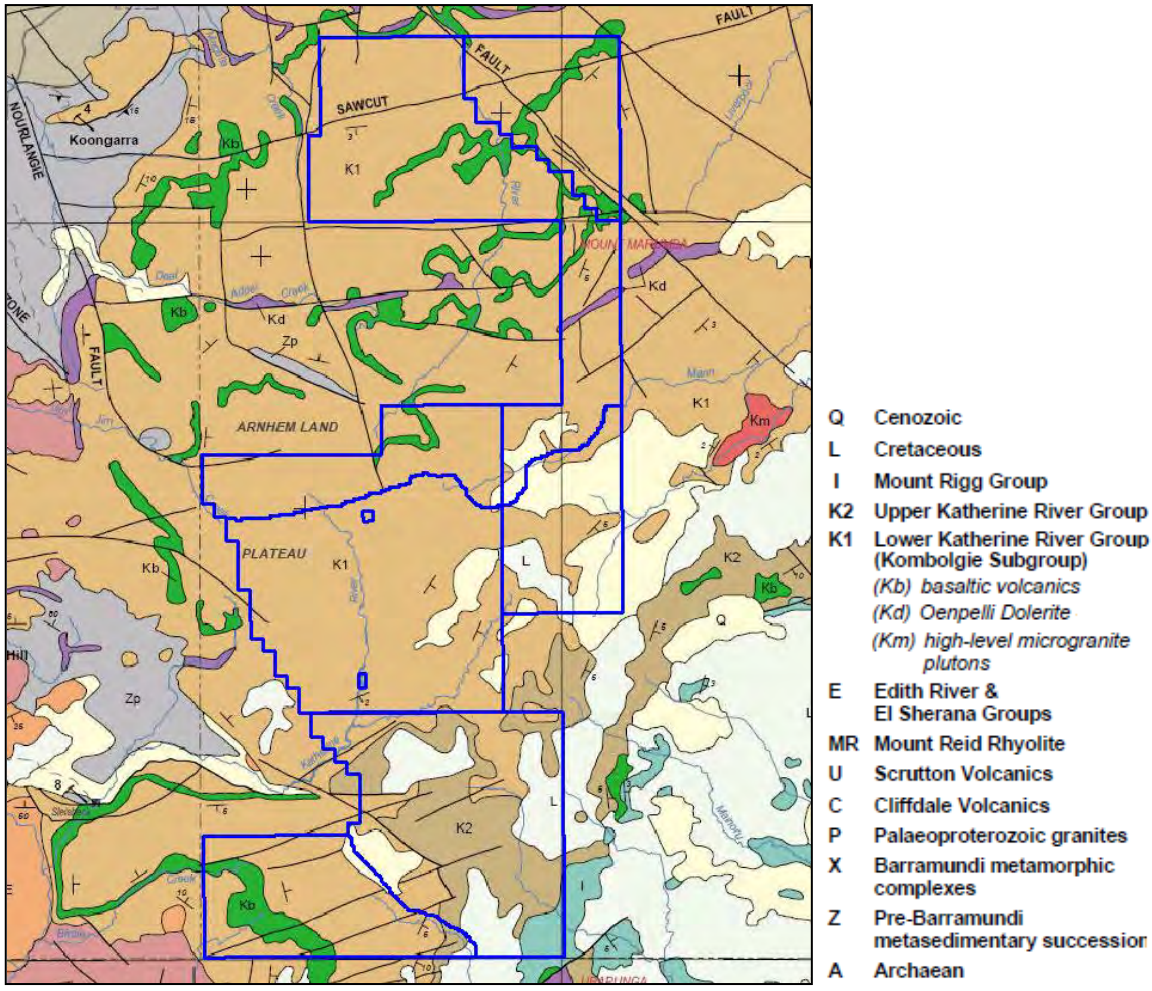

Figure 6: Local geology within the Headwaters tenements, Arnhem Land, Northern Territory (Modified from Rawlings, 2001). Blue boxes are the borders for the Headwaters tenements.

The lowermost unit exposed in the south is the Gumarrirnbang Sandstone which is comprised of a very coarse grained quartz arenite (Carson et al., 1999). It was mainly deposited within a distal braided fluvial system. The thin, extensively lateritised Gilruth Volcanic Member conformably overlies the Gumarrirnbang Sandstone which is conformably overlain by the Marlgowa Sandstone. This unit comprises a fine grained, thickly bedded quartz arenite in a shallow marine, tidal to braided fluvial environment. It contains interbeds of ferruginous sandstone in several sections (Zaluski, 2003). The McKay Sandstone is generally included as a unit within the Marlgowa Sandstone.

2.5 Local Structure

Within the Headwaters tenements there are two predominant conjugate fault sets, one set at 340˚ and 070˚ and another set at 310˚ and 030˚ (Figure 7). The dextral Kub-O-Wer fault displaces the 070˚ fault set by one or two kilometres and the dextral Bulman Fault, along with a major parallel structure further north, displaces the 030˚ fault set by up to 2 kilometres (Drever et al., 1999).

The overprinting relationships in the aforementioned structures suggest that two major generations of deformation occurred within the area (Rosenbaum, 2009). The first generation included dextral strike-slip faulting along the Bulman fault and east-west reverse faulting which occurred along with an early extension trending approximately east-west. A north-south trending extension event followed which occurred along with reactivation of east-west trending and NE-SW trending structures. NE-SW extensional features with dextral movement were also developed.

The north-west and east-west trending lineaments in the area have strong positive magnetic anomalies which suggests that the lineaments may have provided routes for dykes to penetrate the sandstones (Rosenbaum, 2009).

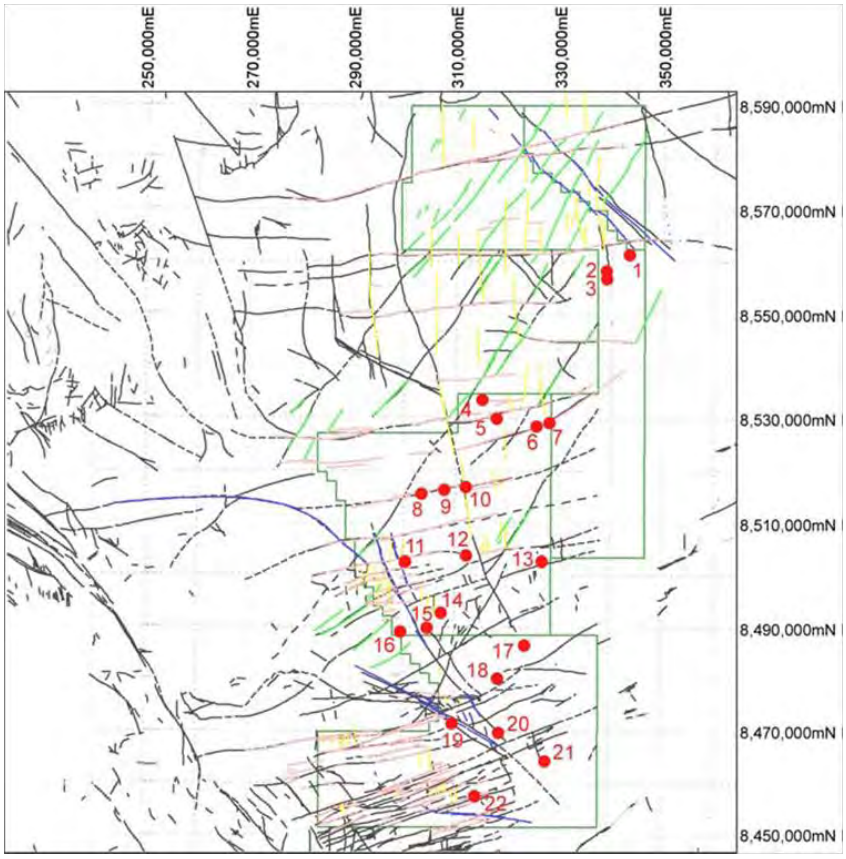

Figure 7: Map of the Headwaters tenements showing different structures along with locations of uranium anomalies. Solid coloured lines represent interpreted structures and red dots represent uranium anomalies (From Rosenbaum, 2009).

2.5 Previous Exploration

Uranium exploration has been conducted within the Headwaters tenements since 1969. Exploration for diamonds was also undertaken with little success.

From 1969 to 1971, a joint venture to search for uranium in the Northern Territory was undertaken by Peko Mines N. L., Electrolytic Zinc Company of A/Asia LTD and Newmont Pty. Ltd (Maynard, 1971). The area of exploration covered parts of EL's 25220 and 27513 within the northern part of the Headwaters tenements. Exploration consisted of photo-interpretation, airborne radiometric and magnetic surveys. Only one uranium anomaly was located within the project area which was determined to be a possible indication of an uranium deposit upstream (Maynard, 1971).

In 1972 and 1973, Queensland Mines Limited conducted exploration in EL's 260 and 264 which included the northern extents of the Headwaters tenements. An exploration program was created to study results from previous exploration and identify any gaps in the data (Queensland Mines Ltd, 1972a; Queensland Mines Ltd, 1972b; Queensland Mines Ltd, 1974a; Queensland Mines Ltd, 1974b; Swingler, 1973). Several uranium prospects (or "windows") in the project area were selected for ground reconnaissance and stream sediment sampling. The majority of anomalies discovered in the two exploration licenses were determined to be lithological anomalies. A total of four zones of uranium mineralisation were located. (Queensland Mines Ltd, 1972a; Queensland Mines Ltd, 1972b; Queensland Mines Ltd, 1974a; Queensland Mines Ltd, 1974b; Swingler, 1973). The four zones of uranium mineralisation were not located within the Headwaters tenements.

From 1995 to 1997, Normanby Exploration's Bulman/Mainoru Project explored for diamonds, zinc, lead, copper and silver in an area that encompasses EL's 27515, 24715 and 24712 in the Headwaters project (Price, 1996; Warren, 1997). Heavy mineral drainage, loam and geochemical samples were taken along with rock chips from various sites within the exploration licenses. One diamond chip and numerous chromite grains were found and several diamond related anomalies defined (Price, 1996; Warren, 1997).

All exploration up to and including exploration by Normanby focused solely on uranium exploration on the surface. Although several areas of possible uranium mineralisation were found, each company determined there was no economical uranium deposit in the area.

2.5.1 Cameco Exploration

Over a period of approximately eight years, Cameco Australia Pty Ltd explored for uranium in two project areas that now make up the majority of the Headwaters project area.

The Deaf Adder project, an area that is now included in EL's 24711,24712,24713,27513 and 27514, was undertaken from 1997 until 2002. Several uranium prospects were identified by airborne magnetic spectrometric survey and radiometric prospecting. Outcrop sampling was subsequently conducted and detailed analyses performed to determine uranium levels. These data were used to better define the prospect in the project area (Drever et al., 2000; Drever et al., 1999; Drever and Marlatt, 2000; Drever et al., 1998; Otto et al., 2001; Otto et al., 2002). Figure 8 shows the location of the prospects within the Headwaters tenements and the areas with high uranium values.

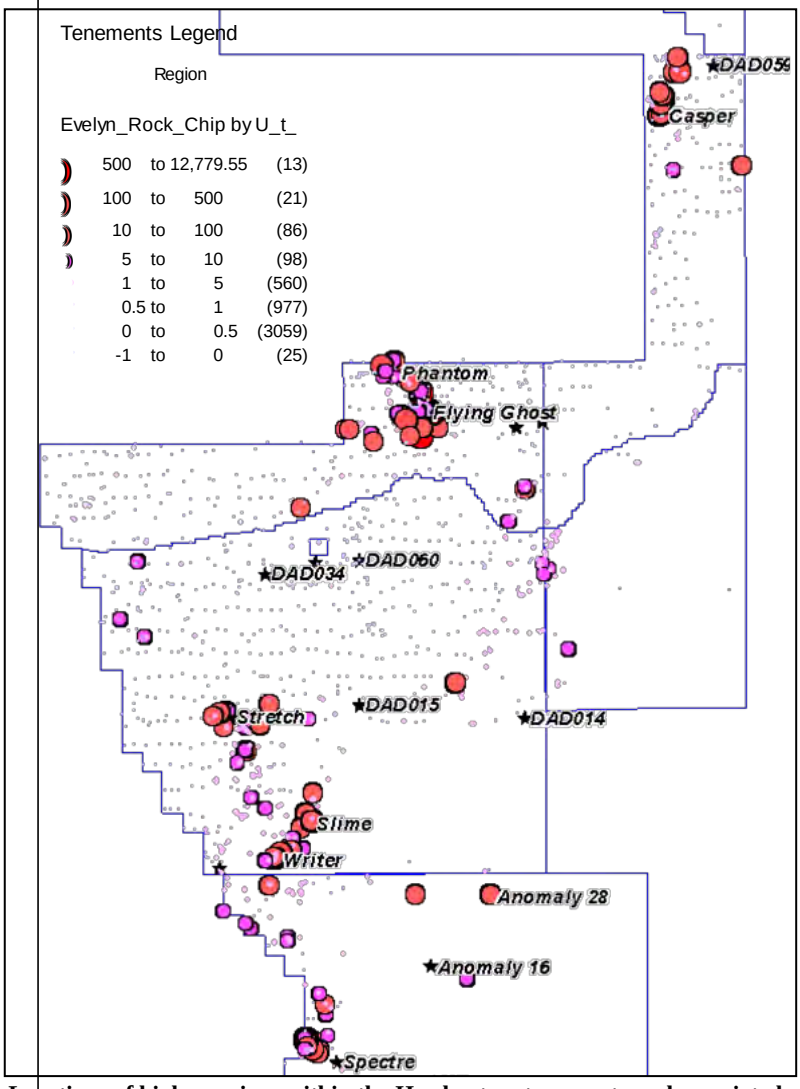

Figure 8: Locations of high uranium within the Headwaters tenements and associated prospects.

During 1998, 1999 and 2000, a total of eight holes were drilled within the Deaf Adder project area. Five holes were drill in the area surrounding the Flying Ghost prospect to determine if

radioactivity occurred below the surface (Drever et al., 1999). Two holes were drilled in the southern part of the project area in a failed attempt to reach the basement (Drever et al., 2000). A drill hole in the western part of the project area was the only one deep enough to reach the unconformity at 993.45 metres (Otto et al., 2001).

After five years of exploration it was determined that the uranium mineralisation in the Deaf Adder project was the result of surface enrichment or that the mineralisation was sourced from possible enrichment at the unconformity. Regardless, it was determined that depth of the unconformity severely diminished the prospectivity of the exploration licenses and they were surrendered in June 2002 (Otto et al., 2002).

The East Alligator project was conducted from 2002 to 2005 within the current exploration license 25220 in the Headwaters tenement. An airborne hyperspectral survey, airborne magnetics, radiometrics and a digital terrain model along with outcrop sampling were undertaken to determine if an unconformity-style uranium deposit occurred in the project area (Carter and Beckitt, 2003).

The airborne radiometrics for uranium showed numerous uranium anomalies within the East Alligator Project area. The majority of these anomalies correspond with exposures of the Gilruth Volcanics. Weaker anomalies (Figure 9) were less common and were generally related to features and dykes within the Gumarrirnbang and Marlgowa sandstones (Carter, 2005).

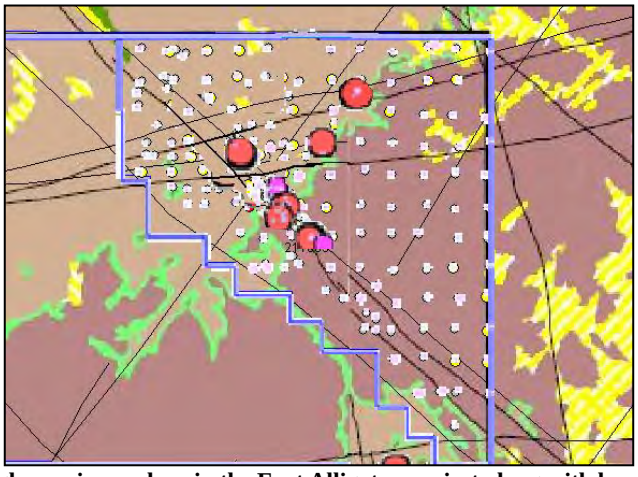

Figure 9: Location of high uranium values in the East Alligator project along with local geology and structure.

Cameco concluded that anomalous uranium values were related to scavenging, inheritance and surficial enrichment from the Gilruth Volcanics. It was determined that analysis of surface samples would not help in determining basement targets within the East Alligator project area (Carter and Otto, 2006).

3. Methods

The majority of geochemical data used in this project were produced by Cameco from rock chip sampling within the Deaf Adder and East Alligator projects. Several samples from exploration in the Bulman/Mainoru project were included in the dataset.

All the samples from the Cameco prospects were analysed by either ICP-MS (G400M) or ICP-OES (G400I). A full list of elements along with the analytical methods and techniques used are shown in Table 1. A few elements, including lead and uranium, were also analysed by G950M with ICP-MS which were measured in parts per billion. Analytical methods for samples collected for the Bulman/Mainoru project are unknown although there were no significant uranium values determined and the samples were not used for geochemical interpretation during this project.

Table 1: Elements analysed by Cameco Australia for the Headwaters samples along with the analytical method, technique, accuracy/precision, detection limit and data units.

Analysis	Analytical Method	Technique	Accuracy/Precision ±%	Detection Limit	Data Units
Au	FA25N_EMS	ICP-MS	10	1	ppb
Pd	FA25N_EMS	ICP-MS	10	1	ppb
Pt	FA25N_EMS	ICP-MS	10	1	ppb
Ag	G400M	ICP-MS	10	0.05	ppm
Al203	G400I	ICP-OES	10	100	ppm
As	G400M	ICP-MS	10	0.5	ppm
Ba	G400I	ICP-OES	10	2	ppm
B	G140I	ICP-OES	10	20	ppm
Be	G400M	ICP-MS	10	0.1	ppm
Bi	G400M	ICP-MS	10	0.2	ppm
CaO	G400I	ICP-OES	10	20	ppm
Ce	G400M	ICP-MS	10	0.01	ppm
Co	G400M	ICP-MS	10	0.05	ppm
Cr	G400I	ICP-OES	10	5	ppm
Cu	G400I	ICP-OES	10	1	ppm
Dy	G400M	ICP-MS	10	0.01	ppm
Er	G400M	ICP-MS	10	0.01	ppm
Eu	G400M	ICP-MS	10	0.01	ppm
Fe2O3	G400I	ICP-OES	10	50	ppm
Ga	G400M	ICP-MS	10	0.01	ppm
Gd	G400M	ICP-MS	10	0.01	ppm
Hf	G400M	ICP-MS	10	0.01	ppm
Ho	G400M	ICP-MS	10	0.01	ppm
K2O	G400I	ICP-OES	10	100	ppm
La	G400M	ICP-MS	10	0.01	ppm
Li	G400I	ICP-OES	10	1	ppm
Lu	G400M	ICP-MS	10	0.01	ppm
MgO	G400I	ICP-OES	10	20	ppm
MnO	G400I	ICP-OES	10	2	ppm
Mo	G400M	ICP-MS	10	0.05	ppm
Na2O	G400I	ICP-OES	10	100	ppm
Nb	G400M	ICP-MS	10	0.05	ppm
Nd	G400M	ICP-MS	10	0.05	ppm

Analysis	Analytical Method	Technique	Accuracy/Precision ±%	Detection Limit	Data Units
Ni	G400M	ICP-MS	10	0.2	ppm
P2O5	G400I	ICP-OES	10	50	ppm
Pb	G400M	ICP-MS	10	0.2	ppm
Pb204	G400M	ICP-MS	10	0.2	ppm
Pb206	G400M	ICP-MS	10	0.2	ppm
Pb207	G400M	ICP-MS	10	0.2	ppm
Pb208	G400M	ICP-MS	10	0.2	ppm
Pr	G400M	ICP-MS	10	0.01	ppm
Rb	G400M	ICP-MS	10	0.01	ppm
S	G400I	ICP-OES	10	20	ppm
Sc	G400M	ICP-MS	10	0.1	ppm
Se	G400M	ICP-MS	10	2	ppm
Sm	G400M	ICP-MS	10	0.01	ppm
So	G400M	ICP-MS	10	0.2	ppm
Sr	G400M	ICP-MS	10	0.05	ppm
Ta	G400M	ICP-MS	10	0.02	ppm
Tb	G400M	ICP-MS	10	0.01	ppm
Th	G400M	ICP-MS	10	0.01	ppm
TiO2	G400I	ICP-OES	10	20	ppm
Tm	G400M	ICP-MS	10	0.01	ppm
U	G400M	ICP-MS	10	0.01	ppm
V	G400I	ICP-OES	10	2	ppm
W	G400M	ICP-MS	10	0.05	ppm
Y	G400M	ICP-MS	10	0.01	ppm
Yb	G400M	ICP-MS	10	0.02	ppm
Zn	G400I	ICP-OES	10	2	ppm
Zr	G400M	ICP-MS	10	0.1	ppm
Hg	G950M	ICP-MS	10	1	ppb
Pb204	G950M	ICP-MS	10	0.01	ppb
Pb206	G950M	ICP-MS	10	0.01	ppb
Pb207	G950M	ICP-MS	10	0.01	ppb
Pb208	G950M	ICP-MS	10	0.01	ppb
Pb Tot	G950M	ICP-MS	10	0.01	ppb
U	G950M	ICP-MS	10	0.01	ppb

In this study the different datasets containing geochemical information, outcrop information (including lithology, formation, alteration and structure) and sample co-ordinates were combined into a single dataset for preparation and interpretation. The majority of elements from the different datasets were measured in parts per million. However, some elements were measured in parts per billion and were therefore recalculated to parts per million before the data could be imported into a statistical program for analysis. The detection limits also varied between different datasets therefore data for each element were set to the highest detection limit used. All results that were blank, negative or zero were corrected to half the detection limit in order to avoid errors when using statistical programs for multivariate analysis.

Data levelling was not conducted as the datasets came from different areas within the tenements. Some of the values in the datasets were from samples that were collected form

mineralised areas. Levelling the data, in the case of the Cameco projects, may have disguised mineralisation. The decision not to conduct data leveling may create bias from the Bulman/Mainoru project. However, as the samples from the Bulman/Mainoru project are few and contain no significant uranium anomalies any such bias will be of negligible importance.

Once the entire dataset (Appendix 1) had been prepared for interpretation, univariate statistics (Appendix 2) were calculated to determine if the values within the dataset seemed appropriate for each element or oxide. These data were then entered into the IOGas statistical program to create histograms and scatter plots in order to determine if any trends were present within the data. Any trends determined in the data were then compared to alteration, lithology and structure in order to determine if any trends were related to mineralisation.

Triplot diagrams were used to determine if the geochemical data could be used to differentiate between different lithologies and alteration. Other statistical programs, such as Statistica and SPSS, were used to conduct principal component analysis and factor analysis on the geochemical data.

As multivariate analysis techniques were carried out during this project, data were standardised so that all major and trace elements could be plotted together. Data were standardised by dividing the value of each element in each sample by average for each element.

Samples previously collected by Cameco were examined to determine what alteration and geochemical changes occurred from unmineralised samples toward mineralised samples in fault zones. Samples from one particular fault located within a known prospect were chosen for closer examination. Samples from one transect were sent to a lab in the USA for polished thin section to be created. Detailed rock and thin section descriptions were written to see if there was an obvious change in mineralogy, lithology, alteration or weathering as uranium values increased.

4. Results and Discussions

4.1 Analysis of Element Distributions

The univariate statistics returned appropriate values for each element suggesting that there were no significant errors during analysis or the input of data rendering the entire dataset suitable to use for geochemical interpretation. Histograms are a useful statistical tool used to determine the variability of data. They help to determine the shape, location and spread of the data distribution. The shape of distribution shows whether the values are symmetric, skewed, bimodal or multi-modal and can identify any outliers (Bulmer, 2005).

The histograms for all major oxides and trace elements are included as Appendix 3. For the different elements from the Headwaters project, three types of statistical distributions were recognised: simple Gausian, skewed and bi-modal. Gausian (bell shaped) distribution were seen in Al_2O_3, Ag, CaO, Co and K_2O. Such a distribution suggests that the concentrations of these elements are more or less homogenous across the project area with some slight variations. The bimodal distributions of Rb, Mo, Li and Fe_2O_3 suggest that these elements have two distinct groups within the dataset. The skewed distributions were seen for several elements including U, As, Ba, Co and MnO. This type of distribution suggests that the majority of values are low with only a few high values recorded. These three distributions are investigated in more detail in section 4.3. For a small number of elements (Be, Na, Nb and Tm), the majority of results were below the analytical detection, and therefore clustered at the lower end of the histograms.

4.2 Geochemical Differentiation of Lithologies and Alteration

Outcrop samples from the Headwaters tenements consist of five lithologies: three types of sandstone and two igneous rocks types. Out of the 2,751 samples only fifteen were igneous, therefore, the three sandstones, the Gumarrirnbang, Marlgowa and McKay Sandstones, were the only lithologies analysed for this project.

The geochemical data from the outcrop samples were investigated to determine if the three different sandstones had different geochemical signatures. Initial investigation to differentiate between the sandstones consisted of plotting aluminium oxide, iron oxide and silica triplots for each sandstone, the results of which are shown in Figures 10, 11 and 12. Triplots for silica, Na + K and Al + Fe were also investigated (Figures 13, 14 and 15).

4.2.1 Triplots for SiO_2, Al_2O_3 and Fe_2O_3

The triplot for the Gumarrirnbang Sandstone (Figure 10) showed that the majority of sandstone samples were high in silica and low in aluminium and iron. There were several samples that contained greater concentrations of iron with silica ranging from fifteen to ninety five percent. There were two samples that contained a higher percentage of aluminium, one contained fifty percent silica and the other contained only ten percent silica.

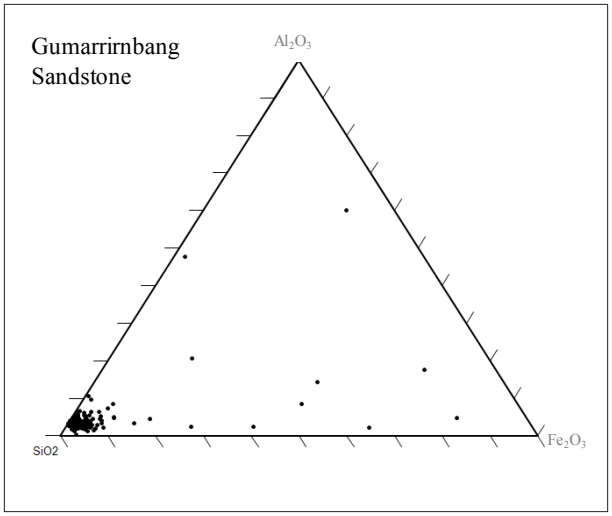

Figure 10: Triplot showing the abundances of silica, aluminium oxide and iron oxide of the Gumarrirnbang Sandstone.

Results from the Marlgowa Sandstone (Figure 11) showed similarities to samples from the Gumarrirnbang Sandstone. The majority of the samples were silica rich and there were several samples that contained higher concentrations of iron with silica percentages ranging from fifteen to ninety five. The major difference in the Marlgowa Sandstone is that there is a greater percentage of aluminium in most of the samples and there appears to be a grouping (circled) that shows a general decrease in silica as aluminium increases.

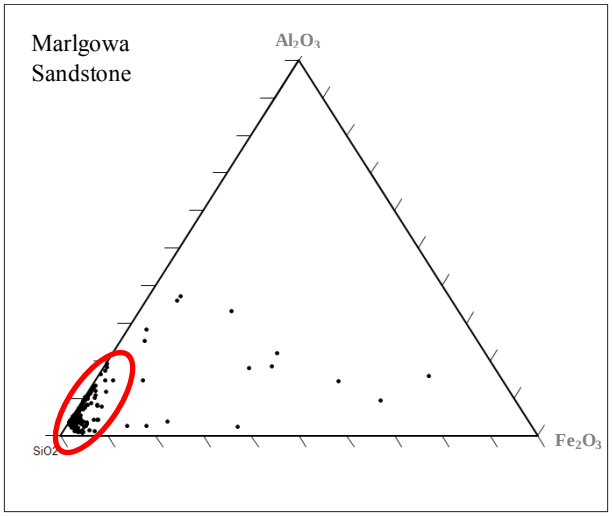

Figure 11: Triplot of the Marlgowa Sandstone showing percentages of silica, aluminium oxide and iron oxide.

The triplot for the McKay Sandstone (Figure 12) shows that it is, in general, more aluminium rich and iron poor than both the Gumarrirnbang and Marlgowa Sandstone. There were only three samples that contained greater than thirty percent iron. A grouping showing a general increase in aluminium with a decrease in silica is also present (red circle).

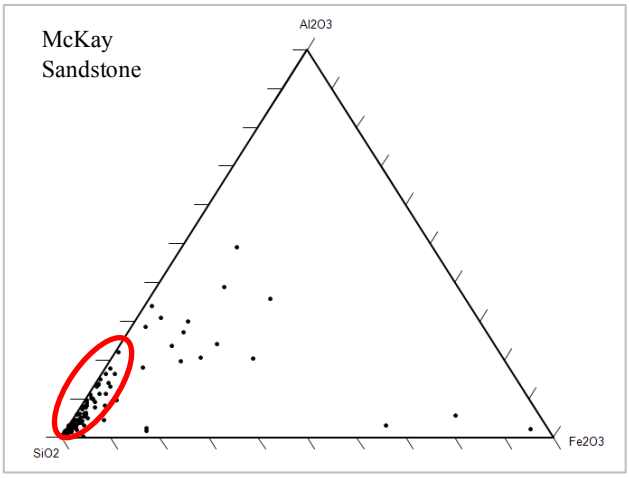

Figure 12: Triplot of silica, aluminium oxide and iron oxide for the McKay Sandstone.

4.2.2 Triplots for SiO_2, Na + K and Al + Fe

Although the triplots above show some minor geochemical differences between the three sandstones it is not enough to be able to differentiate between them using only the three selected oxides. Therefore, silica, Na + K and Al + Fe were plotted for the sandstones to determine if there were differences in alteration or weathering.

The new triplot, shown in Figure 13, for the Gumarrirnbang Sandstone showed that the highest percentage of Na + K in any of the samples was just below ten percent. The majority of the samples had over ninety percent SiO_2 with less than ten percent Al + Fe and very minor percentages of Na + K. However, there were several samples that were higher in Al + Fe and lower in SiO_2 signifying a general trend of increasing Al + Fe with decreasing SiO_2.

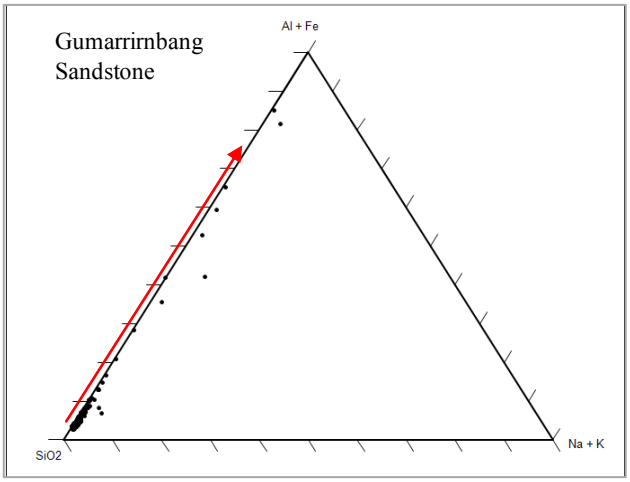

Figure 13: Triplot of SiO_2, AL + Fe and Na + K for the Gumarrirnbang Sandstone.

The new triplot for the Marlgowa Sandstone shows that the results are similar to the new triplot for the Gumarrirnbang Sandstone with the exception of a second trend (blue arrow, Figure 14). The majority of samples contains less than ten percent Al + Fe and contains more than ninety percent SiO_2. As in the Gumarrirnbang Sandstone there is a trend of increasing Al + Fe with decreasing SiO_2. However, in the Marlgowa Sandstone there is also a trend showing an increase in Na + K at the same time.

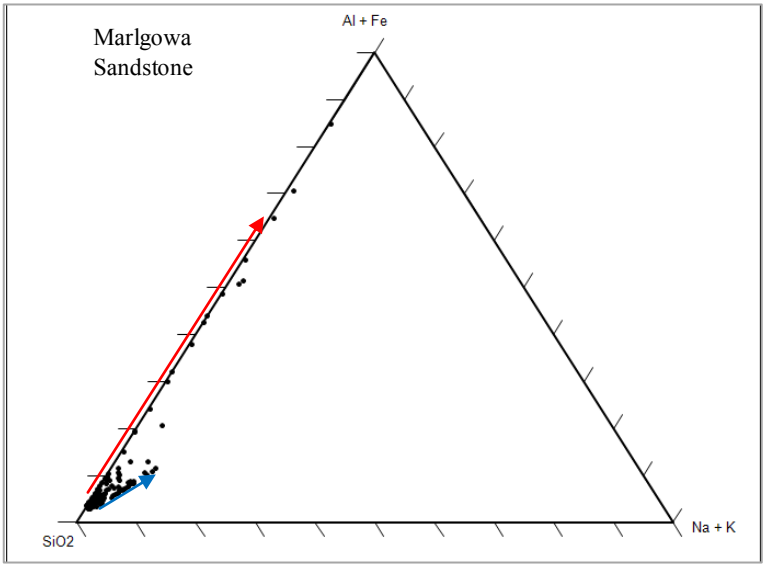

Figure 14: Triplot showing the percentages of SiO2, Al + Fe and Na + K for the Marlgowa Sandstone.

The percentages in the McKay Sandstone were slightly different than both the Gumarrirnbang and Marlgowa sandstones. The majority of samples contain greater than five percent Na + K with a maximum of thirty percent Na + K. The main trend in the McKay Sandstones appears to be an increase in Al + Fe and Na + K with a decrease in SiO_2 (Figure 15). There are a few samples that show the same increase in Al + Fe without the increase in Na + K.

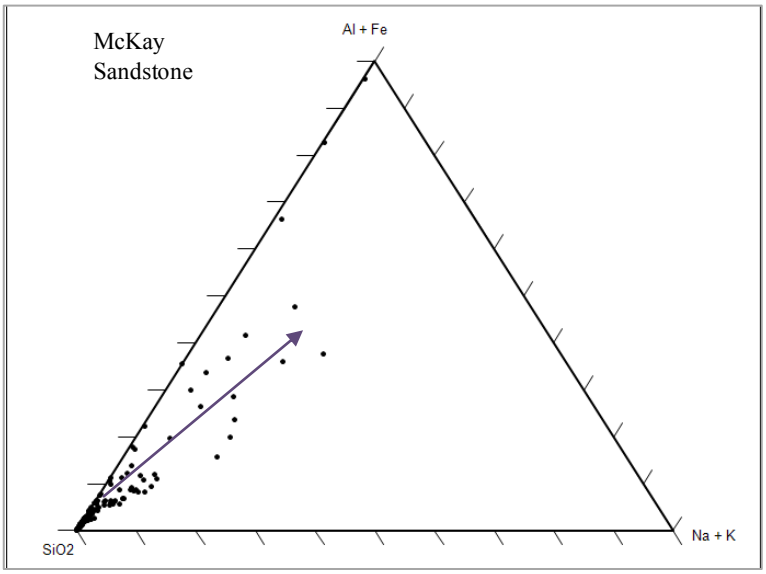

Figure 15: Triplot of SiO_2, Na + K and Al + Fe for the McKay Sandstone.

Although geochemistry does not show a definite differentiation between the major rock types within the Headwaters project, it can still be used to determine different trends in lithology. This may help to define particular types of alteration that are known to occur with uranium mineralisation in the Northern Territory.

4.2.3 Differentiation of Alteration

There are several types of alteration that have previously been recorded within the Headwaters tenements. In the absence of a limonitic-goethitic crust, drusy and smokey quartz along with bright red hematite have been observed in the southern part of the Flying Ghost area (Drever et al., 1998). Strong bleaching of goethite was also seen along some fractures (Drever et al., 1998). None of the aforementioned alteration types were associated with mineralisation. In the areas containing possible uranium mineralisation, blotches of black or purple goethite that were potentially formed by alteration were seen within the sandstones. Goethite was also associated with anomalous values in the Casper prospect (Drever et al., 1998).

Subsequent exploration in the Deaf Adder project area determined that although radiometric anomalies were associated with goethite alteration, it was strongly elevated gold values that were most commonly associated with goethite (Drever et al., 2000). It was also discovered that uranium was, in general, associated with clays in zones of intense fracturing. Clay patterns around known uranium prospects generally consisted of increased kaolinite, chlorite and occasionally increased illite (Drever et al., 2000).

Most mafic samples that were collected from the same area were intensely altered by supergene processes. A few samples not affected by supergene processes were available from which to identify primary minerals and hydrothermal alteration. The main minerals in these samples formed during hydrothermal alteration included adularia, chlorite, albite, sericite, carbonate and clay. This assemblage suggests low pressure and a temperature of between 200°C and 300°C (Drever et al., 1999). Similar minerals have been discovered with unconformity type uranium mineralisation at Nabarlek (Polito et al., 2004a) and Jabiluka (Polito et al., 2005b) as well as the sandstone-hosted uranium deposits in Westmoreland (Polito et al., 2005a).

Hand samples were inspected in section 4.4.6 in order to determine if alteration differed in mineralised and unmineralised areas. To determine which alteration minerals occur in each sample, further analysis, such as SEM or XRD analysis, would need to be undertaken.

4.3 Uranium Associations

Probability plots were produced for each major oxide and trace element. The high values for uranium were highlighted so that the corresponding samples could be seen in graphs of other elements. The purpose of this was to determine if the high uranium values matched high values in other elements. This may suggest a particular elemental association in mineralisation within the Headwaters tenements. The main elements that generally appear to be associated with uranium include arsenic (Figure 16), gold, lead, platinum and lower silica. The remaining probability plots can be seen in Appendix 4.

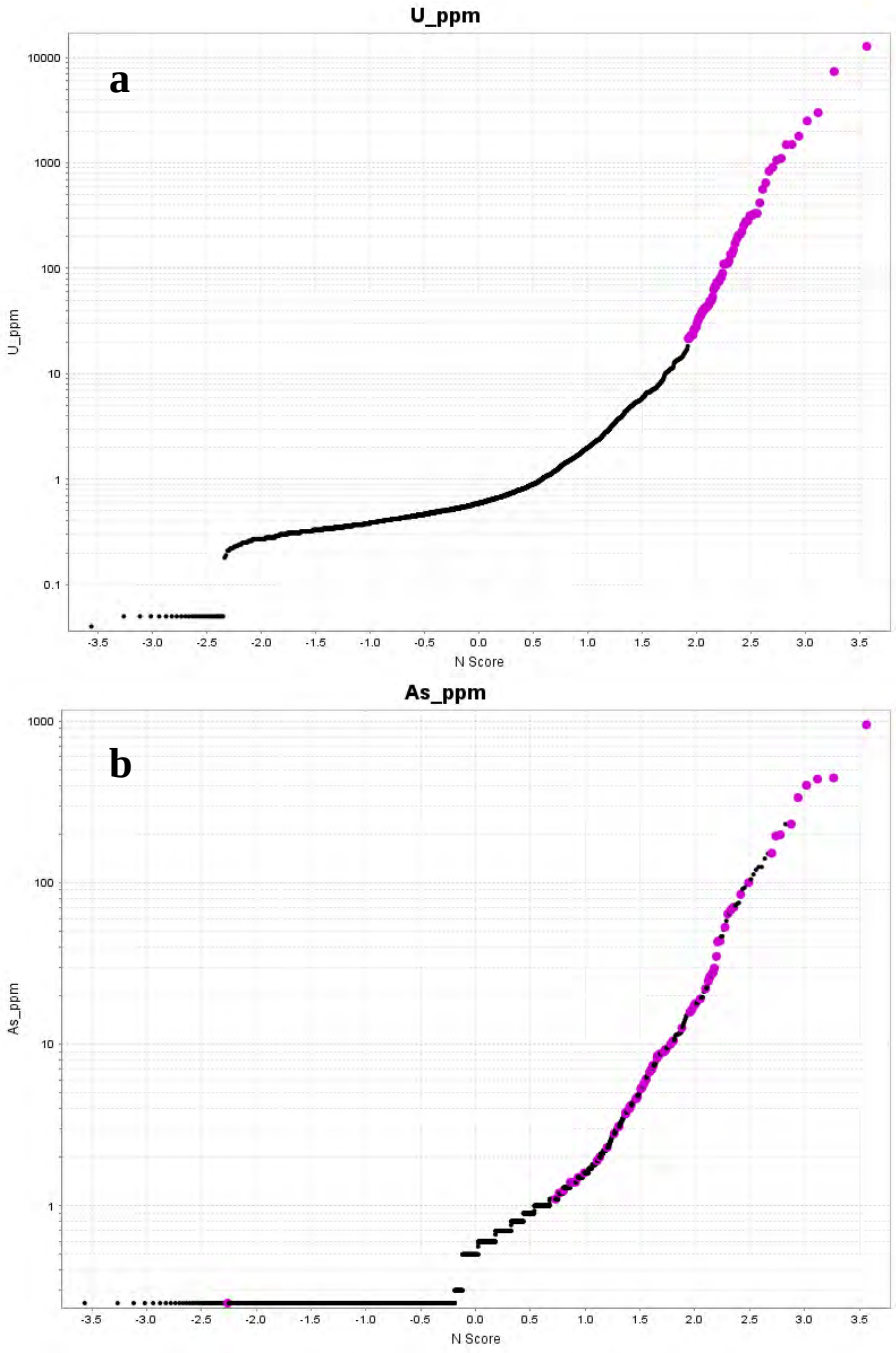

Figure 16: Probability plots with high uranium values (purple dots) in a) and the corresponding samples (purple dots) highlighted in arsenic b).

4.3.1 Similarities to Uranium Associations in Other Deposits

Uranium deposits in the Westmoreland area, namely the Redtree deposit, comprise stratiform and discordant sandstone-hosted uranium mineralisation. Stratiform mineralisation occurs wholly within the Westmoreland Conglomerate which lies beneath the Siegal volcanics. Discordant mineralisation occurs in the conglomerate and dolerite dikes. Mineralisation in the Junnagunna deposit is flat lying and occurs at a fault intersection (Polito et al., 2005a).

The mineral assemblage associated with uranium mineralisation in the Westmoreland area is characterised by uraninite, hematite, illite and minor rutile around 1655Ma. This mineral assemblage was found to have replaced an earlier chlorite-illite assemblage. Uranium deposits were formed in structural and chemical traps when uraniferous brines between 150° and 250°C migrated through the conglomerate (Polito et al., 2005a).

In the Alligator Rivers uranium field, mineralisation is hosted in metamorphic rocks below the unconformity between the Kombolgie Formation and schists from the Cahill Formation (Dodson et al., 1974). In the Jabiluka deposit, uraninite was precipitated with chlorite, quartz, sericite and hematite when oxidized basinal brine around 200°C was drawn into the basement rocks. Diagenetic aquifers in the Kombolgie Subgroup are believed to be the source of the fluid (Polito et al., 2005b). The same mechanisms and alteration assemblages were found at the Nabarlek, Koongarra and ranger deposits (Kendell, 1990; Komninou and Sverjensky, 1995b; Ludwig et al., 1987; Polito et al., 2004a).

Uranium minerals in the Alligator Rivers uranium field may be accompanied by chlorite, pyrite, lead and copper sulfides as well as gold (Dodson et al., 1974). Alteration haloes surrounding ore deposits were generally enriched in Ti, Cu, Ni, Co, Rb, Zn, Pb, Li and uranium (Wilde and Wall, 1987).

It appears that processes for the formation of both sandstone-hosted and unconformity-type uranium deposits, as well as their alteration assemblages, are very similar in the McArthur Basin. In the case of unconformity-type deposits, for uranium to be deposited on the surface it would have had to have been taken back into solution and transported to the surface. Subsequent processes may mask or replace features that would indicate an unconformity-type deposit depth. This makes it difficult to determine if the uranium anomalies in the Headwaters project are related to either type of deposit.

4.3.2 Trends in Uranium Associations

All major oxides and trace elements in the geochemical database were graphed with uranium to determine if there were any trends in the data. In graphs for several trace elements and major oxides two trends were identified (Figure 17) which may represent mineralisation and heavy metal trends. There were in some cases outliers or smaller trends occurring between the two main trends. The remainder of the scatter plots can be seen in Appendix 5.

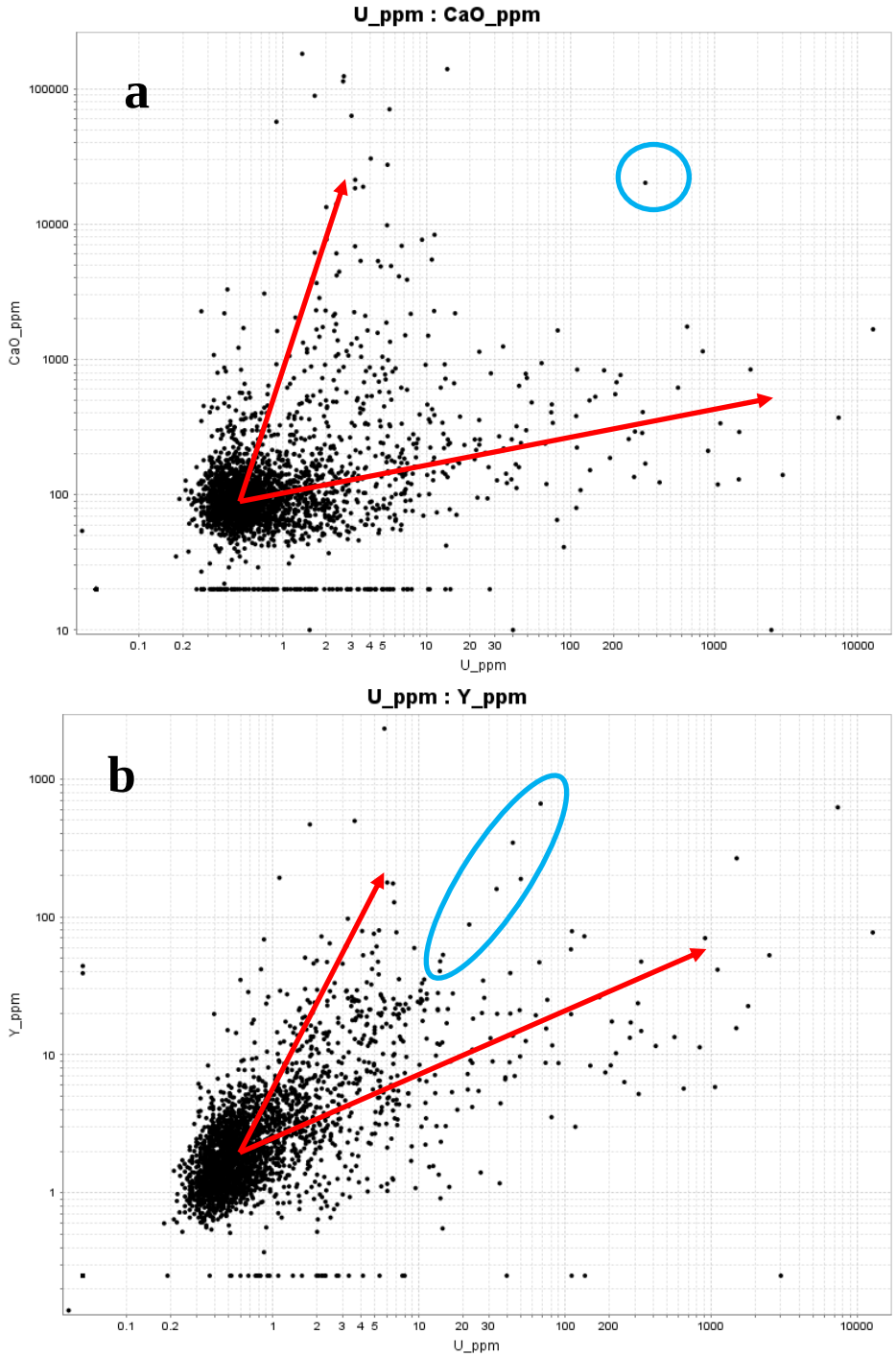

Figure 17: Scatter plots of a) CaO and b) Y against uranium showing direction of trends and location of outliers or smaller trends.

Samples within one of the trends seen above were highlighted so that the same samples could be located in other graphs. This was to determine if the trends seen in other elements were the same as the trends seen above. It was revealed that for several elements, the samples in the lower trends were generally the same samples that occurred in the lower trend of the calcium oxide (Figure 18). The remainder of the scatter plots with highlighted samples can be seen in Appendix 6.

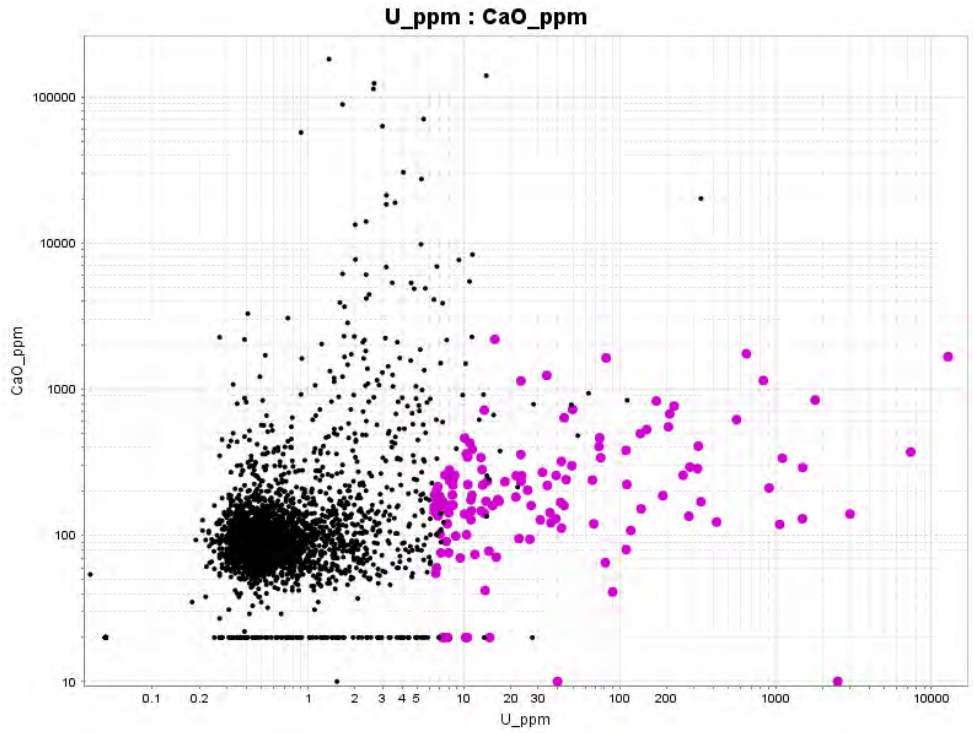

Figure 18: Scatter plot of calcium oxide against uranium with samples in one trend highlighted in purple.

Samples within the trends seen in the scatter plots were then selected so they appeared highlighted on a map of the Headwaters tenements that showed the location of known prospects (Figure 19). The samples from the lower trend (trend B) are located within known uranium prospects. The majority of samples from the higher trend (trend A) are located in areas that are not identified as prospects although there are several samples located within the prospects. The location of the highlighted samples suggests that trend B is a mineralisation trend where as trend A may be related to heavy metals.

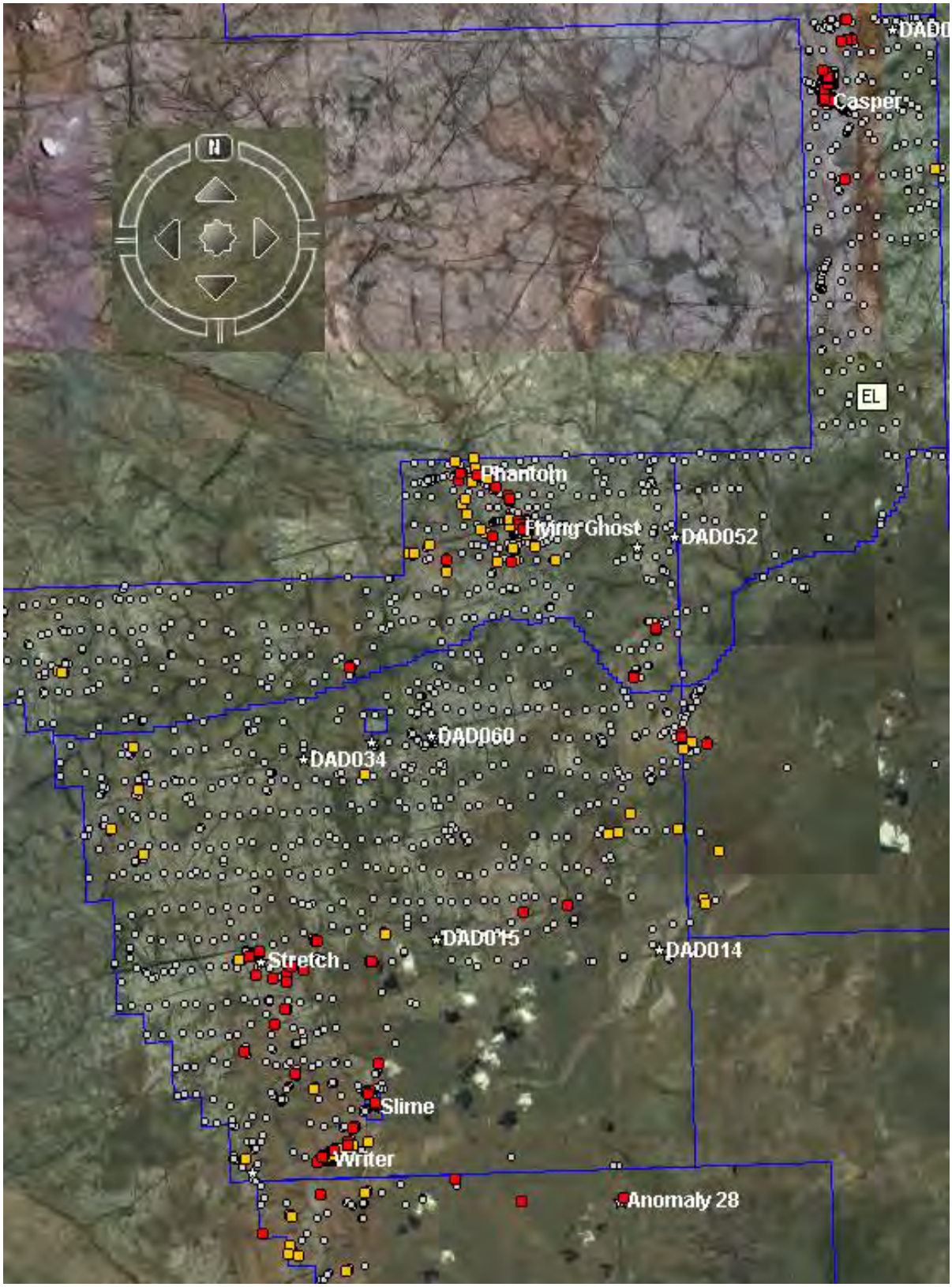

Figure 19: Location of samples within the trends seen in the scatter plots comparing uranium to all other elements in the geochemical database. Local structure can be seen in the Google image and known uranium prospects are labelled. Red squares represent samples that occurred in trend B. Orange squares represent samples that occurred in trend A (Google Earth, 2009).

4.3.3 Alteration associated with trends

The trends in the scatter plots were colour coded to represent different types of alteration in order to determine if either trend contained more altered samples than the other. This would help in determine whether trend B was a mineralisation trend. Major oxides, for example Figure 20a, and trace elements (Figure 20b) were again plotted with results showing that all but one altered sample for CaO and all but three altered samples for Th were located along trend B. Scatter plots with associated alteration for other elements can be seen in Appendix 7.

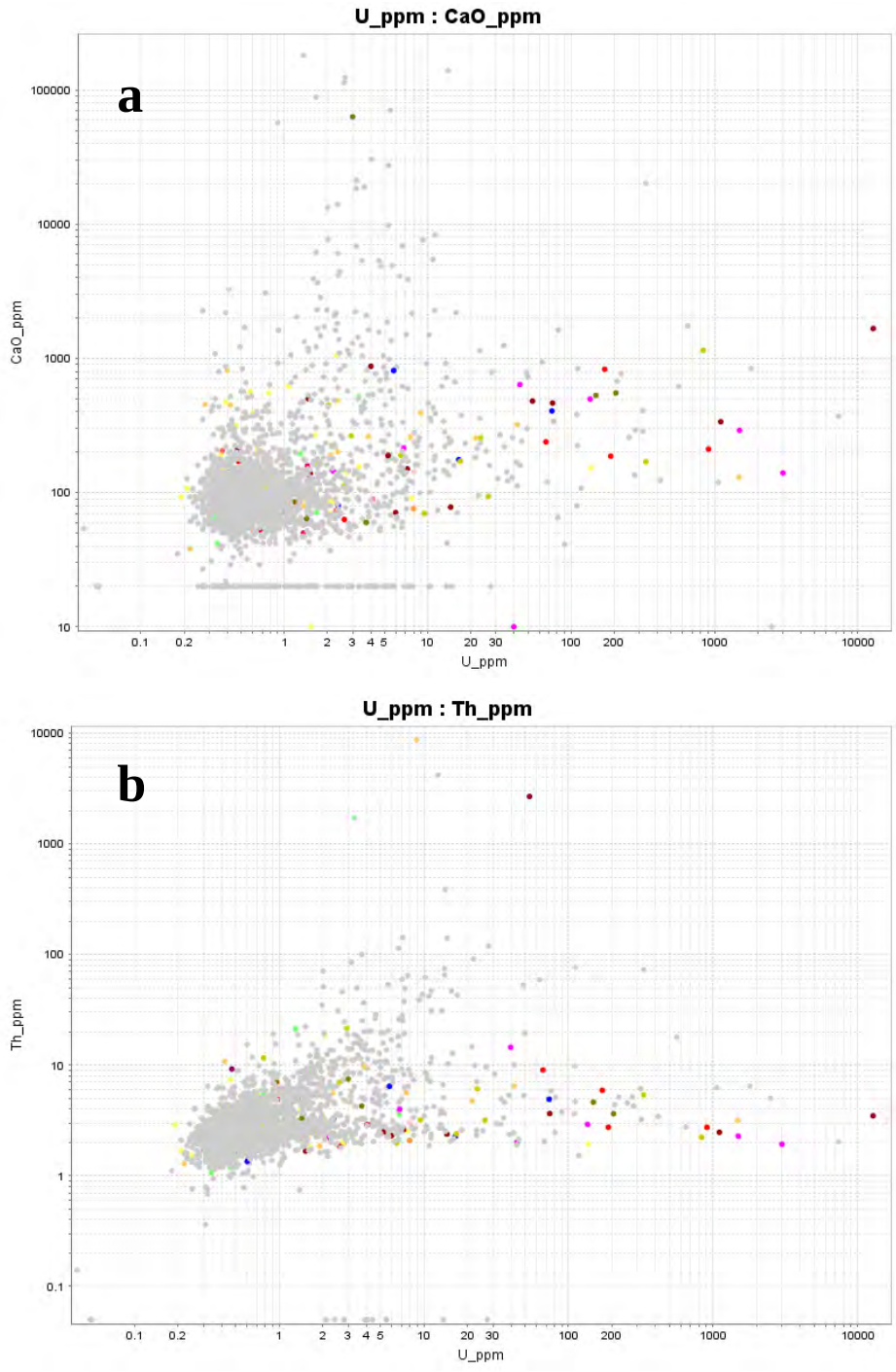

Figure 20: Scatter plots of (a) CaO and (b) Th showing altered (coloured) and unaltered (grey) samples.

There were several different types of alteration described in the outcrop samples taken by Cameco. These types included bleaching, silicification, hematite, limonite, goethite and quartz veining. Secondary uranium minerals and radioactivity readings were generally associated with the alteration types mentioned in areas within or surrounding fractures and brecciation. This also suggests that the trend containing the altered samples is a mineralisation trend.

4.3.4 Structure associated with trends

The same trends were also compared to the different types of structure known to occur within or around the samples. The results show that all samples associated with different structures occurred in trend B of the CaO (Figure 21a). However, in the scatter plot for thorium (Figure 21b), structures were not limited to trend B. Three samples that contained jointing, one that contained a fracture and one that showed signs of shear were located in trend A. Plots for other elements can be found in Appendix 7.

Some samples related to structures in the Headwaters area were located in the upper trend. Regardless, the majority of structures related to the major faults detailed previously, and brecciation related to faulting, occurred within the lower trend. This also supports the assumption that the lower trend is associated with mineralisation.

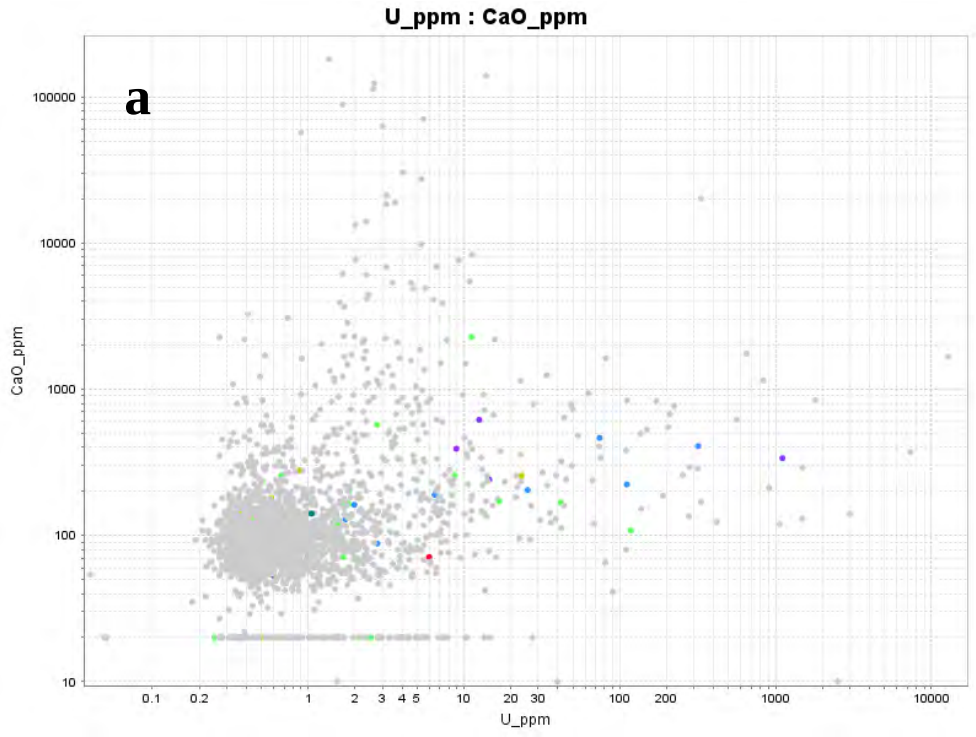

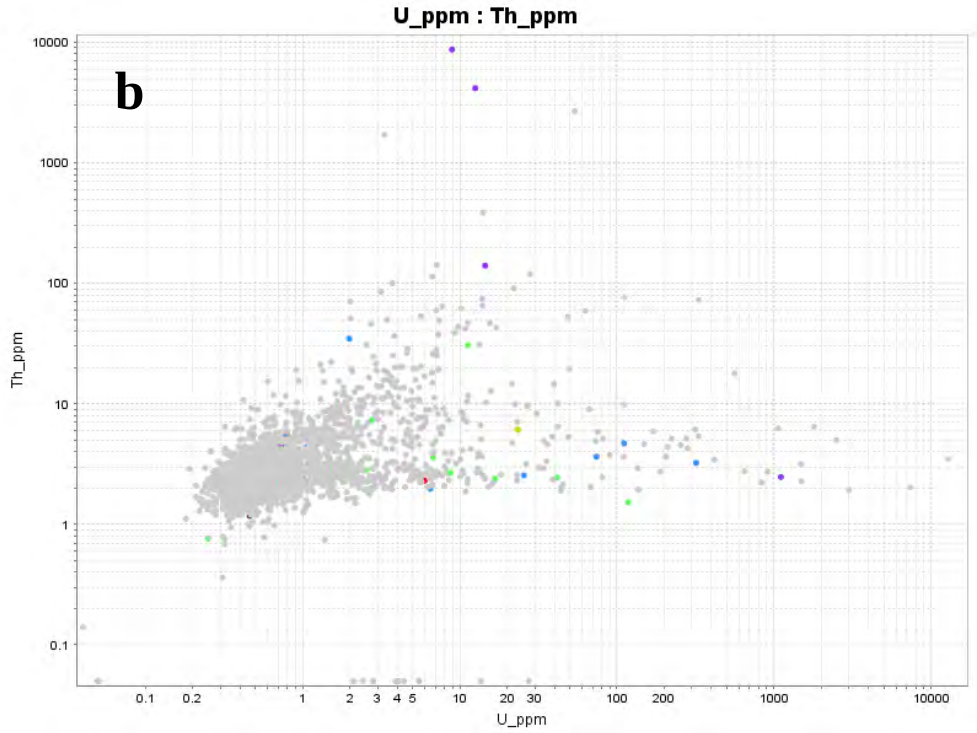

Figure 21: Scatter plots comparing a) CaO and b) Th to structures in or around samples (coloured dots).

4.3.5 Lithology associated with trends

The trends seen above were also compared to lithology to determine if the trends were made up of one lithology more than any others. Figure 22a for CaO, and Figure 22b for Th, show that the majority of samples in trend B for are from the Gumarrirnbang Sandstone and the majority of samples in trend A are from the McKay Sandstone. Samples from the Marlgowa Sandstone were seen in both trends. Plots for other elements are in Appendix 7.

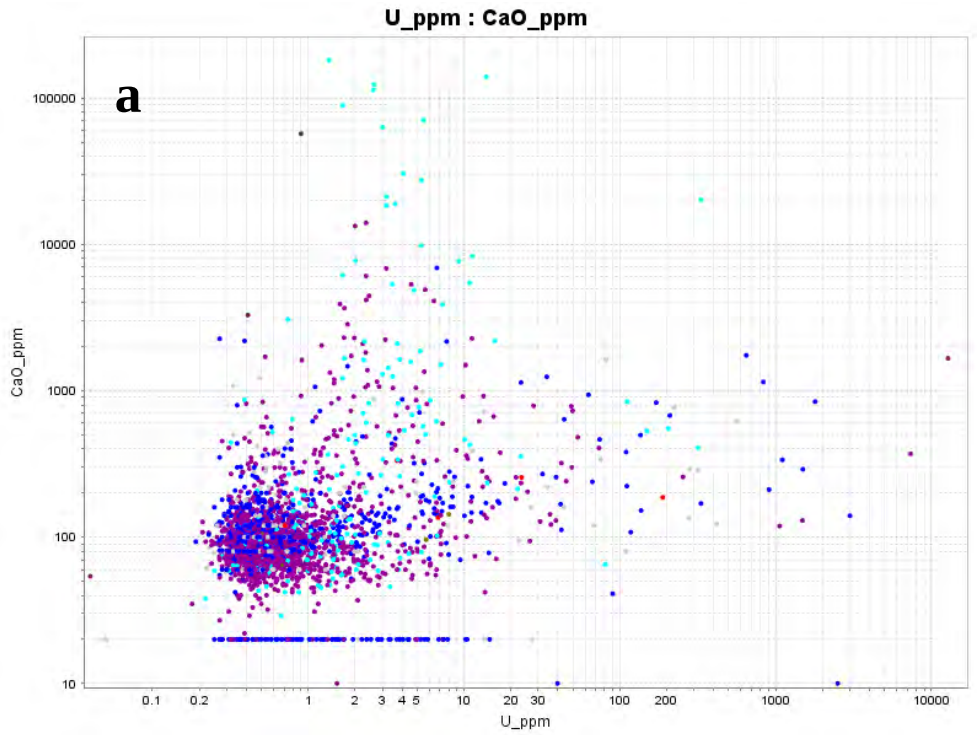

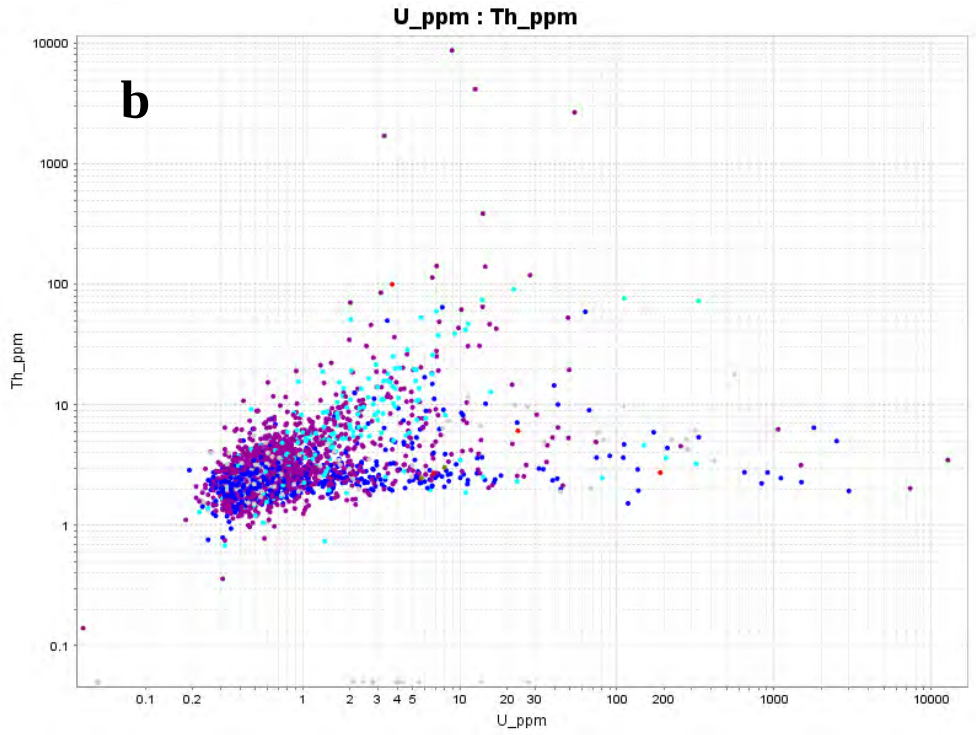

Figure 22: Scatter plots coloured by lithology for a) CaO and b) Th. Dark blue indicates Gummarrirnbang Sandstone, light blue indicates McKay Sandstone and purple indicates Marlgowa Sandstone. Red dots show volcanic or dolerite samples.

Although the type of lithology does not lend any support to the theory that one of the trends is a mineralisation trend, it can help to determine the location of different mineralised zones as the different types of sandstone outcrop in different areas within the Headwaters project. The McKay sandstone outcrops only in the south; the Gumarrirnbang Sandstone outcrops in the central area; and the Marlgowa Sandstone occurs throughout the project area.

The Flying Ghost and Casper prospects are located within this unit which may suggest that these two prospects are formed due to mineralisation. The McKay sandstone contains the Writer prospect in the southern part of the project area. This would suggest that uranium anomalies in the Writer prospect are formed through a different process or by a different mineralisation event.

4.4 Structural Transects

Four transects were taken from different prospects which were located with different structures within the Headwaters tenements (Figure 23). The Casper prospect in the north is situated along a north-east trending fault zone mentioned earlier in this report. The Phantom prospect in the middle of the tenements is situated on a north-west trending structure which is not believed to be one of the common fault zones in the area. The Flying Ghost prospect, which is also located in the centre of the project, is situated on one of the 70 degree faults which were also mentioned in the local geology section. In the south, the Writer prospect appears to be related to a similar north-west trending structure as the Phantom prospect.

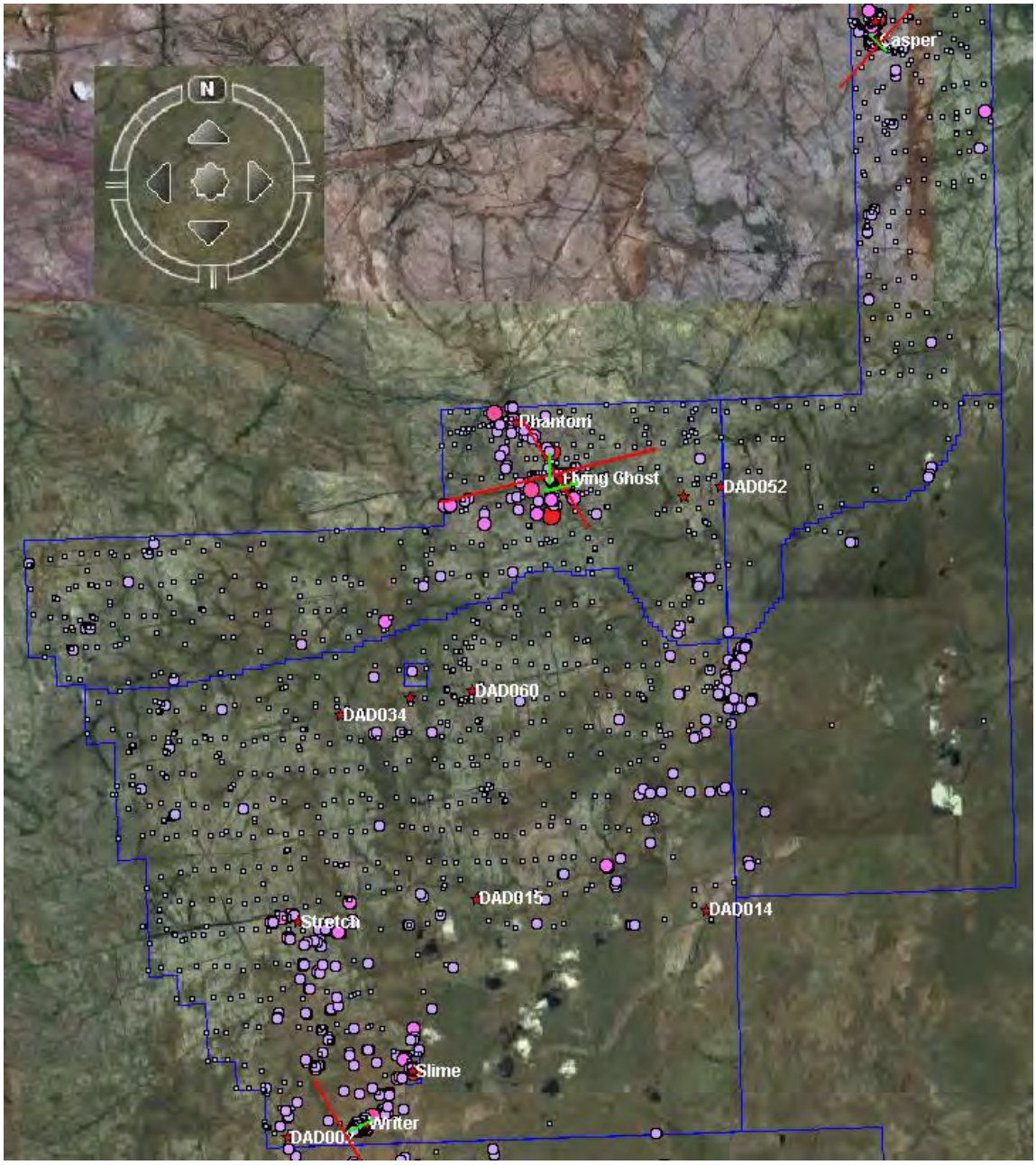

Figure 23: Part of the Headwaters tenements showing the location of prospects, uranium values (pink and purple dots) and the trend (red lines) of structures in the four areas chosen for the transects (green lines) (From Google Earth, 2009).

When the geochemical data were analysed for each transect it was discovered that the samples from the 1997 sampling program were not analysed for all trace elements. Therefore, it was not possible to compare the rare earth elements in the Writer prospect to those in the Flying Ghost and Casper prospects. Elements other than rare earth elements were analysed for all areas therefore elements seen in the two trends determined with PCA (Figure 30) could be compared.

4.4.1 Casper Transect

The transect from the Casper prospect was taken across a fault from the 30° fault set. Uranium values for each sample (Figure 24) were compared to the values for rare earth and other trace elements. Graphs were constructed for major oxides, metals and other trace elements other than REEs. Graphs for the Casper transects can be seen in Appendix 8.

The sample that contained the highest uranium value was from the 1997 sampling program where as all other samples in the transect came from the 1998 sampling program. Differences in analysis between the two years could result in false associations; therefore results will be compared to other prospects before any conclusions are made.

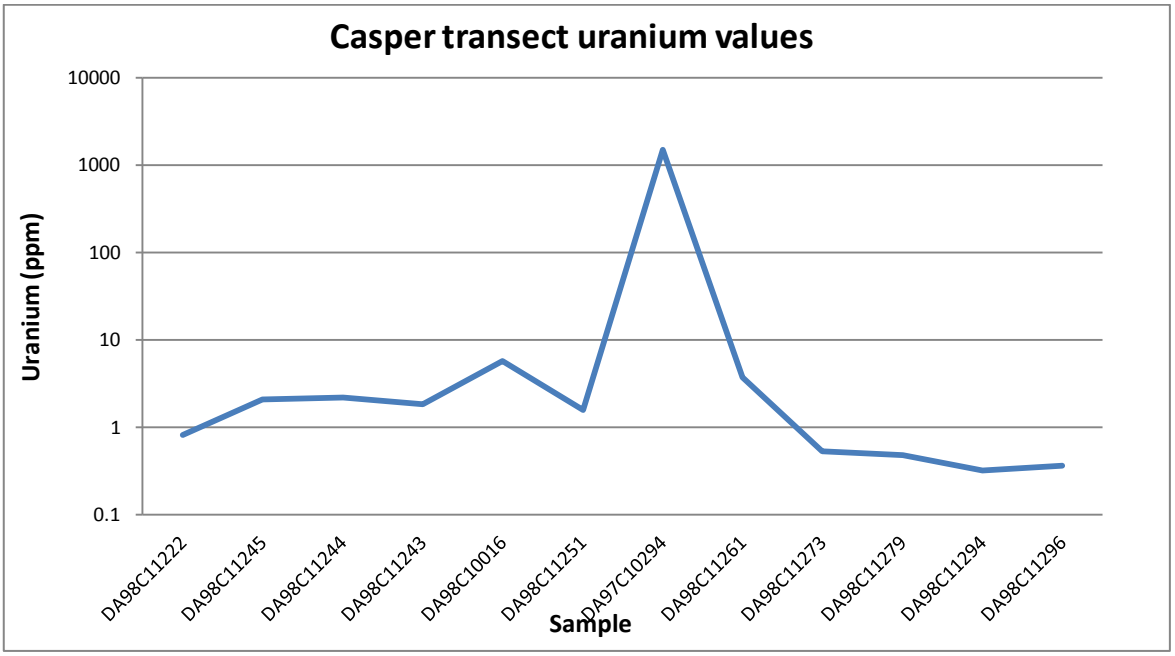

Figure 24: Transect across a fault zone in the Casper prospect showing uranium values of samples.

The results show that increased uranium values in the Casper prospect are related to increases in major oxides including Fe_2O_3, MnO, MgO and P_2O_5. CaO and Al_2O_3 showed only slight increases in association with uranium. K_2O did not appear to be related to uranium at all and SiO_2 decreased with the highest uranium concentration.

The only rare earth measured was La which showed increased values with increased uranium. Although analysis was not undertaken for the sample with the highest uranium value, trends in all other rare earths followed the same trend as La which suggests that they may all increase. Y also showed an association with uranium along with all the metals and platinum group elements.

Other trace elements that showed an association with uranium include As, Ba, Co, Li, Mo, S and Sr. Elements Be, Bi and Nb were not measured but follow the same trend as uranium therefore they possibly increase as well. Rb, Th, V, Zr and B appear to have no association with uranium concentrations.

The elemental associations above suggest a possible association between rare earth elements, platinum group elements, metals, several major oxides and uranium. Similar associations are known to occur at other uranium deposits in the Northern Territory (Rich et al., 1980).

4.4.2 Flying Ghost E-W Transect

Samples in the Flying Ghost area were collected in the 1997 sampling program therefore there are no values for most rare earth elements. Uranium values for samples in the east-west transect generally increased towards the fault zone with the exception of sample DA97C10190 (Figure 25). The uranium concentration in this sample dropped well below the uranium concentrations of adjacent samples although it was still higher than the samples further away from the fault zone. This transect cuts across a structure trending 150° which is parallel to the Bulman Fault in the north.

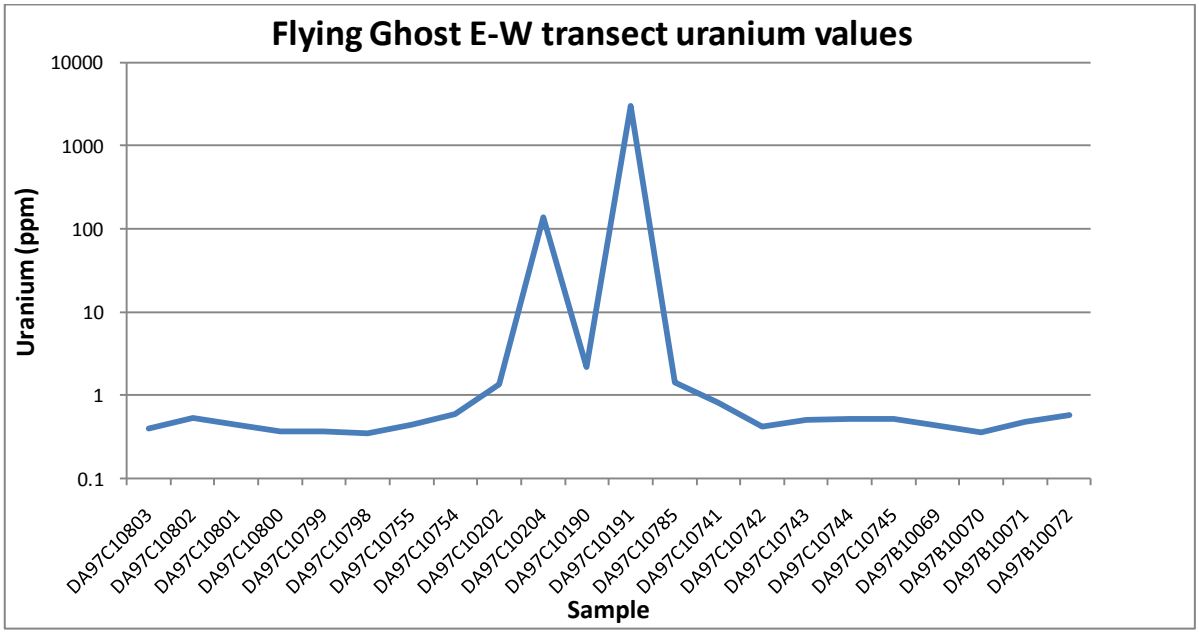

Figure 25: Graph showing the uranium concentrations for samples along the east-west transect in the Flying Ghost area.

The graphs for this transect showed some differences from the graphs for the Casper prospect. Of the major oxides, only Fe_2O_3 and P_2O_5 showed increased values for the same samples that contained high uranium. However, these oxides also occurred in higher concentrations in samples that did not contain high concentrations of uranium. Oxides such as Al_2O_3, CaO and K_2O appear to have no association with uranium. Increased concentrations of MgO and MnO occurred in the same samples as the uranium spikes but occur over a larger area and do not decrease when the uranium decreases. Decreases in concentrations were seen in SiO_2, which was the same for the Casper transect, and inTiO_2 by a small degree.

The graph for metals and platinum group elements was more similar to the Casper transect graphs than the major oxides. All metals and PGEs increased in concentration in association with the highest uranium reading. Elements including Au, Ni, total Pb, Pd and Zn also showed spikes in association with the smaller uranium spike. However, some elements, notably Au, Pb and Zn also showed spikes where there were no increases in uranium. Three elements, Ag, Cu and Pt, did not increase with the smaller uranium spike but also showed spikes where there was no increase in uranium.

Of the other elements analysed for the Flying Ghost area, only As was strongly associated with uranium. Elements such as B, Ba, La and Rb had weak correlations with uranium and Mo and Li appear to have a negative association with uranium.

4.4.3 Flying Ghost N-S Transect

The north-south transect in the Flying Ghost area cut across a fault in the 70° trending fault set. Uranium generally increases towards the fault zone with some slight variation.

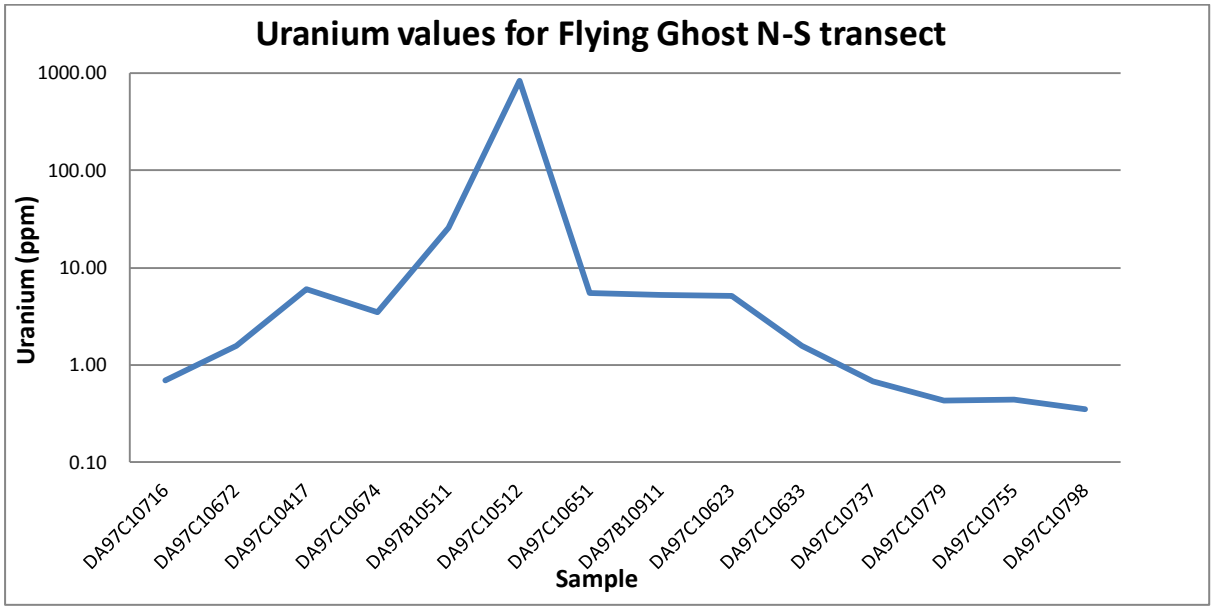

Figure 26: Uranium values for a transect running north-south through the Flying Ghost area.

Similar to the east-west transect (Figure 25), the oxides associations in the north-south transect differ from oxide associations in the Casper transect (Figure 24). Oxides that appear to be associated to some extent with uranium include Fe_2O_3, MgO, Na_2O, MnO and P_2O_5. Silica oxide once again has a negative correlation to uranium which was seen in the Casper and east-west Flying Ghost transects. Oxides that have little or no correlation to uranium concentrations include Al_2O_3, K_2O and TiO_2.

The metals and platinum group elements were all associated with uranium to some extent. All had spikes corresponding to the spikes in uranium and generally had increased or increasing concentrations when uranium was still relatively high (Appendix 8). The major different between this transect and the transects mentioned above is the drop in total Pb and Pd in sample DA97C10737 which is most likely due to those elements not returning values for that sample as they both drop to half the detection limit.

Other elements that showed an association with uranium include As, Co, Y and to a small V and Li. Most other elements showed very little or no correlation with uranium with the exception of Sr, Zr and La which have slightly negative associations with uranium. La was seen to have a positive correlation with uranium in the Casper transect.

4.4.4 Writer Transect

The samples selected across the Writer transect were collected during the 1998 sampling program and were all analysed for all 54 elements in the dataset including the rare earths. Uranium concentrations generally increased towards a structure which is at a similar orientation to the structure in the east-west Flying Ghost transect. Uranium concentrations on the western side of the fault were generally higher than concentrations on the eastern side. This may be due to the close proximity of another structure to the west of the Writer prospect.

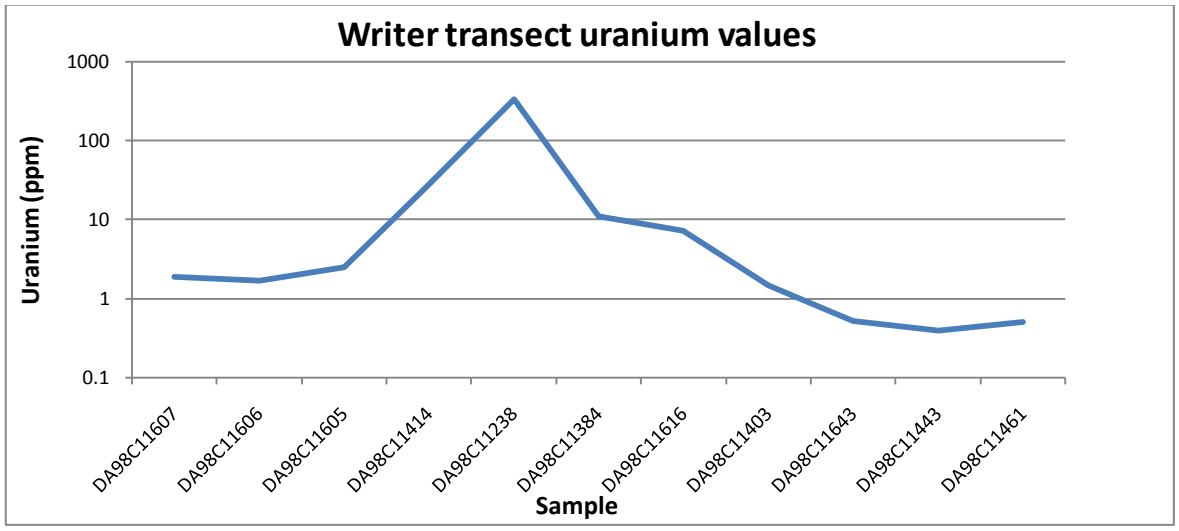

Figure 27: Uranium concentrations across a transect through the Writer prospect.

The oxides in the Writer transect are much more varied than the oxides in any of the previous transects. The only oxides that appear to be associated with uranium are CaO and P_2O_5 (Appendix 8). Two oxides appear to increase in concentration towards the structure and decrease as the uranium concentration increases. Most of the other oxides steadily decrease from the west to the east. This may be related somehow to the structure further west. The one exception is for SiO_2. In all other transects the silica oxide percentage decreases when uranium concentration increases. In the Writer transect the silica content steadily decreases from the east to the west in opposition to the oxides trending the other way. This may also be related to the structure towards the west.

The rare earth elements generally followed the same trend as the uranium with some small differences. The highest values of all the light REEs were seen in the sample to the west of the one with the highest uranium concentration. They did not show the same spike as seen in the uranium trend. The mid and high REEs also followed the same trend as the uranium concentrations and although the highest values occur in the same sample as the highest uranium, there was no spike in their trends.

The metal values in the Writer prospect were similar to those recorded in the transects mentioned above. Although values were not returned for Ni and Zn in the sample with high uranium they appear to follow the same trend on either side. Values were not recorded for Pt or Pd. Of the remaining metals all but Ag and total Pb increased with an increase in uranium. Values for Ag increased toward the sample with high uranium but dropped within that sample. Total Pb was generally high on the west side of the transect with a small increase in the sample to the east of the uranium high. It then steadily decreased. Copper also shows a spike to the west which is not associated with uranium or any other metal.

The remaining elements varied greatly in their associations with uranium. The elements that showed increased concentrations with the highest uranium value include Sr, S and Ba none of which followed the same special concentration trend as the uranium. Both Ba and Sr generally increased from east to west and S varied across the whole transect with the highest value occurring in the east. Four elements, Bi, Th, V and Pr, followed the same trend as the light rare earth elements. Elements including As, Co, Nb and Zr increased with uranium towards the centre of the transect but dropped when uranium peaked. The other elements with the exception of Rb showed a general increase towards the centre of the transect with high values occurring in samples other than the one containing the highest uranium. Rubidium values steadily increased from east to west.

4.4.5 Correlations Between Transects

Since the samples from different transects, and in the case of the Casper area within the transect, were collected and analysed during different sampling programs, there may be some differences that could affect the results. Data levelling may have reduced these possible errors but may have also masked mineralisation occurrences so it was not performed.

As mentioned earlier, values for rare earth elements were not recorded during analysis of the 1997 samples therefore only values in the Writer and Casper transects can be compared. Values for all other elements were generally recorded therefore have been compared with a degree of caution.

Associations between uranium trends and the oxide trends varied between the different transects. In Casper and the east-west trending Flying Ghost transect, increases in uranium were strongly associated with increases in Fe_2O_3 and weakly to moderately associated with increases in Al_2O_3, MgO, MnO and P_2O_5. Increases in uranium were very strongly associated with decreases in SiO_2. Associations were similar in the north-south Flying Ghost transect with uranium increases weakly to moderately associated with increases in Al_2O_3, Fe_2O_3, MgO and P_2O_5 were strongly associated with a decrease in SiO_2. One difference was that increased CaO appeared to be moderately associated with an increase in uranium. Associations in the Writer transect varied greatly from those seen in other transects. Oxides, including Al_2O_3, K_2O, MgO, Na_2O and SiO_2, showed no association with uranium at all. All values increased from east to west, with the exception of SiO_2 which dipped in the opposite direction. This suggests there may be increased alteration in the fault zone to the west. Oxides including P_2O_5, CaO, and TiO showed slight to moderate associations with uranium and Fe_2O_3 decreased with the spike in uranium.

Rare earth elements could only be tentatively compared between the Casper and Writer transects. In both transects all rare earth elements generally increased in association with uranium concentrations. The only exception was in the Writer transect where light rare earths were highest in one sample to the west of the sample with the highest uranium value. Yttrium generally followed the same trend as the Heavy rare earths.

Metals and platinum group elements were fairly similar for all transects with a few differences. All metals and PGEs were very strongly associated with uranium in the Casper transect but were weakly to strongly associated with uranium in the Flying Ghost transects. In the north-south transect Pd had no real association with uranium. Once again the Writer

transect showed the majority of differences with Ag and Pb decreasing with the highest concentrations of uranium. PGEs Pt and Pd did not return values therefore could not be compared.

The association of remaining elements with uranium varied greatly across all transects. In the Casper transect, elements that showed a strong association with uranium included As, Ba, Co, Li, Mo, S, Sr, Nb, Be and Bi. In the east-west Flying Ghost transect As was the only element that showed a strong positive association with uranium. Weak associations were seen in Ba, Co, S, Sr, B and possibly Li and Mo. In the north-south Flying Ghost transect As, Co and, to a lesser extent, Li showed strong positive correlations with uranium with Sr showing a negative association. In the writer transect only Ba and Bi showed a weak positive association with uranium. Elements As, Co, Li and Nb dropped as uranium reached its highest levels.

The differences in element associations between transects may be caused by several different things. There may be differences in alteration types, degrees of alteration or weathering in different transects. Differences may have also been caused by different mineralisation events. The type of structure may also have an effect on the types of elements present as some faults contain only breccia and quartz veining where as some have acted as pathways for dykes. One possibility for the major difference between the Writer transect and the other three transects is that the Writer prospect lies to the east of a well defined fault. This fault may itself contain higher concentrations of elements associated with mineralisation.

4.4.6 Hand Sample Variations across Transects

Hand samples previously collected by Cameco Australia were inspected for variations in alteration and mineralogy along three of the aforementioned transects. Due to time limitations, thin sections were unable to be inspected or analysed. Detailed hand sample descriptions are included as Appendix 9.

Alteration seen in hand samples varied within each transect. The main types of alteration that were obvious in hand samples included hematite alteration and silicification with occasional veins and clay patches observed.

In the Writer transect, sandstones were generally silicified with the exception of DA98C11403 which was slightly crumbly. Samples generally became darker towards the mineralised sample with sample DA98C11616 (two from the sample with high uranium) showing dark red/black colours. The sample with the highest uranium content and the two

samples on either side were coarser grained that the other samples with orange, yellow and green minerals visible in fractures, veins and on the surface.

In the Casper transect the sandstones on one side of the fault zone are dark red in colour and getting progressively lighter towards the sample with the highest uranium reading. This sample was dark brown in colour with visible yellow clay in the surface. On the other side of this sample, DA98C11261 is a dark purple colour. This colour disappears in the next sample but returns and gradually darkens towards the sample furthest from the uranium anomaly.

Alteration in the east-west Flying Ghost transect varies far more than alteration in the other two transect. Starting from the east, samples go from purple to pink to dark red then back to a light orange/pink colour for a few samples. Darker colours come back in at sample DA97C10755 which is followed by two light pink samples (one with yellow on the surface) and two medium purple sandstones.

Sample DA97C10191 is the sample with the highest uranium content. This sample is a light pink sandstone but has dark brown patches with yellow clay on the surface. The light pink colour continues through the next two samples that also have red colours associated with weathering surfaces. The purple colour seen on the other side of the fault returns for three samples that become increasingly incompetent further away from the fault. The purple colour then gives way to a light pink/orange colour for the rest of the transect.

There appears to be different alteration progressions through each of the transects. The colour became darker and sample coarser towards the centre in Writer where as in Casper alteration on one side of the fault appears different to alteration on the other side. In the Flying Ghost transect alteration occurs in a similar sequence on either side of the fault going from light pink to purple towards the centre. There were no purple samples in the Writer transect.

This difference in alteration in between the transects may suggest that there were different processes occurring in each area. Purple samples occur in the Casper and Flying Ghost transects suggesting hematite alteration. Hematite alteration is known to occur with uranium mineralisation in the Northern Territory which suggests that the uranium within the two prospects is due to mineralisation.

The absence of purple from the Writer prospect does not discount the possibility of mineralisation occurring in the area. Analysis of clays within the Writer samples would have to be analysed in order to determine if there is mineralisation within the Writer prospect.

4.5 Principal Component Analysis

Principal component analysis (PCA) is a multivariate analysis technique that is used to reduce a large number of variables in a dataset to a smaller amount of uncorrelated variables which can be viewed in a variation diagram at the same time. If only a few principal components account for the majority of variation in the data, the other components are generally discarded which reduces the amount of variables even further (Rollinson, 1993).

As the values for the elements to be used in the PCA were in different units, and some elements recorded much higher values than others, these data had to be standardised in order for all elements to be plotted together.

The principal component analysis was initially performed on the entire data set which included a total of 2,751 samples analysed for 54 elements or oxides. The entire data set proved too large to provide interpretable results. It was decided to divide the elements into major oxides and trace elements to improve the principal component analysis results. When all trace elements were analysed with PCA it became apparent that there were still too many factors. As a result, the trace elements were divided into rare earth elements (REEs) and trace elements not including REEs.

4.5.1 Rare Earth Elements

The correlation matrix that was used for the REE PCA is shown in Appendix 10. The calculated eigenvalues and variances which were used to define the components are shown in Table 1. Initial analysis of the REEs showed that the data contained an outlier (DA98B13663) that anomalously high in rare earth elements. This outlier disguised trends in these data therefore it was removed and the PCA was rerun.

Table 2: Eigenvalues for the rare earth element principal component analysis.

Explained Variance (Eigenvalues)													
Value	PC 1	PC 2	PC 3	PC 4	PC 5	PC 6	PC 7	PC 8	PC 9	PC 10	PC 11	PC 12	PC 13
Eigenvalue	8.832	2.928	0.638	0.32	0.11	0.07	0.05	0.03	0.007	0.005	0.003	0.001	0.001
% of Var.	67.93	22.52	4.907	2.48	0.87	0.53	0.40	0.21	0.056	0.038	0.024	0.010	0.007
Cum. %	67.93	90.45	95.36	97.8	98.7	99.2	99.6	99.9	99.92	99.96	99.98	99.99	100.0

The results showed that there were two principle components in within the REEs. The other components had eigenvalues less than one therefore they were not considered to be principal components.

A principle component plot was then constructed which showed that the REEs contained two main trends in the headwaters samples (Figure 28). One trend was associated mainly with Ce,

Pr, Nd and La which are all light REEs. The other trend was mostly associated with Lu, Dy, Ho, Er and Tm which are all mid/heavy REEs.

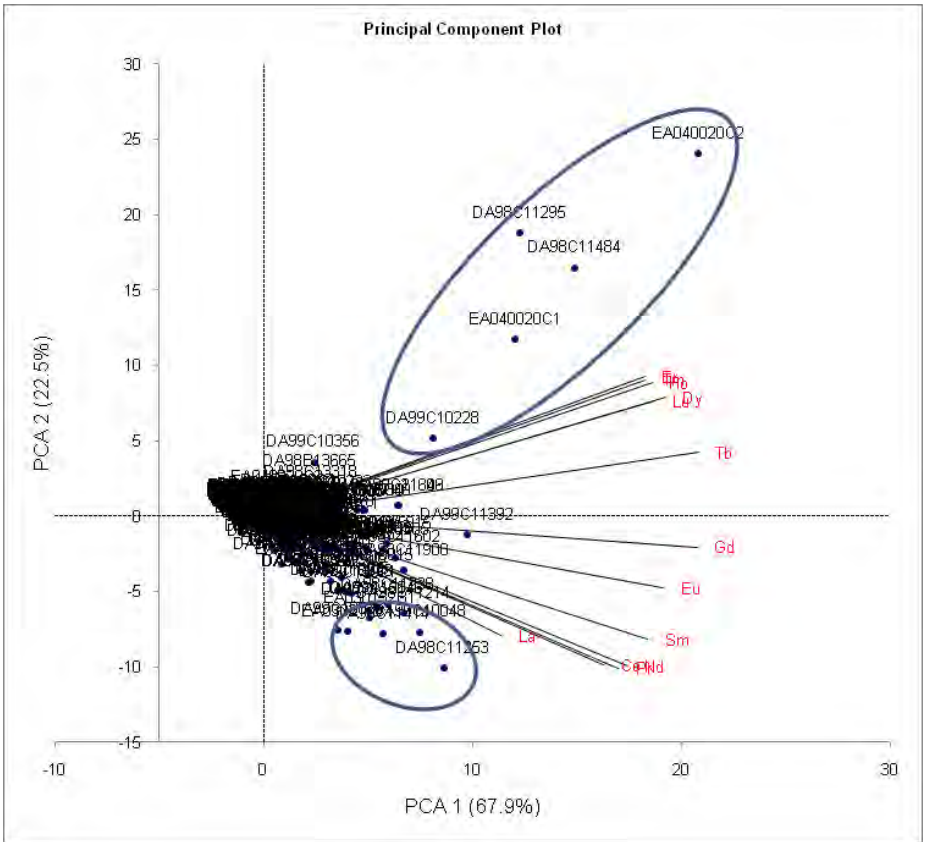

Figure 28: Principle component plot of the rare earth elements.

The samples that occurred within the two main trends were plotted on a map to determine if the different trends correlated to different lithologies or structure (Figure 29). The locations of known uranium prospects were also included.

Samples in the upper trend were located in the Casper and Writer prospect as well as in structure intersections in the north. Samples from the lower trend were located near the Casper and Writer prospects. This may suggest a separation of REEs during mineralisation with the HREEs located with mineralisation and LREEs precipitated at a different time.

The mobility of rare earth elements varies in literature with scientists often putting forward contradicting views on the subject. REEs are generally regarded by all scientists as some of the least soluble trace elements that are relatively immobile during hydrothermal alteration and weathering (Rollinson, 1993). Some scientists concluded that the mobility of REEs is controlled by the availability of carbonate, fluorine, phosphate or sulphate complexes in low temperature alkaline solutions (Michard, 1989; Wood, 1990). Others determined that most REEs are transported as carbonate, fluorine and sulphate complexes in alkaline fluid (Felshe and Herrman, 1978). Rollinson (1993) came to the conclusion that a direct comparison

between rare earth elements and other trace elements cannot give an indication of mobility in altered and unaltered rocks.

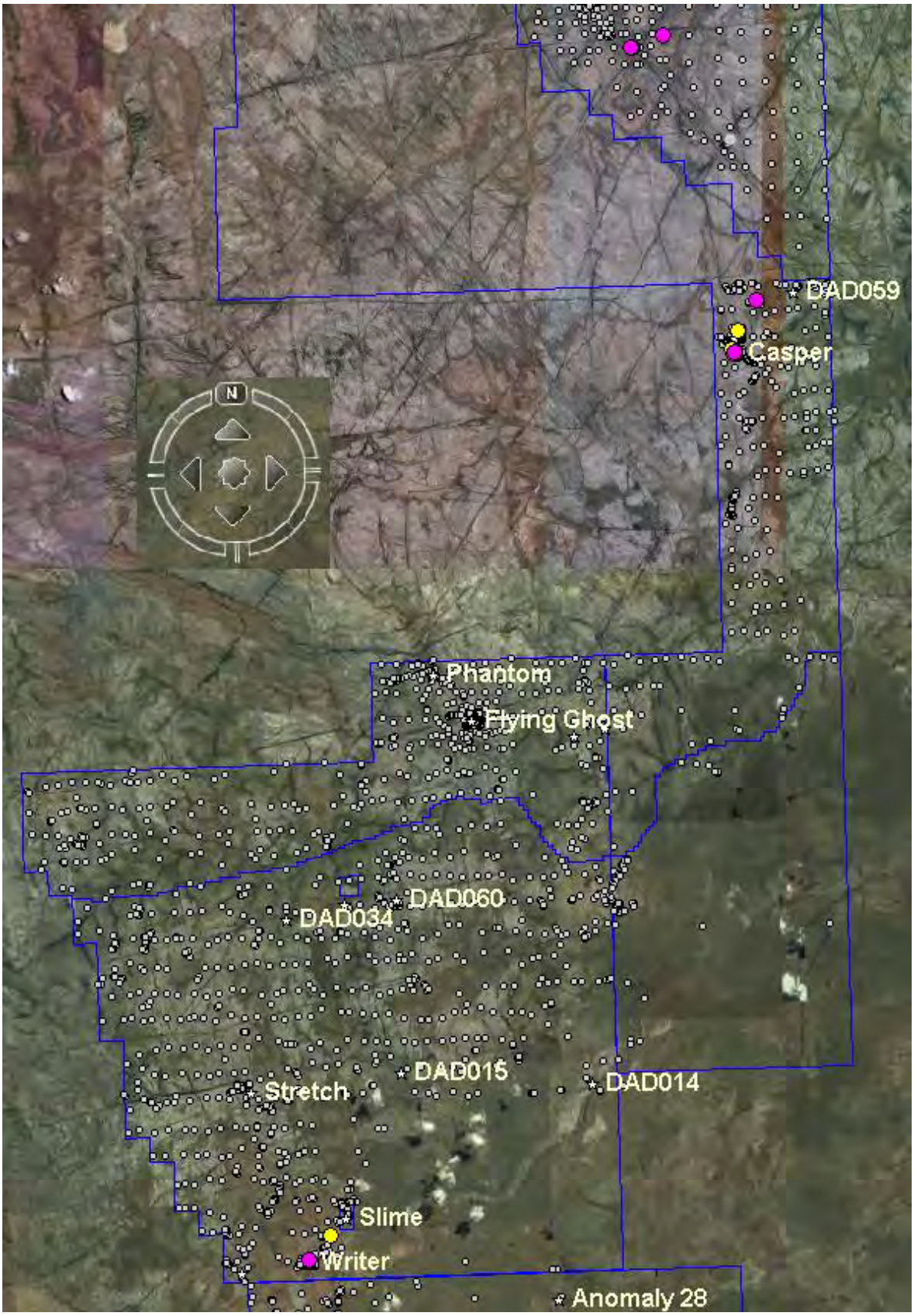

Figure 29: Location of samples in different REE trends in relation to the Headwaters tenements (blue lines) and known prospects (white stars). Yellow circles indicate samples in the upper trend and pink circles indicate samples in the lower trend (Google Earth, 2009).

Some scientists have detailed findings of the separation of light and heavy rare earth elements. Pirajno (1992), suggested that heavy rare earths form more stable complexes with ligands than light rare earths. As a result they stay in solution longer which leads to a concentration of heavy rare earths later on in the hydrothermal process.

In a recent paper by Gaboreau et. al. (2007), the authors described light rare earth rich compositions of aluminum phosphate-sulphate (APS) minerals in hydrothermally altered sandstones around unconformity-type uranium deposits. It was determined that the disseminated APS minerals were commonly present in association with host-rock clay alteration around unconformity-type uranium deposits (Gaboreau et al., 2005).

During a study on the Pine creek Geosyncline, McLennan & Taylor (1979) discovered rare earth element mobility associated with uranium mineralisation in the metasedimentary rocks. They determined that REEs and uranium were moved by carbonate complexes in an oxidizing, low temperature alkaline solution.

4.5.2 Other Trace Elements

The correlation matrix that was used for the PCA of trace elements of than REE's is shown in Appendix 10. The calculated eigenvalues and variances which were used to define the components are shown in Table 2. As for the rare earth elements there was an outlier that disguised any trends in these data (DA98B13663). Therefore, the outlier was removed and the PCA was run again.

Table 3: Eigenvalues for the principal component analysis of trace elements other than REE's.

Eigenvalues																									
Value	PC 1	PC 2	PC 3	PC 4	PC 5	PC 6	PC 7	PC 8	PC 9	PC 10	PC 11	PC 12	PC 13	PC 14	PC 15	PC 16	PC 17	PC 18	PC 19	PC 20	PC 21	PC 22	PC 23	PC 24	PC 25
Eigenvalue	4.344	2.519	1.751	1.726	1.587	1.403	1.199	1.129	1.062	1.002	0.974	0.872	0.816	0.743	0.658	0.608	0.534	0.459	0.372	0.318	0.281	0.218	0.190	0.163	0.073
% Var.	17.378	10.076	7.005	6.904	6.346	5.611	4.794	4.518	4.246	4.006	3.897	3.488	3.263	2.973	2.630	2.431	2.136	1.835	1.488	1.270	1.126	0.873	0.759	0.654	0.293
Cum.%	17.378	27.453	34.458	41.363	47.709	53.320	58.114	62.632	66.878	70.884	74.781	78.269	81.532	84.505	87.135	89.566	91.702	93.537	95.025	96.295	97.421	98.294	99.053	99.707	0

The principle component analysis showed that there were also two main principle components. However, the scree plot shows that there were many other smaller components since the start of the smaller slope is above 1.5 and gradually decreases towards zero.

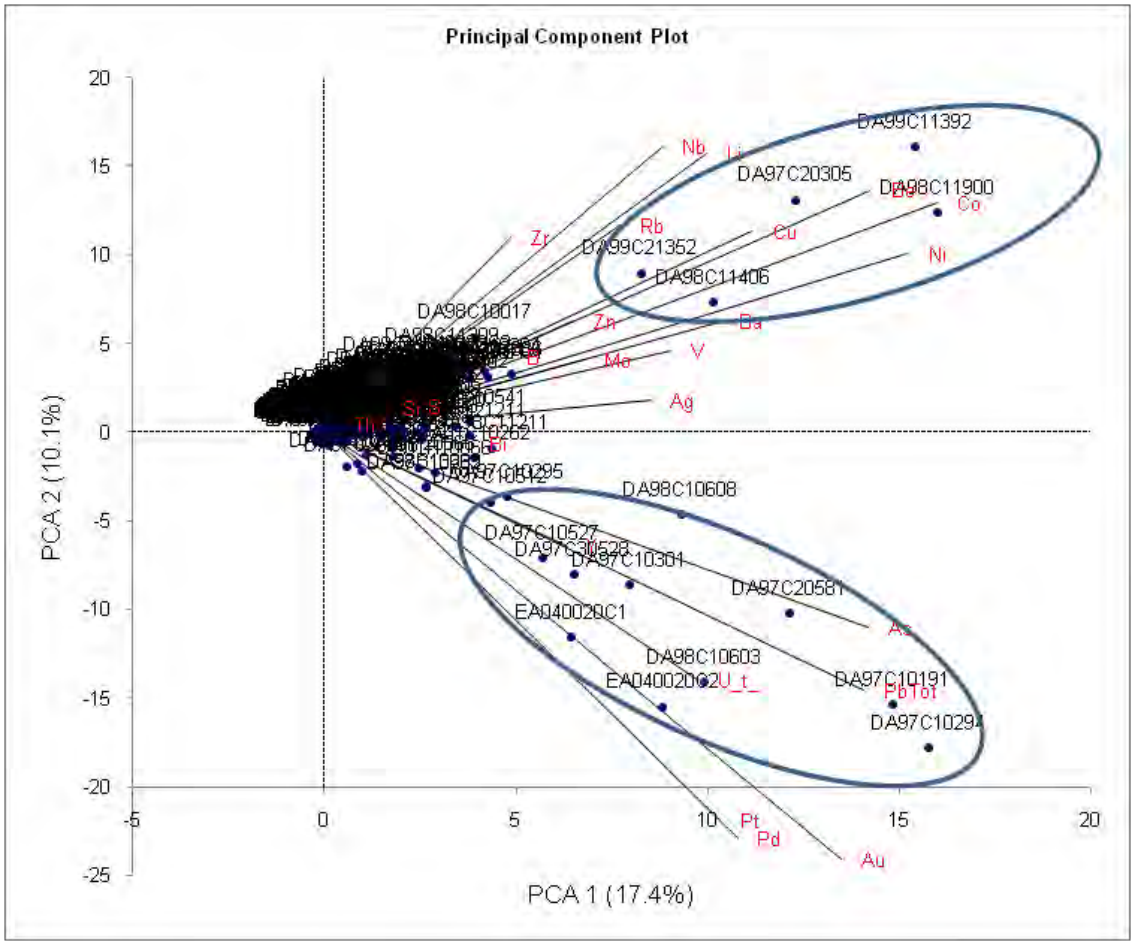

Figure 30: Principal component plot for trace elements other than REE's.

A principle component plot was constructed which showed the trace elements other than REE's also had two main trends (Figure 30). One trend was mainly associated with copper, cobalt, nickel and beryllium. The other trend was mainly associated with uranium, arsenic, lead, gold, platinum, palladium and a small part of yttrium.

The samples shown within the two trends were plotted on a map containing known uranium prospects, geology and structure to determine if the trends occurred either within a particular lithology or close to structures in the area (Figure 31).

Samples in the upper trend were located mainly in the Writer prospect with one sample located to the north of the Casper prospect. Samples from the lower trend were located either in the Casper prospect or Flying Ghost prospect. There is one sample from the lower trend situated in a fault intersection in the northern most tenement.

The different locations for the two trends may indicate that there are two different processes involved with mineralisation within the Headwaters project. It may also indicate different mineralisation events.

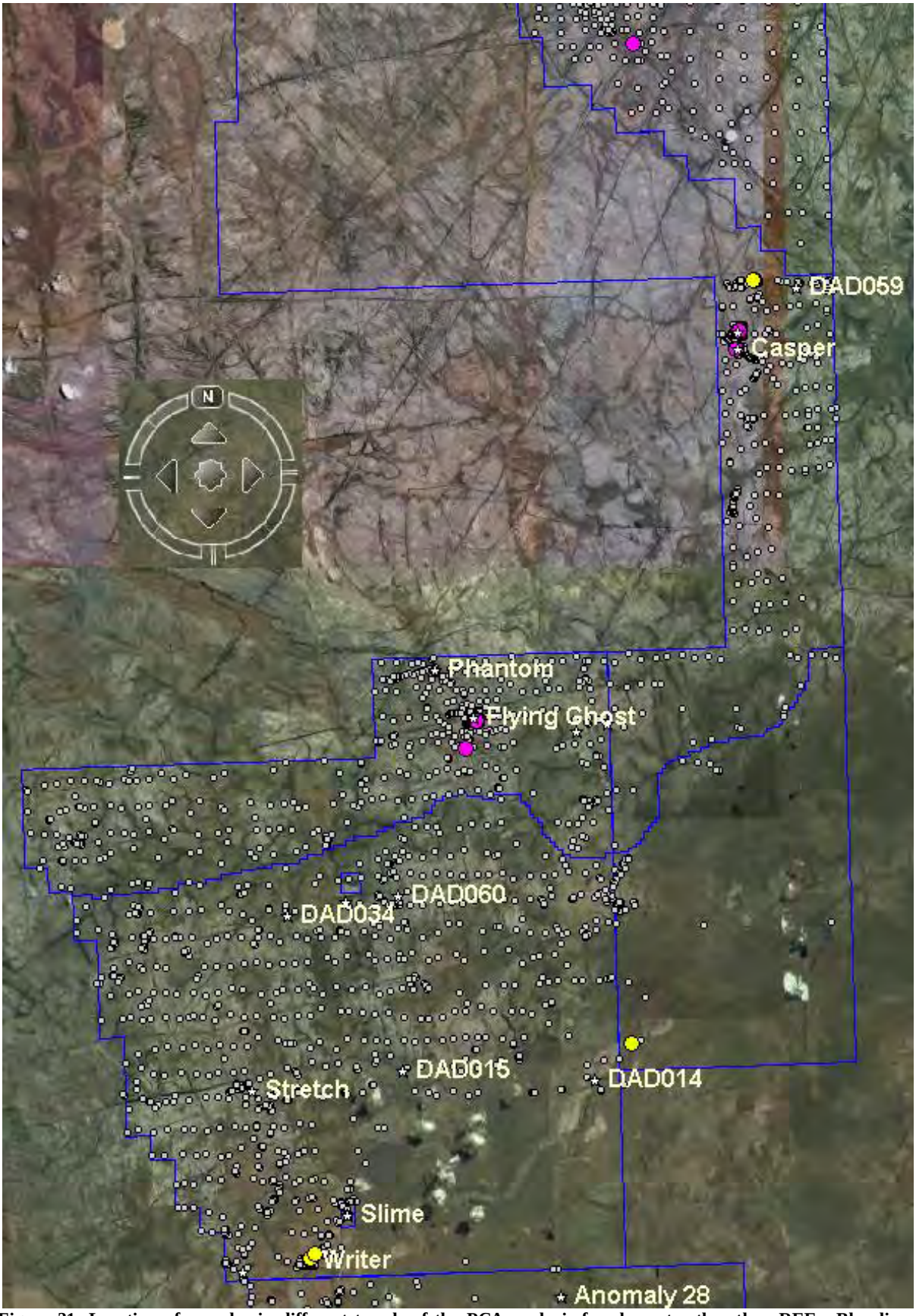

Figure 31: Location of samples in different trends of the PCA analysis for elements other than REEs. Blue lines indicate the boundaries of the Headwaters tenements and white stars indicate locations of known uranium anomalies. The upper trend is indicated by yellow circles and pink circles indicate samples in the lower trend (Google Earth, 2009).

Elements can be distributed by a variety of processes. The main processes that relate to this study include hypogene and supergene precipitation of metals and associated elements. Uranium anomalies in the Headwaters project were formed by one of two processes. In the case of unconformity-type or sandstone-hosted uranium mineralisation, mineralisation would have occurred as a result of hydrothermal fluid movement through structure in the area. The other possibility is that the anomalies were formed by scavenging of certain elements from volcanic units on or near the surface.

As mentioned in the section for rare earth elements, different elements have different solubilities and form different bonds. For example, chalcophile metals such as Cu, Ag, Pb, Zn, Cd and Bi have an affinity for sulfur. The solubilities of elements such as Mn and Fe, along with Pb and Zn vary as an exponential function of the concentration of chlorite (Robb, 2007). This suggests that a difference in fluid composition could account for the differentiation of elements.

There are also several factors that can account for the precipitation or adsorption of metals. A change in oxidation state either by increasing pH or H_2S, or by decreasing the chloride ion concentration can result in precipitation. Changes in temperature and pressure can also have an effect on precipitation as can fluid mixing and fluid/rock interactions (Robb, 2007).

Fluid mixing can also result in precipitation if meteoric or ground water has scavenged uranium and other oxide-soluble metals from overlying volcanic rocks. Oxide soluble metals include Cu, Se, Co, As and Mo (Robb, 2007). Most of these metals are seen in the trends above so a supergene process is a possibility. Both the hypogene and supergene processes will be discussed in section 4.6.2 in relation to factor analysis trends.

4.6 Factor Analysis

The main aim of factor analysis was to explain variation in a multivariate data set with as few "factors" as possible. It recognises that the total variation in the dataset is not necessarily explained by the common factors. This allows for factor analysis to show unique factors that may behave differently than the other factors in the dataset (Reimann et al., 2002).

The trace elements in the data set were once again divided into rare earth elements and trace elements without the REE's. The trends seen above in the principal component analysis were rotated to the two main axes in order to show the different factors in separate graphs. An R^2 value was then calculated to determine if the rotation had affected any of the values. R^2 values close to one show that values had a very high level of confidence and were suitable to use in further analysis.

4.6.1 Rare Earth Elements

With an R^2 value of 0.999, the factor analysis for the rare earth elements was accurate and no data were lost during the rotation. The measure of data confidence is high and values could be used to create plots for each factor.

Table 4: Total variances explained for components of the REE's.

Total Variance Explained									
	Initial Eigenvalues			Extraction Sums of Squared Loadings			Rotation Sums of Squared Loadings		
Component	Total	% of Variance	Cumulative %	Total	% of Variance	Cumulative %	Total	% of Variance	Cumulative %
1	8.387	64.514	64.514	8.387	64.514	64.514	7.391	56.853	56.853
2	3.679	28.300	92.814	3.679	28.300	92.814	4.675	35.961	92.814
3	.566	4.351	97.166						
4	.221	1.703	98.868						
5	.052	.397	99.265						
6	.045	.343	99.608						
7	.028	.216	99.824						
8	.017	.128	99.952						
9	.003	.023	99.975						
10	.002	.012	99.987						
11	.001	.008	99.996						
12	.000	.002	99.998						
13	.000	.002	100.000						

The initial eigenvalues show that components one and two make up 92.8% of the total variance in the rare earth elements (Table 4). As for the principal component analysis, the two factors are generally divided into light rare earth elements (Figure 32) and mid/heavy rare

earth elements (Figure 33). The major difference is that Sm contributes slightly to the heavy rare earths factor, Gd contributes slightly to the light rare earths factor and Eh is divided between the two factors.

The mid/heavy rare earth elements (Factor 1) are the most important factor as they explain 64.5% of the variance with a contribution of only 8.2%. The light earth elements have a contribution of 91.77% but only account for 28% of the variance. This may be due to a separation of rare earths during hydrothermal alteration as mentioned above. Heavy rare earths may have remained in solution longer and may have been deposited slightly later than the light rare earths.

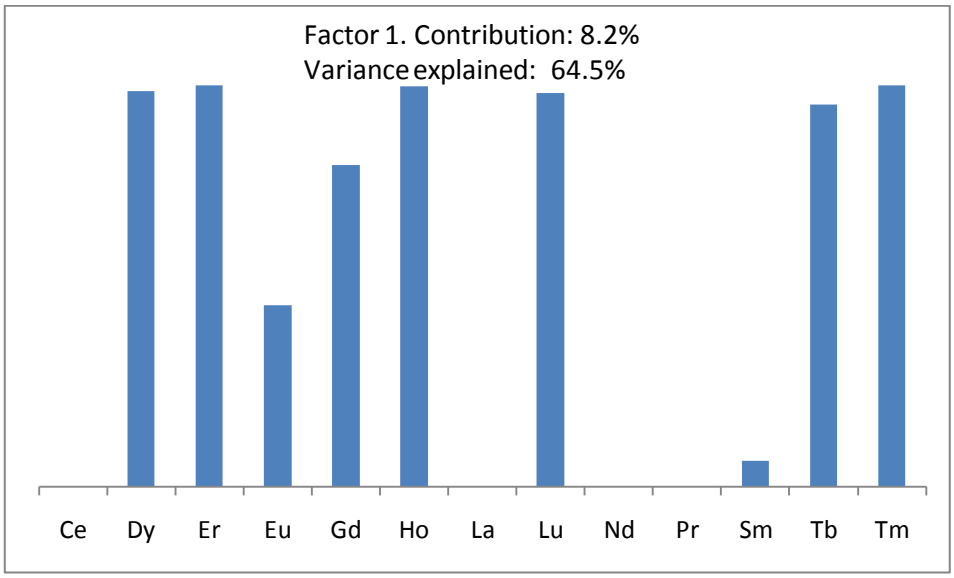

Figure 32: Figure showing factor one of the factor analysis for the rare earth elements.

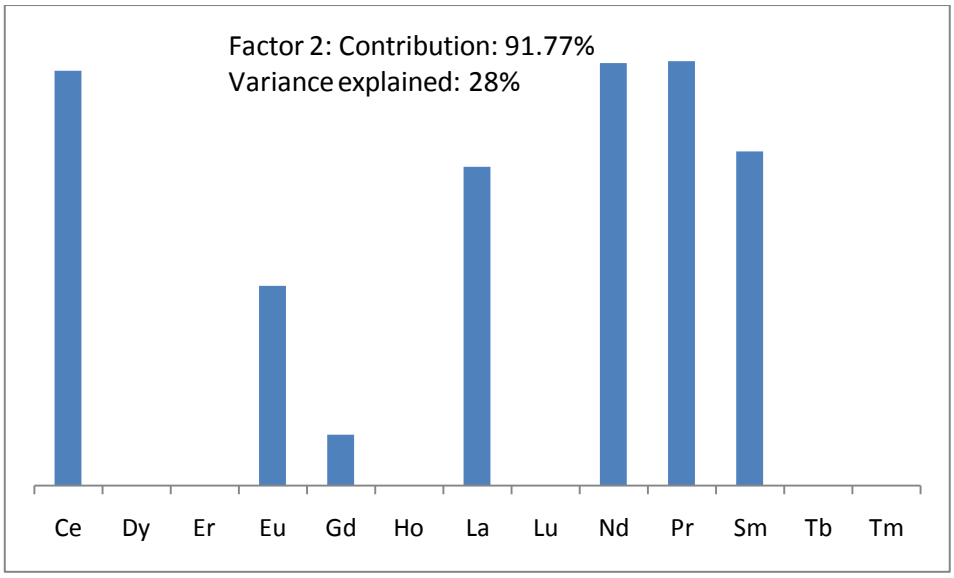

Figure 33: Figure showing factor 2 of the factor analysis for the rare earth elements.

4.6.2 Trace elements other than REE's

The Sum Calc for elements other than REE's was not as linear as for the rare earth elements but still had an R^2 value of 0.9917 which shows that data were not affected by the rotation.

The total variance of the trace elements other than REEs was explained by ten factors (Table 5). These factors are described in detail below.

Table 5: Total variance explained for the factor analysis of trace elements other than REE's.

Total variance explained									
	Initial Eigenvalues			Extraction Sums of Squared Loadings			Rotation Sums of Squared Loadings		
Component	Total	% of Variance	Cumulative %	Total	% of Variance	Cumulative %	Total	% of Variance	Cumulative %
1	4.745	18.980	18.980	4.745	18.980	18.980	4.166	16.664	16.664
2	3.340	13.359	32.340	3.340	13.359	32.340	2.395	9.580	26.243
3	1.727	6.910	39.249	1.727	6.910	39.249	2.107	8.426	34.669
4	1.716	6.863	46.113	1.716	6.863	46.113	1.872	7.487	42.157
5	1.563	6.252	52.365	1.563	6.252	52.365	1.688	6.753	48.909
6	1.322	5.290	57.655	1.322	5.290	57.655	1.594	6.375	55.284
7	1.171	4.685	62.340	1.171	4.685	62.340	1.593	6.374	61.658
8	1.077	4.310	66.650	1.077	4.310	66.650	1.157	4.627	66.285
9	1.008	4.032	70.682	1.008	4.032	70.682	1.098	4.394	70.679
10	1.001	4.004	74.686	1.001	4.004	74.686	1.002	4.007	74.686
11	.957	3.827	78.513						
12	.898	3.592	82.105						
13	.815	3.258	85.363						
14	.736	2.945	88.308						
15	.569	2.277	90.585						
16	.490	1.962	92.546						
17	.466	1.864	94.411						
18	.344	1.374	95.785						
19	.299	1.198	96.983						
20	.240	.959	97.942						
21	.225	.901	98.844						
22	.169	.677	99.520						
23	.120	.479	99.999						
24	.000	.001	100.000						

The factors that explained the variance in the geochemical data were different than was expected after seeing the results of the PCA. Factor one (Figure 34), which explained 19% of the variance, included the same elements that were contained in one of the trends seen above with the exception of uranium. It also contained small amounts of B, Be, Cu, Mo, S, Sr and Zr. The absence uranium in this factor suggests that even though it was present in the PCA analysis, it may not be related to the metals in factor one.

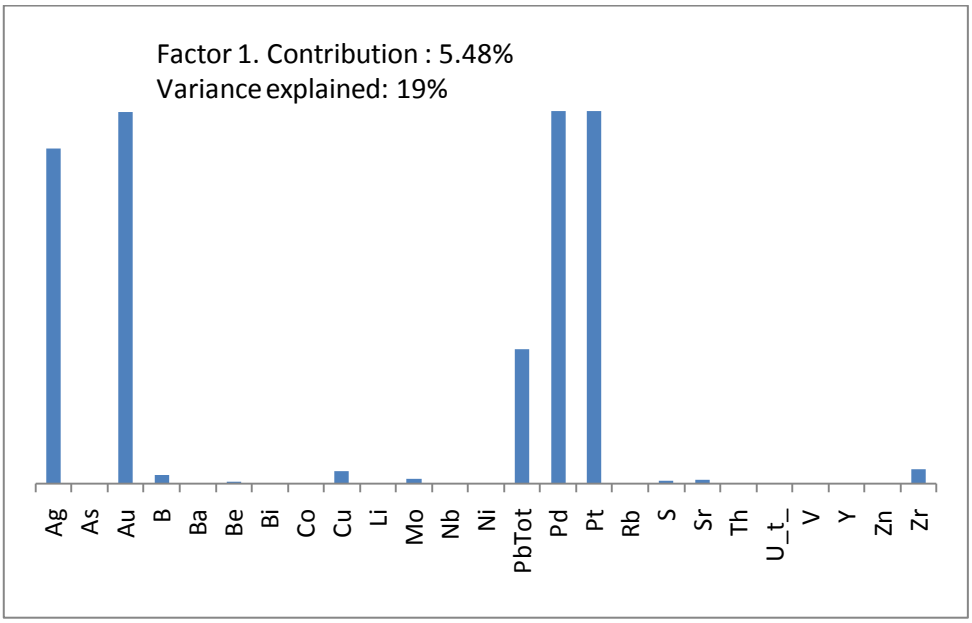

Figure 34: Factor one of the factor analysis of trace elements other than REEs.

Factor two, which explained 13.4% of the variation, consisted mainly of Cobalt, nickel and lithium with small amounts of barium, zinc, strontium and thorium (Figure 35). Cobalt and nickel were two elements which made up the second trend in the PCA analysis. The line representing zinc was in the same direction as the upper trend although was not as long as the lines for the other elements. Therefore, zinc was not considered part of the trend. Lithium was also not one of the elements included in the trend. However, it was generally associated with the elements in the trend which can be seen in Figure 30 above. Barium, strontium and thorium were not associated with the upper trend at all.

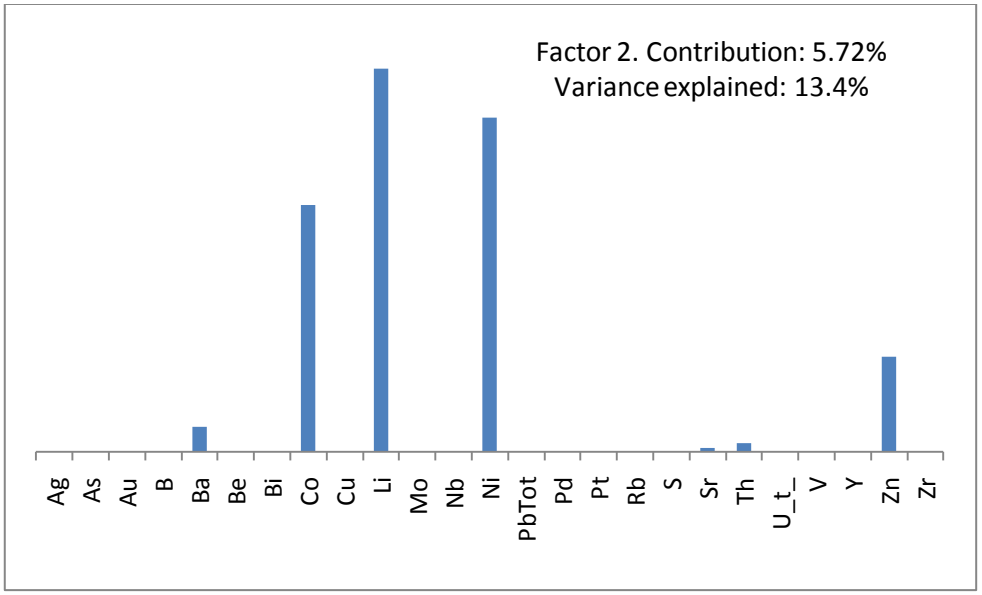

Figure 35: Factor two of the factor analysis of trace elements other than REEs.

Factor three explained 6.9% of the variance for trace elements not including REEs (Figure 36). It contained the remaining elements from the upper trend in Figure 30 that were not seen

in factor 2. Molybdenum and vanadium were similar to zinc in that the lines representing them were not as long as lines for other elements in the trend. Therefore, they were also not included in the trend. One main difference with factor three is that it contained very small contributions from elements such as silver, gold, palladium and platinum which were seen in the lower trend in Figure 30.

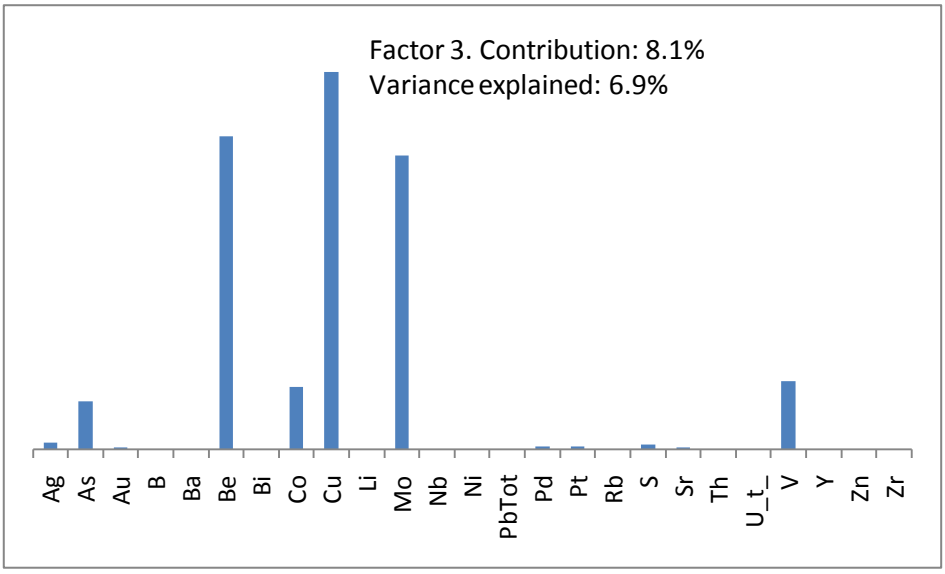

Figure 36: Factor three of the factor analysis for trace elements other than REEs.

Uranium, which is the main focus of this study, was not seen until factor four (Figure 37). Factor four accounts for only 6.86% of the variance and contains all but a small part of the uranium. The other main element in this factor is arsenic which is seen to be related to uranium in some of the transects. Also seen in factor four are total lead, yttrium, vanadium and some zinc. Arsenic, uranium, total lead and some yttrium were in the lower trend of the PCA.

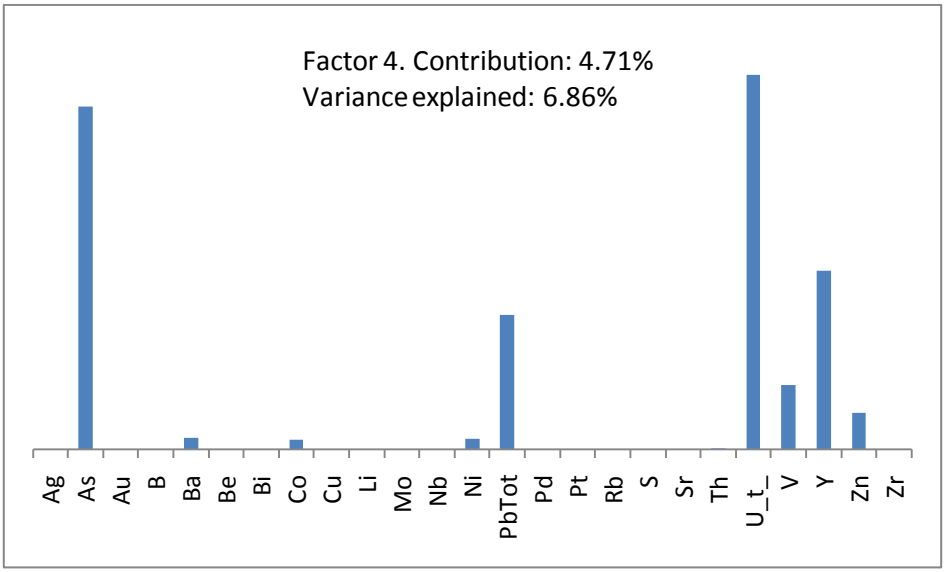

Figure 37: Factor four of the factor analysis for trace elements other than REEs.

Factors five to ten generally contained elements that were not included in the two trends calculated from the PCA above. However, there were some relationships that are not related to uranium mineralisation that may still be of interest. Factor five, for example, showed a very strong relationship between strontium and sulfur (Figure 38). There were also small contributions by several other elements which were either slightly related or not related to the two main trends.

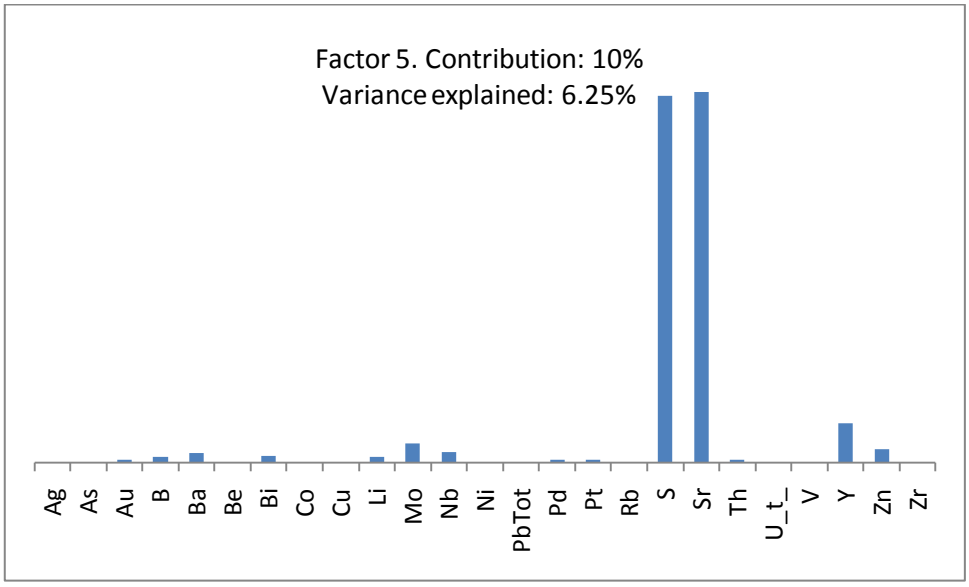

Figure 38: Factor five of the factor analysis for trace elements other than REEs.

Factor six showed a strong relationship between barium and rubidium with minor inputs from beryllium, total lead, yttrium and silver. There were also very minor inputs from cobalt, copper and zircon (Figure 39).

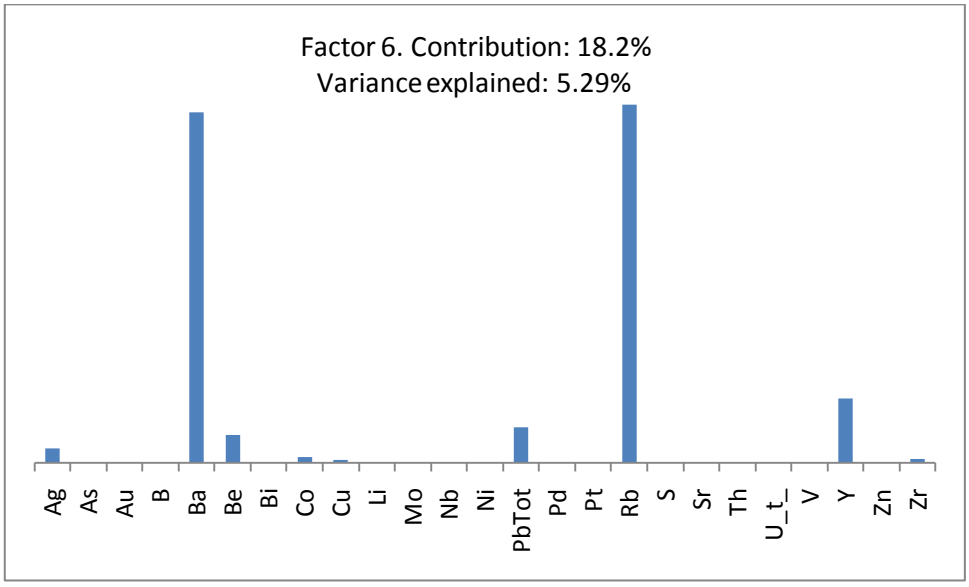

Figure 39: Factor six of the factor analysis for trace elements other than REEs.

The factors shown in the figures below showed elemental relationships that were not of major interest in this study. Factor seven (Figure 40) showed a relationship between niobium, zinc, and zircon with small inputs from silver, vanadium, yttrium and bismuth. Factor eight (Figure 41) showed a relationship between boron and vanadium with minor inputs from Zr, Be, Bi, Li, Mo, Nb, Ni, Rb, Ag, As and uranium. Factor nine (Figure 42) showed a relationship between bismuth and total lead with minor inputs from silver and the non metals.

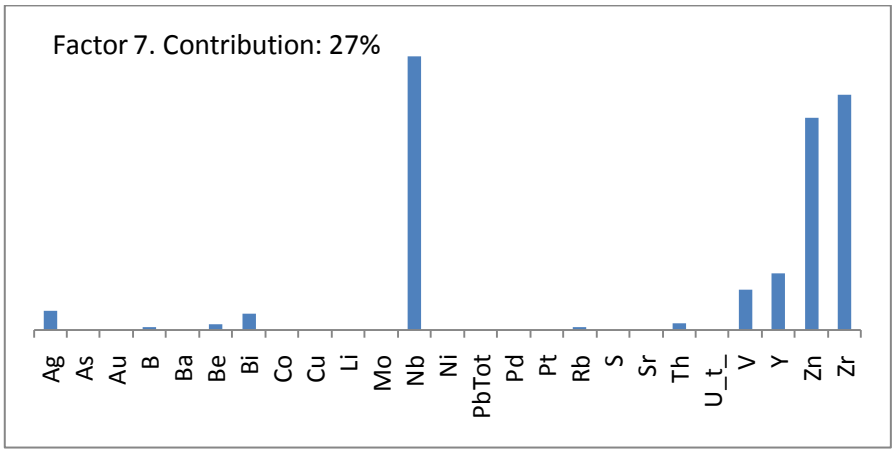

Figure 40: Factor seven for the factor analysis of elements other than REEs.

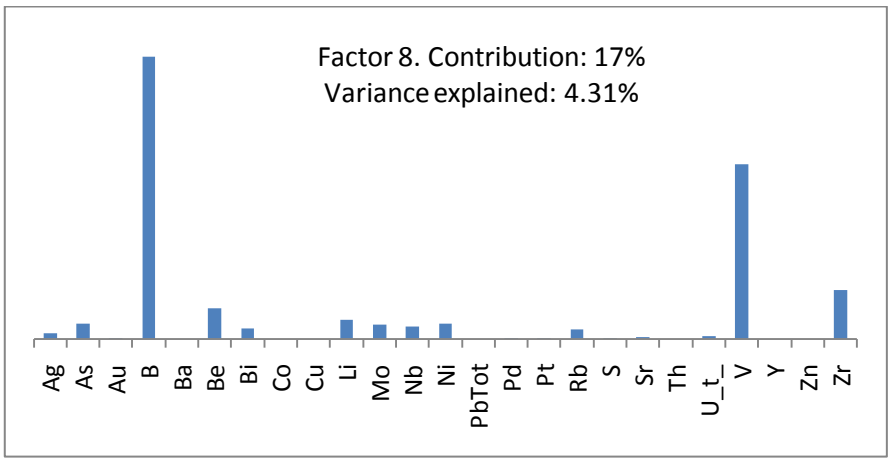

Figure 41: Factor eight for the factor analysis of elements other than REEs.

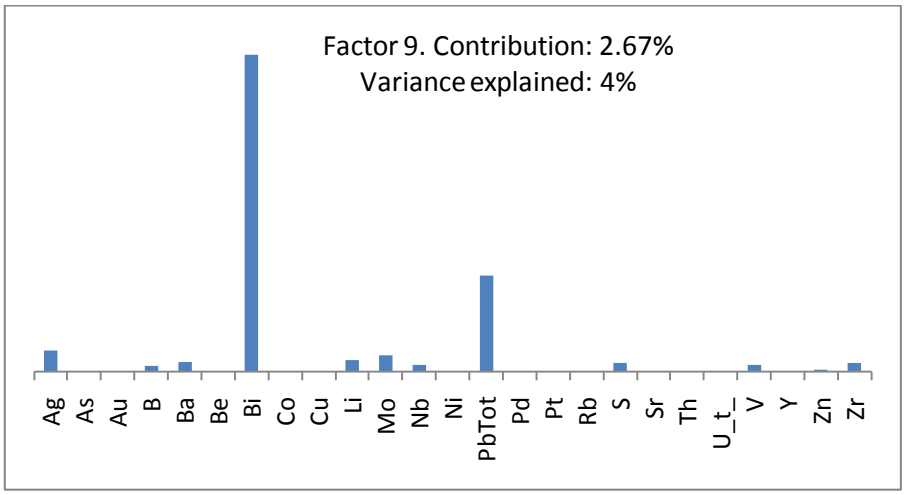

Figure 42: Factor nine of the factor analysis for elements other than REEs.

Factor ten (Figure 43) consists of all but a small portion of thorium associated with small amounts of some metals (Ag, Cu and Ni) and elements such as Zr, Bi, Co, Li, S and Sr.

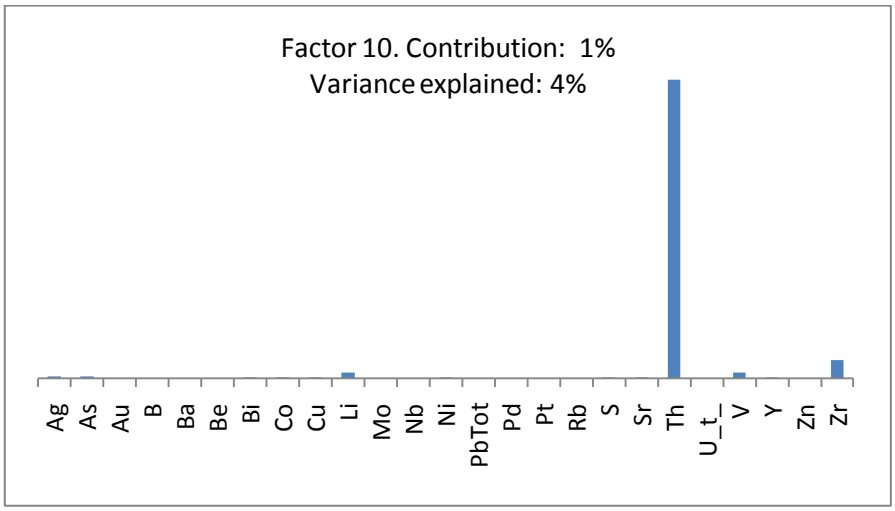

Figure 43: Factor ten for factor analysis of elements other than REEs.

As mentioned in section 4.5.2, there are many processes that will lead to the precipitiation of different types of metals and other elements. Supergene processes may lead to the precipitation of metals that are soluble in oxidised water. Hypogene process may lead to the precipitation of metals that form complexes with chloride of sulphide complex if redox reactions occur.

The metals in factor one (Ag, Au, Pb, Pd, Pt) are all metals that like to form complexes with chloride or sulfer. This may suggest that factor one produced by is hypogene process. Elements such as Co, Mo, As, V and Cu, which are found in factor two, can form soluble metal-oxide complexes. This may suggest that a supergene process was responsible for the precipitation of those metals. However, elements from each factor are known to be desposited by more than process which makes determining the type of process more difficult.

The presence of uranium and arsenic in a separate factor to the elements that were assumed to be associated with uranium is unexpected. This may be the result of the precipitation of uranium and arsenic during a seperate mineralisation event than the elements in the first three factors.

5. Drill Core Geochemistry

Eight holes were drilled by Cameco Australia within their Deaf Adder project area. Three holes were stratigraphic and five were drilled within the vicinity of the Flying Ghost uranium prospect to determine if the radioactivity located on the surface continued at depth. Details of the four drill holes examined in this project are shown in Table 6.

Table 6: Drill hole data for the five drill holes in the Flying Ghost prospect.

Drillhole	UTM N	UTM E	RL	Total Depth
DAD-0001	8529970	318240	322.56	419.00
DAD-0002	8530051	318092	319.78	794.00
DAD-0003	8530025	318355	331.89	83.00
DAD-0004	8529944	318203	321.85	275.00

The geochemistry of four of the drill holes in the Flying Ghost area (Figure 44) were examined to determine if peaks in the uranium were associated with particular lithologies. The drill hole geochemistry can be found in Appendix 11. It was also determined if uranium peaks were related to peaks in any other element.

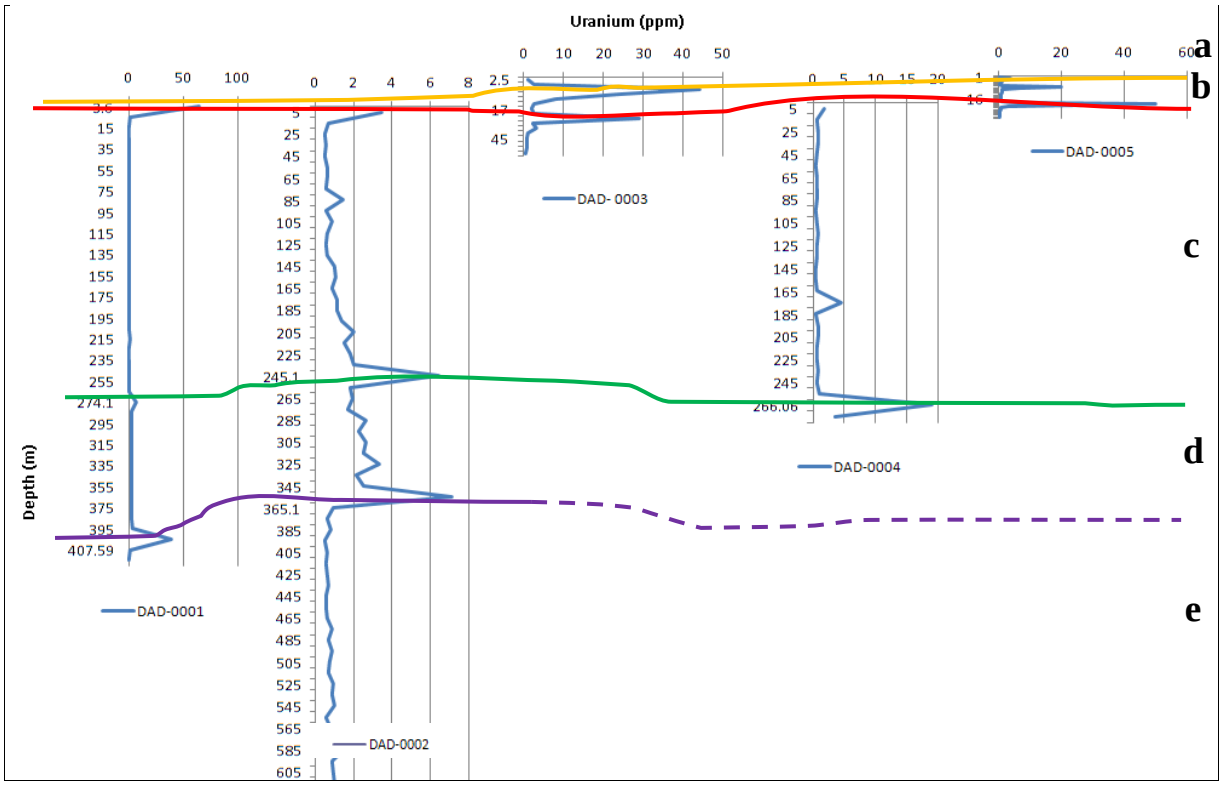

Figure 44: Correlation of drill holes in the Flying Ghost area showing uranium concentrations and lithological contact. The lithologies include the a) Marlgowa Sandstone, b) Gilruth Volcanics, c) Gumarrirnbang Sandstone, d) Nunngbalgarri Volcanics and e) Mamadawerre Sandstone. The solid lines represent the lower contact of each lithology. The dotted line represents an inferred lower contact for the Nunngbalgarri Volcanics.

Graphs were constructed for drill holes DAD-0001 to DAD-0004. There were no geochemical data available for DAD-0005. The concentration of uranium was compared to the concentration of all other elements analysed. The resulting graphs are included as Appendix 12.

5.1 DAD-0001

All elements analysed in DAD-0001 were higher within the Nunngbalgarri Volcanics than the surrounding sandstone with the exception of Mo and SiO_2 which decreased. Within the volcanic unit there were some variations in the element concentrations. Several elements remained constant within the unit (e.g. Al_2O_3, Fe_2O_3, SiO_2, MREE, HREE, Cu, Th. V, Zr), while some varied. There generally two types of variation, elements either varied throughout the unit (e.g. K_2O and MgO) or increased towards the centre of the unit (e.g. CaO, Na_2O, Cu and Sr).

In relation to uranium, some elements had peaks that corresponded to both uranium spikes. These included As, B, Be Li and the LREEs. Elements with spikes correlating to uranium at only the upper contact of the volcanic unit included K2O, MnO and Rb although the oxides values did increase within the volcanic unit. Elements with spikes that correlated with the uranium spike at only the lower contact include Au, Ni, Pd, S and Zn.

5.2 DAD-0002

Element concentrations in DAD-0002 were very similar to the concentrations in DAD-0001. All oxide values were higher within the volcanic unit than the surrounding sandstone with the exception of SiO2. P2O5 was the only oxide that appeared to have a peak at the upper contact of the volcanic unit in association with uranium. A peak in Au also corresponded to a peak in the uranium at the base of the volcanic unit.

The rare earth elements were more closely related in this drill hole than any other. They all increase from the surface to the upper contact of the volcanic unit. There is a small drop in LREE's just below the contact then all REEs increase until the base of the volcanic unit where values all drop steeply. The concentration of all REEs then increases with depth. From the remaining elements, peaks are seen in B, Be, Rb and Th in association with uranium spikes.

5.3 DAD-0003

Drillhole DAD-0003 only encountered the contacts between the Marlgowa Sandstone and the Gilruth Volcanics and between the Gilruth Volcanics and the Gummarrirngbang Sandstone. Values for the oxides were all higher within the Gilruth volcanics with the exception of SiO_2

which decreased. Peaks in the oxide concentrations were generally associated with peaks in uranium. There were several elements (CaO, MnO and P_2O_5) that only had peaks in association with the uranium peak at the lower contact.

Metals and PGEs that had similar concentration trends as uranium include Au, Ni, Pb and Zn. Rare earth elements in DAD-0003 once again varied between light and mid/heavy rare earths. The LREEs are negatively correlated with uranium until 17 metres then steadily decrease with depth. The MREEs and HREEs all have the same trend which increases within the volcanic unit then drops at the lower contact before peaking again at 35 metres. Of the other elements, only B, Be, Li, V and Zr appear to have any association with uranium.

5.4 DAD-0004

DAD-0004 only encountered the upper contact of the Nunngbalgarri volcanics. The spike in uranium at the contact appears to be associated with only two oxides, CaO and P_2O_5. Out of the metals and PGEs, only Au Pb and Zn showed an association with uranium.

The light rare earth elements have a closer association than in any of the previous drill holes as they all increase to some extent with the increase in uranium at the contact. However, above the contact, the LREEs have peaks at approximately 50 metres and 125 metres where the MREEs and HREEs have peaks at 115 metres and 135 metres. The only other elements that showed any association with uranium were Ba, Bi, Li, Rb, S, Sr and V.

The uranium spikes are generally larger at the base of the Gilruth Volcanics and the Nunngbalgarri Volcanics. Spikes in some elements associated with uranium in the transects also occurred at the base of the volcanic units. This may be due to precipitation of metals from a redox reaction when hydrothermal fluids encountered the volcanic units on the way to the surface. However, high concentrations may also be due to scavenging of elements from within the volcanic unit. These elements may have been precipitated by supergene processes when water from the surface came into contact with redox reaction at the boundary. The increase in CaO and P_2O_5 at contacts between the volcanic units and sandstones is of interest and should be looked at in more depth.

6. Conclusion

The geochemical data was investigated and analysed in order to determine the type of uranium mineralisation discovered at Headwaters. This has resulted in a number of interesting conclusions. Unfortunately it has also left many questions unanswered.

The mineralisation at Headwaters was compared to two different mineralisation types that occur in the Northern Territory. Similarities exist between unconformity-type and sandstone-hosted uranium deposits and uranium at Headwaters in terms of alteration assemblages. All deposits generally have similar assemblages consisting of chlorite, sericite, illite, hematite and kaolinite.

Although there are similarities between the different deposits, there are several differences between Headwaters and the other deposits that make it difficult to determine which type of deposit is most likely to occur in the area.

Unconformity-type deposits in the Northern Territory are generally found below the unconformity between the Kombolgie Formation and metamorphic basement. The basement rocks in the Alligator River uranium field are comprised of the Cahill Formation where as in the Headwaters project the basement rocks are from the Nimbuwah Complex although both are known to be chloritic schists. Another major difference is the depth of the unconformity. In the Headwaters tenements only one hole intersected the basement rock at approximately 994m. This makes it difficult to determine if the metasedimentary rocks in Headwaters have the necessary characteristics to host a uranium deposit. No uranium anomalies were found at the unconformity which may indicate that uranium has come from a different source.

Sandstone hosted uranium deposits in the Westmoreland area are known to be precipitated by similar hydrothermal fluids to those in the Alligator River uranium field. However, the uranium deposits are hosted by the Westmoreland conglomerate beneath the Seigal Volcanics. There is also no evidence in the drill core data to support similar deposits being present in the Headwaters project.

Inspection of hand samples has determined that different types of alteration occur in different areas. This suggests that the prospects and may have been formed by more than one process. Transects across uranium anomalies associated with structures has shown that uranium minerals are associated with different elements in different areas. This may be the result of different ore forming processes or even perhaps different mineralisation events.

Geochemical analysis of drill holes determined that high uranium concentrations are also present below the surface. These high concentrations generally occur at the contacts between sandstone and volcanic units. These high concentrations may also be the result of two different types of ore forming processes namely hypogene and supergene processes.

Analysis of multivariate statistics and scatter plots also raised the possibility of two different processes for mineralisation. One trend in the multivariate data suggests that uranium mineralisation may have been precipitated by an uraniferous hydrothermal fluid bringing uranium up from the unconformity. The second trend may be the result of groundwater scavenging uranium from volcanic rocks on or near the surface.

In order to define which process is responsible for the uranium anomalies in the Headwaters project further investigations will be needed. Determining the type of mineralisation at each prospect as well as the origin of the fluid which precipitated the uranium minerals will enable the type of uranium deposit to be established.

7. Recommendations for Further Work

Due to time limitations on this project only a limited amount of analysis was able to be carried out on the geochemical data collected by Cameco Australia. In order to fully determine if uranium anomalies in the Headwaters area are related to unconformity-type or sandstone-hosted uranium deposits further investigation would be needed. Following are several suggestions that may help to further define the uranium anomalies:

- Mapping and sampling along structures within the Headwaters tenements.
- Whole rock analysis of samples collected.
- Analysis of thin sections to observe any diagenesis within the samples
- SEM (Microprobe or EDS) or XRD analysis of samples to identify alteration and uranium minerals. Determining the different minerals will help to define differences between mineralisation events or processes.
- Lead, uranium or Sr/Rb isotope dating of uranium and alteration minerals to determine the age of alteration and mineralisation in different areas.
- H, O and C isotope analysis to determine the origin of fluid involved in the transportation of uranium and other metals.

References

Bulmer, M., 2005. Data Analysis. University of Queensland, Brisbane.

Carson, L.J., Haines, P.W., Brakel, A., Pietsch, B.A. and Ferenczi, P.A., 1999. Milingimbi SD 53-2 1:250 000 geological map series Explanatory Notes., Northern Territory Geological Survey, Department of Mines and Energy and Australian Geological Survey Organisation.

Carter, M., 2005. Exploration Licence EL23522, East Alligator - Northern Territory: Annual Report for the period 26th February 2004 - 25th February 2005, Second Year of Exploration.

Carter, M. and Beckitt, G., 2003. Exploration Licence 23522, East Alligator - Northern Territory: Annual Report, Cameco Australia Pty Ltd.

Carter, M. and Otto, G., 2006. Exploration Licence EL23522, East Alligator Project - Northern Territory: Surrender and Final Report - 26 February 2003 to 26 February 2006. EA06-02.

Dodson, R.G., Needham, R.S., Wilkes, P.G., Page, R.W. and Watchman, A.L., 1974. Uranium mineralisation in the Rum Jungle-Alligator Rivers Province, Northern Territory, Australia, Formation of Uranium Ore Deposits. International Atomic Energy Agency, Vienna, pp. 551-568.

Drever, G., Beckitt, G., Otto, G. and Rosewall, D., 2000. Exploration Licences EL 5061 & EL 5062, Deaf Adder Project - Northern Territory, Annual report for period 27th May 1999 to 26th May 2000, Cameco Australia PTY LTD.

Drever, G., Beckitt, G., Otto, G., Rosewall, D. and Mackie, A., 1999. Exploration Licences EL 5061 & EL 5062, Deaf Adder Project - Northern Territory, Annual report for period 27th May 1998 to 26th May 1999, Cameco Australia PTY LTD.

Drever, G. and Marlatt, J., 2000. EL 5061 and EL 5062, Deaf Adder Project, 2000 proposed work program., Cameco Australia PTY LTD.

Drever, G., Thevissen, J. and Beckitt, G., 1998. Exploration Licences EL 5061 and EL 5062, Deaf Adder Project - Northern Territory, 1997 annual report, volume 1 of 3.

Felshe, J. and Herrman, A.G., 1978. Yttrium and lanthanides. In: K. Wedepohl (Editor), Handbook of Geochemistry. Springer-Verlag, New York, pp. 57-71.

Foster, C.B., Robbins, E.I. and Bone, Y., 1990. Organic tissues, graphite, and hydrocarbons in host rocks of the Rum Jungle Uranium Field, northern Australia. Ore Geology Reviews, 5: 509-523.

Gaboreau, S., Beaufort, D., Vieillard, P., Patrier, P. and Bruneton, P., 2005. Aluminium phosphoate-sulphate minerals associated with Proterozoic unconformity-type uranium deposits in the East Alligator River Uranium Field, Northern Territory, Australia. Canadian Mineralogist, 43: 813-827.

Gaboreau, S. et al., 2007. Significance of aluminum phosphate-sulfate minerals associated with U unconformity-type deposits: The Athabasca Basin, Canada. American Mineralogist, 92(2-3): 267-280.

Google Earth, 2009. Satellite Image of the Headwaters Project area.

Hein, K.A.A., 2002. Geology of the Ranger Uranium Mine, Northern Territory, Australia: structural constraints on the timing of uranium emplacement. Ore Geology Reviews, 20: 83-108.

Isobe, H., Murakami, T. and Ewing, R.C., 1992. Alteration of uranium minerals in the Koongarra deposit, Australia: Unweathered zone. Journal of Nuclear Materials, 190: 174-187.

Kendell, C.J., 1990. Ranger uranium deposits. In: F.E. Hughes (Editor), Geology of the Mineral Deposits of Australia and Papua New Guinea. The Australian Institute of Mining and Metallurgy, Melbourne, pp. 799-805.

Komninou, A. and Sverjensky, D.A., 1995b. Hydrothermal alteration and the chemistry of ore-forming fluids in an unconformity-type uranium deposit. Geochimica et Cosmochimica Acta, 59(13): 2709-2723.

Komninou, A. and Sverjensky, D.A., 1996. Geochemical modeling of the formation of an unconformity-type uranium deposit. Economic Geology, 91(3): 590-606.

Ludwig, K.R. et al., 1987. Age of uranium mineralization at the Jabiluka and Ranger deposits, Northern Territory, Australia; new U-Pb isotope evidence. Economic Geology, 82(4): 857-874.

Maynard, C.C., 1971. Report on exploration (1971) in Liverpool River Project Area A.P. 2364, Electrolytic Zinc Co. of A/asia Limited and P.E.N Joint Venture.

McLennan, S.M. and Taylor, S.R., 1979. Rare earth element mobility associated with uranium mineralisation. Nature, 282: 247-250.

Michard, A., 1989. Rare earth element systematics in hydrothermal fluids. Geochimica et Cosmochimica Acta, 53(3): 745-750.

Otto, G., Beckitt, G. and O'Connor, T., 2001. Exploration Licences EL 5061 & EL 5062, Deaf Adder Project - Northern Territory, Annual report for period 27th May 2000 to 26th May 2001, Cameco Australia Pty Ltd.

Otto, G., Zaluski, G. and O'Connor, T., 2002. Exploration Licences EL 5061 & EL 5062, Deaf Adder Project, Arnhem Land - Northern Territory, Annual and final report for period 27th May 2001 to 26th May 2002, Cameco Australia Pty Ltd.

Pirajno, F., 1992. Hydrothermal Mineral Deposits. John Wiley and Sons, Sydney.

Polito, P.A. et al., 2004a. Significance of alteration assemblages for the origin and evolution of the Proterozoic Nabarlek unconformity-related uranium deposit, Northern Territory, Australia. Economic Geology, 99(1): 113-139.

Polito, P.A., Kyser, T.K., Rheinberger, G. and Southgate, P.N., 2005a. A paragenetic and isotopic study of the Proterozoic Westmoreland uranium deposits, southern McArthur Basin, Northern Territory, Australia. Economic Geology, 100: 1243-1260.

Polito, P.A., Kyser, T.K., Thomas, D., Marlatt, J. and Drever, G., 2005b. Re-evaluation of the petrogenesis of the Proterozoic Jabiluka unconformity-related uranium deposit, Northern Territory, Australia. Mineralium Deposita, 40(3): 257-288.

Price, A.T., 1996. Annual Report on Exploration licenses 6352, 6353, 6354, 6355 and 8436, Bulman/Mainoru Project. 13/11/95 to 12/11/96.

Queensland Mines Ltd, 1972a. Exploration Licence No. 260 - Northern Territory, Annual report - year ending 31 December 1972.

Queensland Mines Ltd, 1972b. Exploration Licence No. 264 - Northern Territory, Annual report - year ending 31 December 1972.

Queensland Mines Ltd, 1974a. E.L. No 264 - Northern Territory, Annual report year ending Dec. 31 1973.

Queensland Mines Ltd, 1974b. Exploration licence No. 260 - Northern Territory, Annual report year ending December 31, 1973.

Rawlings, D.J., 1999. Stratigraphic resolution of a multiphase intracratonic basin system: the McArthur Basin, northern Australia. Australian Journal of Earth Sciences, 46: 703-723.

Rawlings, D.J., 2001. Tectonostratigraphy of the McArthur Basin (1:100 000 scale map). Northern Territory Geological Survey, Darwin.

Reimann, C., Filzmoser, P. and Garrett, R.G., 2002. Factor analysis applied to regional geochemical data: problems and possibilities. Applied Geochemistry, 17(3): 185-206.

Rheinberger, G.M., Hallenstein, C.P. and Stegman, C.L., 1998. Westmoreland uranium deposits. In: D.A. Berkman and D.H. Mackenzie (Editors), Geology of Australian and Papua New Guinea mineral deposits. Australian Institute of Mining and Metallurgy, Melbourne, pp. 807-814.

Rich, R.A., Holland, H.D. and Peterson, U., 1980. Hydrothermal Uranium Deposits. Developments in Economic Geology, 6. Elsevier Scientific Publishing Company, Amsterdam.

Robb, L., 2007. Introduction to ore-forming processes. Blackwell Science Ltd, Victoria.

Rollinson, H.R., 1993. Using geochemical data: Evaluation, presentation, interpretation. Pearson Education Limited, Essex, England.

Rosenbaum, G., 2009. Structural geology of the Headwaters project area (Unpubl.). University of Queensland, Brisbane.

Sullivan, C.J. and Matheson, R.S., 1952. Uranium-copper deposits, Rum Jungle, Australia. Economic Geology, 47(7): 751-758.

Swingler, N., 1973. Notes on ground reconnaissance, various localities within EL 244, EL 260, EL 264 and EL 261, Queensland Mines Limited, Internal Report.

Warren, K.R., 1997. Annual Report on Exploration Licenses 6352, 6353, 6354, 6355 and 8436, Bulman/Mainoru Project, 13/11/96 to 12/11/97.

Wilde, A.R. and Wall, V.J., 1987. Geology of the Nabarlek Uranium Deposit, Northern Territory, Australia. Economic Geology, 82: 1152-1168.

Woinarski, J., 2009. Arhnem Land: Landscapes and Climarte. Savanna Explorer: North Australian Information Resource.

Wood, S.A., 1990. The aqueous geochemistry of the rare-earth elements and yttrium: 2. Theoretical predictions of speciation in hydrothermal solutions to 350°C at saturation water vapor pressure. Chemical Geology, 88(1-2): 99-125.

Zaluski, G., 2003. Processing and Interpretation of Hymap Mk 1 Hyperspectral Scanner Data for the East Alligator Project (ELA 23522).

Appendix 1 – Geochemical Data

See attached CD

Appendix 2 – Univariate Statistics

Univariate	U	Ag	Al2O3	As	Au	B	Ba	Be
Min	0.04	0.02	50	0.25	0.5	10	1	0.1
Max	12779.6	16.87	262441	948.3	236550	980	6369	32.6
Mean	16.4472	0.060	13927.85	3.44693	93.6676	22.4907	62.7922	0.2354
Median	0.59	0.02	9185	0.5	0.5	10	12	0.1
St. Dev	298.871	0.361	19594.56	26.8043	4511.04	40.0781	244.298	0.87883
Int Range	0.71	0.01	11850	0.83126	0	14	19	0
Range	12779.5	16.85	262391	948.05	236550	970	6368	32.5
1 percentile	0.19	0.02	50	0.25	0.5	10	1	0.1
5 percentile	0.31	0.02	50	0.25	0.5	10	3	0.1
10 percentile	0.35	0.02	2210	0.25	0.5	10	4.08142	0.1
25 percentile	0.43178	0.02	4700	0.25	0.5	10	7	0.1
75 percentile	1.14	0.03	16534	1.02703	0.5	23	25	0.1
90 percentile	3.72	0.09	26975	2.9	1	43	78	0.3
95 percentile	7.7	0.17	36618	7.6	4	66	251	0.7
99 percentile	135.7	0.52	96508	64.3	74	147	1115	2.1

Univariate	Bi	CaO	Ce	Co	Cu	Dy	Er	Eu
Min	0.01	10	0.05	0.02	0.5	0.005	0.005	0.005
Max	110.992	181732	316	300.04	1532	380.96	226.4	20.19
Mean	0.33122	556.1474	17.4822	1.415597	5.283421	0.96951	0.506	0.299811
Median	0.01	94	14.14	0.25	0.5	0.31	0.15	0.17
St. Dev	3.67876	6177.931	25.9356	8.624884	35.19092	8.09058	4.832	0.66966
Int Range	0.02	59.629	20.95	0.63	1.5	0.585	0.275	0.305
Range	110.982	181722	315.95	300.02	1531.5	380.955	226.4	20.185
1 percentile	0.01	10	0.05	0.02	0.5	0.005	0.005	0.005
5 percentile	0.01	20	0.05	0.025	0.5	0.005	0.005	0.005
10 percentile	0.01	55	0.05	0.06	0.5	0.005	0.005	0.005
25 percentile	0.01	72	0.05	0.11	0.5	0.005	0.005	0.005
75 percentile	0.03	131	20.98	0.73	1.96913	0.59	0.28	0.31
90 percentile	0.12	269	33.99	2.11	6.6	1.37	0.64	0.59
95 percentile	0.41	566	49.9	4.31	21	2.94	1.38	1.1
99 percentile	4.4	4872	135.3	16.29	84	9.85	4.8	2.86

Univariate	Fe2O3	Gd	Ho	K2O	La	Li	LOI	Lu
Min	25	0.005	0.005	50	0.005	0.5	0.05	0.01
Max	817365	205.58	81.87	130443	381.1	1082	26	23.63
Mean	11167.7	1.24914	0.18614	3165.27	13.2793	4.30199	0.501254	0.08131
Median	1673.1	0.63	0.05	1511	10.07	2	0.2	0.03
St. Dev	53917.6	4.61673	1.73824	7334.32	16.6765	26.8217	1.373466	0.49873
Int Range	3797.22	1.115	0.095	2344	6.55	2.16989	0.45	0.05
Range	817340	205.575	81.865	130393	381.095	1081.5	25.95	23.62
1 percentile	25	0.005	0.005	50	0.005	0.5	0.05	0.01
5 percentile	237.38	0.005	0.005	50	0.22	0.5	0.05	0.01
10 percentile	386.1	0.005	0.005	200	4.7	0.5	0.05	0.01
25 percentile	713	0.005	0.005	714	7.49	0.5	0.05	0.01
75 percentile	4508	1.11741	0.1	3046	14.03	3	0.5	0.06
90 percentile	11716	2.26	0.24	5637	21.88	8	0.8	0.17
95 percentile	27384.5	4.57	0.53	8582	32.79	13.8869	1.2	0.24
99 percentile	302358	13.13	1.96	39450	80.82	30	7.7	0.61

Univariate	MgO	MnO	Mo	Na2O	Nb	Ni	P2O5	Pb
Min	10	1	0.025	50	0.01	0.1	25	0.08
Max	108788	24800	88	23217	46.04	436	34800	891
Mean	756.2901	49.68836	0.3952	95.8008	0.803657	3.35018	583.811	5.97333
Median	193	2.582	0.05	50	0.38	1	161	1.27
St. Dev	4740.423	578.2575	2.75714	488.159	2.388981	15.5265	1895.83	33.335
Int Range	281	3.873	0.085	0	0.79	0.5	250	1.55
Range	108778	24799	87.975	23167	46.03	435.9	34775	890.92
1 percentile	10	1	0.025	50	0.01	0.7	25	0.33
5 percentile	10	1	0.025	50	0.01	0.7	25	0.56
10 percentile	68	1	0.025	50	0.01	0.7	58	0.66
25 percentile	108	1.291	0.025	50	0.01	0.7	99	0.88
75 percentile	389	5.164	0.11	50	0.8	1.4	350	2.42
90 percentile	911	19	0.46646	50	1.42	5.7	998	7.04
95 percentile	1731	49.058	1.8	165	2.19	9.7	2095	18.81
99 percentile	7040	840	4.91	1245	9.5	43.8	8258	66.78

Univariate	Pd	Pr	Pt	Rb	S	SiO2	Sm	Sr
Min	0.25	0.005	0.25	0.1	10	1	0.23	0.69
Max	49580	40.51	8034	225.9	5191	99.809	42.01	8960
Mean	19.5218	2.05668	3.426736	7.21843	49.38018	91.53596	1.51768	49.0624
Median	0.25	1.67	0.25	3.29	10	98.0553	0.99	15.73
St. Dev	945.494	3.08606	153.2183	17.3605	185.4711	22.42247	2.52129	256.364
Int Range	0	2.505	0	4.73	30	2.6324	1.29	29.61
Range	49579.8	40.505	8033.75	225.8	5181	98.809	41.78	8959.31
1 percentile	0.25	0.005	0.25	0.21	10	1	0.23	0.97
5 percentile	0.25	0.005	0.25	0.61	10	1	0.23	1
10 percentile	0.25	0.005	0.25	0.95	10	90.6985	0.23	3.77
25 percentile	0.25	0.005	0.25	1.61	10	96.3269	0.25	8.42
75 percentile	0.25	2.51	0.25	6.33	39.1875	98.9596	1.54	38
90 percentile	0.5	3.95	0.25	11.73	79	99.3334	2.79	100.3
95 percentile	1.2	6	0.5	18.39	134	99.481	5.23	156.46
99 percentile	13	15.95	3	99.46	581	99.6623	13.72	392.54

Univariate	Tb	Th	TiO2	Tm	V	Y	Zn	Zr
Min	0.005	0.05	10	0.005	1	0.14	0.5	0.05
Max	54.52	8737	55224	30.71	2200	2312	4600	3037.5
Mean	0.178096	10.612	716.49	0.07739	14.5285	6.56939	6.18372	89.14621
Median	0.07	2.65	316	0.02	4	1.97	1	52
St. Dev	1.134095	194.335	2466.79	0.64954	78.5161	50.8834	92.7017	176.76804
Int Range	0.125	1.5	270	0.045	5	2.24	1	46.8
Range	54.515	8736.95	55214	30.705	2199	2311.86	4599.5	3037.45
1 percentile	0.005	0.05	10	0.005	1	0.14	0.9	0.05
5 percentile	0.005	1.49	156	0.005	1	0.79	0.9	10.4
10 percentile	0.005	1.77	179	0.005	1	0.97	0.9	19.8
25 percentile	0.005	2.14	229	0.005	2	1.29	0.9	35.6
75 percentile	0.13	3.64	500	0.04886	7	3.52	1.9	82.3
90 percentile	0.289707	6.22	889	0.14815	15	8.7	4	153.3
95 percentile	0.587461	9.81	1488	0.22	27	19.22	7.48087	240
99 percentile	1.77	46.04	9424	0.63	273	61.01	64	861.5

Appendix 3 – Frequency Histogram Plots

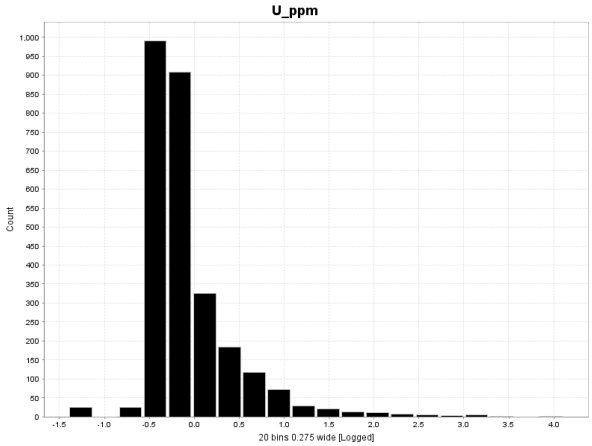

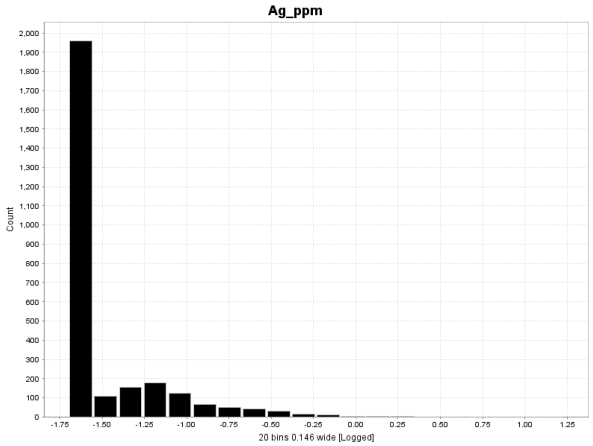

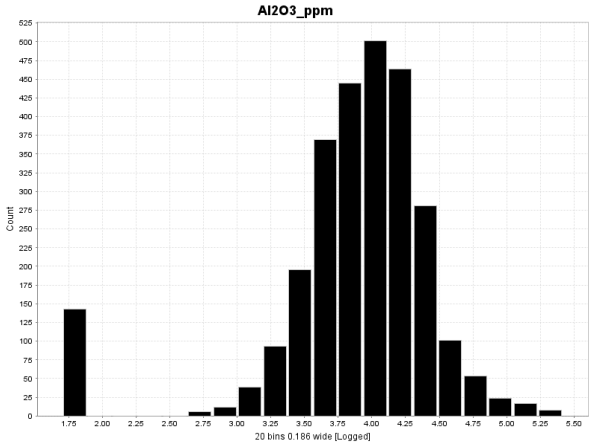

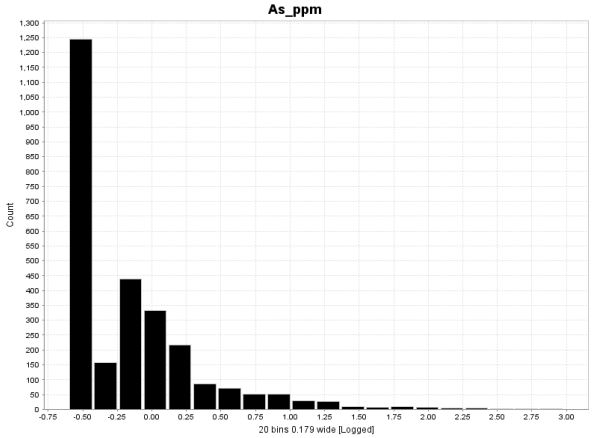

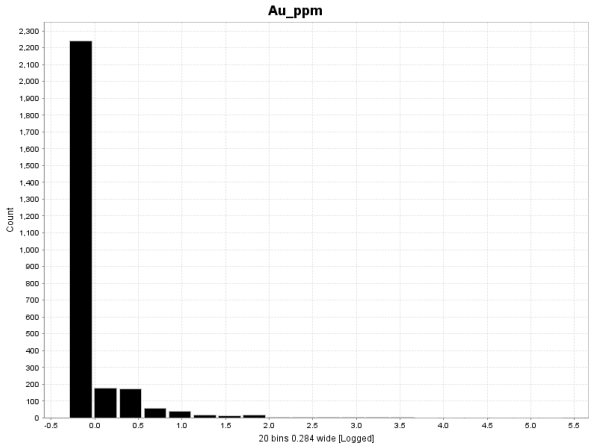

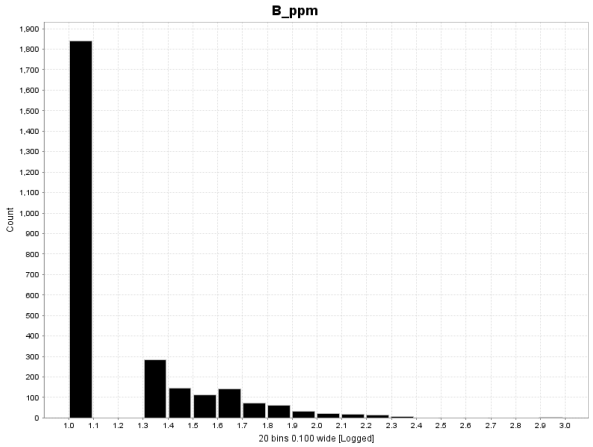

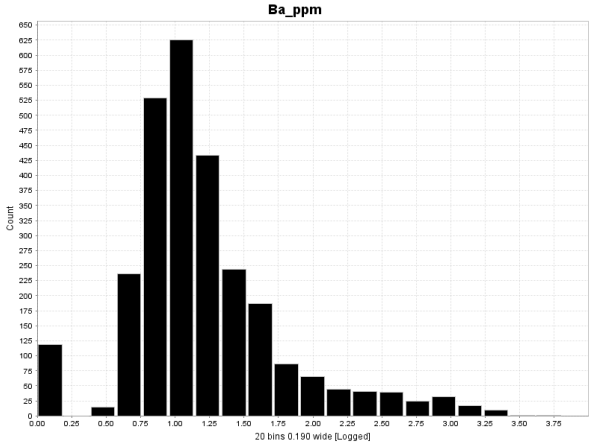

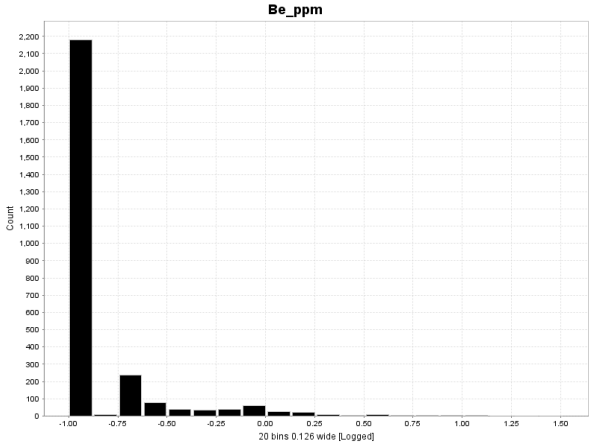

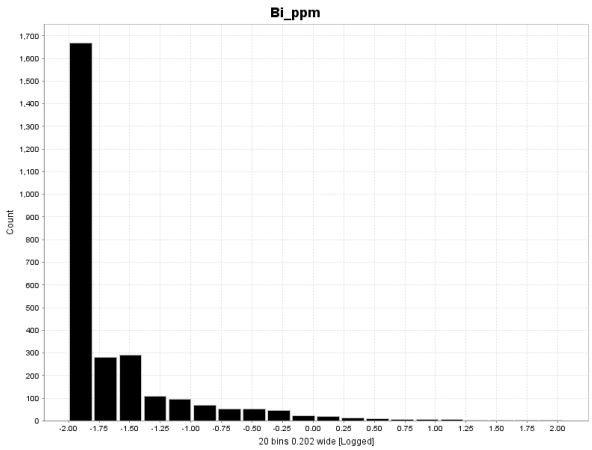
Bi_ppm
Count
20 bins 0.202 wide [Logged]

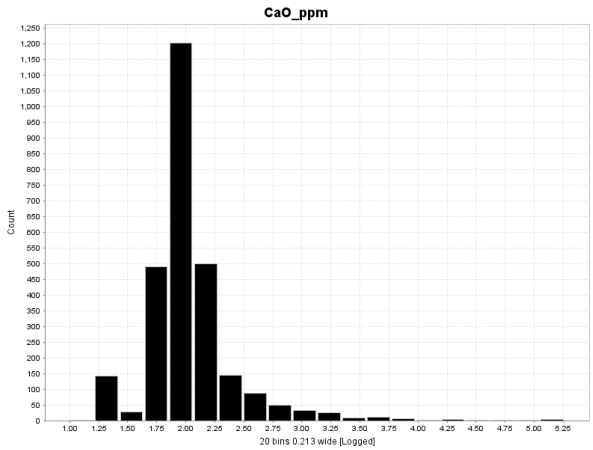
CaO_ppm
Count
20 bins 0.213 wide [Logged]

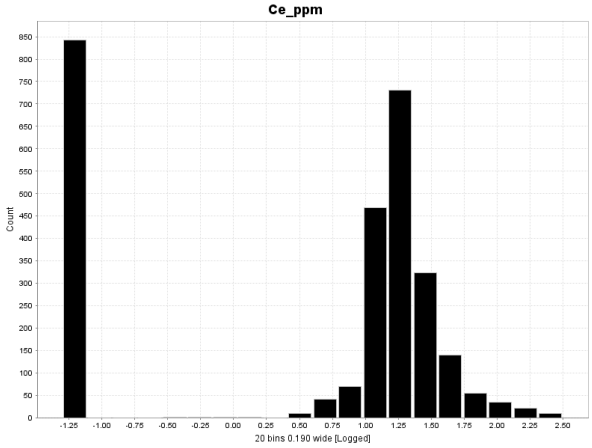
Ce_ppm
Count
20 bins 0.190 wide [Logged]

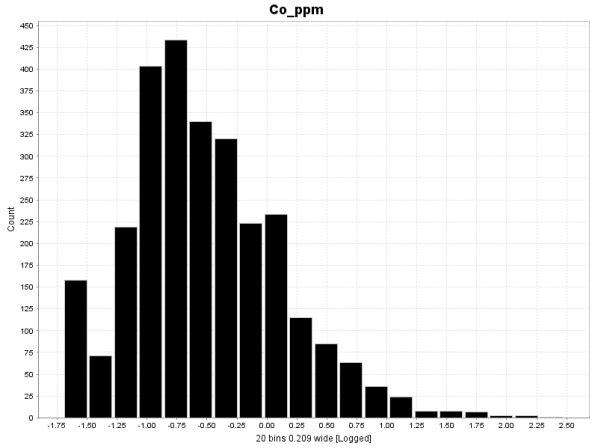
Co_ppm
Count
20 bins 0.209 wide [Logged]

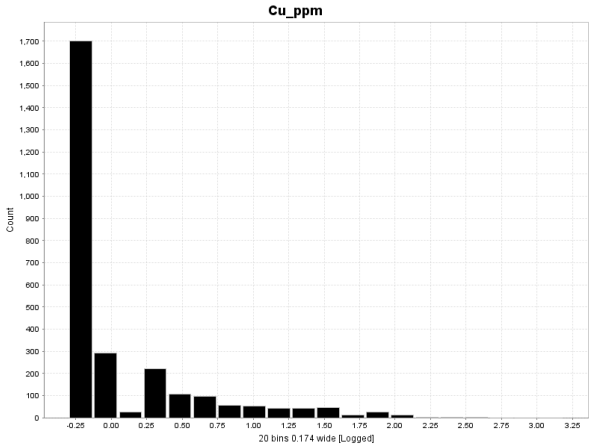
Cu_ppm
Count
20 bins 0.174 wide [Logged]

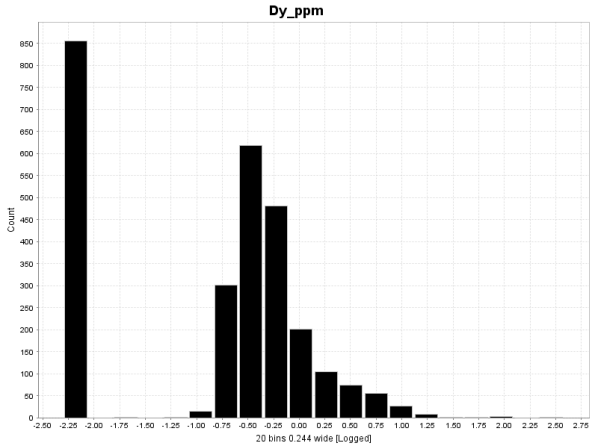
Dy_ppm
Count
20 bins 0.244 wide [Logged]

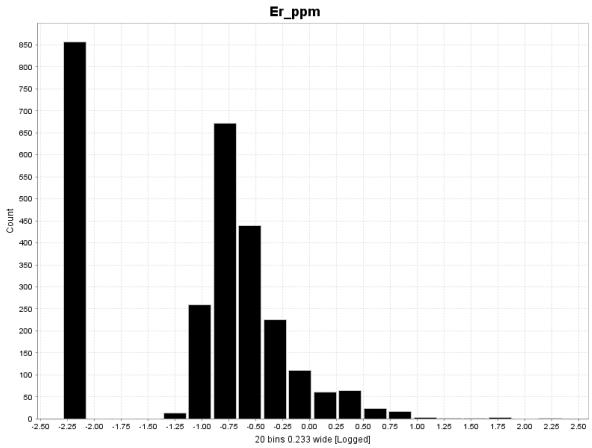
Er_ppm
Count
20 bins 0.233 wide [Logged]

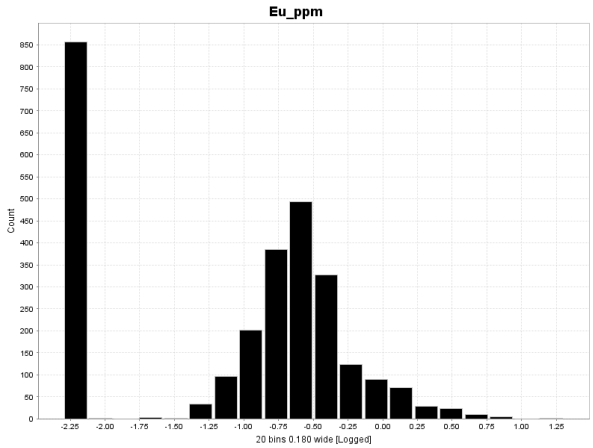
Eu_ppm
Count
20 bins 0.180 wide [Logged]

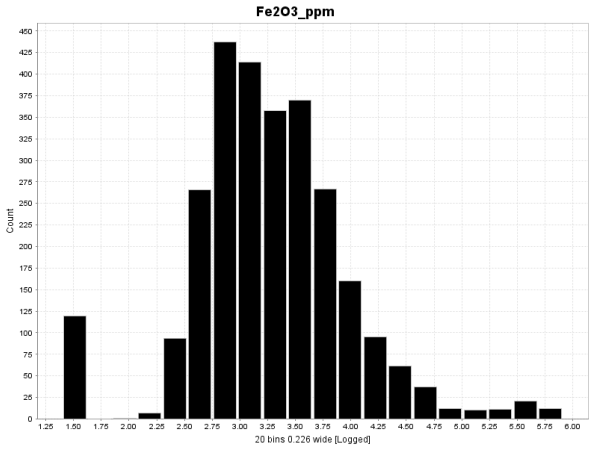
Fe2O3_ppm
Count
20 bins 0.226 wide [Logged]

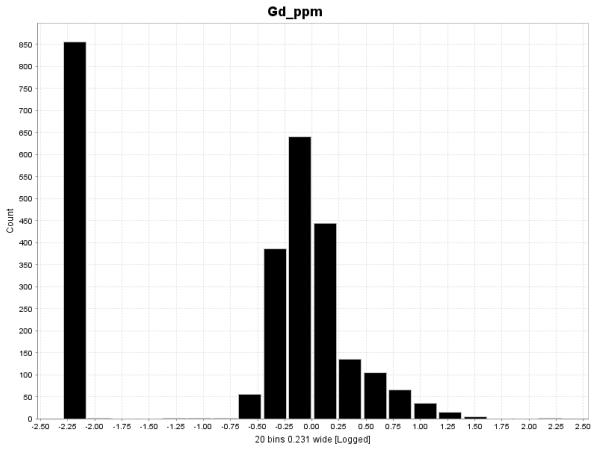
Gd_ppm
Count
20 bins 0.231 wide [Logged]

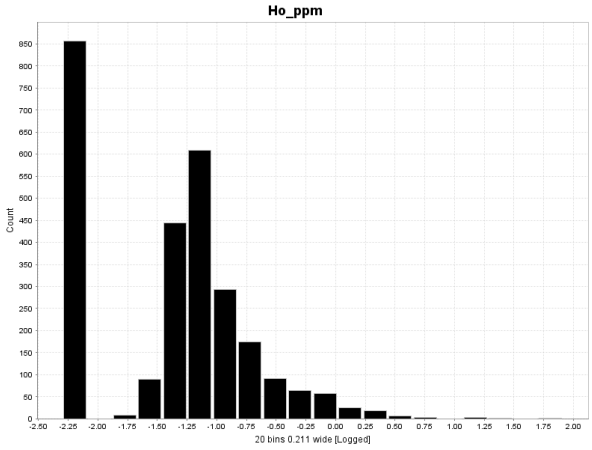
Ho_ppm
Count
20 bins 0.211 wide [Logged]

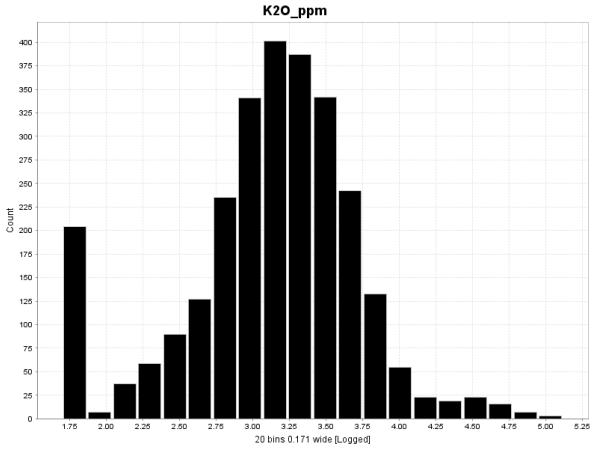
K2O_ppm
Count
20 bins 0.171 wide [Logged]

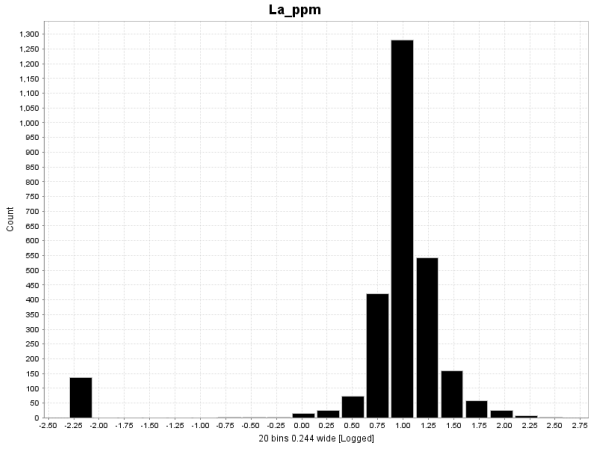
La_ppm
Count
20 bins 0.244 wide [Logged]

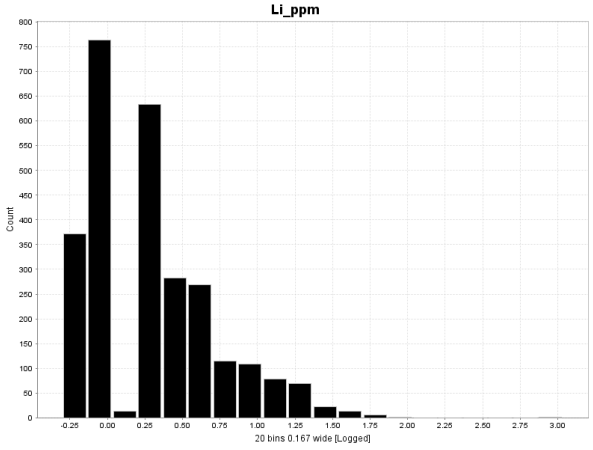
Li_ppm
Count
20 bins 0.167 wide [Logged]

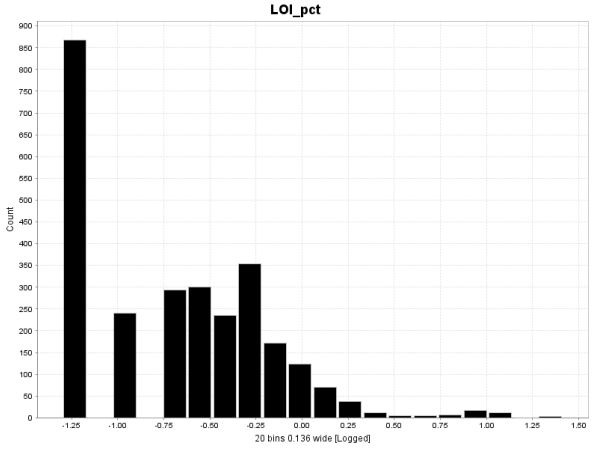
LOI_pct
Count
20 bins 0.136 wide [Logged]

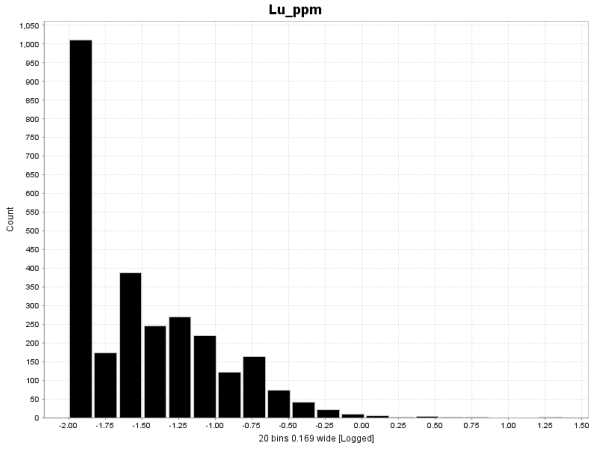
Lu_ppm
Count
20 bins 0.169 wide [Logged]

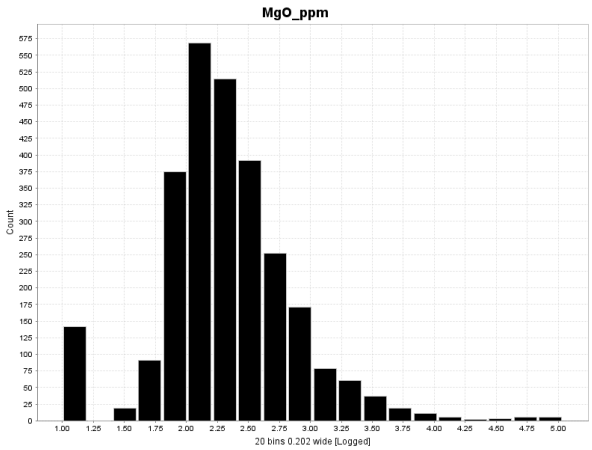
MgO_ppm
Count
20 bins 0.202 wide [Logged]

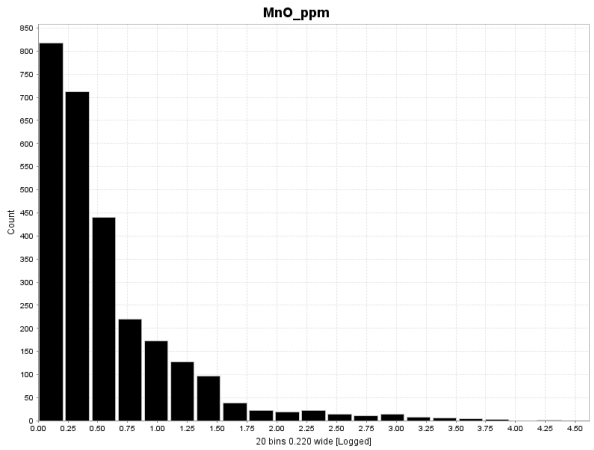
MnO_ppm
Count
20 bins 0.220 wide [Logged]

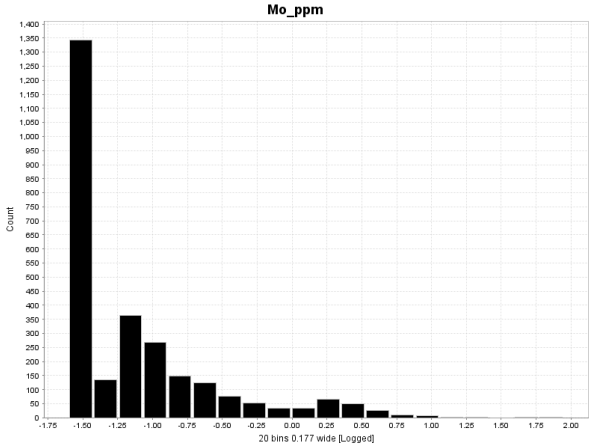
Mo_ppm
Count
20 bins 0.177 wide [Logged]

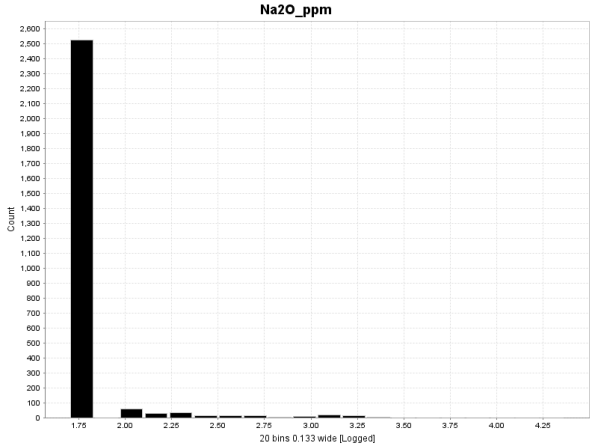
Na2O_ppm
Count
20 bins 0.133 wide [Logged]

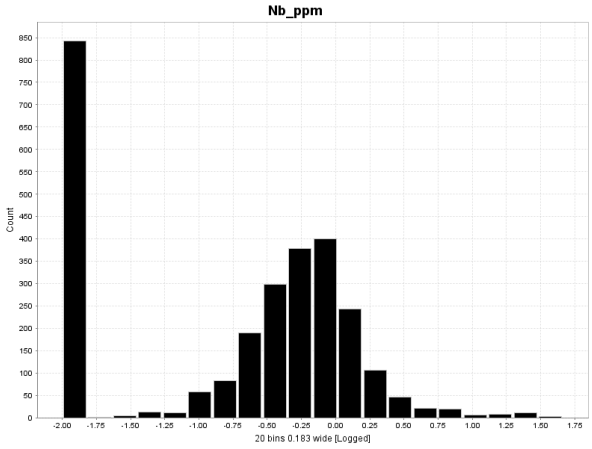
Nb_ppm
Count
20 bins 0.183 wide [Logged]

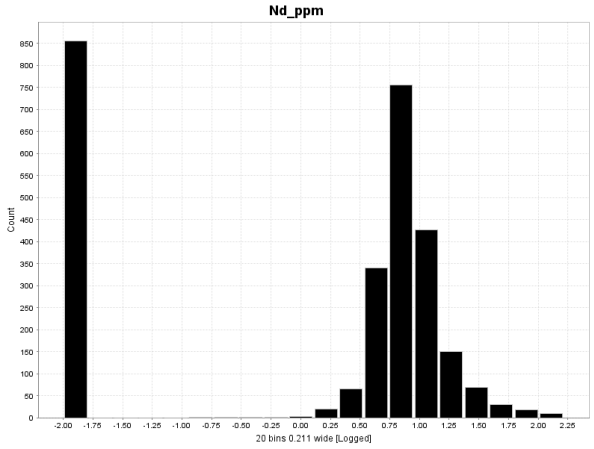
Nd_ppm
Count
20 bins 0.211 wide [Logged]

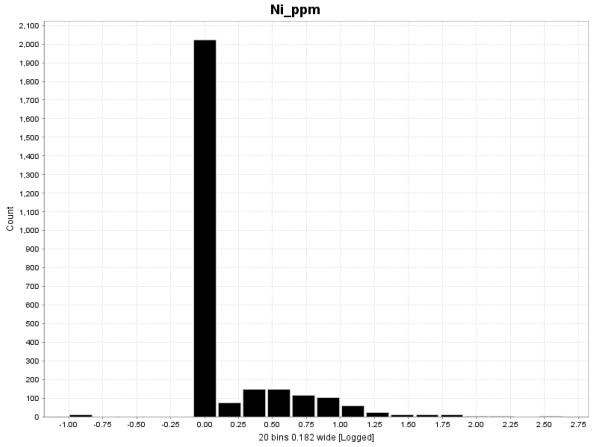
Ni_ppm
Count
20 bins 0.182 wide [Logged]

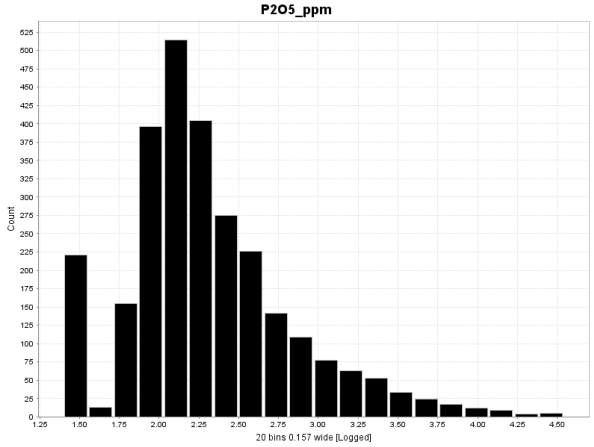
P2O5_ppm
Count
20 bins 0.157 wide [Logged]

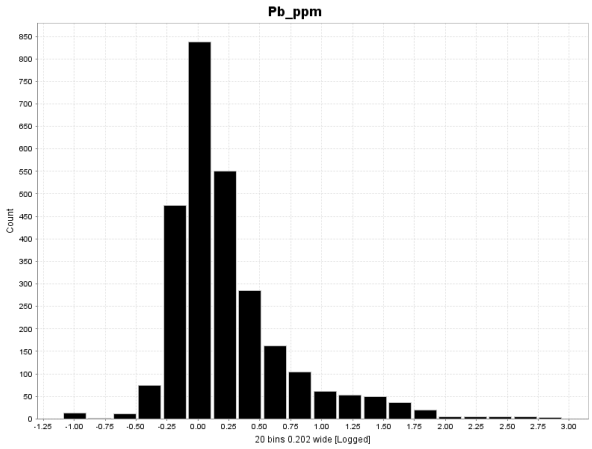
Pb_ppm
Count
20 bins 0.202 wide [Logged]

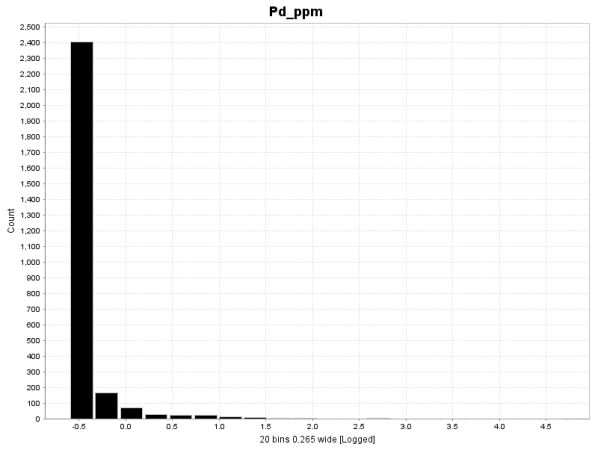
Pd_ppm
Count
20 bins 0.265 wide [Logged]

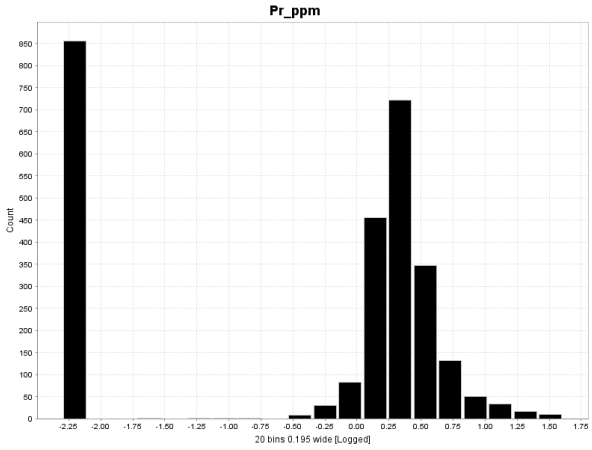
Pr_ppm
Count
20 bins 0.195 wide [Logged]

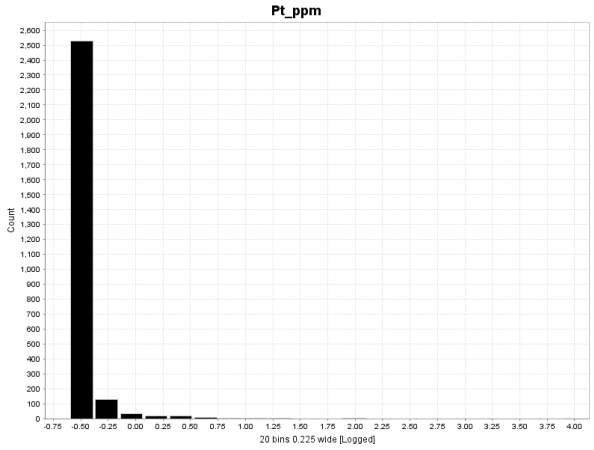
Pt_ppm
Count
20 bins 0.225 wide [Logged]

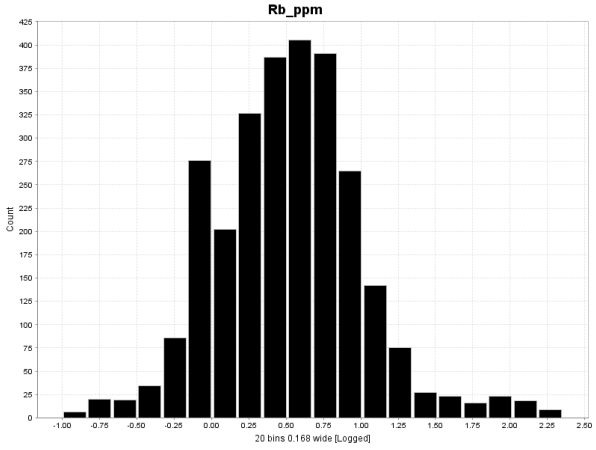
Rb_ppm
Count
20 bins 0.168 wide [Logged]

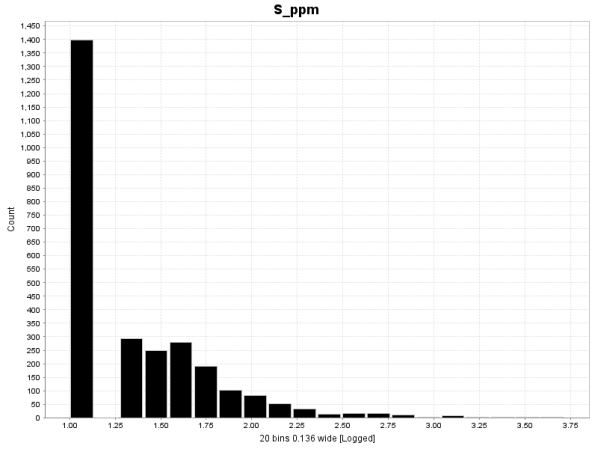
S_ppm
Count
20 bins 0.136 wide [Logged]

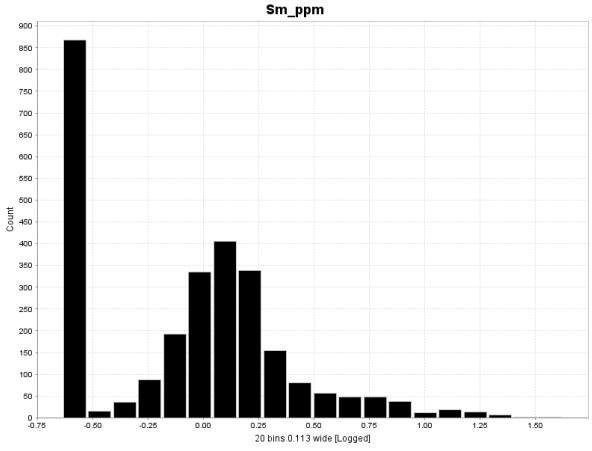
Sm_ppm
Count
20 bins 0.113 wide [Logged]

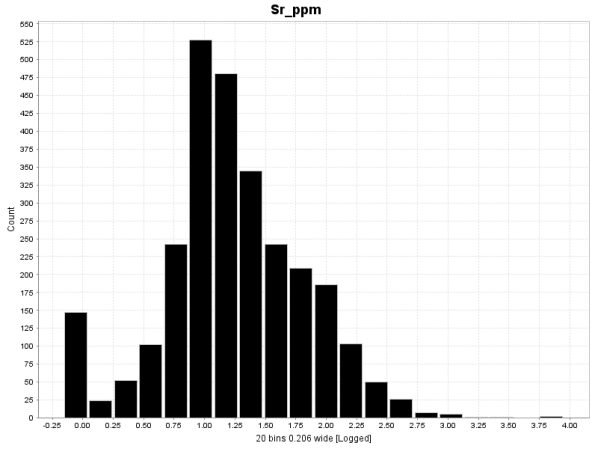
Sr_ppm
Count
20 bins 0.206 wide [Logged]

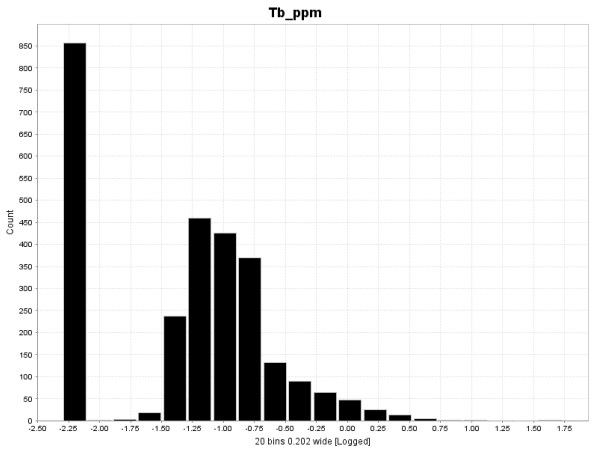
Tb_ppm
Count
20 bins 0.202 wide [Logged]

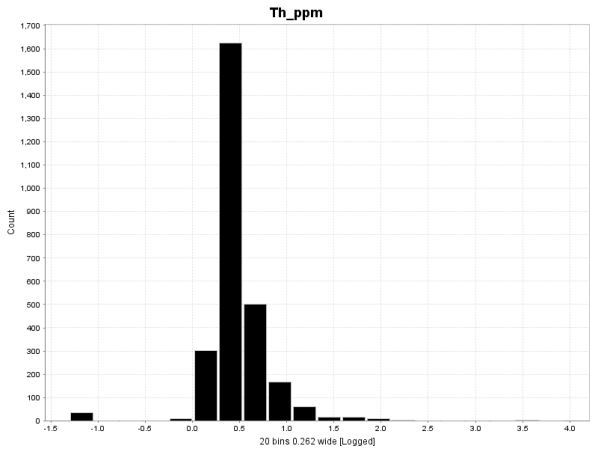
Th_ppm
Count
20 bins 0.262 wide [Logged]

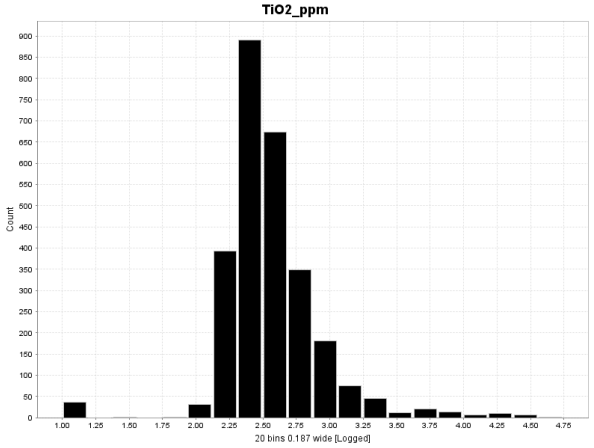
TiO2_ppm
Count
20 bins 0.187 wide [Logged]

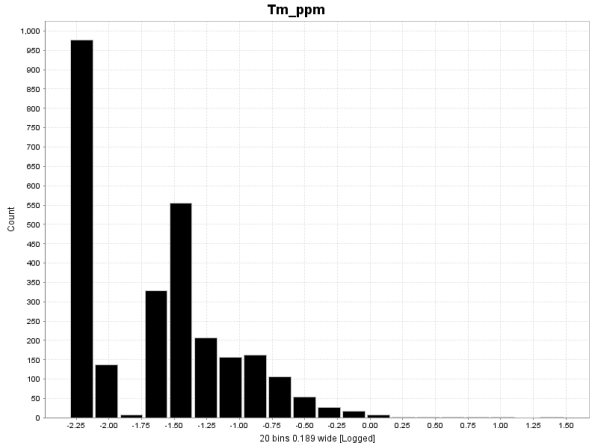
Tm_ppm
Count
20 bins 0.189 wide [Logged]

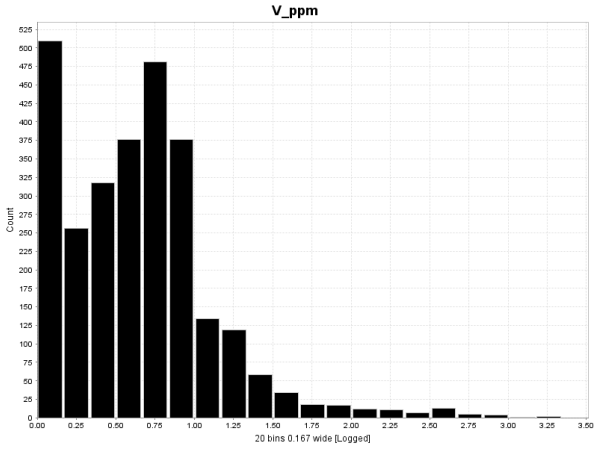
V_ppm
Count
20 bins 0.167 wide [Logged]

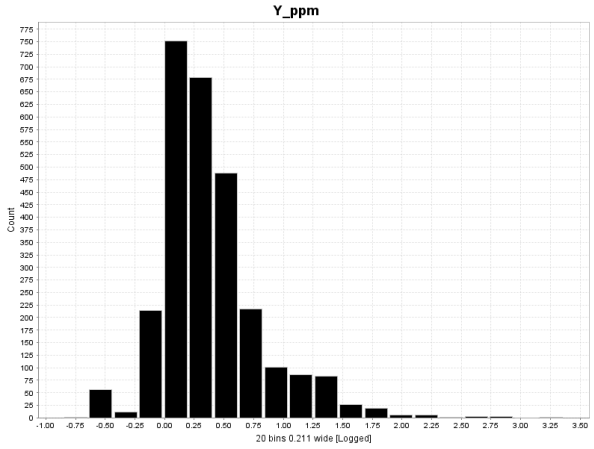
Y_ppm
Count
20 bins 0.211 wide [Logged]

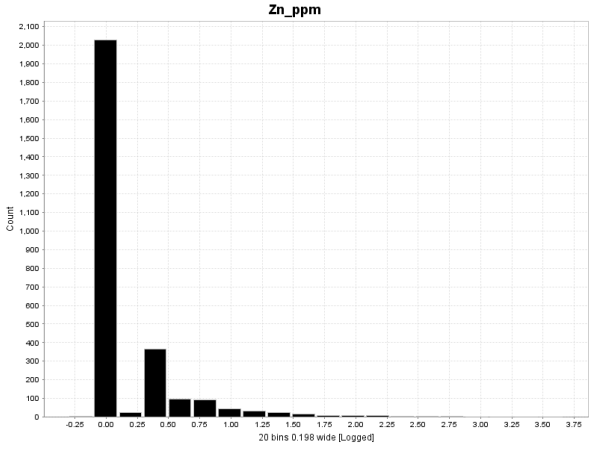
Zn_ppm
Count
20 bins 0.198 wide [Logged]

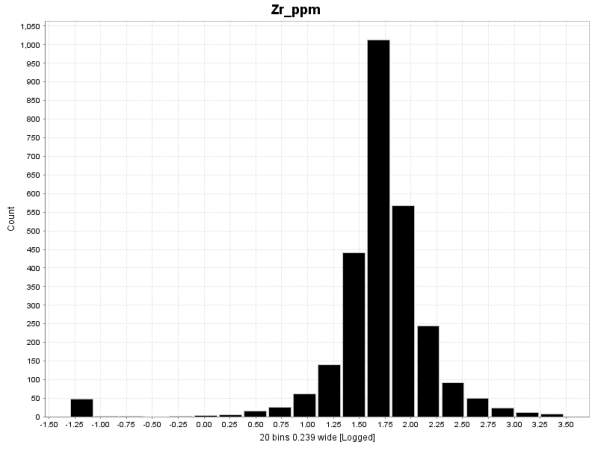
Zr_ppm
Count
20 bins 0.239 wide [Logged]

Appendix 4 – Probability plots for each element

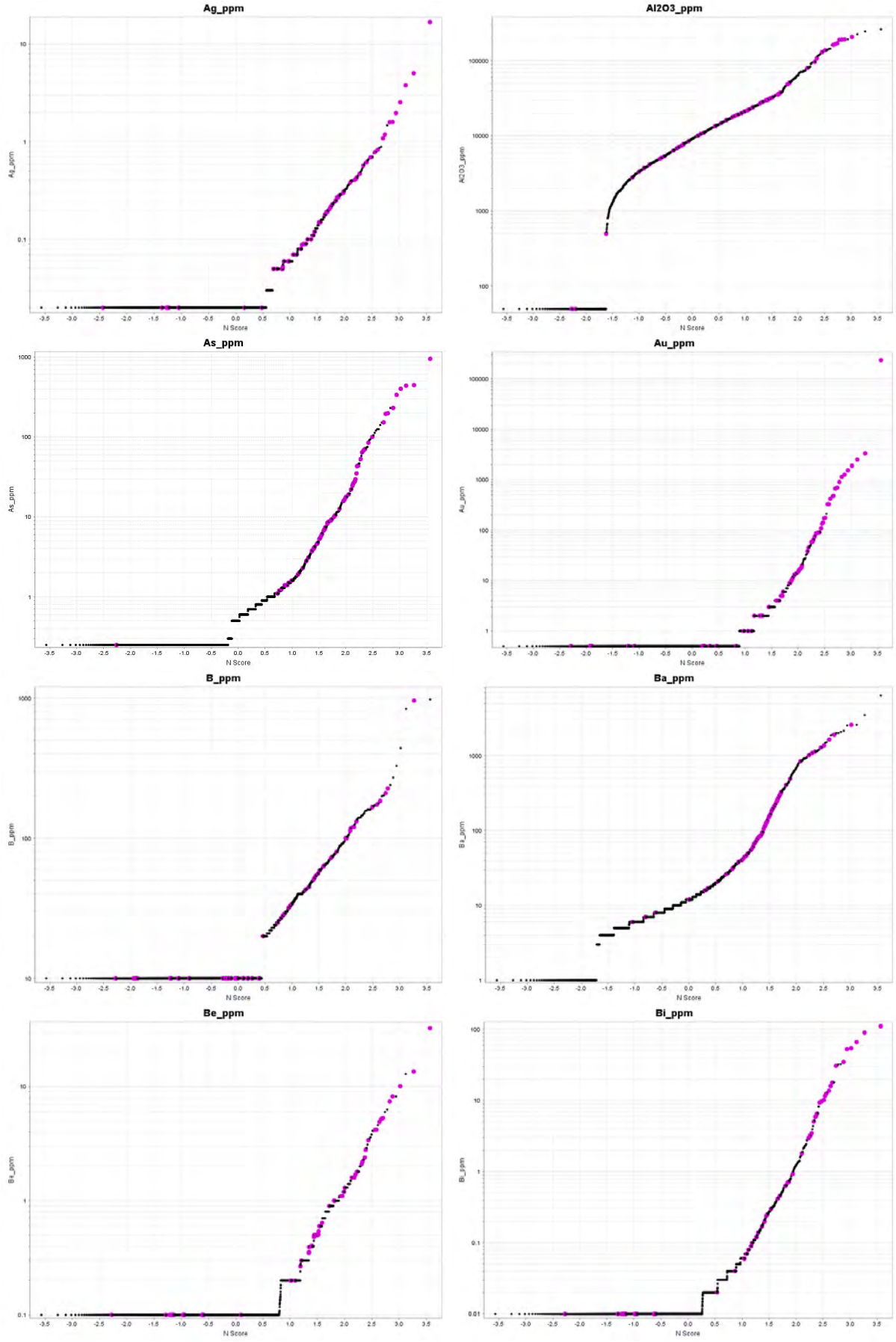

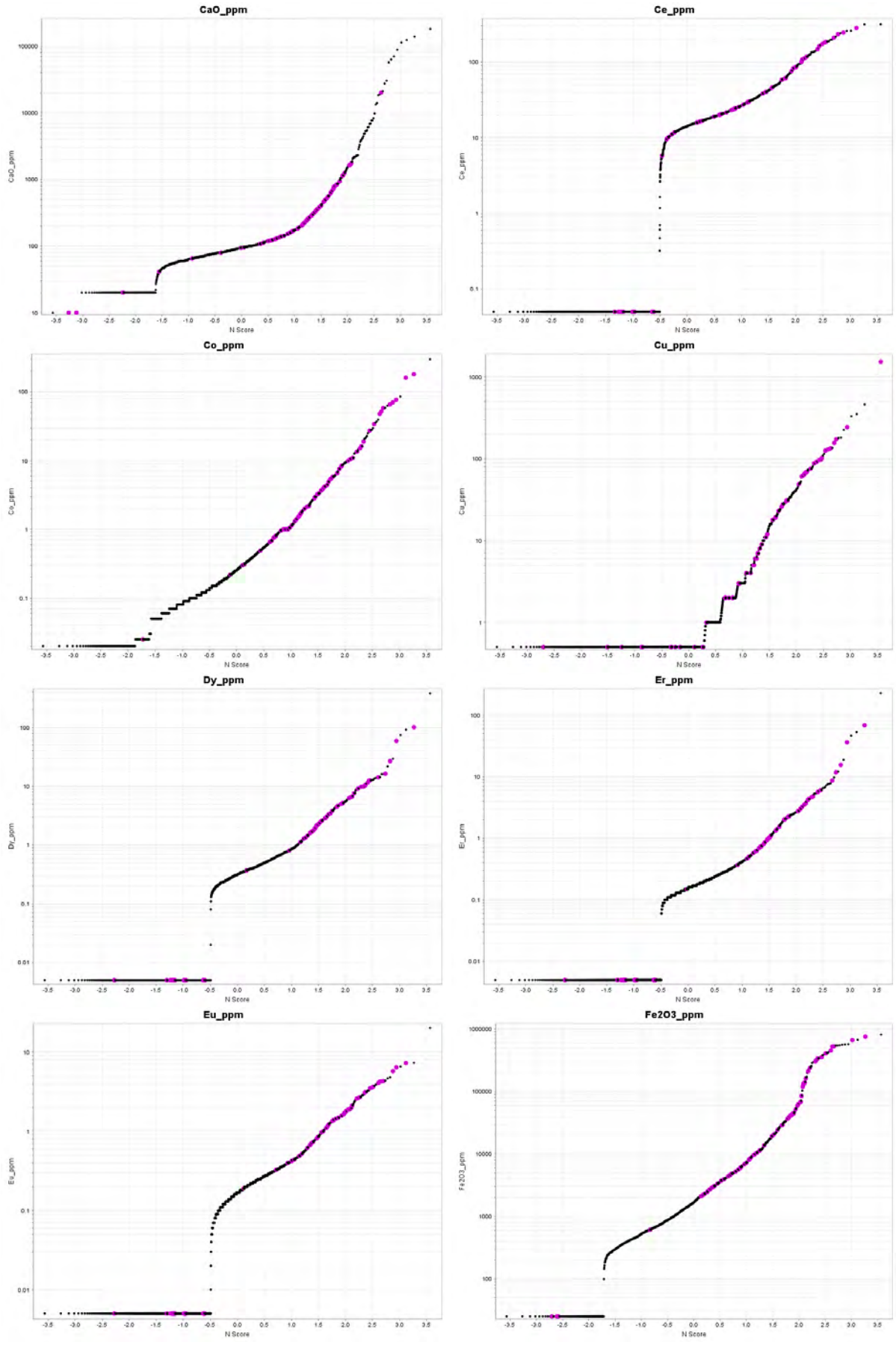
CaO_ppm
Ce_ppm
Co_ppm
Cu_ppm
Dy_ppm
Er_ppm
Eu_ppm
Fe2O3_ppm
N Score

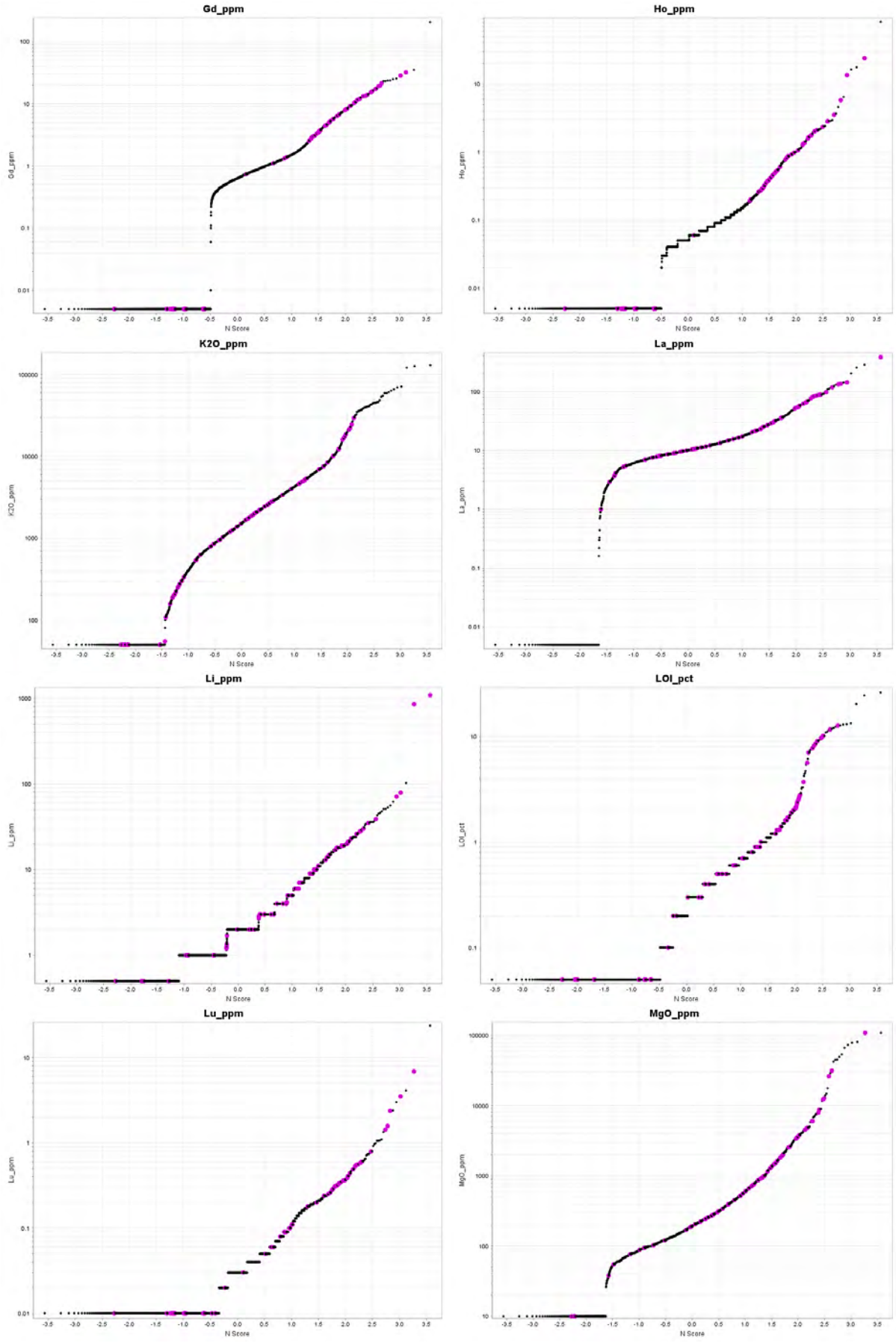
Gd_ppm
Gd_ppm
N Score
Ho_ppm
Ho_ppm
N Score
K2O_ppm
K2O_ppm
N Score
La_ppm
La_ppm
N Score
Li_ppm
Li_ppm
N Score
LOI_pct
LOI_pct
N Score
Lu_ppm
Lu_ppm
N Score
MgO_ppm
MgO_ppm
N Score

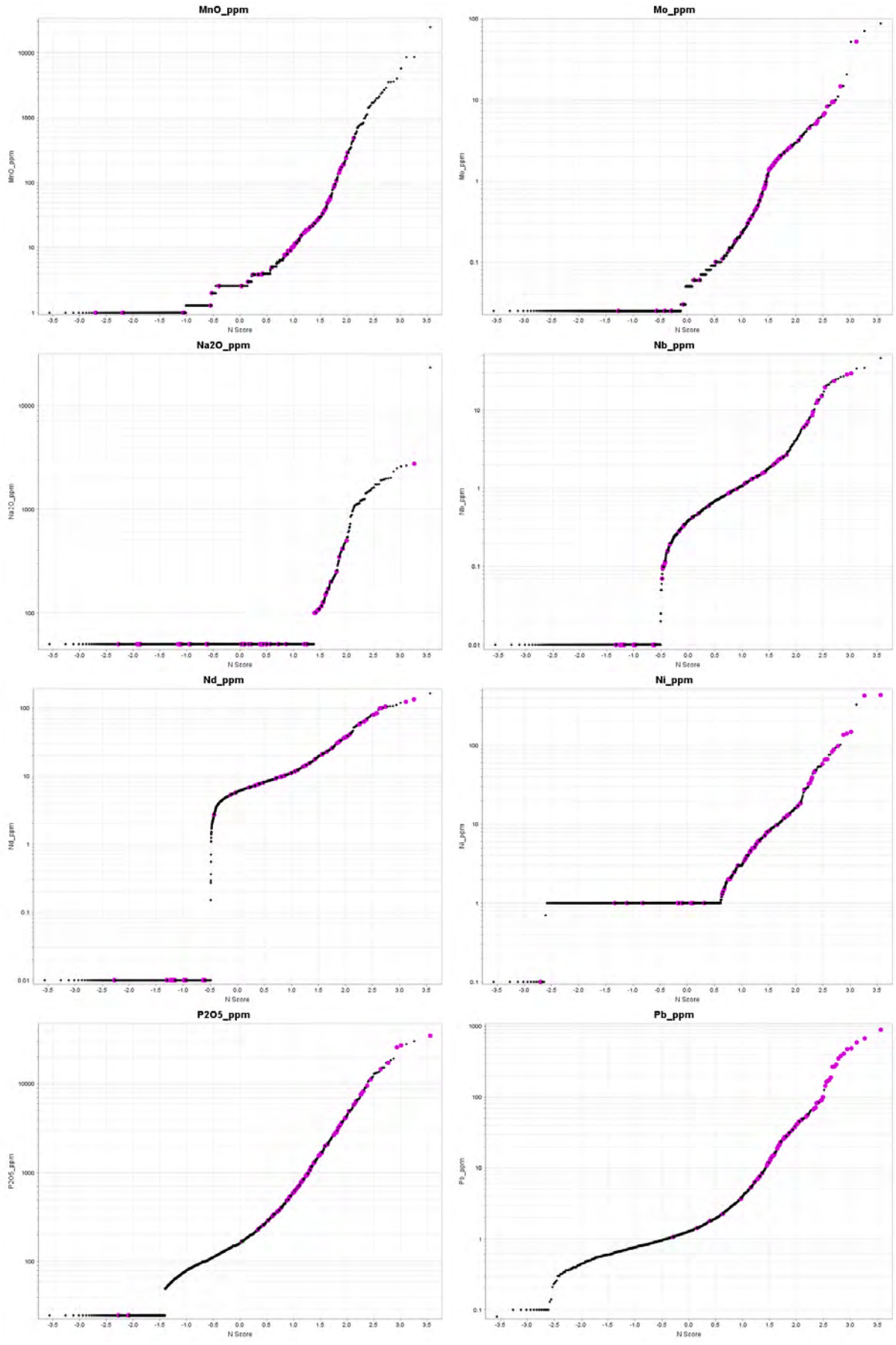
MnO_ppm
Mo_ppm
Na2O_ppm
Nb_ppm
Nd_ppm
Ni_ppm
P2O5_ppm
Pb_ppm
N Score

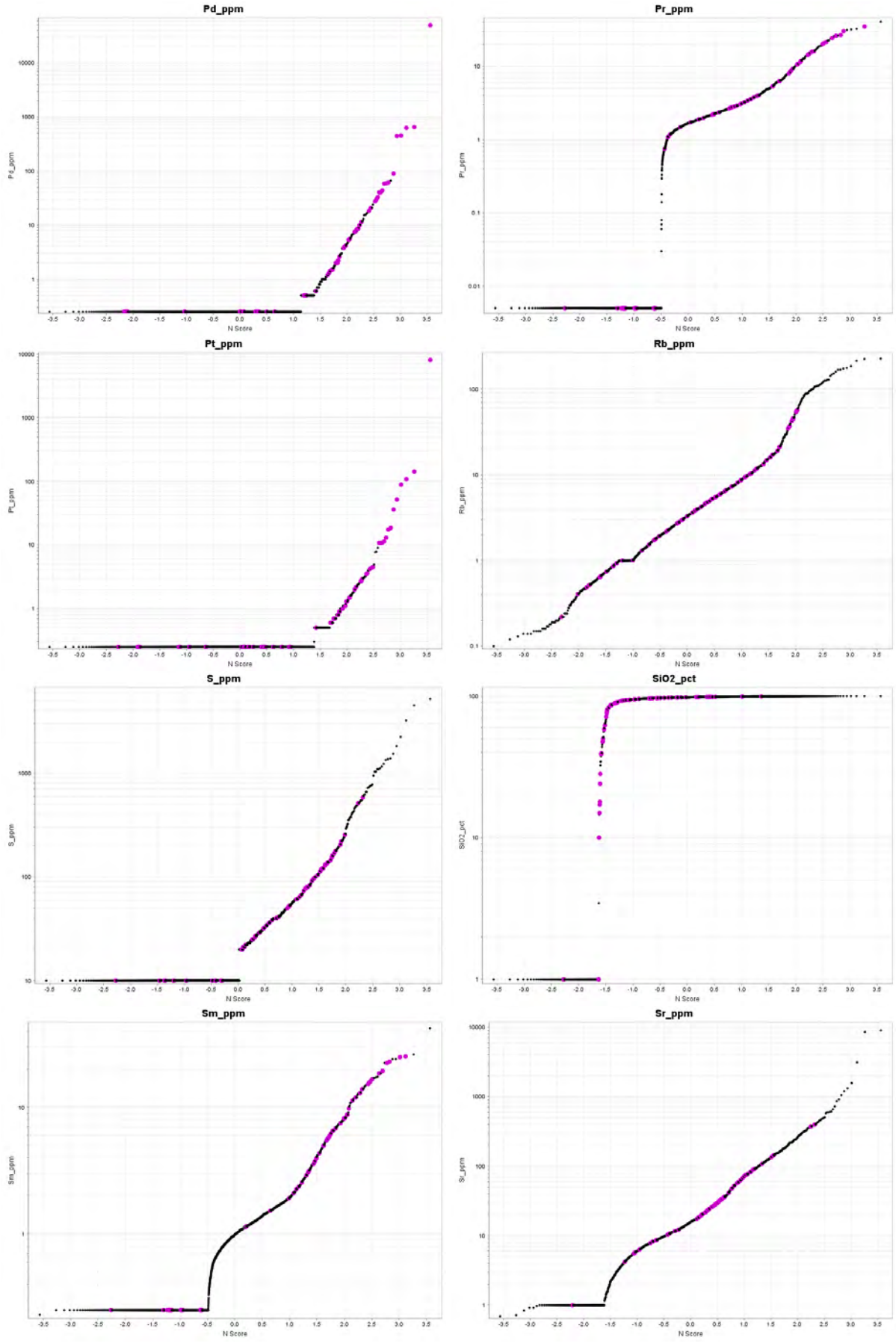
Pd_ppm
Pr_ppm
Pt_ppm
Rb_ppm
S_ppm
SiO2_pct
Sm_ppm
Sr_ppm
N Score

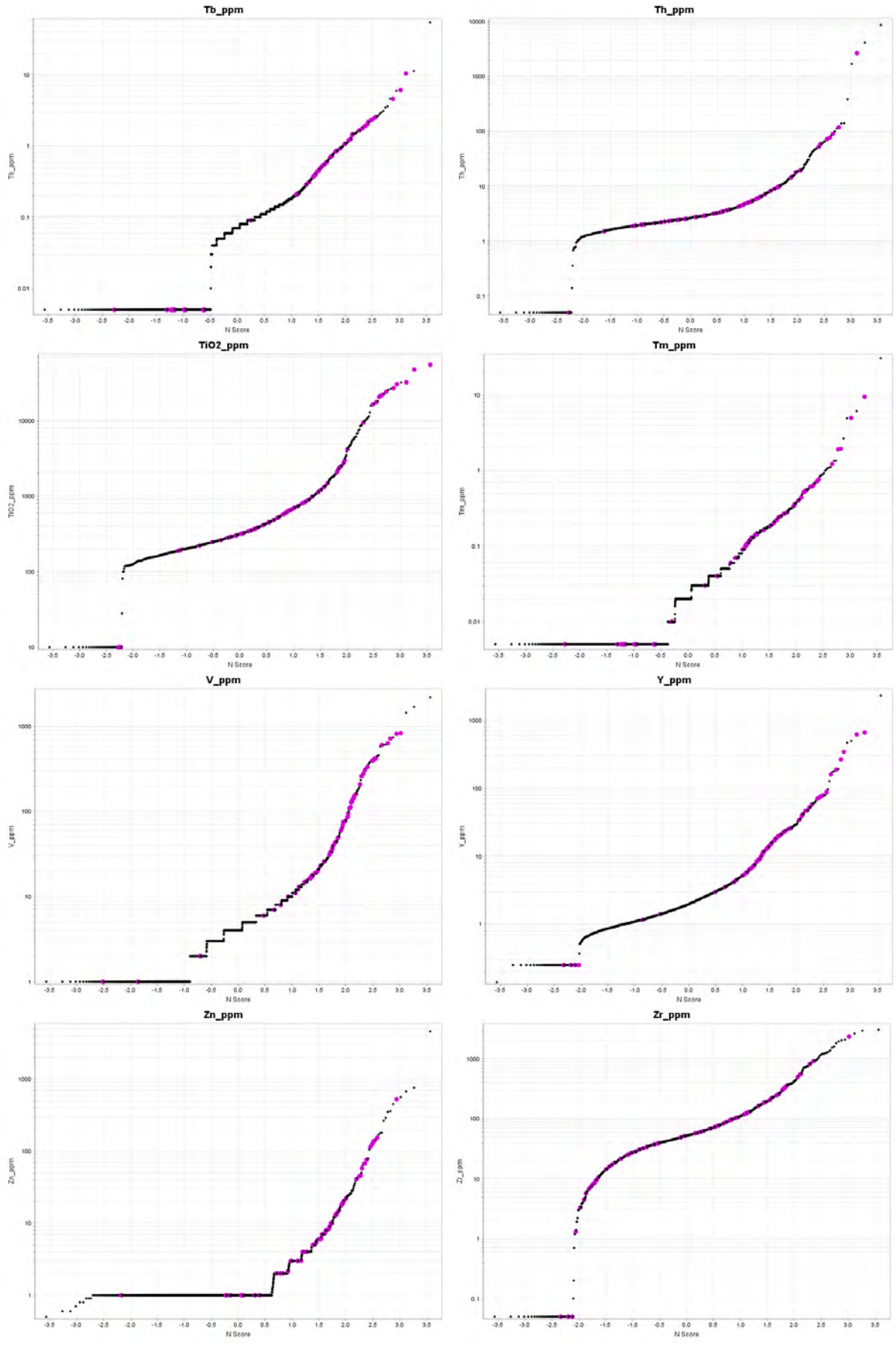
Tb_ppm
Th_ppm
TiO2_ppm
Tm_ppm
V_ppm
Y_ppm
Zn_ppm
Zr_ppm
N Score

Appendix 5 – Scatter Plots for all elements

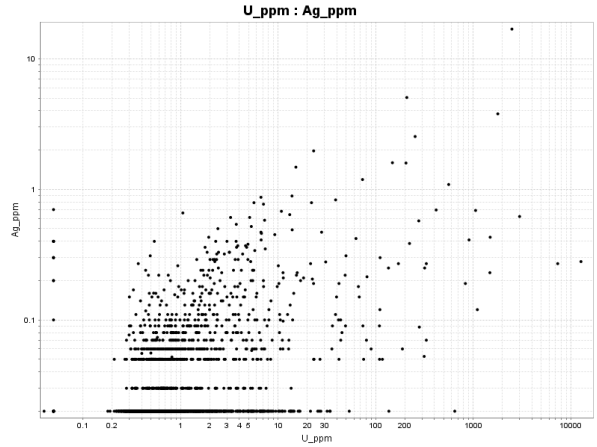

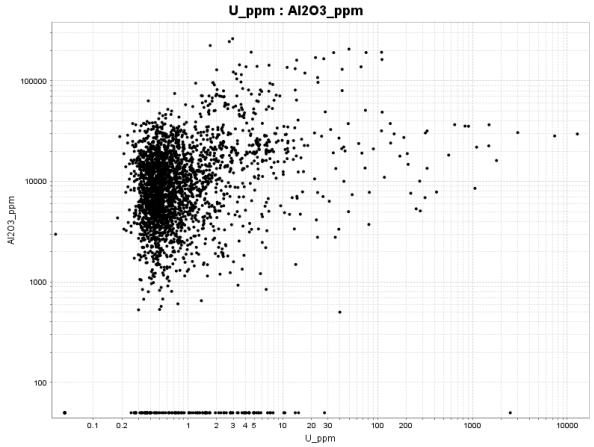

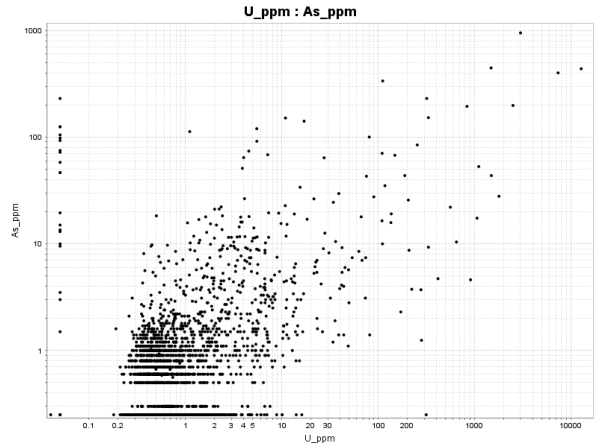

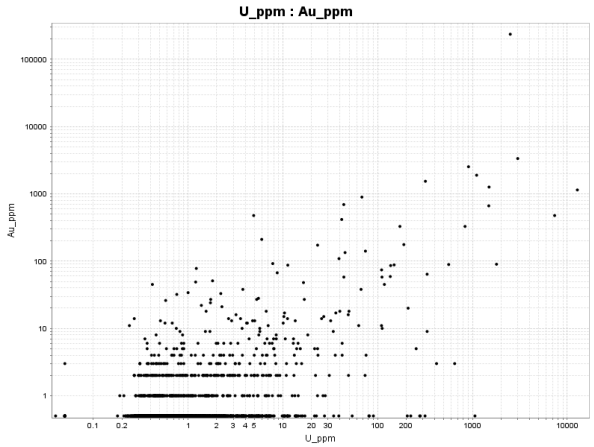

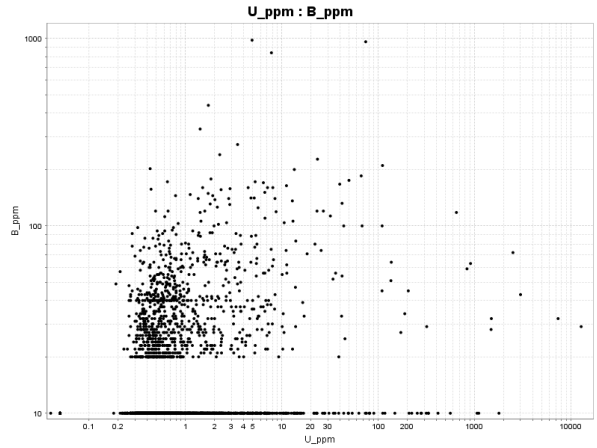

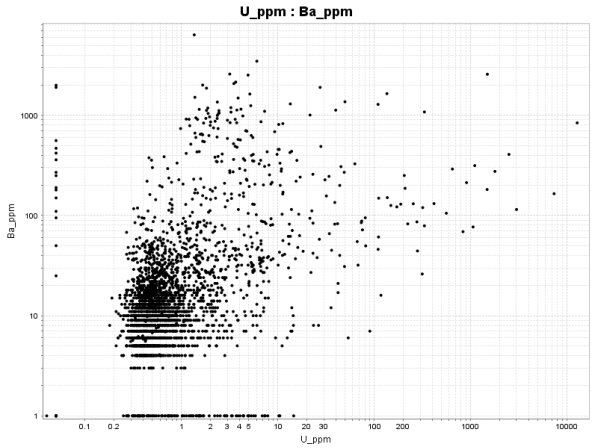

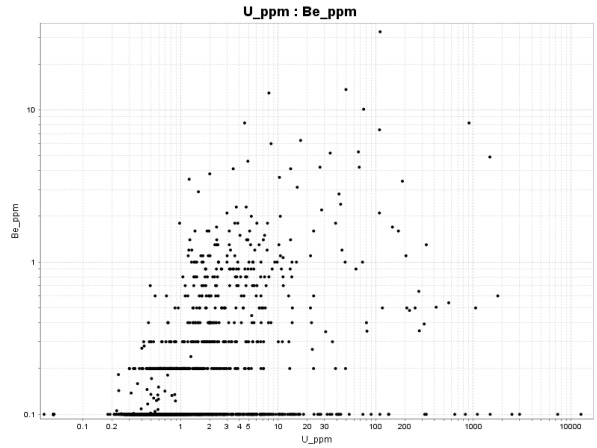

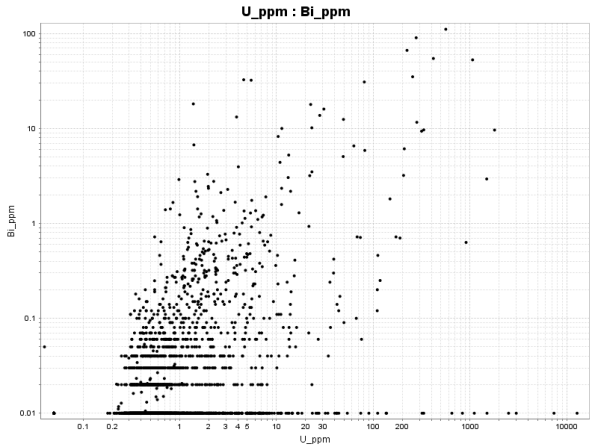

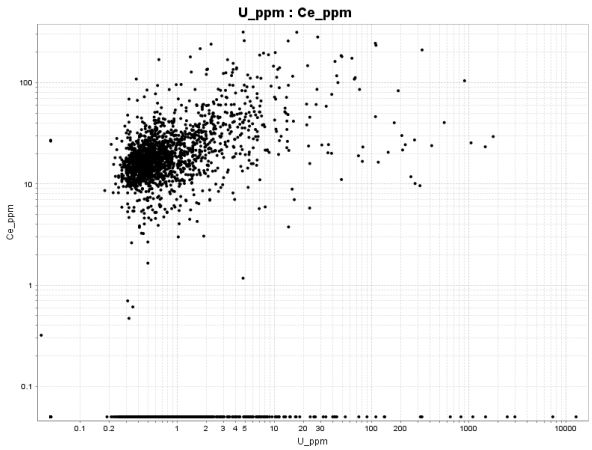
U_ppm : Ce_ppm
Ce_ppm
U_ppm

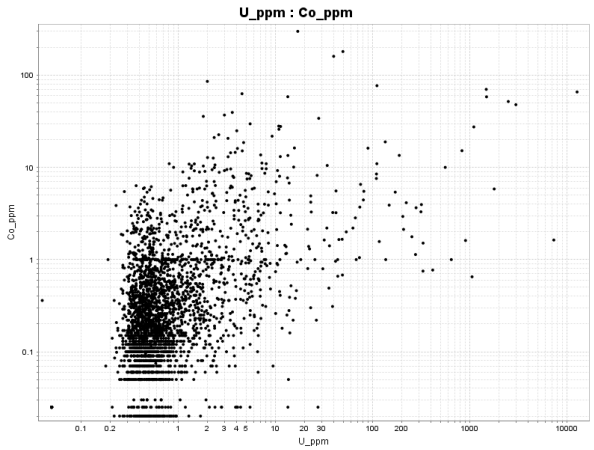
U_ppm : Co_ppm
Co_ppm
U_ppm

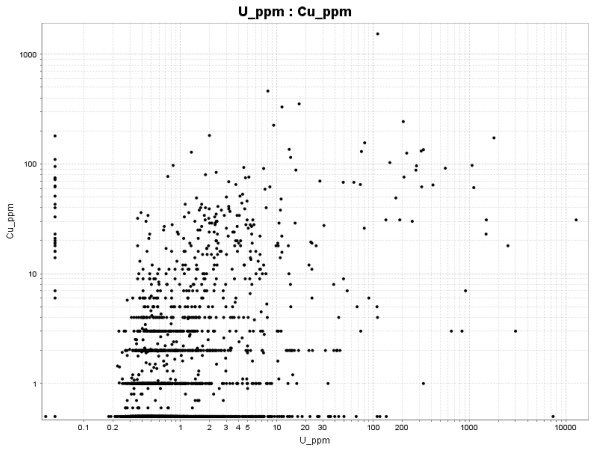
U_ppm : Cu_ppm
Cu_ppm
U_ppm

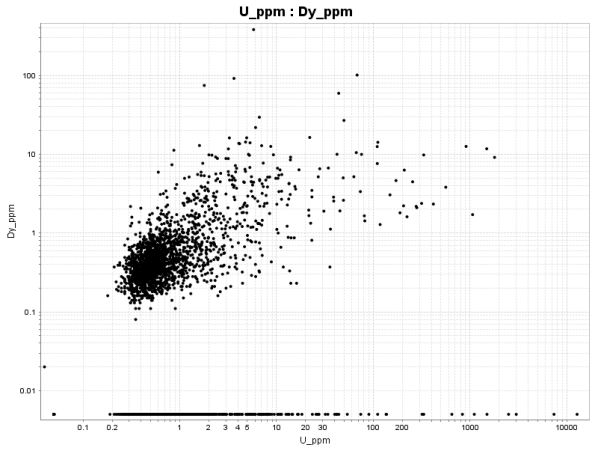
U_ppm : Dy_ppm
Dy_ppm
U_ppm

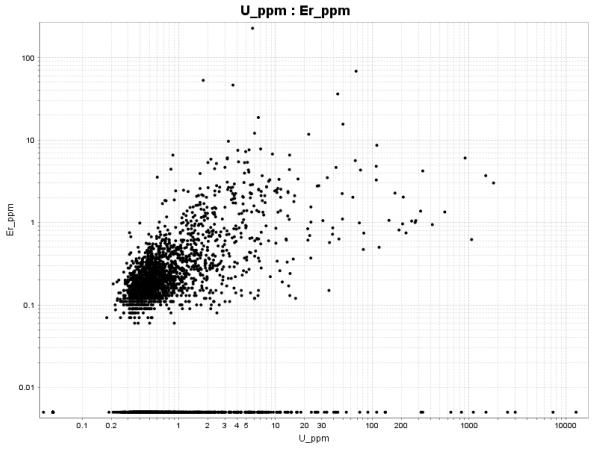
U_ppm : Er_ppm
Er_ppm
U_ppm

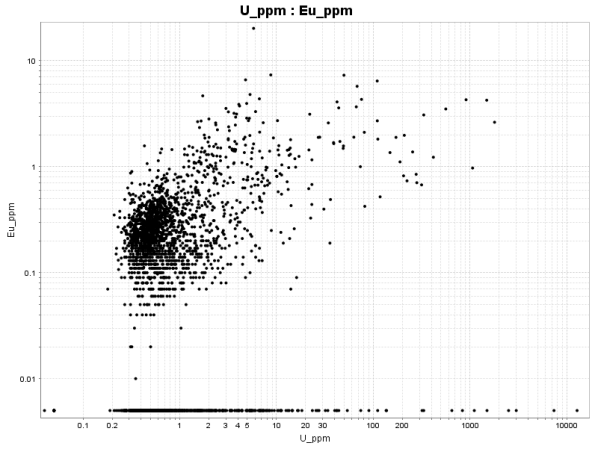
U_ppm : Eu_ppm
Eu_ppm
U_ppm

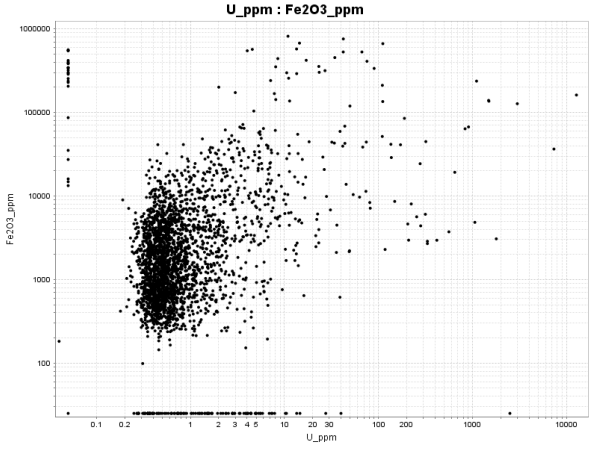
U_ppm : Fe2O3_ppm
Fe2O3_ppm
U_ppm

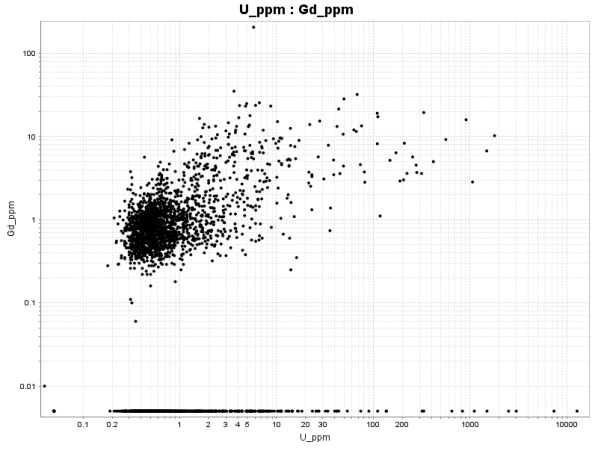
U_ppm : Gd_ppm
Gd_ppm
U_ppm

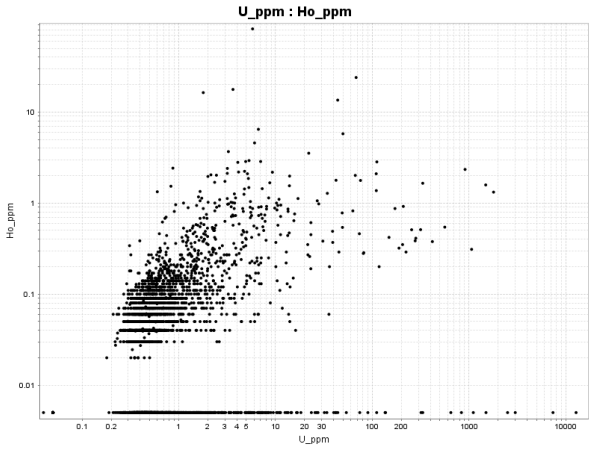
U_ppm : Ho_ppm
Ho_ppm
U_ppm

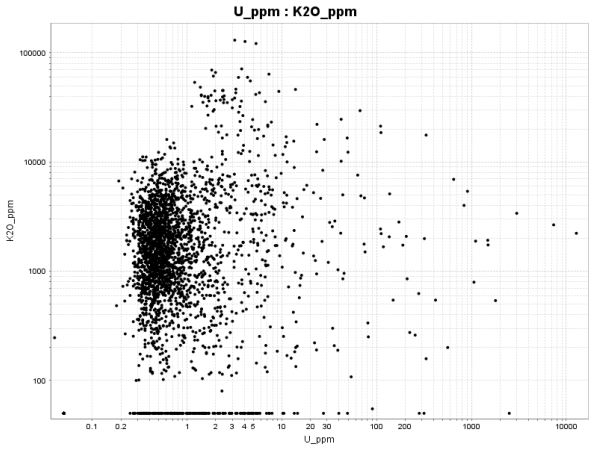
U_ppm : K2O_ppm
K2O_ppm
U_ppm

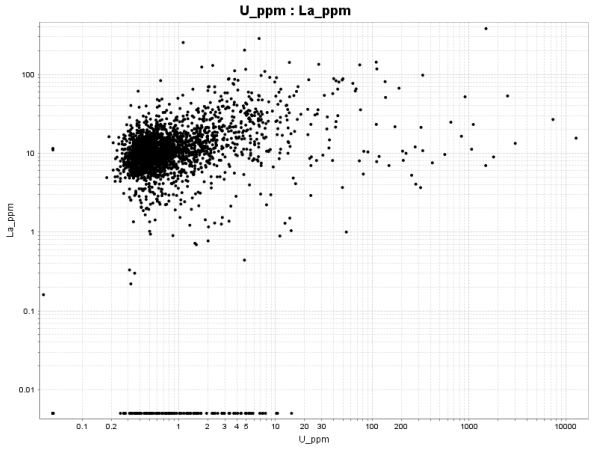
U_ppm : La_ppm
La_ppm
U_ppm

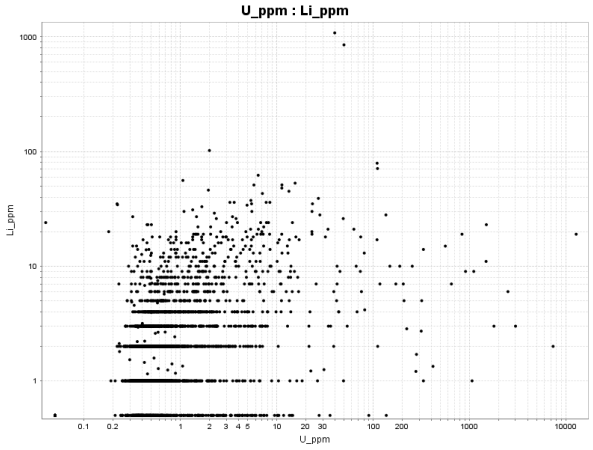
U_ppm : Li_ppm
Li_ppm
U_ppm

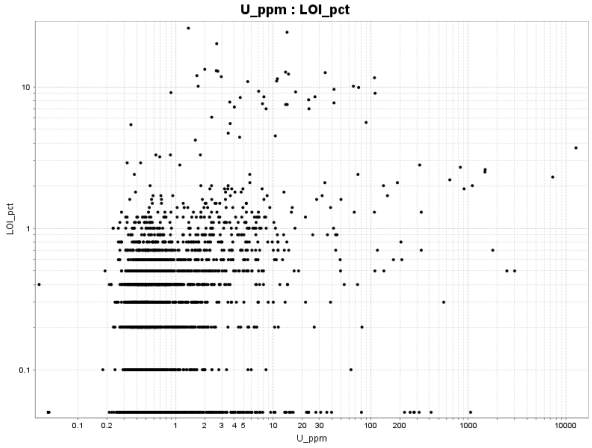
U_ppm : LOI_pct
LOI_pct
U_ppm

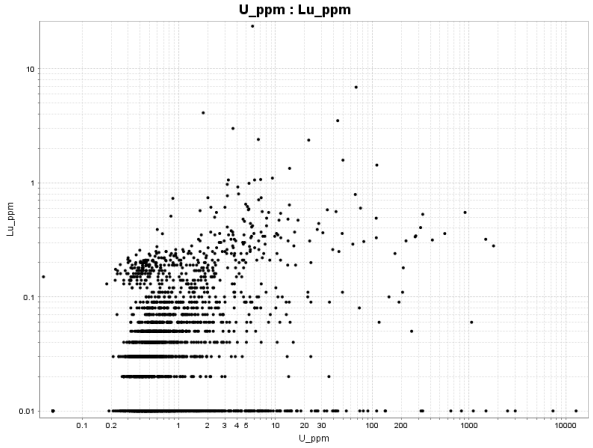
U_ppm : Lu_ppm
Lu_ppm
U_ppm

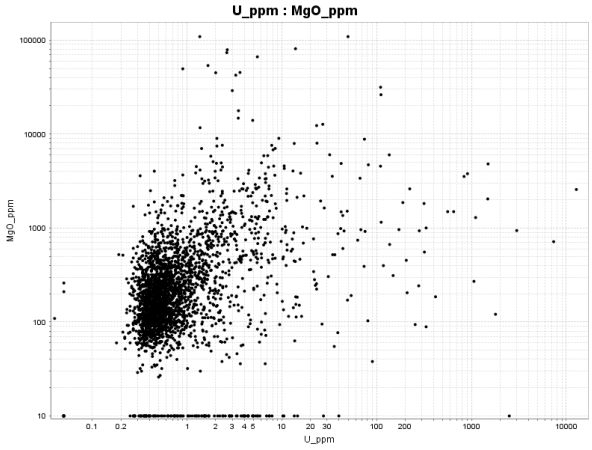
U_ppm : MgO_ppm
MgO_ppm
U_ppm

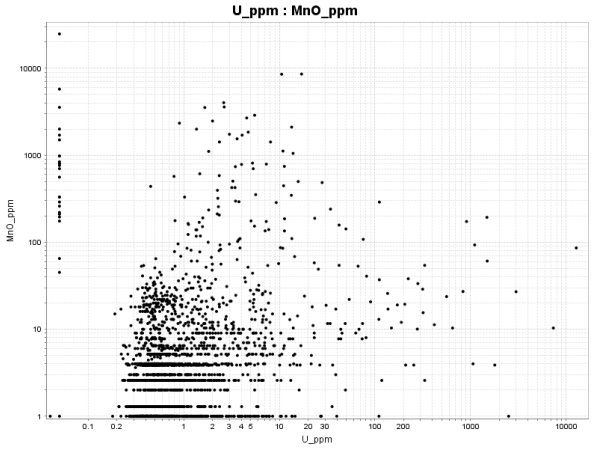
U_ppm : MnO_ppm
MnO_ppm
U_ppm

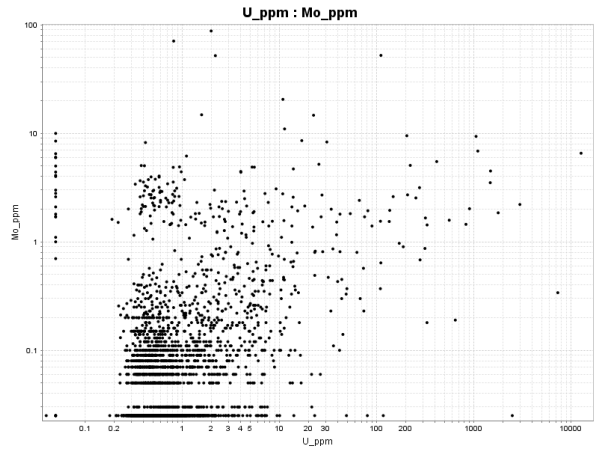
U_ppm : Mo_ppm
Mo_ppm
U_ppm

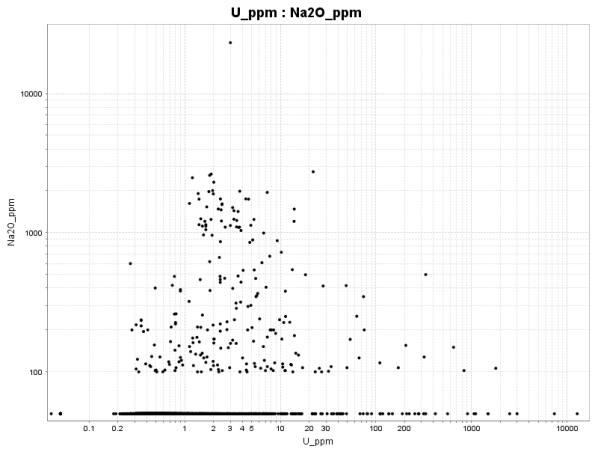
U_ppm : Na2O_ppm
Na2O_ppm
U_ppm

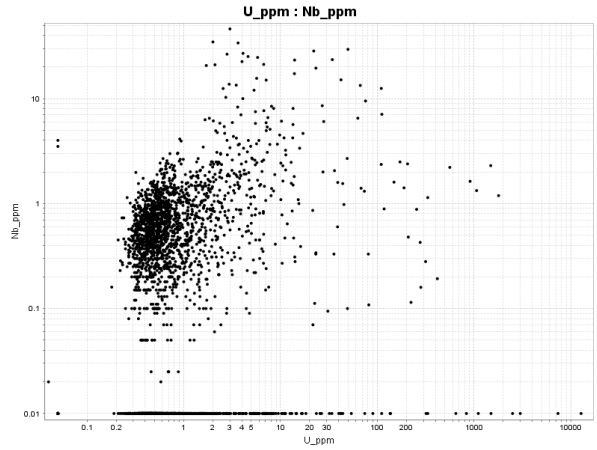
U_ppm : Nb_ppm
Nb_ppm
U_ppm

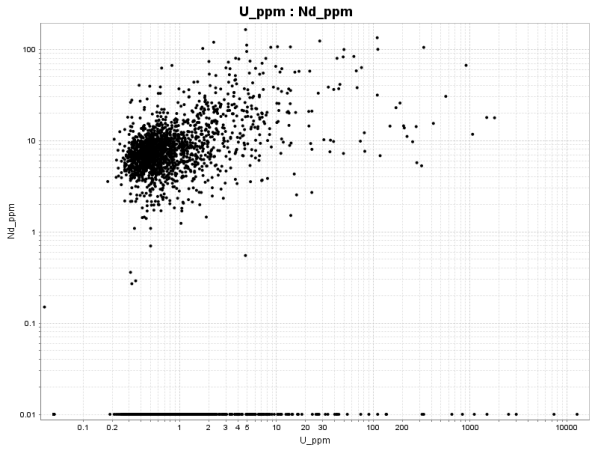
U_ppm : Nd_ppm
Nd_ppm
U_ppm

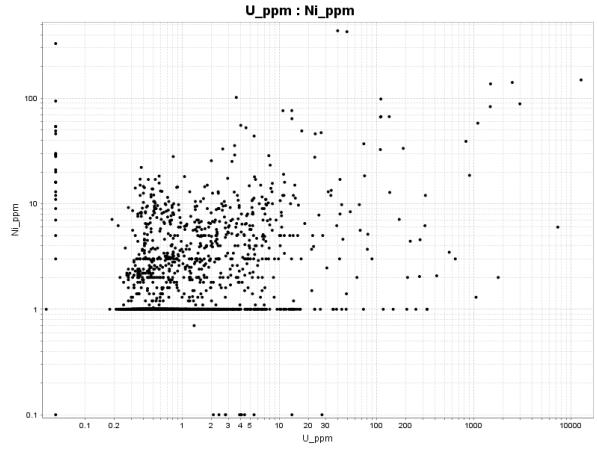
U_ppm : Ni_ppm
Ni_ppm
U_ppm

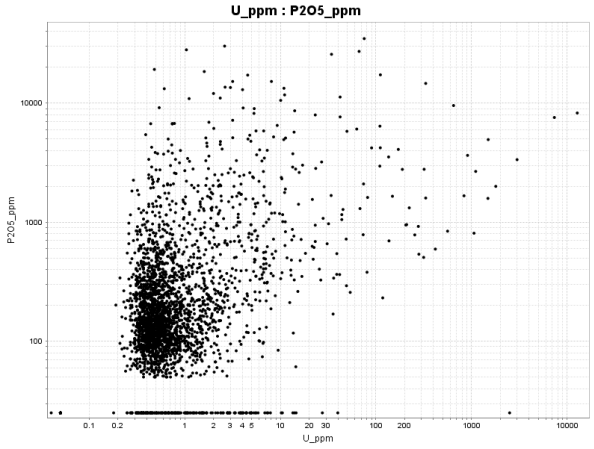
U_ppm : P2O5_ppm
P2O5_ppm
U_ppm

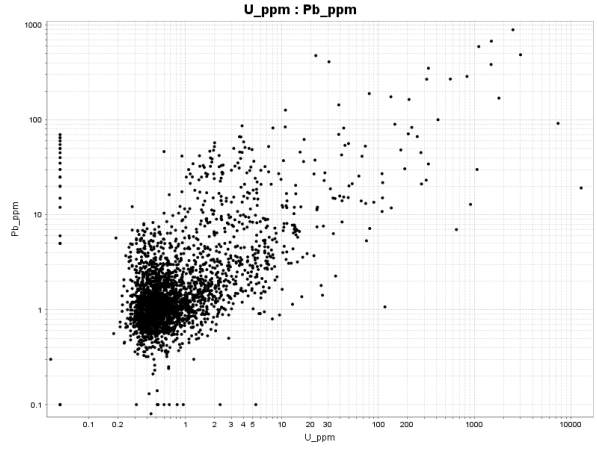
U_ppm : Pb_ppm
Pb_ppm
U_ppm

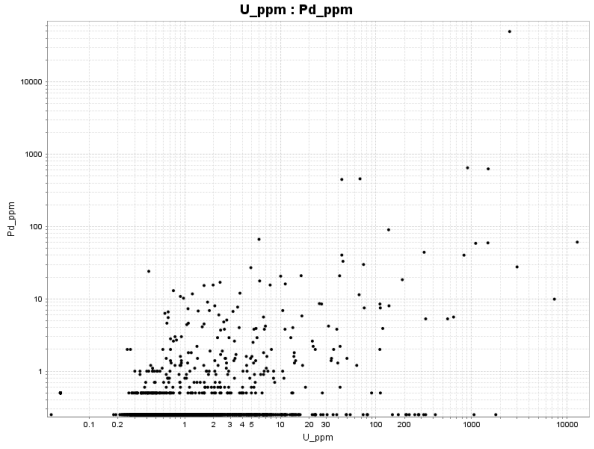
U_ppm : Pd_ppm
Pd_ppm
U_ppm

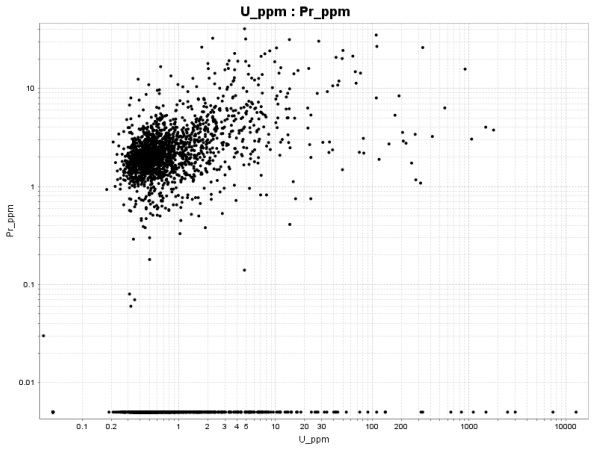
U_ppm : Pr_ppm
Pr_ppm
U_ppm

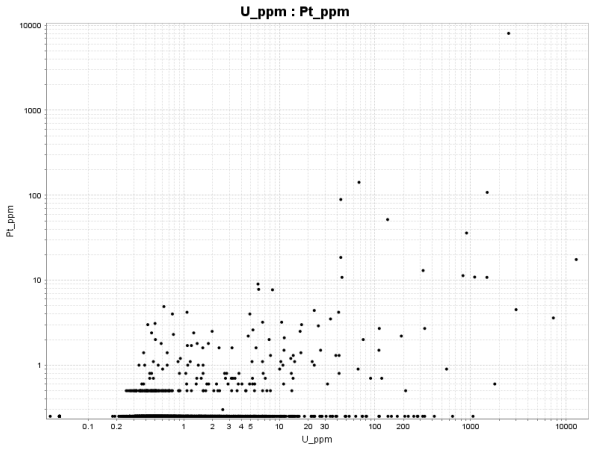
U_ppm : Pt_ppm
Pt_ppm
U_ppm

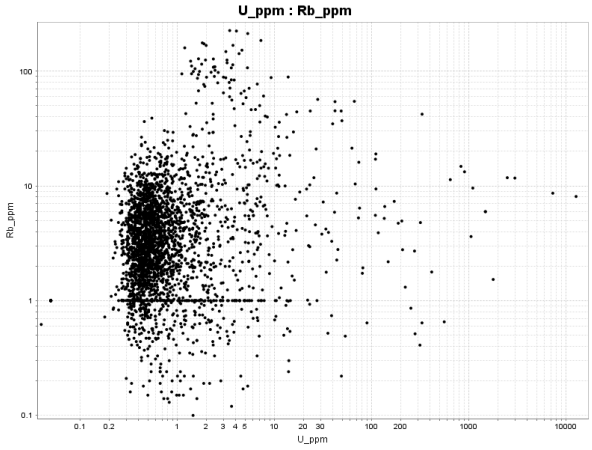
U_ppm : Rb_ppm
Rb_ppm
U_ppm

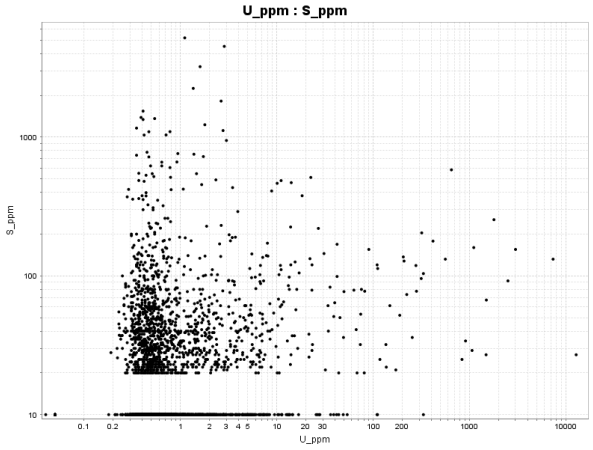
U_ppm : S_ppm
S_ppm
U_ppm

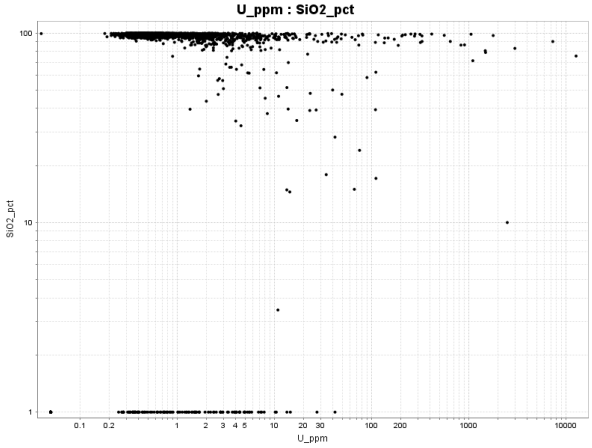
U_ppm : SiO2_pct
SiO2_pct
U_ppm

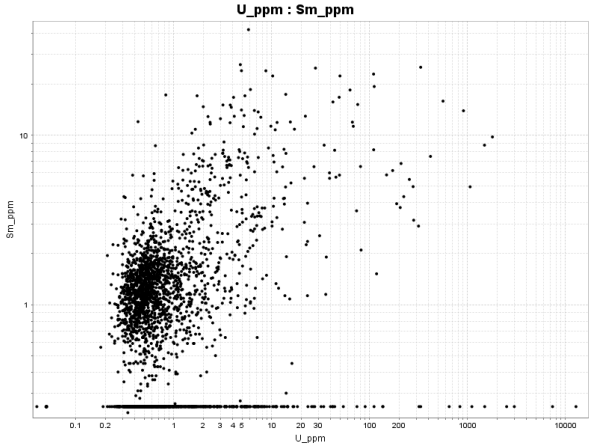
U_ppm : Sm_ppm
Sm_ppm
U_ppm

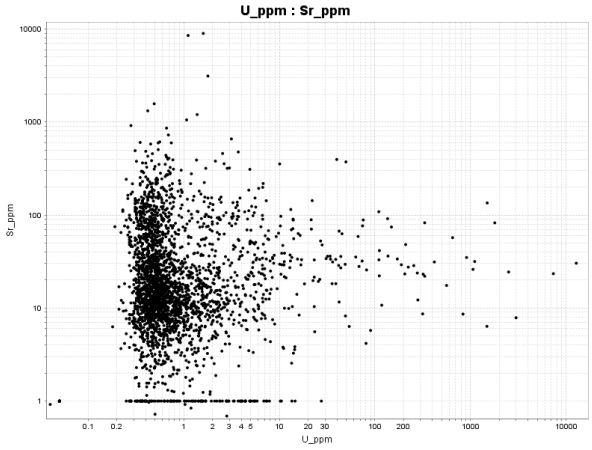
U_ppm : Sr_ppm
Sr_ppm
U_ppm

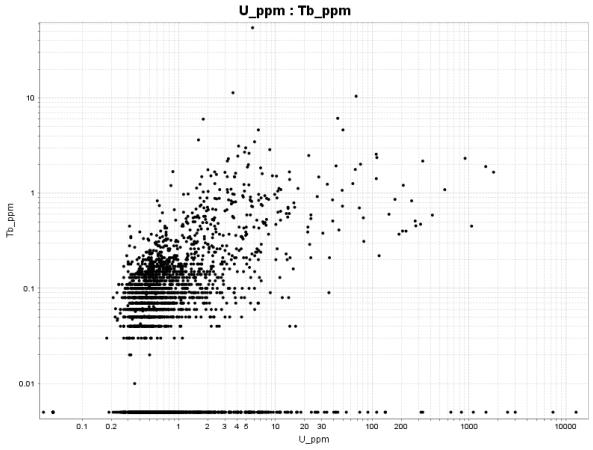
U_ppm : Tb_ppm
Tb_ppm
U_ppm

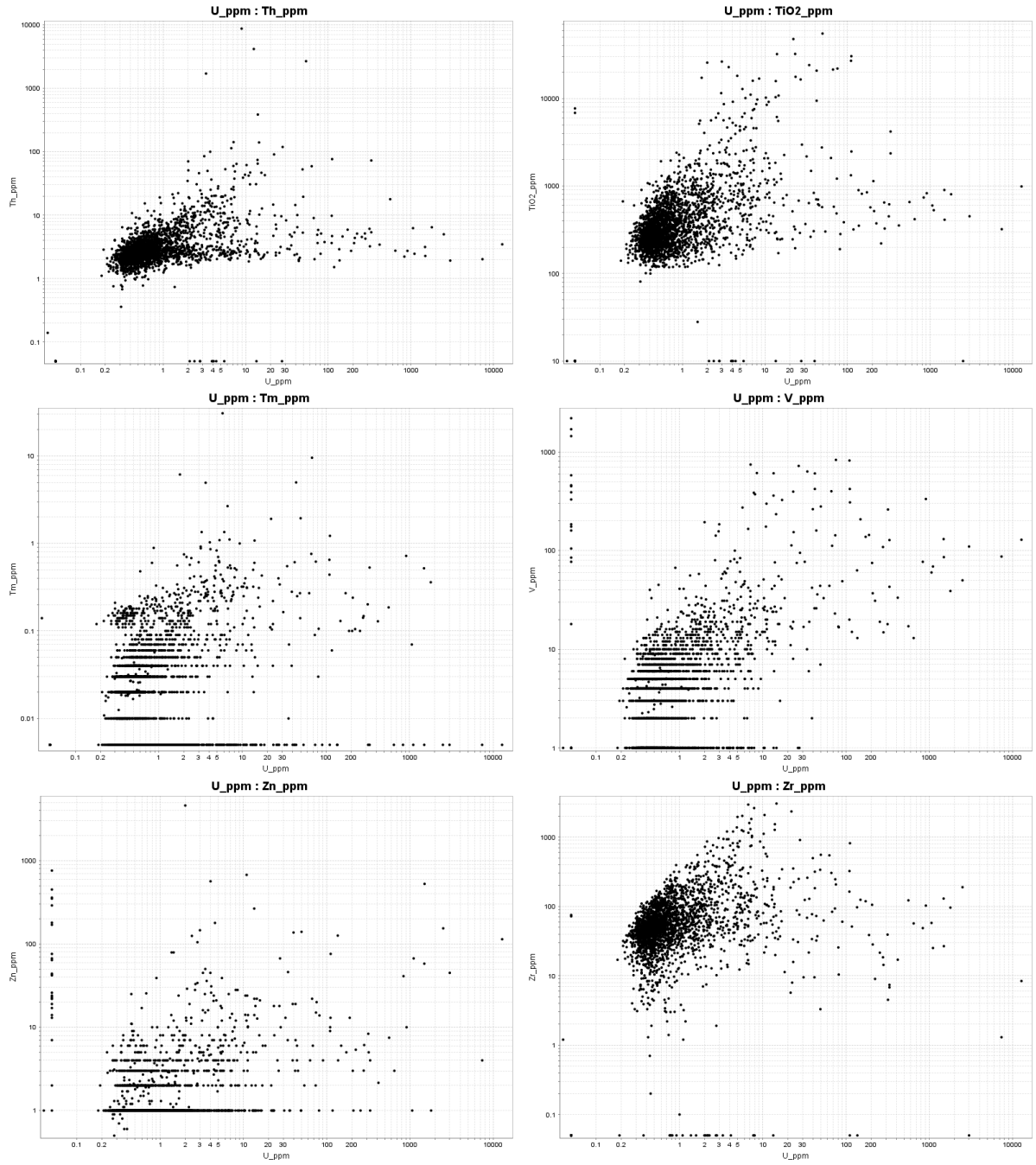
U_ppm : Th_ppm
Th_ppm
U_ppm
U_ppm : TiO2_ppm
TiO2_ppm
U_ppm
U_ppm : Tm_ppm
Tm_ppm
U_ppm
U_ppm : V_ppm
V_ppm
U_ppm
U_ppm : Zn_ppm
Zn_ppm
U_ppm
U_ppm : Zr_ppm
Zr_ppm
U_ppm

Appendix 6 – Scatter plots with CaO trend B highlighted

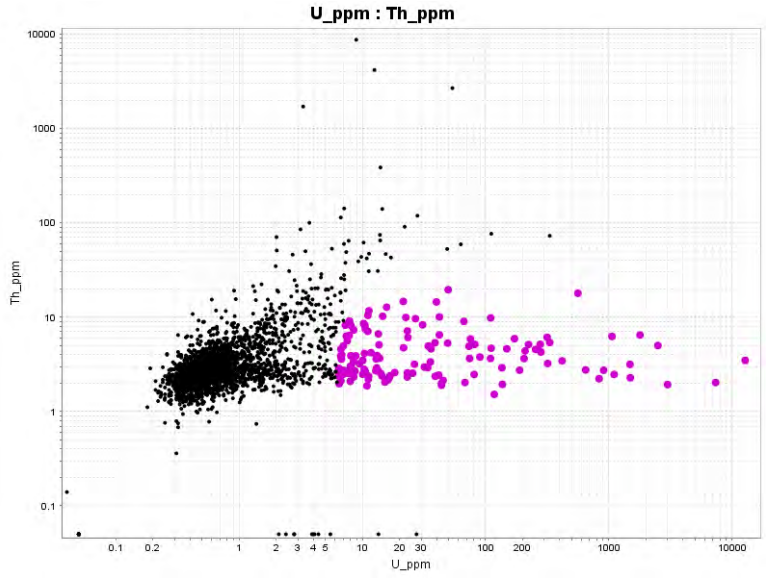

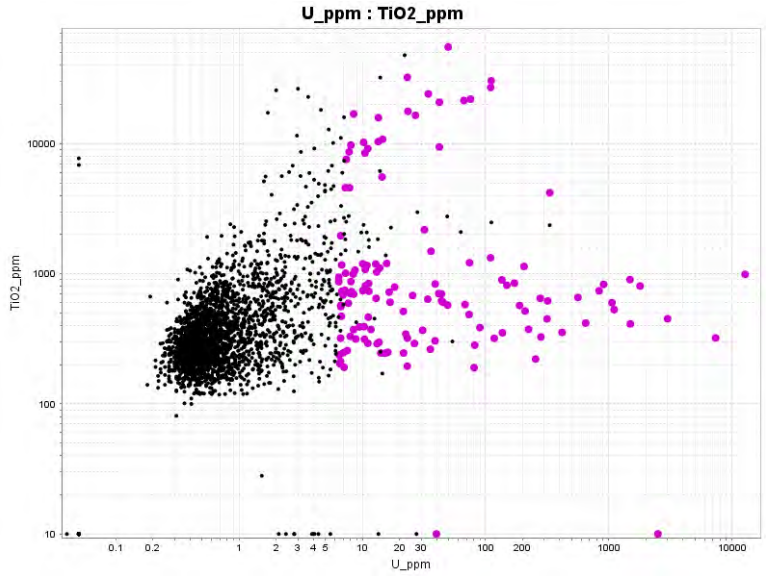

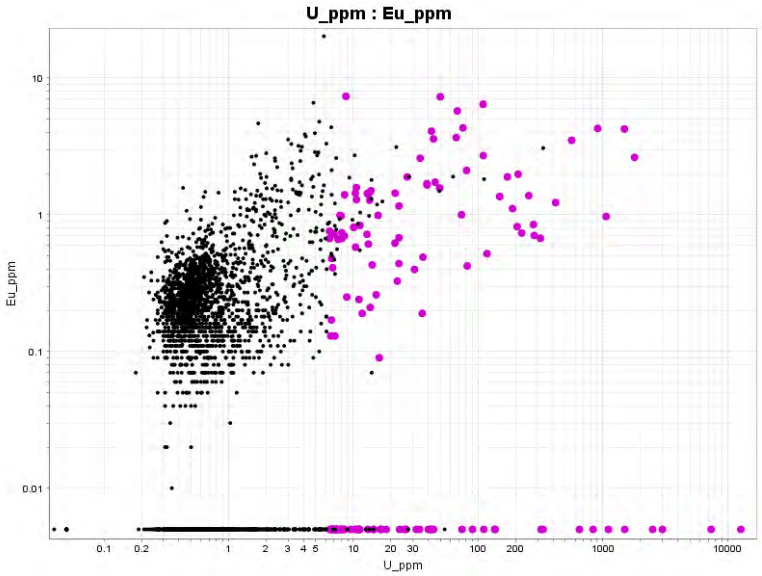
U_ppm : Eu_ppm
Eu_ppm
10
1
0.1
0.01
0.1 0.2 1 2 3 4 5 10 20 30 100 200 1000 10000
U_ppm

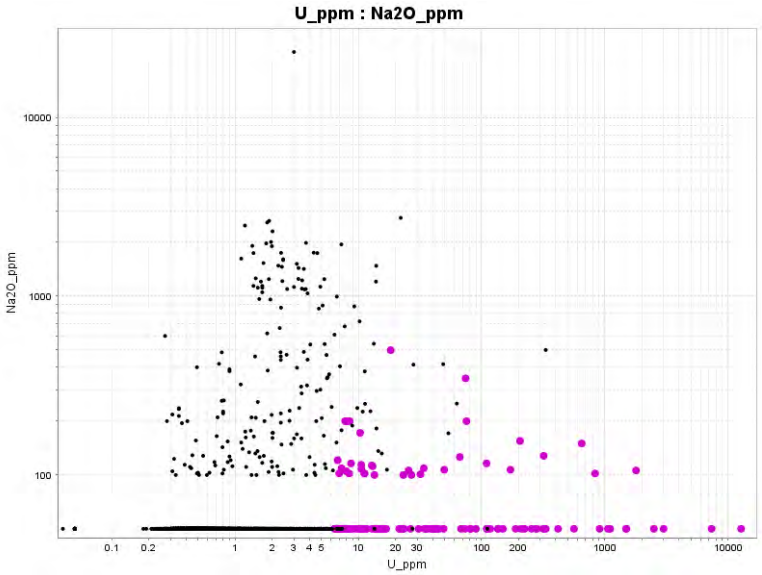
U_ppm : Na2O_ppm
Na2O_ppm
10000
1000
100
0.1 0.2 1 2 3 4 5 10 20 30 100 200 1000 10000
U_ppm

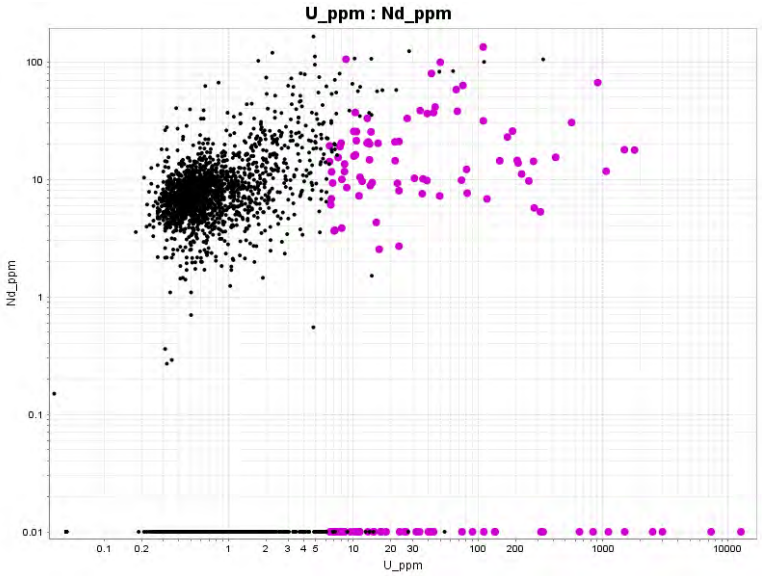
U_ppm : Nd_ppm
Nd_ppm
100
10
1
0.1
0.01
0.1 0.2 1 2 3 4 5 10 20 30 100 200 1000 10000
U_ppm

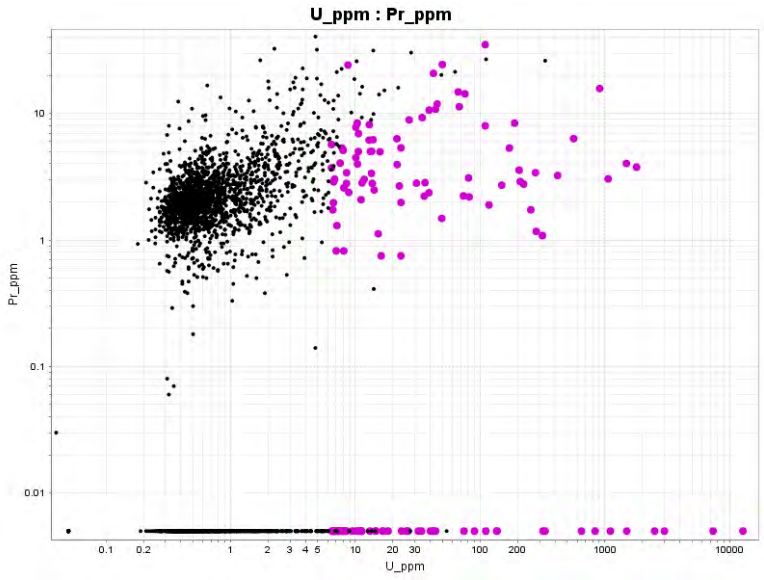
U_ppm : Pr_ppm
Pr_ppm
10
1
0.1
0.01
0.1
0.2
1
2
3
4
5
10
20
30
100
200
1000
10000
U_ppm

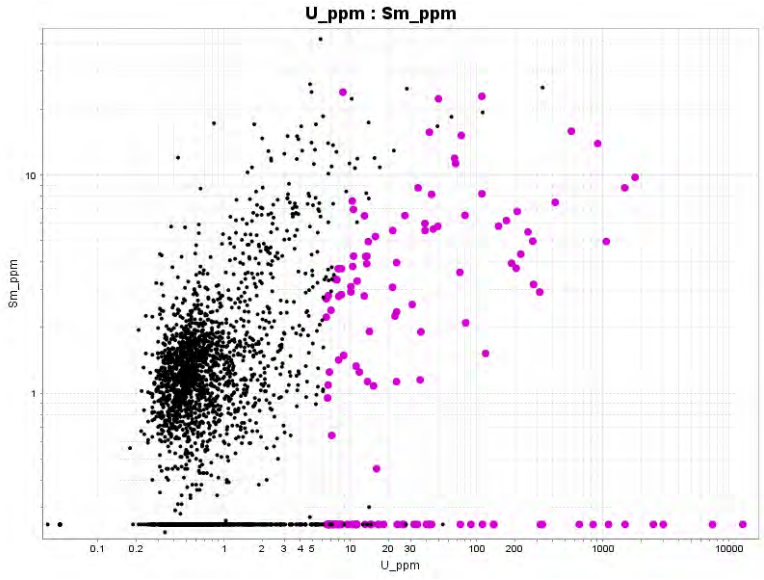
U_ppm : Sm_ppm
Sm_ppm
10
1
0.1
0.2
1
2
3
4
5
10
20
30
100
200
1000
10000
U_ppm

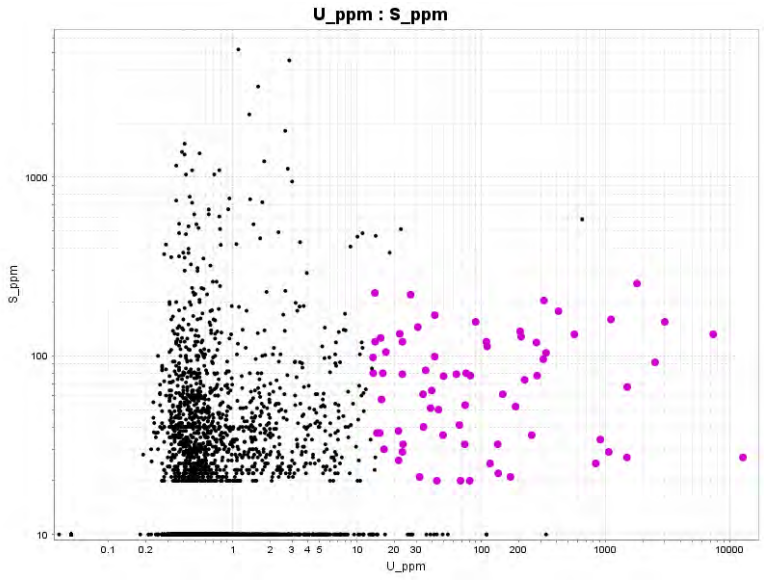
U_ppm : S_ppm
S_ppm
1000
100
10
0.1
0.2
1
2
3
4
5
10
20
30
100
200
1000
10000
U_ppm

Appendix 7 – Scatter plots with alteration, structure and lithology

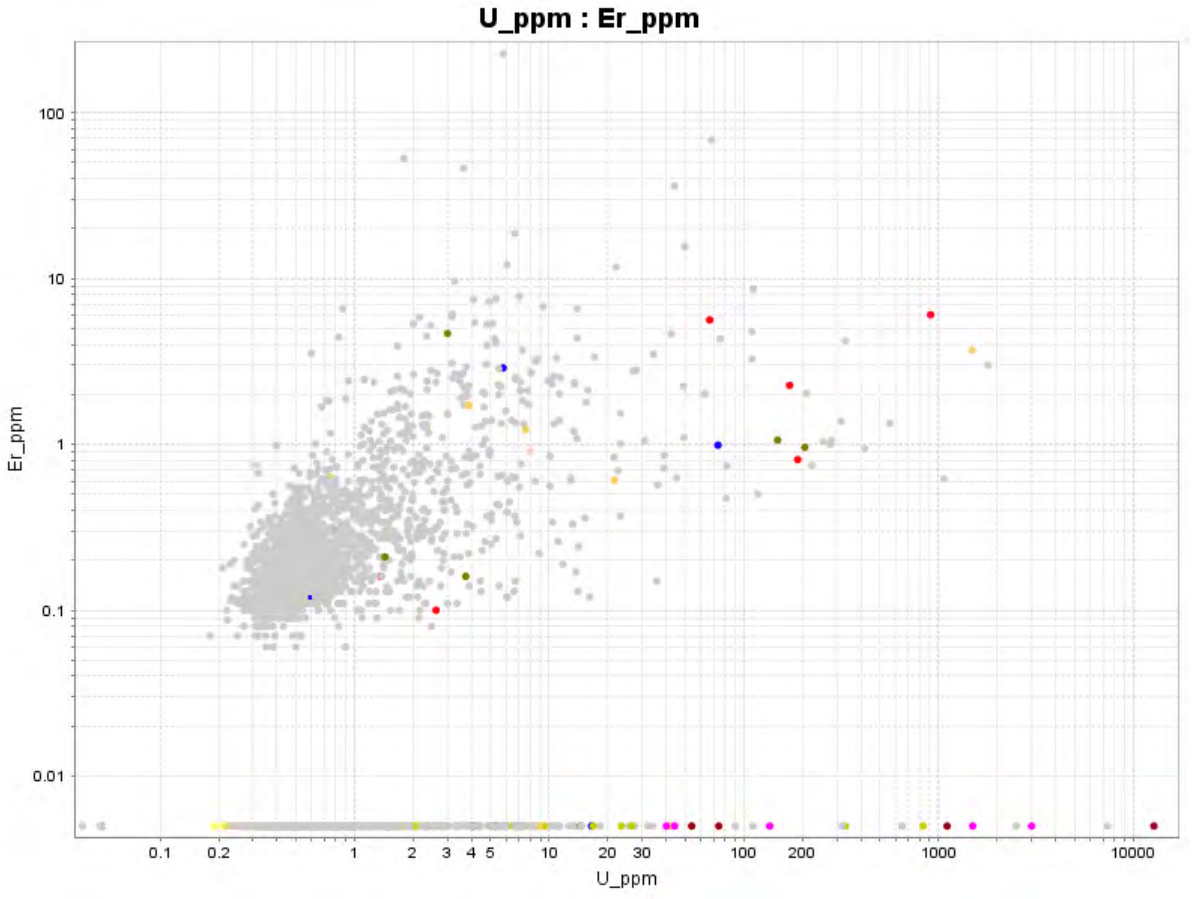

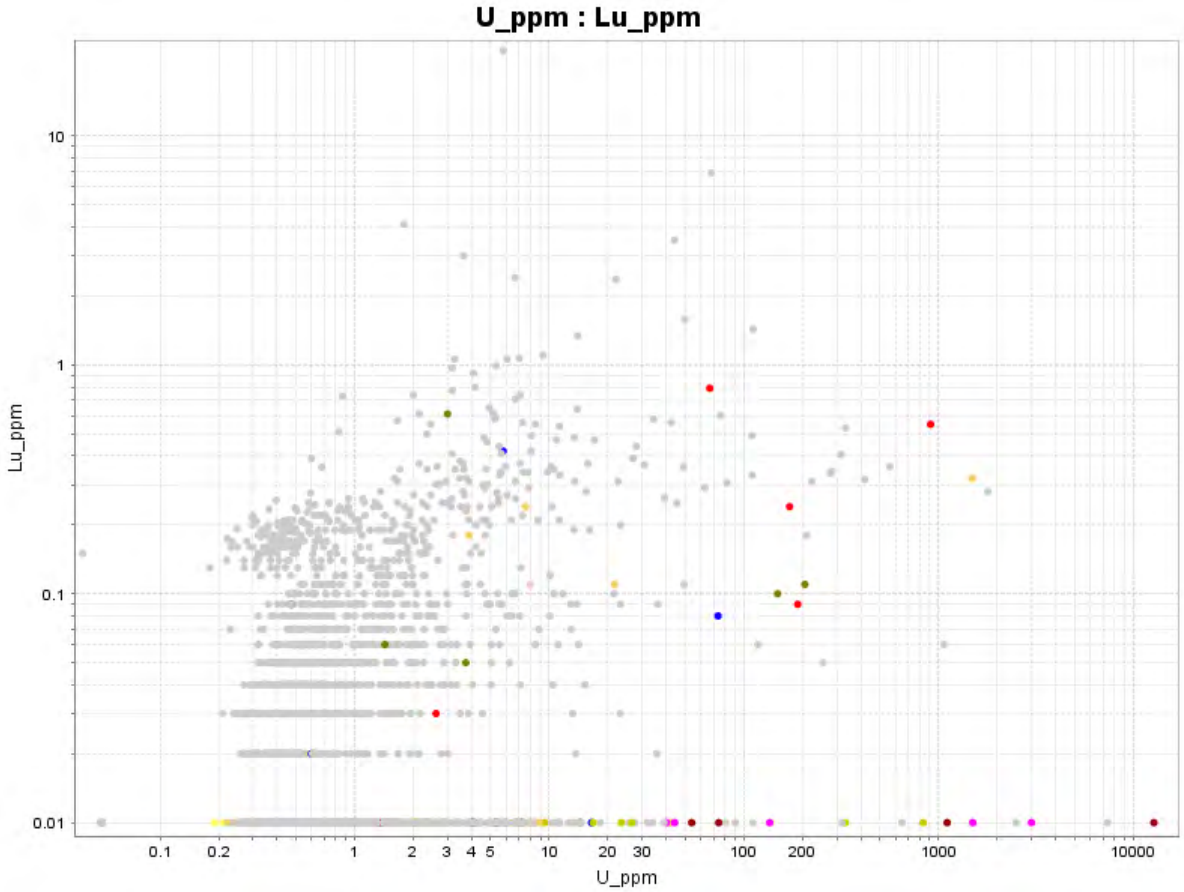
U_ppm : Lu_ppm
Lu_ppm
10
1
0.1
0.01
0.1
0.2
1
2
3
4
5
10
20
30
100
200
1000
10000
U_ppm

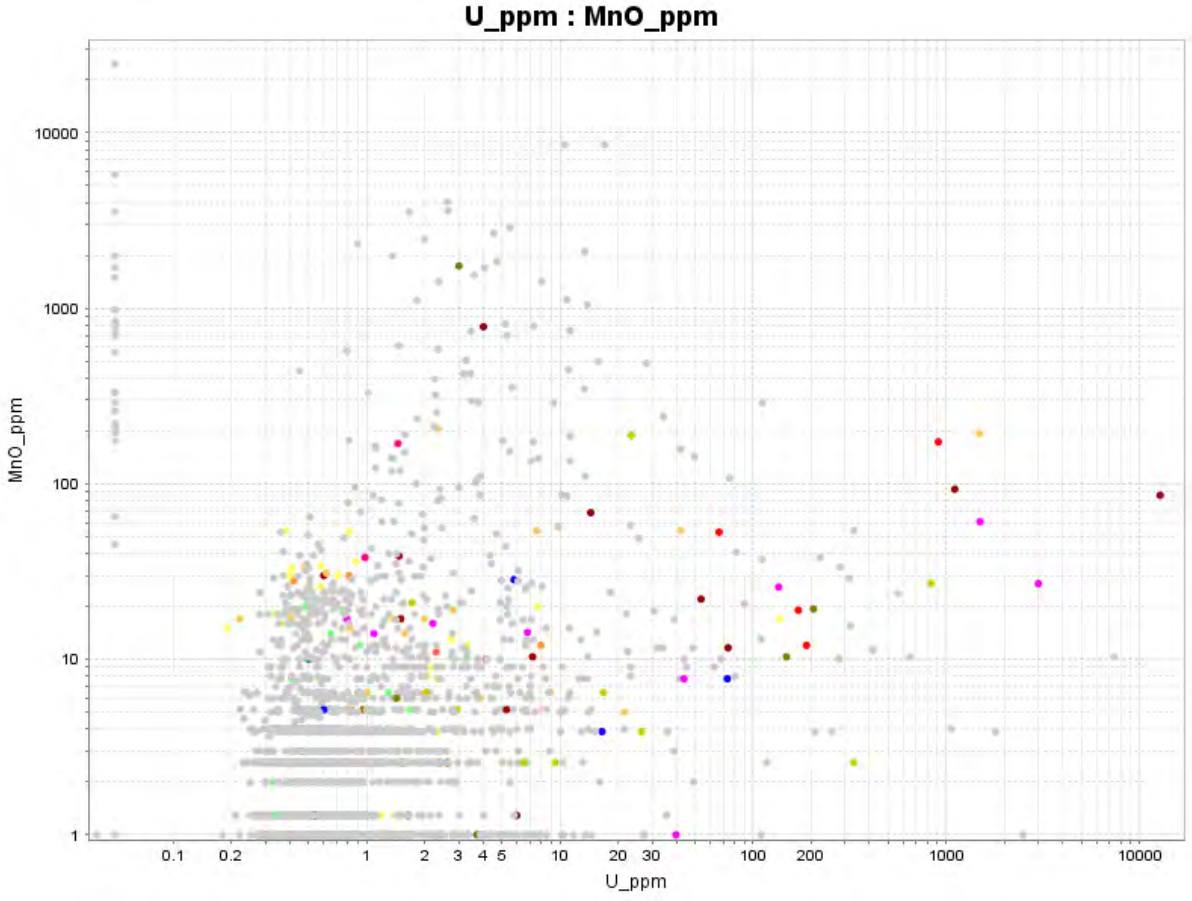
U_ppm : MnO_ppm
MnO_ppm
10000
1000
100
10
1
0.1
0.2
1
2
3
4
5
10
20
30
100
200
1000
10000
U_ppm

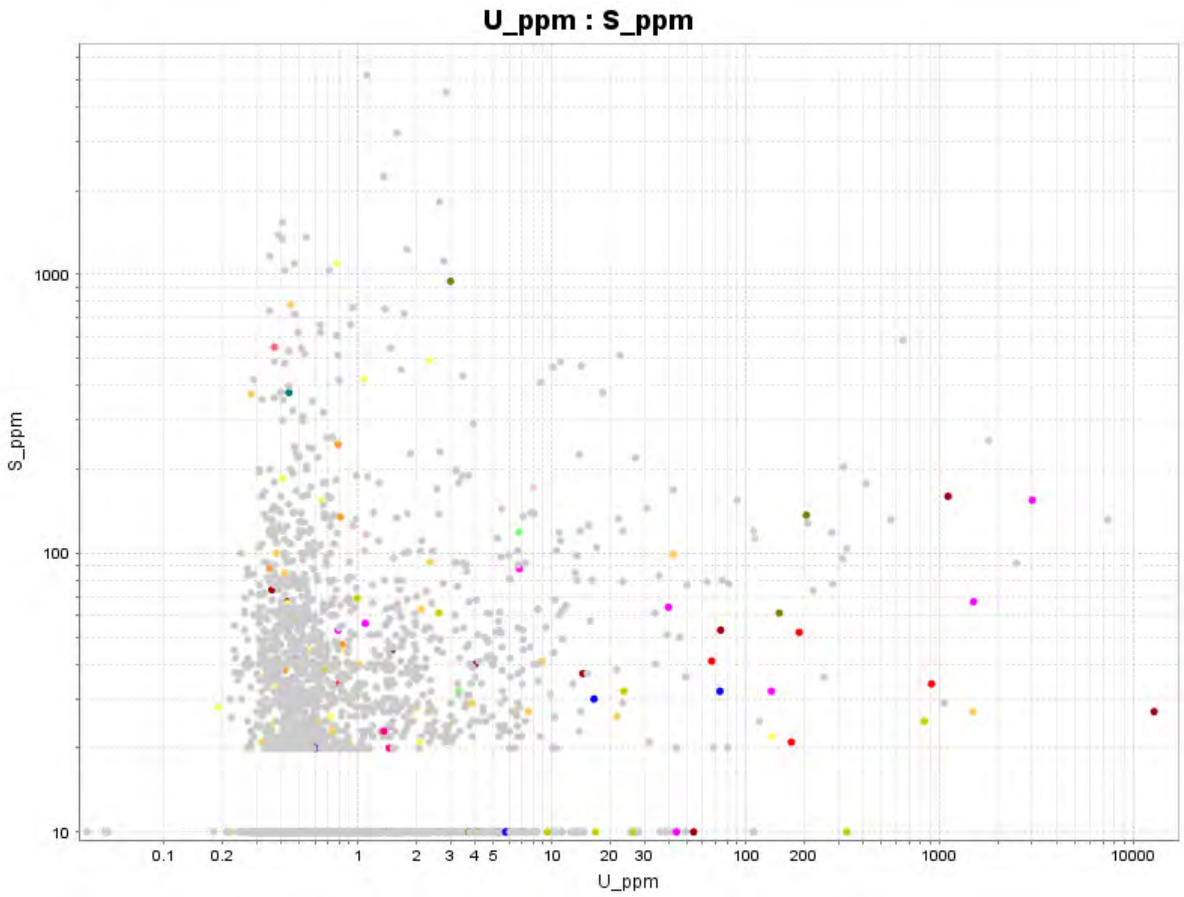
U_ppm : S_ppm
S_ppm
1000
100
10
0.1
0.2
1
2
3
4
5
10
20
30
100
200
1000
10000
U_ppm

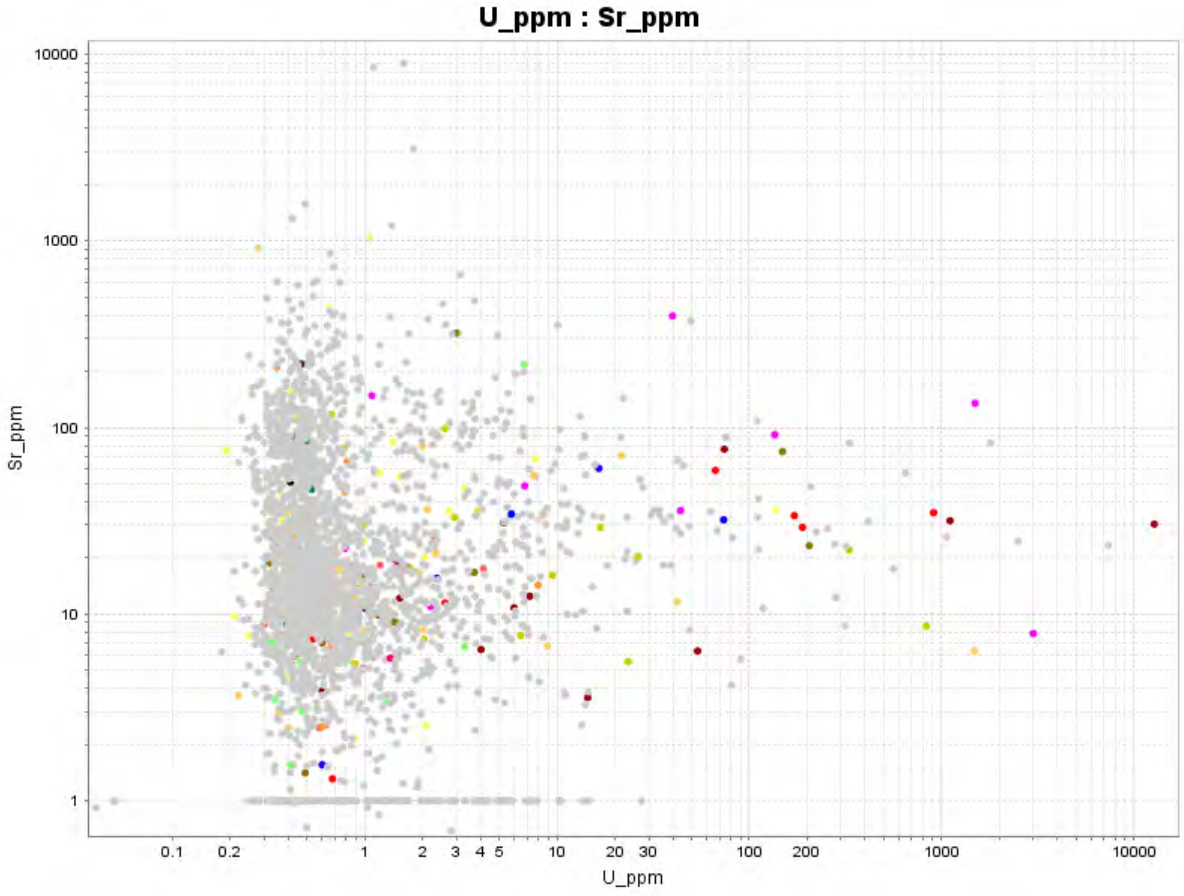
U_ppm : Sr_ppm
Sr_ppm
10000
1000
100
10
1
0.1
0.2
1
2
3
4
5
10
20
30
100
200
1000
10000
U_ppm

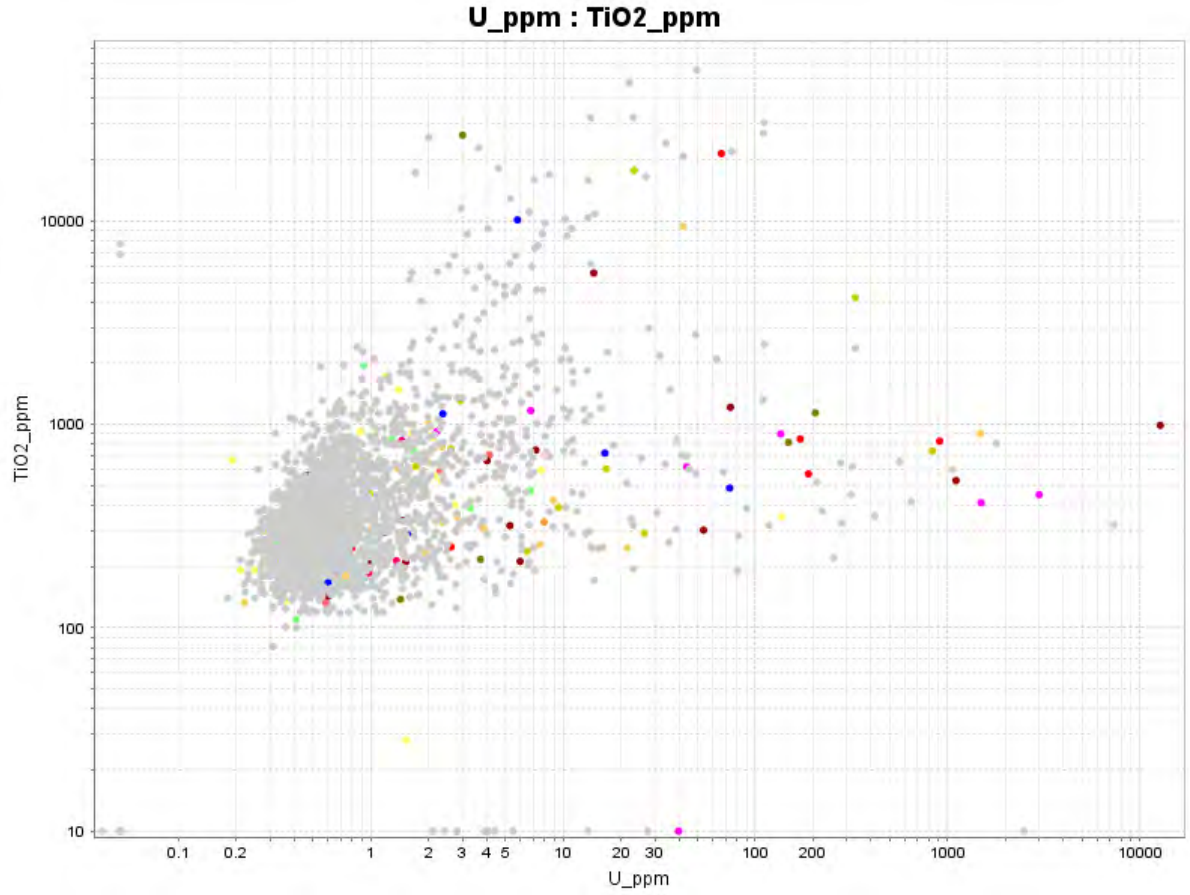
U_ppm : TiO2_ppm
TiO2_ppm
10000
1000
100
10
0.1
0.2
1
2
3
4
5
10
20
30
100
200
1000
10000
U_ppm

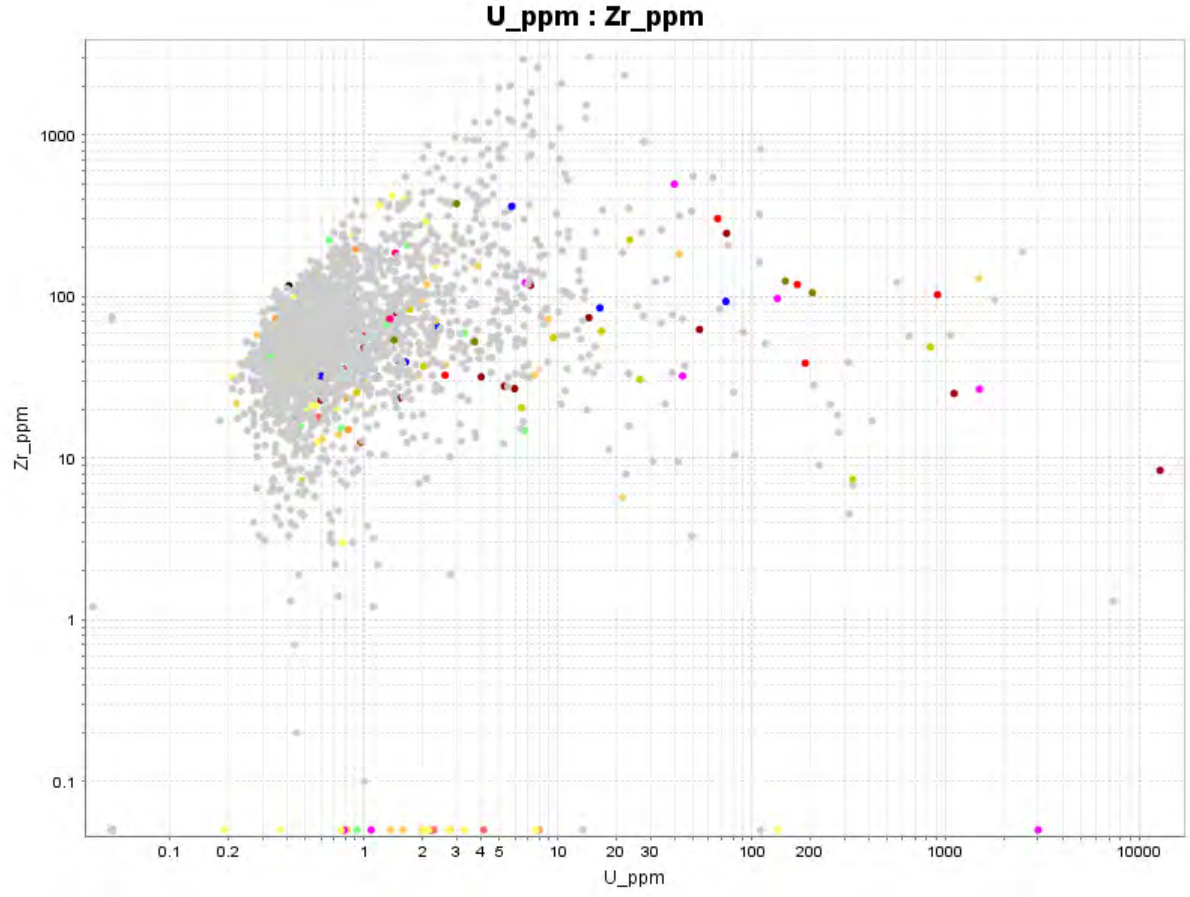
U_ppm : Zr_ppm
Zr_ppm
1000
100
10
1
0.1
0.1
0.2
1
2
3
4
5
10
20
30
100
200
1000
10000
U_ppm

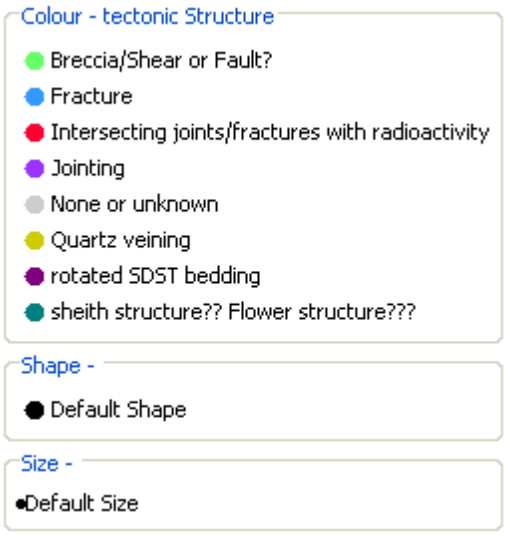
Colour - tectonic Structure
Breccia/Shear or Fault?
Fracture
Intersecting joints/fractures with radioactivity
Jointing
None or unknown
Quartz veining
rotated SDST bedding
sheith structure?? Flower structure???
Shape -
Default Shape
Size -
Default Size

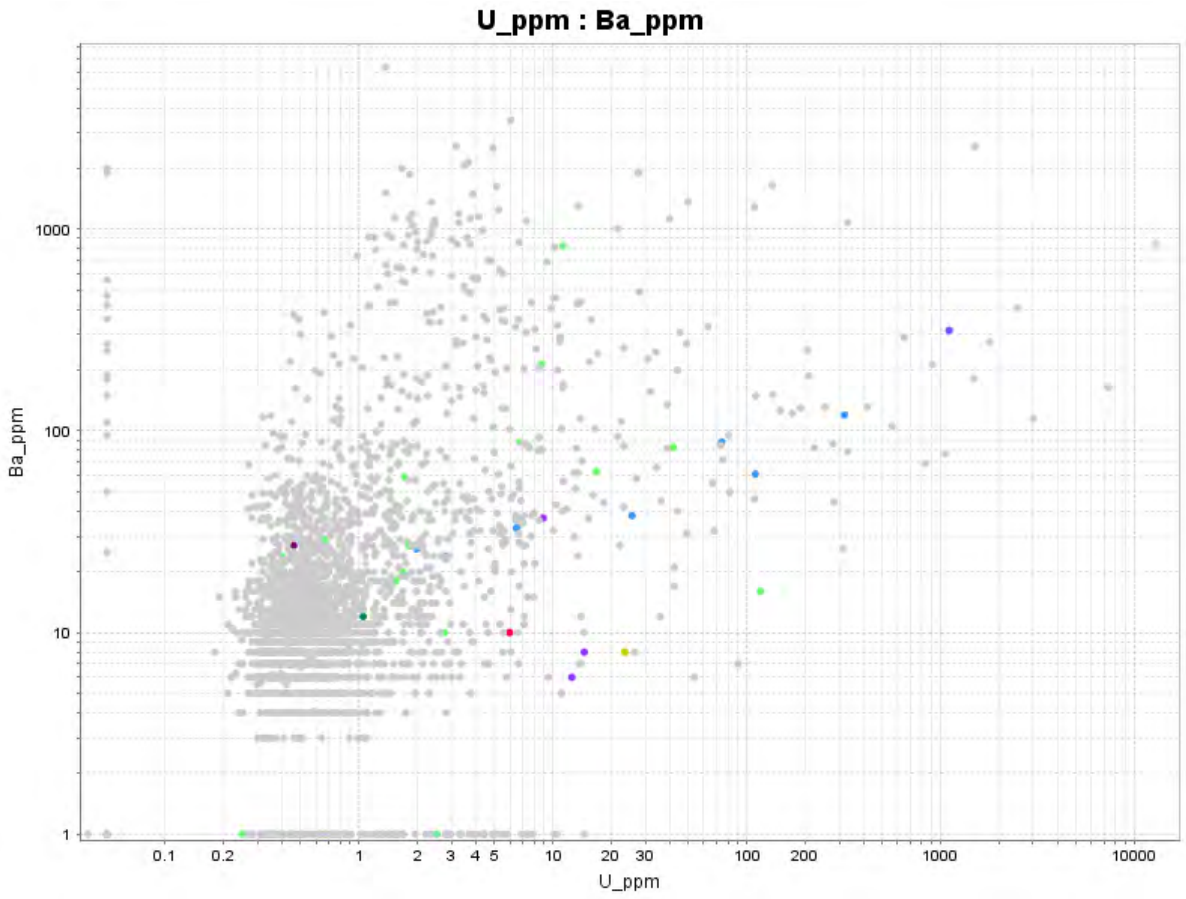
U_ppm : Ba_ppm
Ba_ppm
1000
100
10
1
0.1
0.2
1
2
3
4
5
10
20
30
100
200
1000
10000
U_ppm

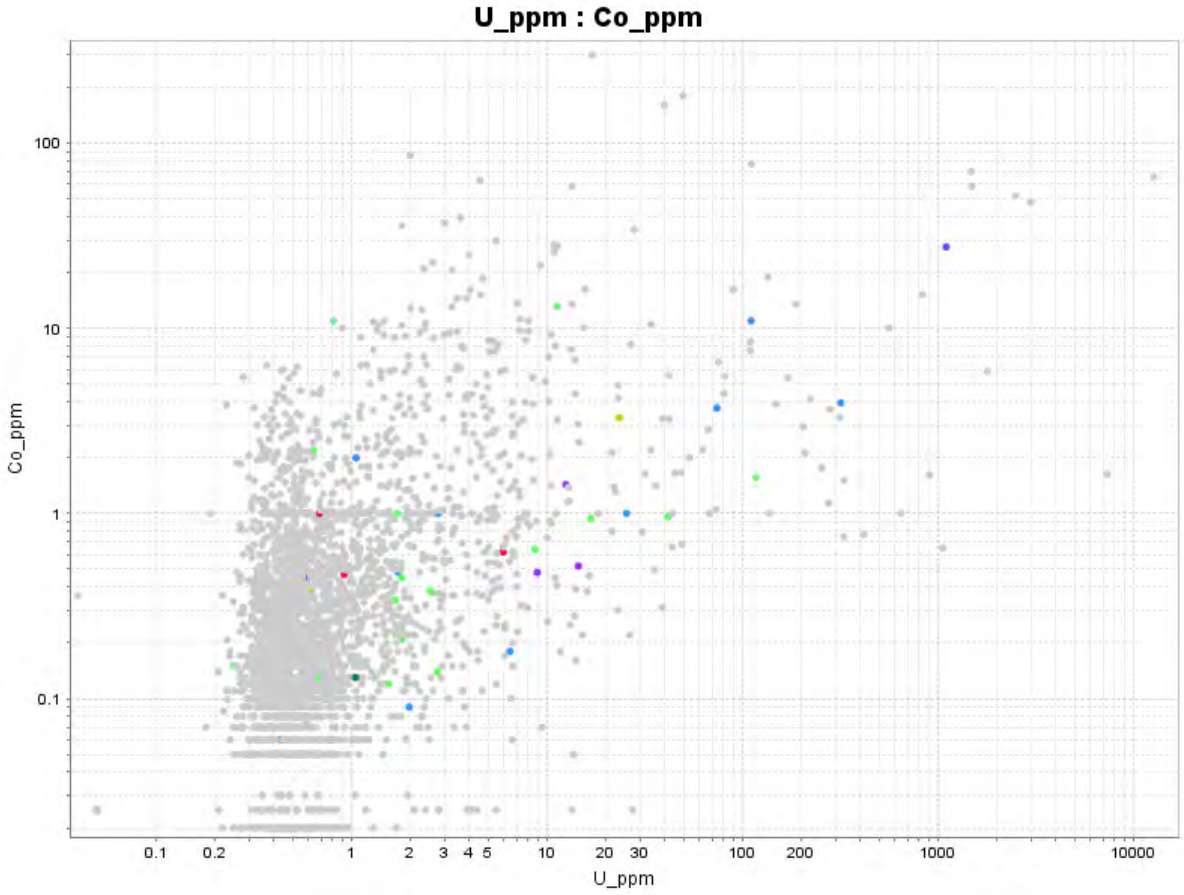
U_ppm : Co_ppm
Co_ppm
100
10
1
0.1
0.1
0.2
1
2
3
4
5
10
20
30
100
200
1000
10000
U_ppm

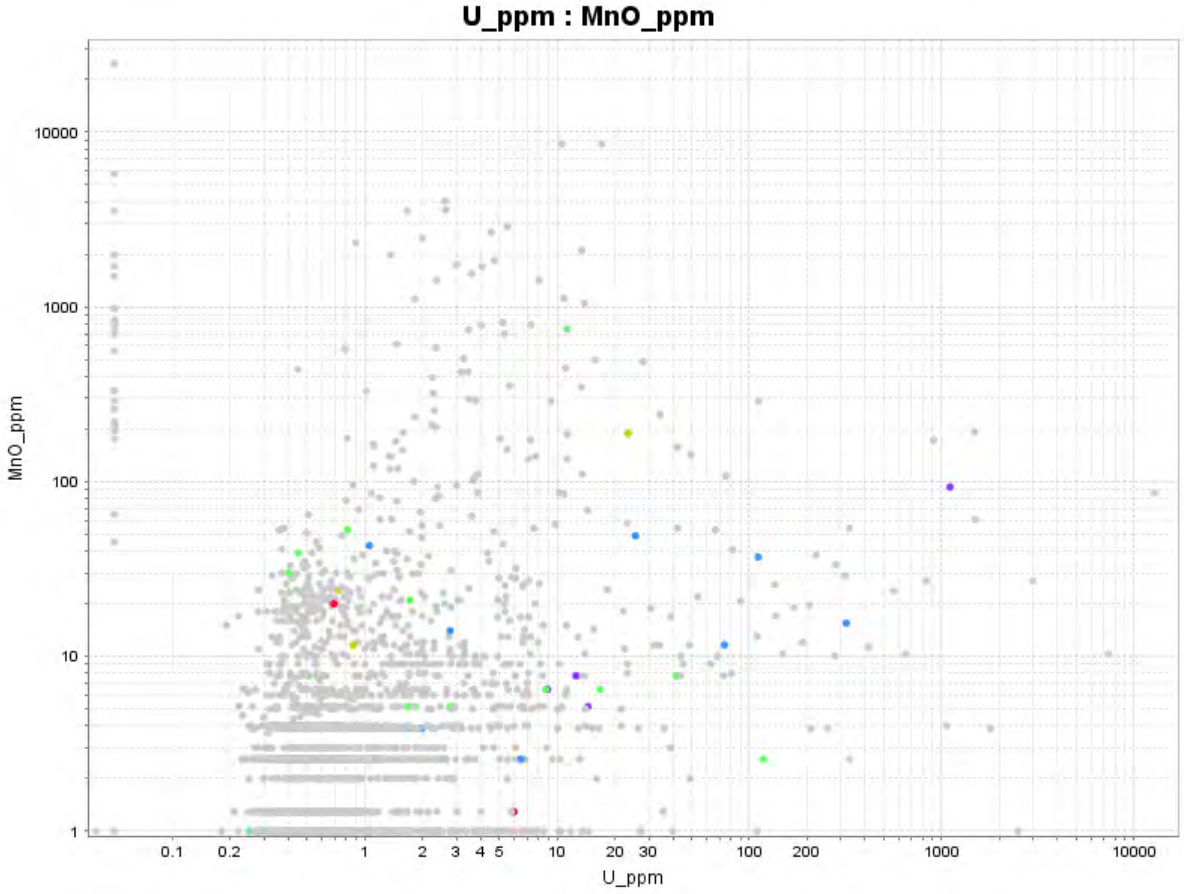
U_ppm : MnO_ppm
MnO_ppm
10000
1000
100
10
1
0.1
0.2
1
2
3
4
5
10
20
30
100
200
1000
10000
U_ppm

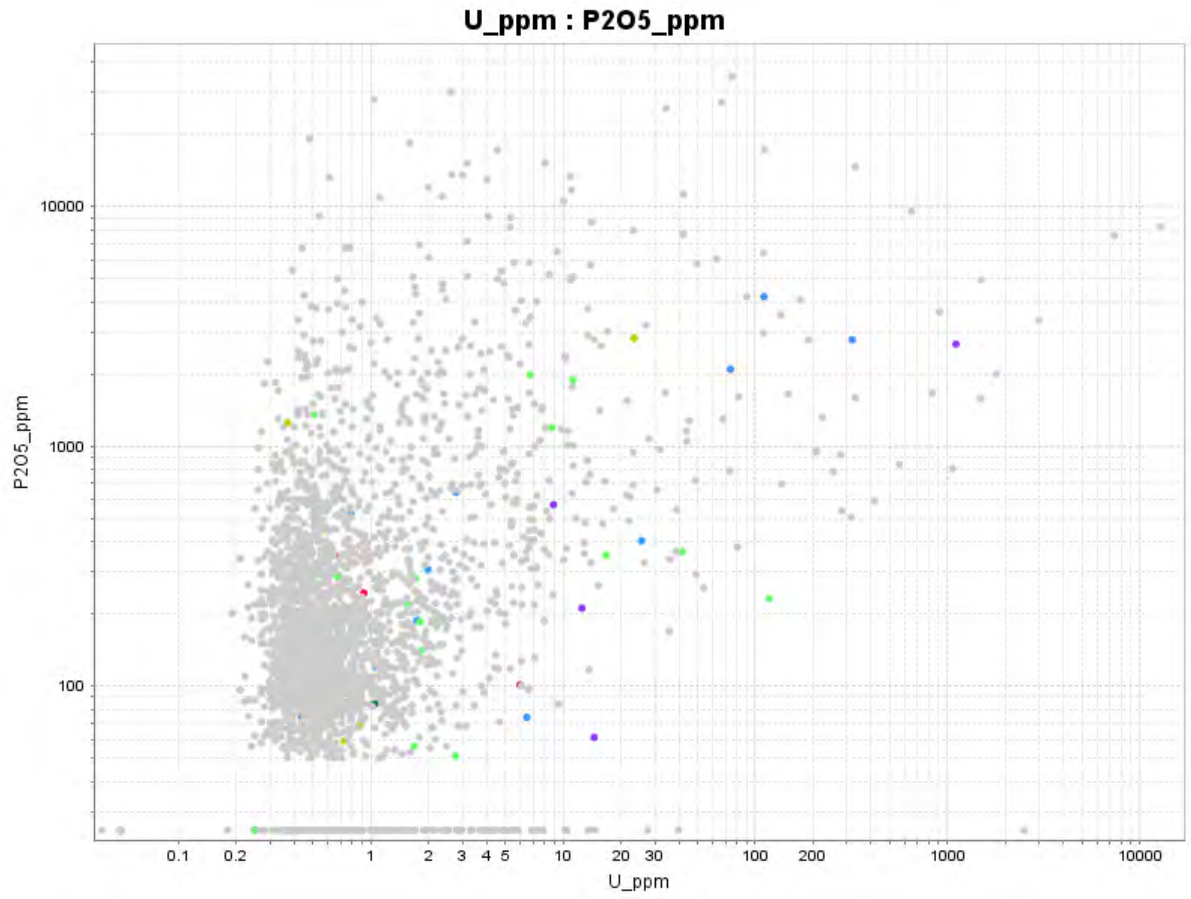
U_ppm : P2O5_ppm
P2O5_ppm
10000
1000
100
0.1
0.2
1
2
3
4
5
10
20
30
100
200
1000
10000
U_ppm

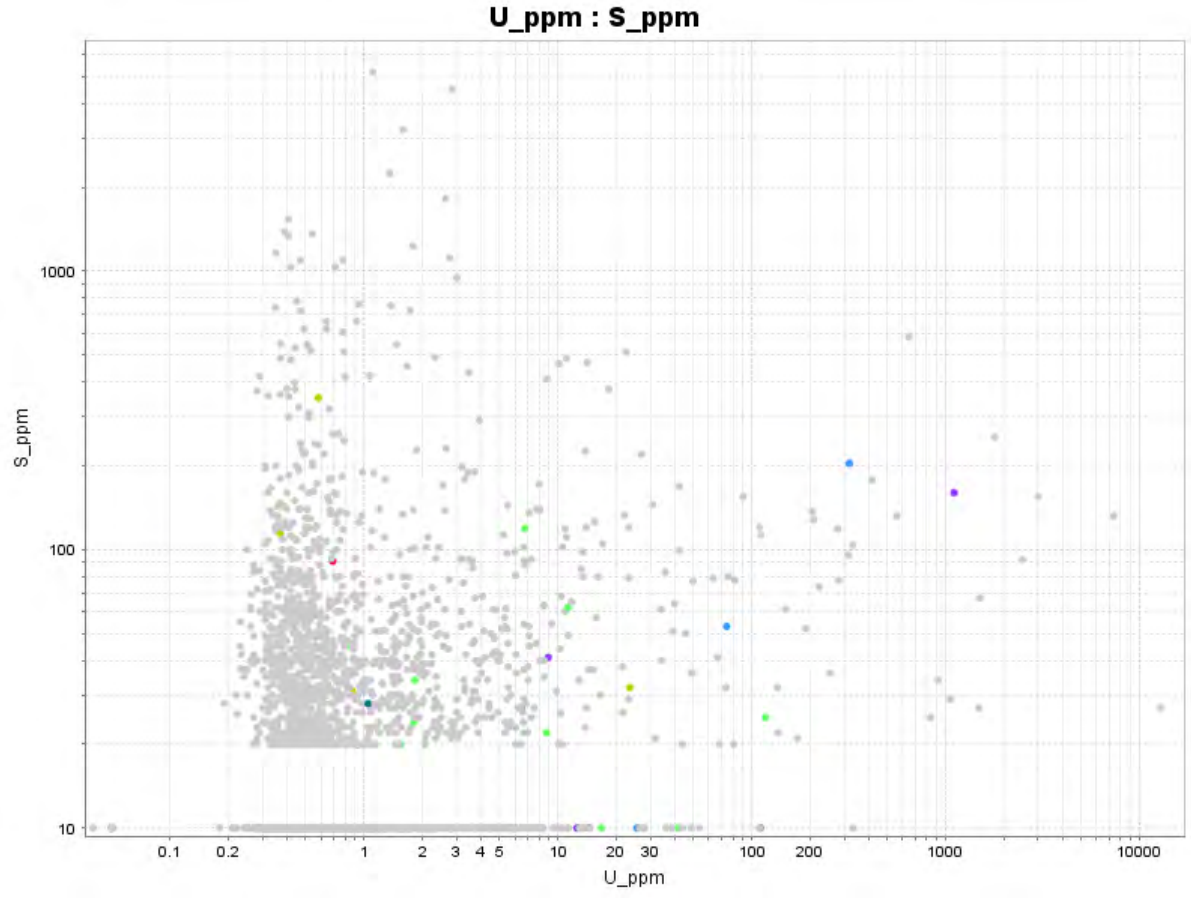
U_ppm : S_ppm
S_ppm
1000
100
10
0.1
0.2
1
2
3
4
5
10
20
30
100
200
1000
10000
U_ppm

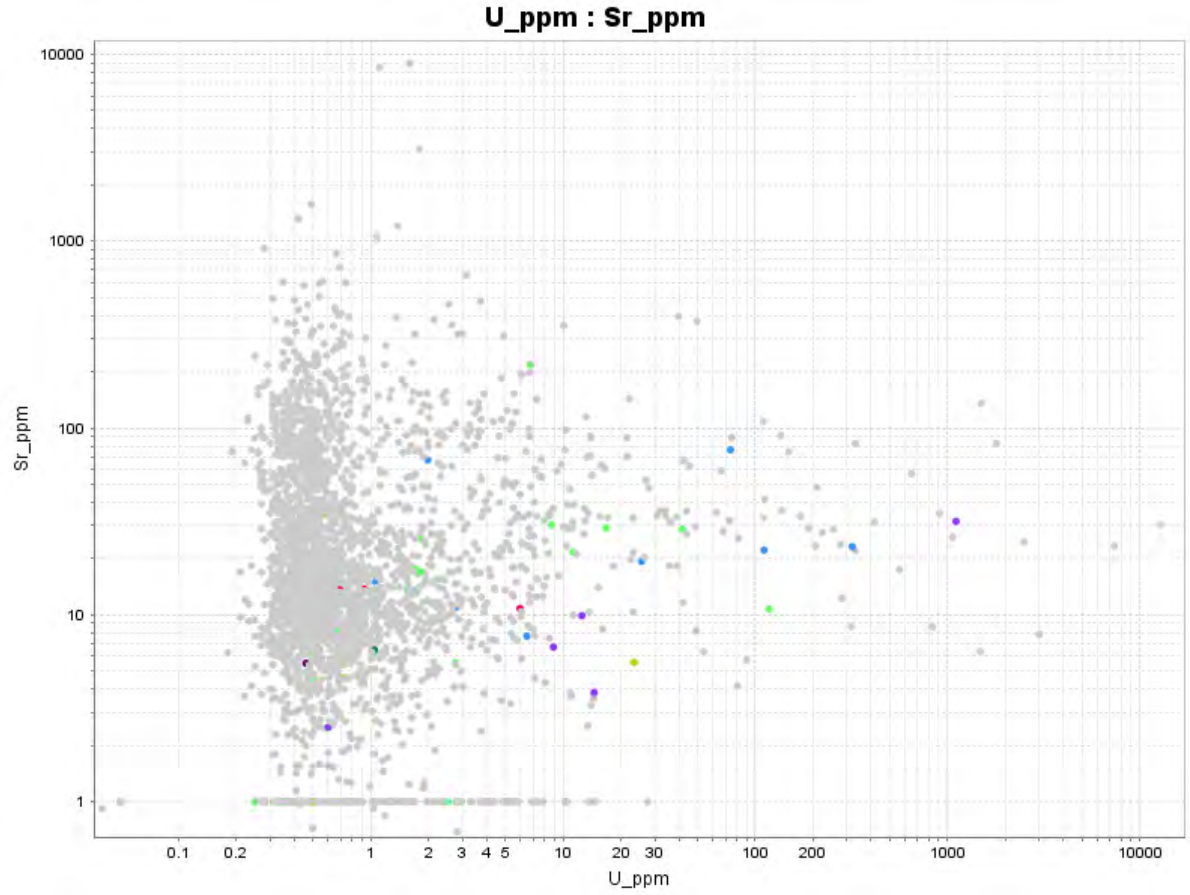
U_ppm : Sr_ppm
Sr_ppm
10000
1000
100
10
1
0.1
0.2
1
2
3
4
5
10
20
30
100
200
1000
10000
U_ppm

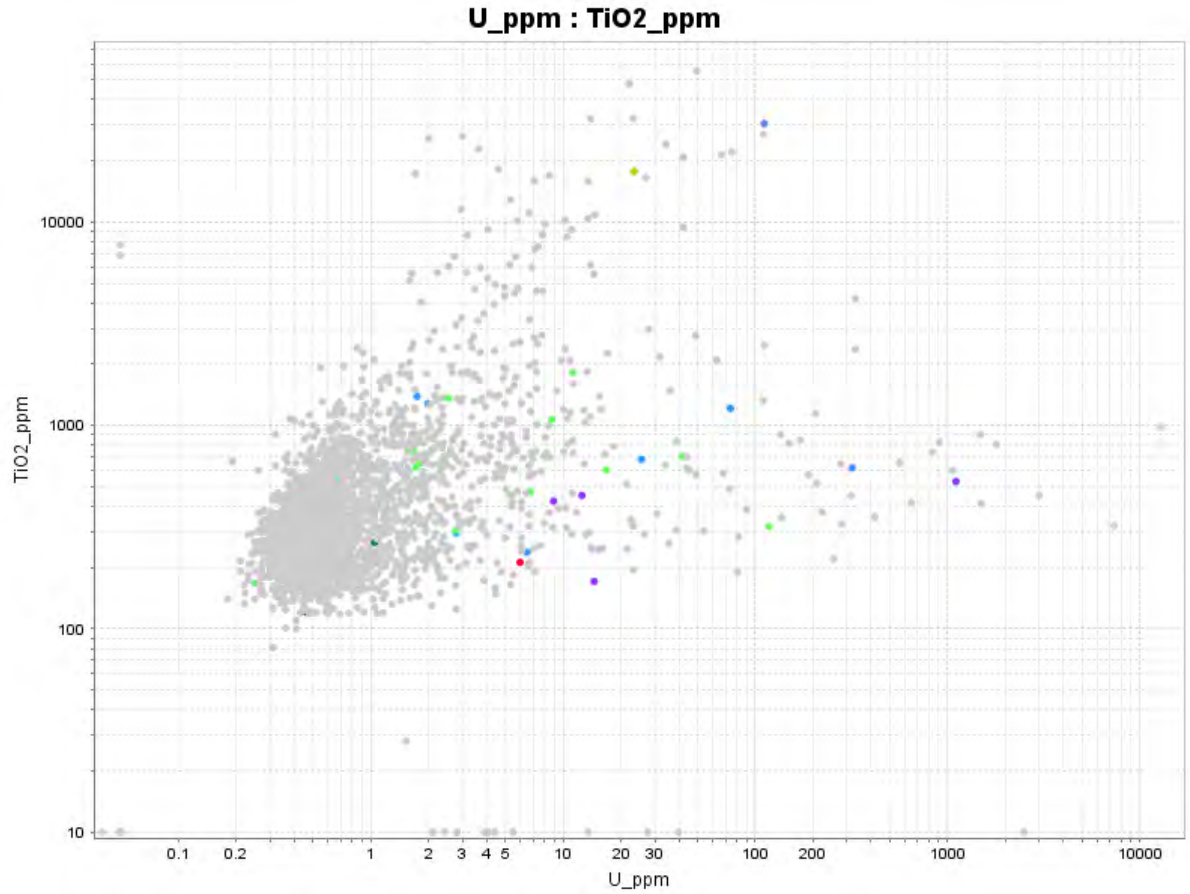
U_ppm : TiO2_ppm
TiO2_ppm
10000
1000
100
10
0.1
0.2
1
2
3
4
5
10
20
30
100
200
1000
10000
U_ppm

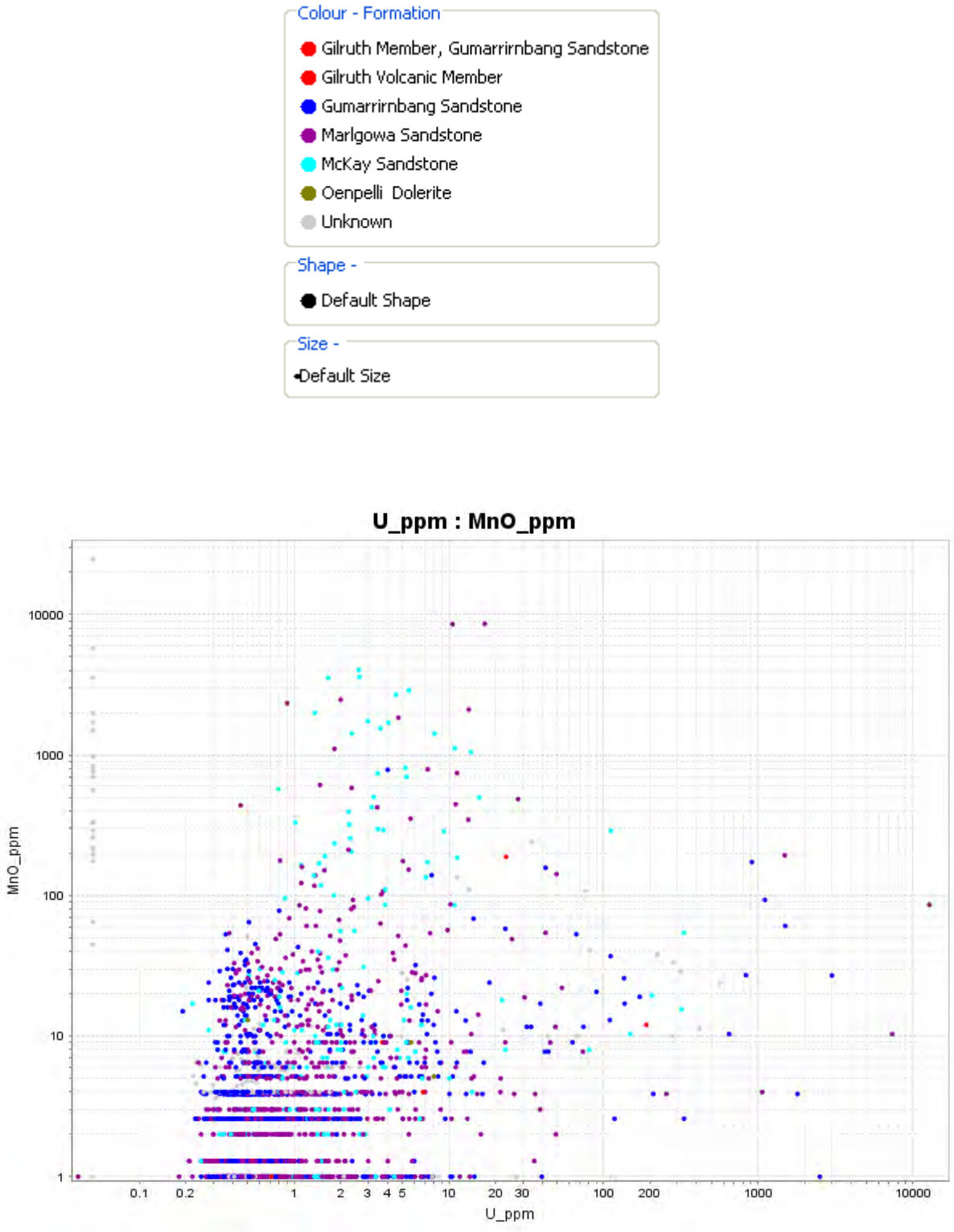
Colour - Formation
Gilruth Member, Gumarrirnbang Sandstone
Gilruth Volcanic Member
Gumarrirnbang Sandstone
Marlgowa Sandstone
McKay Sandstone
Oenpelli Dolerite
Unknown
Shape -
Default Shape
Size -
Default Size
U_ppm : MnO_ppm
MnO_ppm
10000
1000
100
10
1
0.1
0.2
1
2
3
4
5
10
20
30
100
200
1000
10000
U_ppm

Appendix 8 – Graphs of elements in prospect transects

Casper Transect

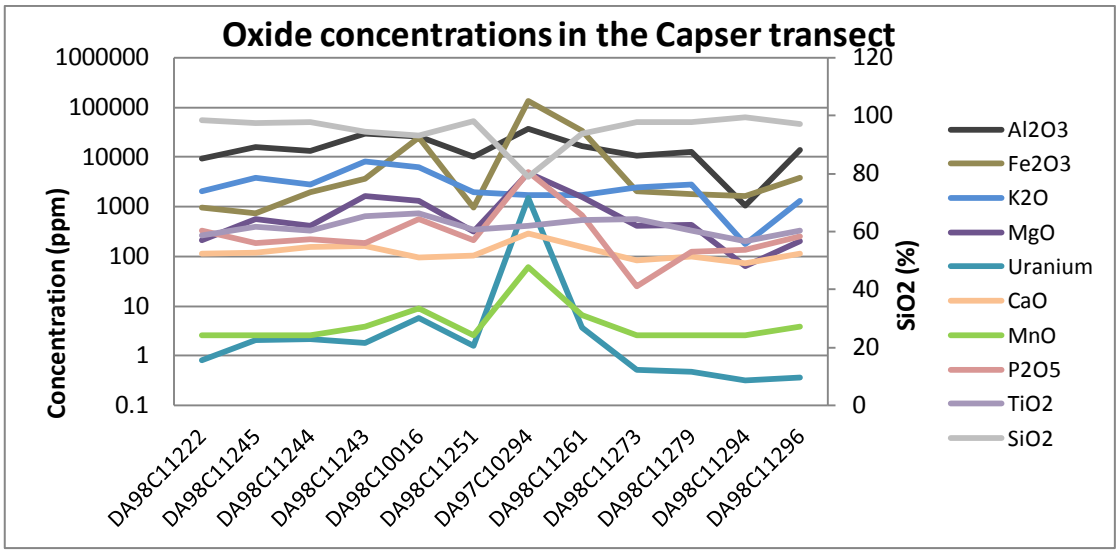

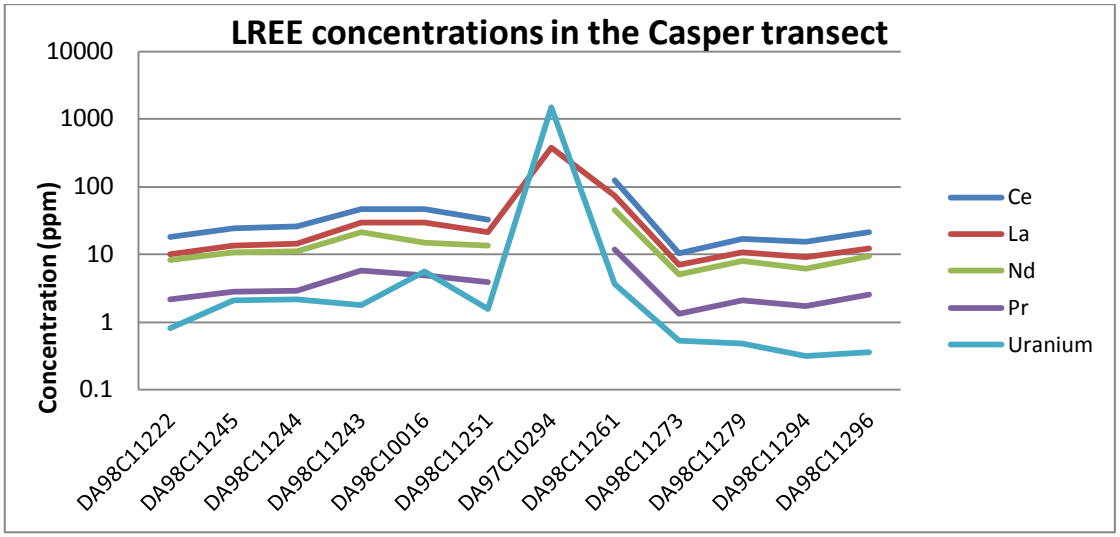

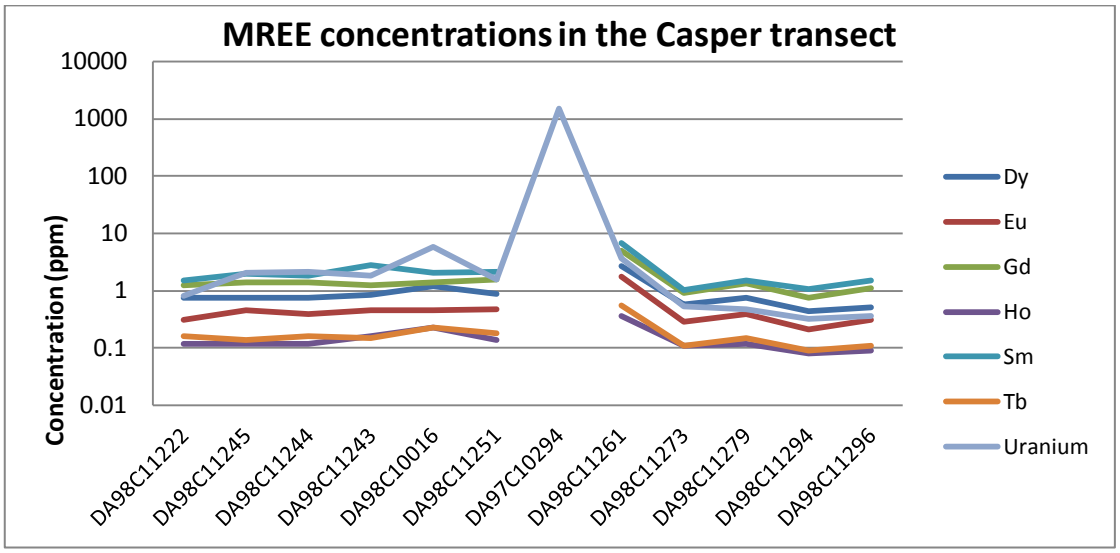

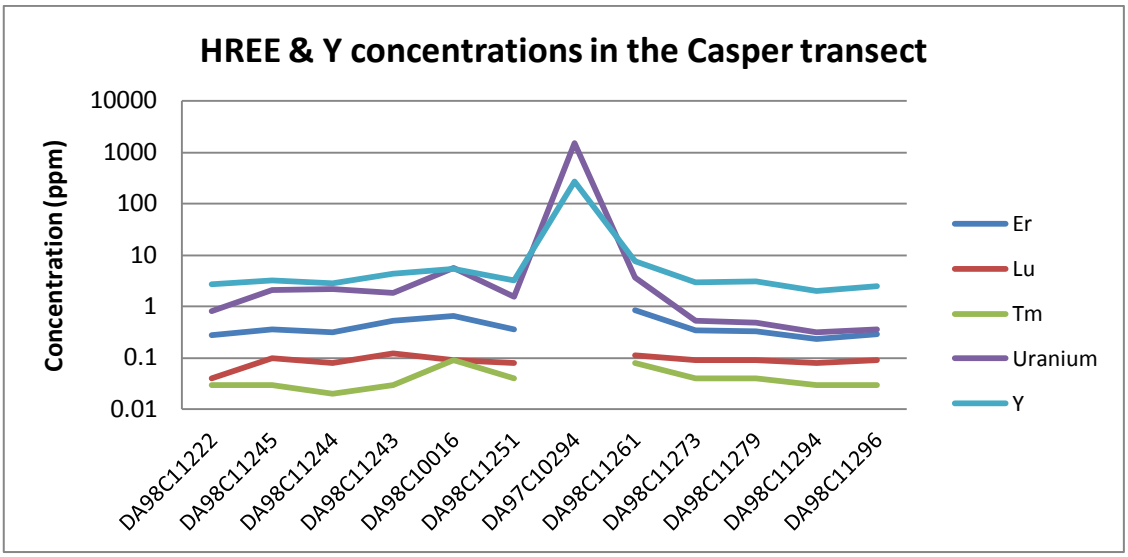
HREE & Y concentrations in the Casper transect
Concentration (ppm)
10000
1000
100
10
1
0.1
0.01
DA98C11222
DA98C11245
DA98C11244
DA98C11243
DA98C10016
DA98C11251
DA97C10294
DA98C11261
DA98C11273
DA98C11279
DA98C11294
DA98C11296
Er
Lu
Tm
Uranium
Y

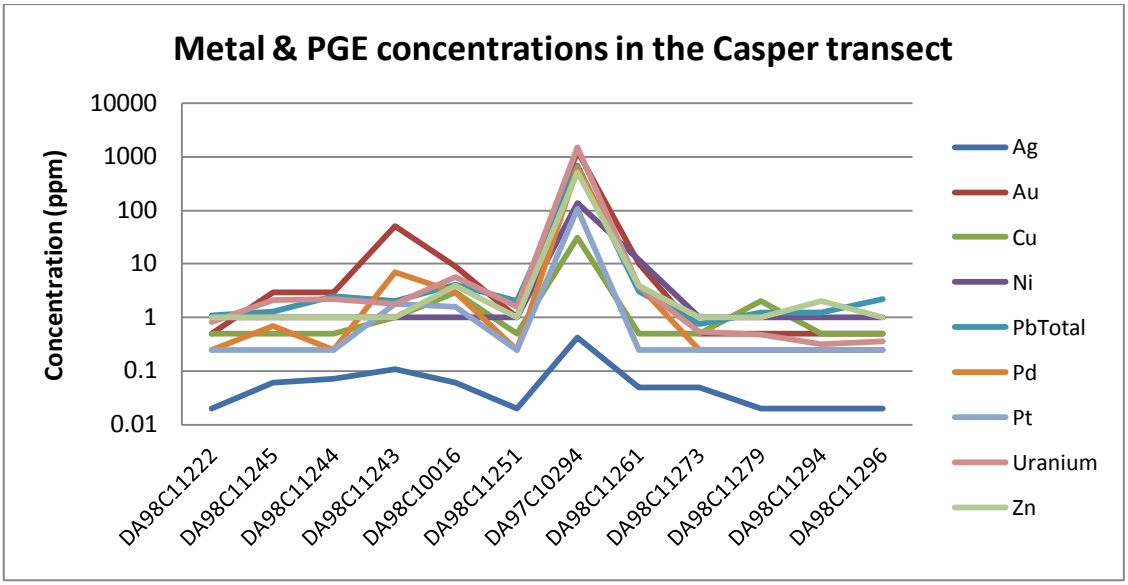
Metal & PGE concentrations in the Casper transect
Concentration (ppm)
10000
1000
100
10
1
0.1
0.01
DA98C11222
DA98C11245
DA98C11244
DA98C11243
DA98C10016
DA98C11251
DA97C10294
DA98C11261
DA98C11273
DA98C11279
DA98C11294
DA98C11296
Ag
Au
Cu
Ni
PbTotal
Pd
Pt
Uranium
Zn

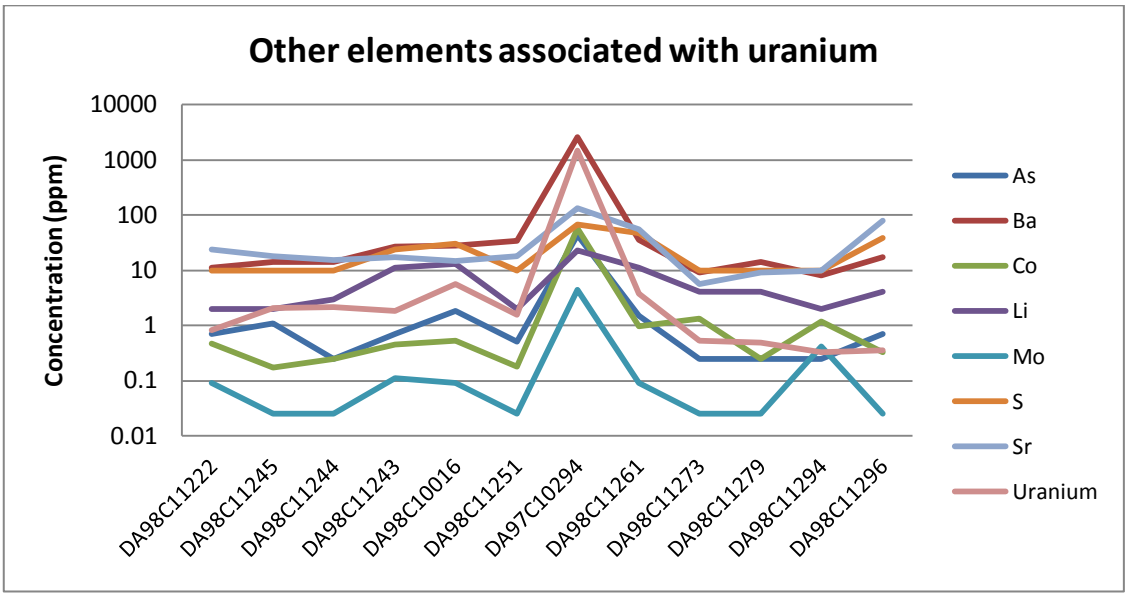
Other elements associated with uranium
Concentration (ppm)
10000
1000
100
10
1
0.1
0.01
DA98C11222
DA98C11245
DA98C11244
DA98C11243
DA98C10016
DA98C11251
DA97C10294
DA98C11261
DA98C11273
DA98C11279
DA98C11294
DA98C11296
As
Ba
Co
Li
Mo
S
Sr
Uranium

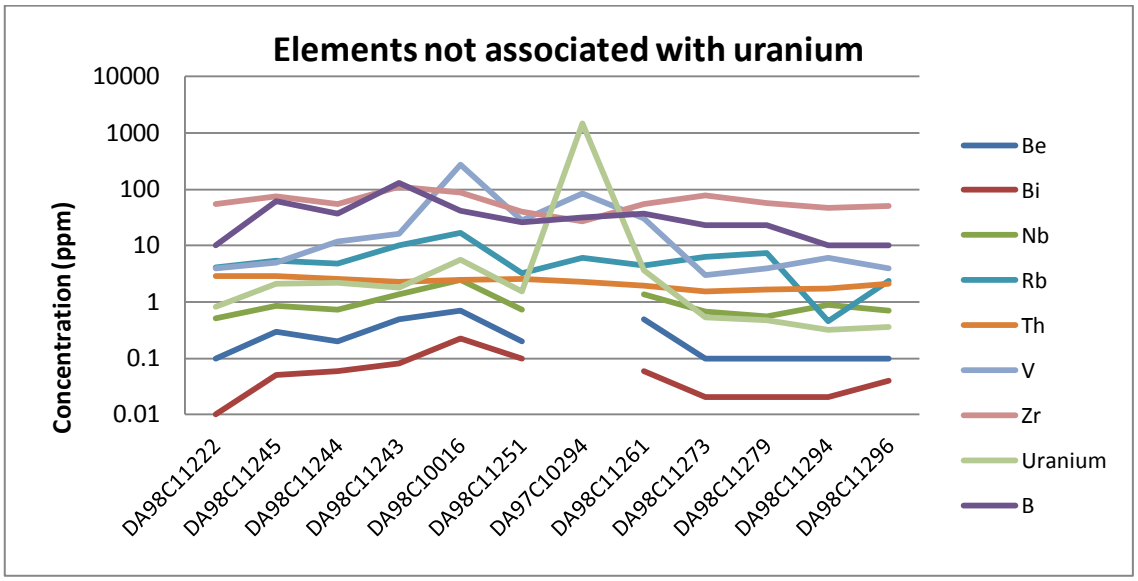

Flying Ghost EW Transect

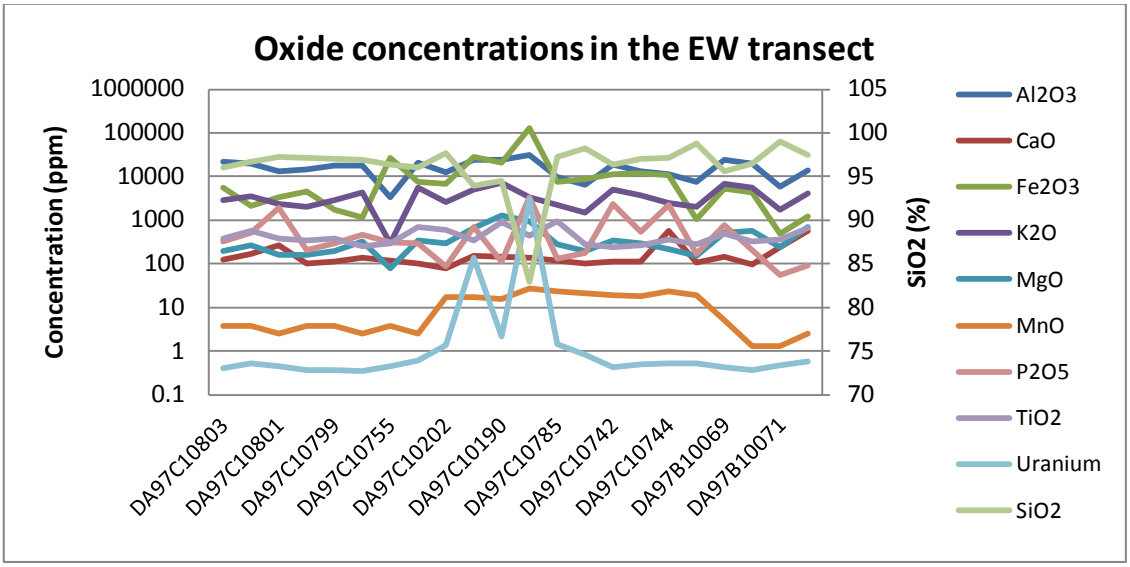

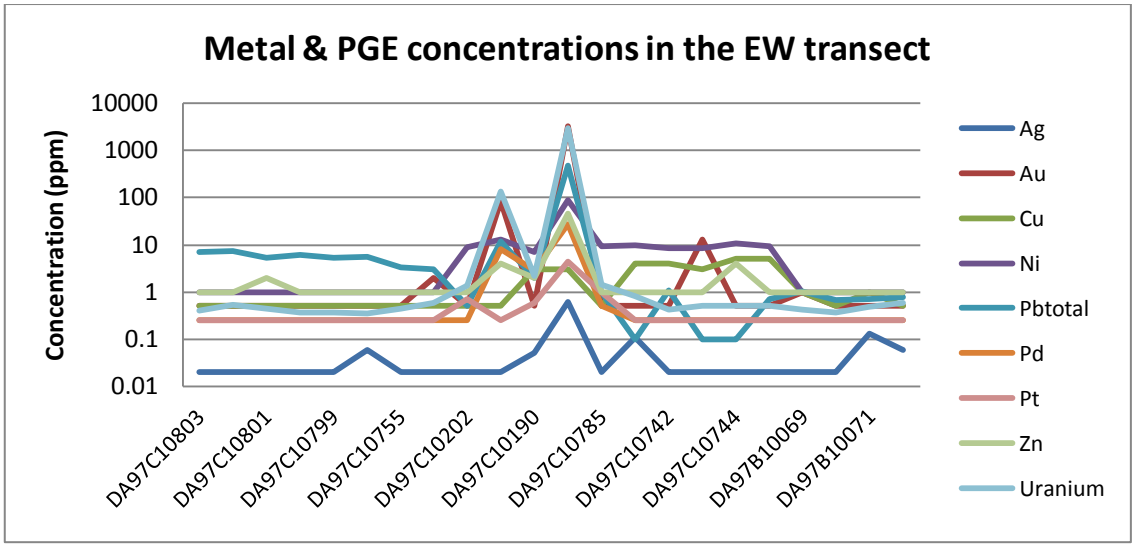

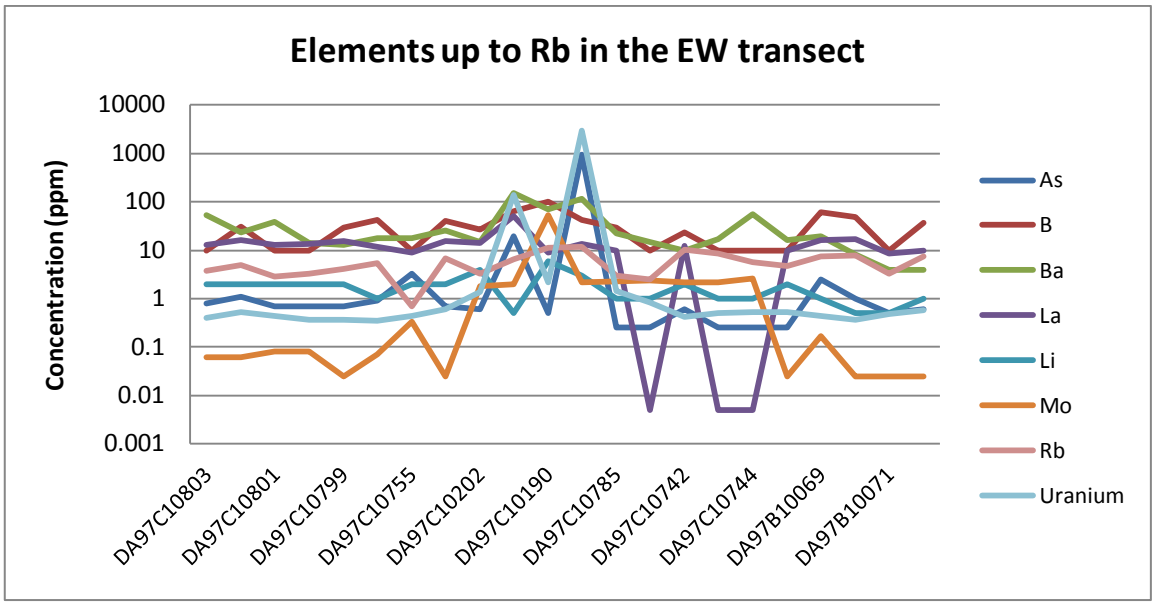

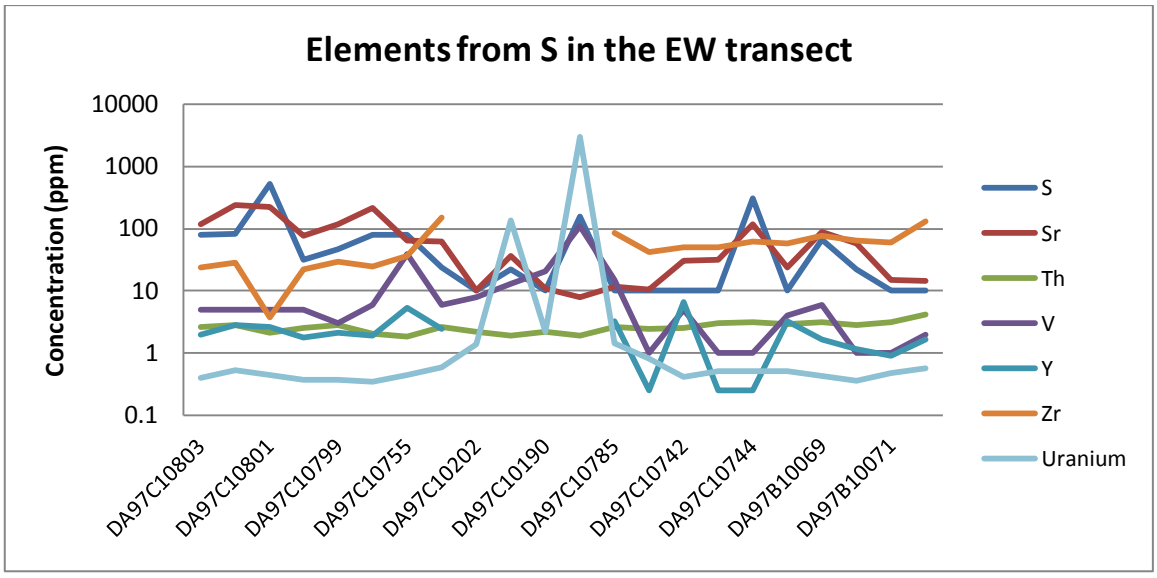

Flying Ghost NS Transect

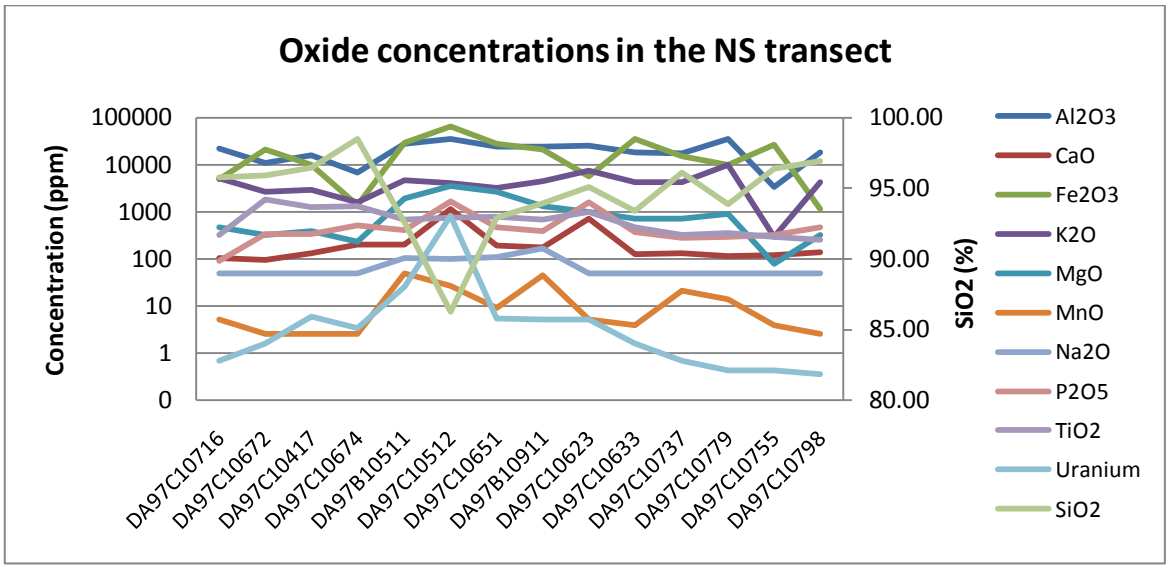

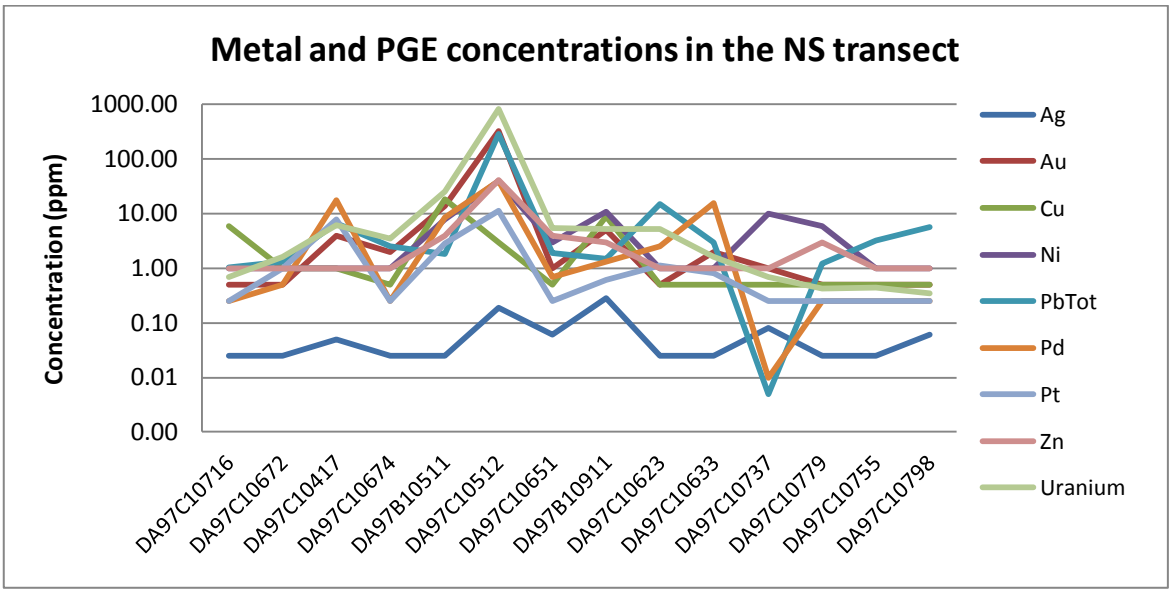
Metal and PGE concentrations in the NS transect
Concentration (ppm)
1000.00
100.00
10.00
1.00
0.10
0.01
0.00
DA97C10716
DA97C10672
DA97C10417
DA97C10674
DA97B10511
DA97C10512
DA97C10651
DA97B10911
DA97C10623
DA97C10633
DA97C10737
DA97C10779
DA97C10755
DA97C10798
Ag
Au
Cu
Ni
PbTot
Pd
Pt
Zn
Uranium

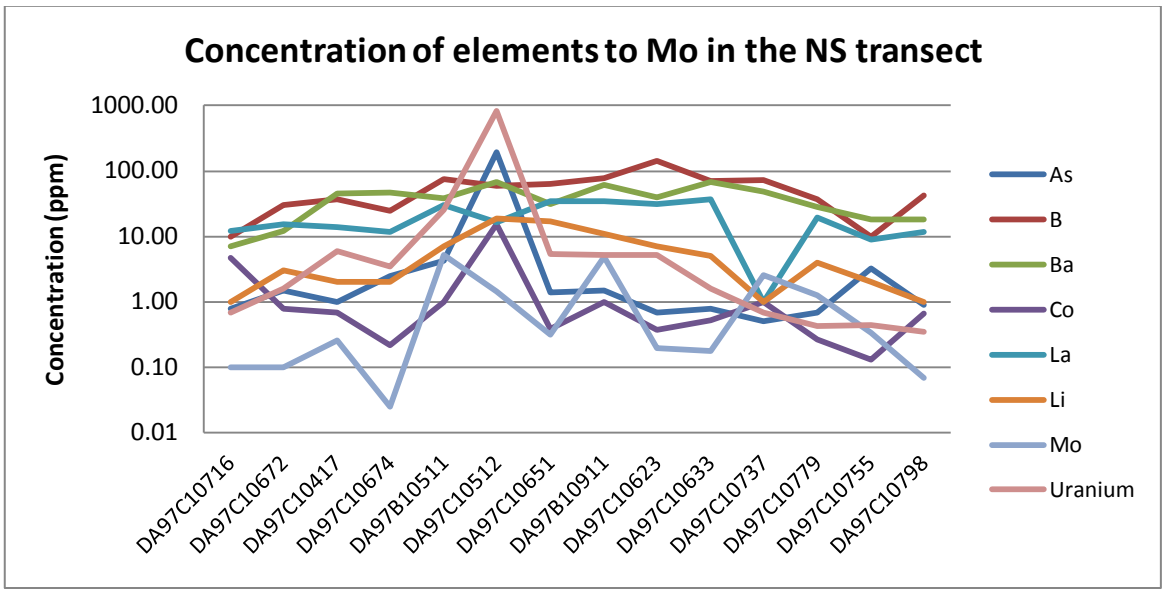
Concentration of elements to Mo in the NS transect
Concentration (ppm)
1000.00
100.00
10.00
1.00
0.10
0.01
DA97C10716
DA97C10672
DA97C10417
DA97C10674
DA97B10511
DA97C10512
DA97C10651
DA97B10911
DA97C10623
DA97C10633
DA97C10737
DA97C10779
DA97C10755
DA97C10798
As
B
Ba
Co
La
Li
Mo
Uranium

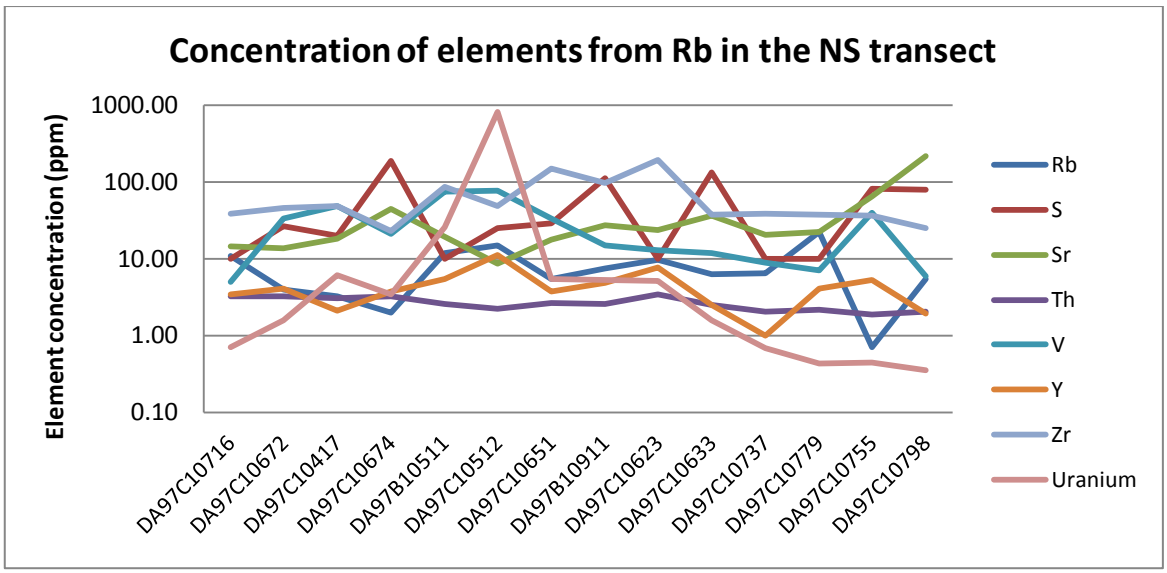
Concentration of elements from Rb in the NS transect
Element concentration (ppm)
1000.00
100.00
10.00
1.00
0.10
DA97C10716
DA97C10672
DA97C10417
DA97C10674
DA97B10511
DA97C10512
DA97C10651
DA97B10911
DA97C10623
DA97C10633
DA97C10737
DA97C10779
DA97C10755
DA97C10798
Rb
S
Sr
Th
V
Y
Zr
Uranium

Writer Transect

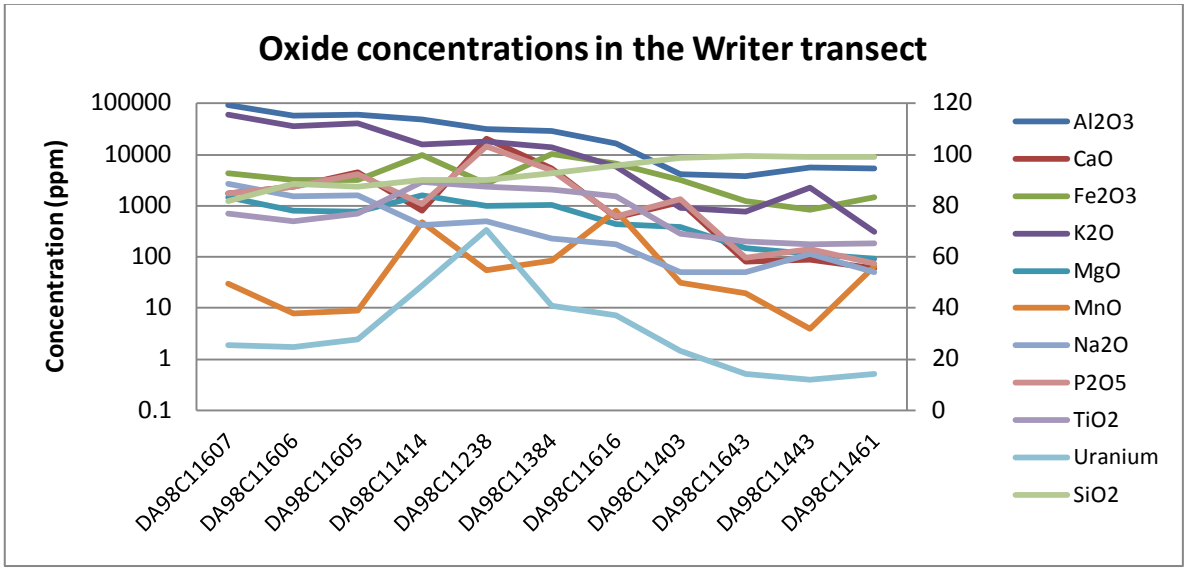

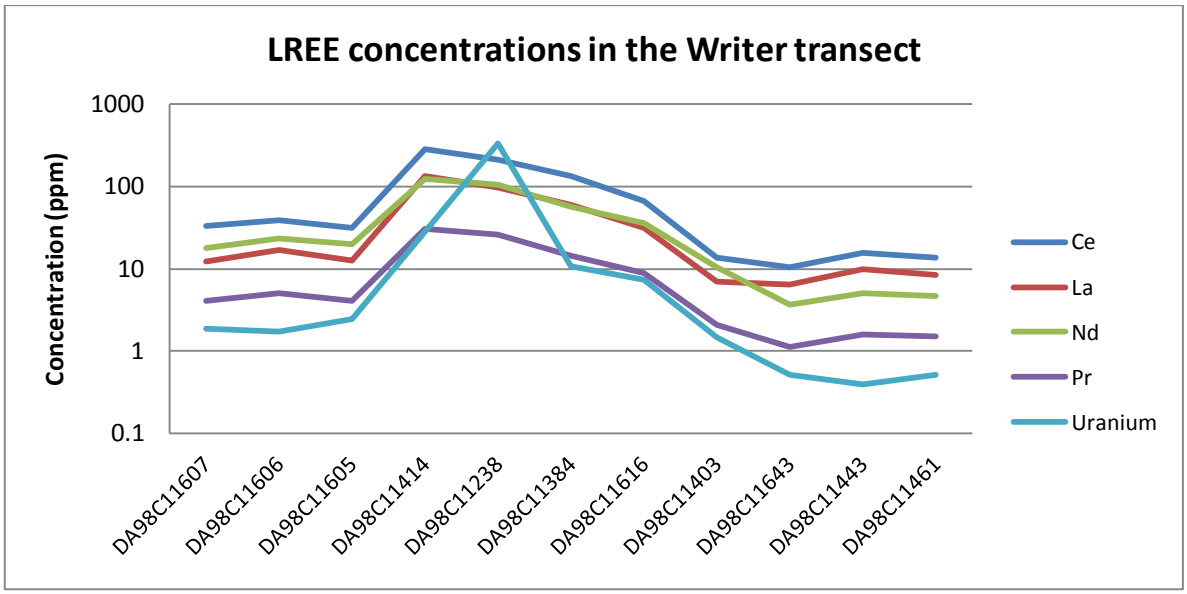

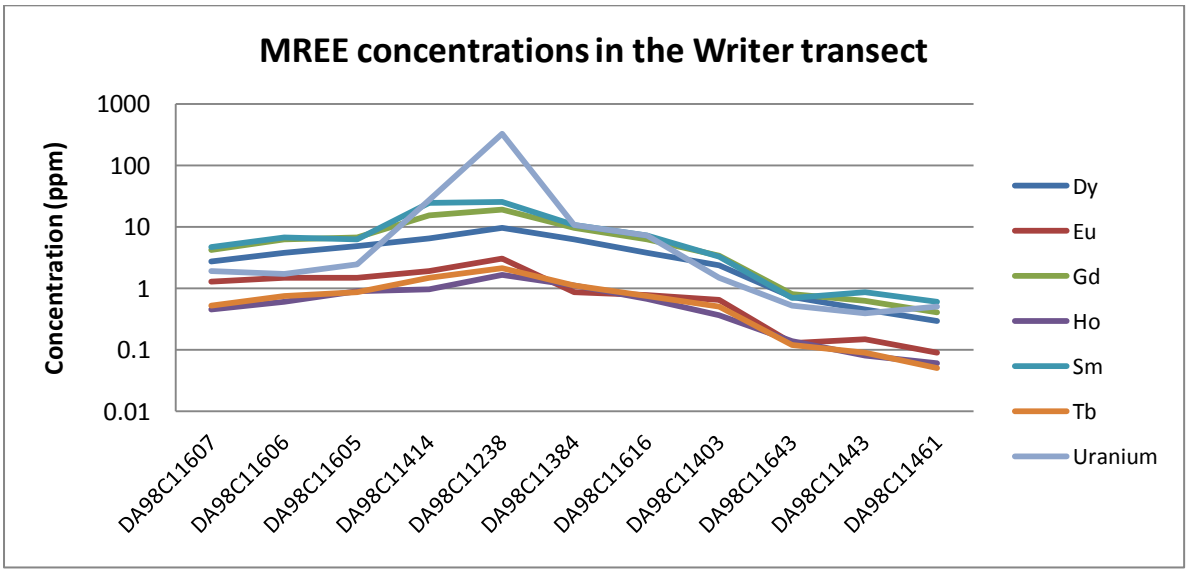

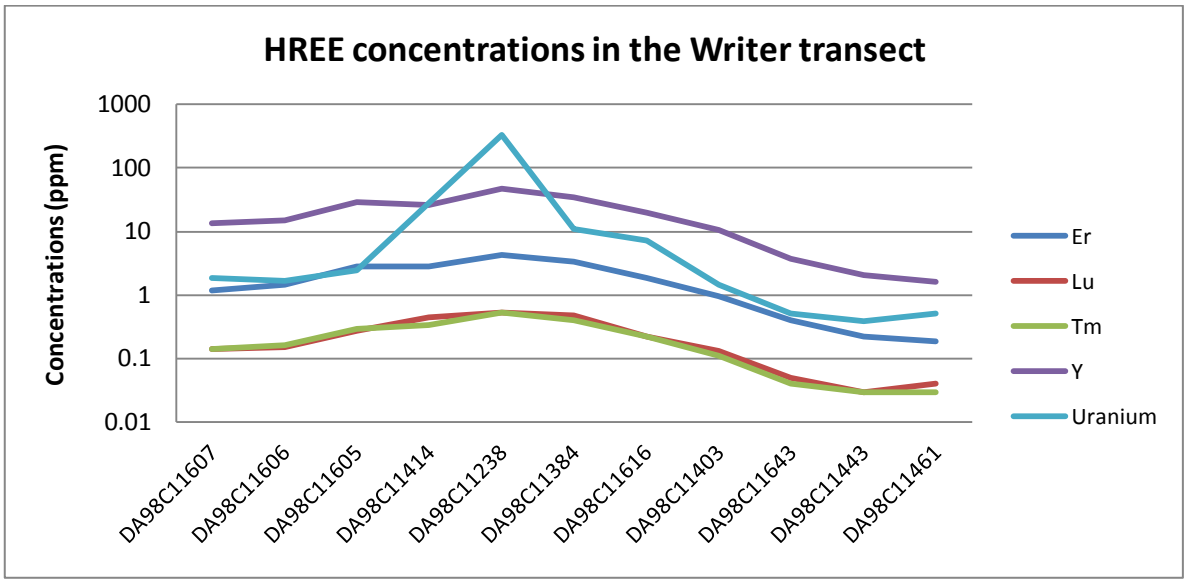
HREE concentrations in the Writer transect
Concentrations (ppm)
1000
100
10
1
0.1
0.01
DA98C11607
DA98C11606
DA98C11605
DA98C11414
DA98C11238
DA98C11384
DA98C11616
DA98C11403
DA98C11643
DA98C11443
DA98C11461
Er
Lu
Tm
Y
Uranium

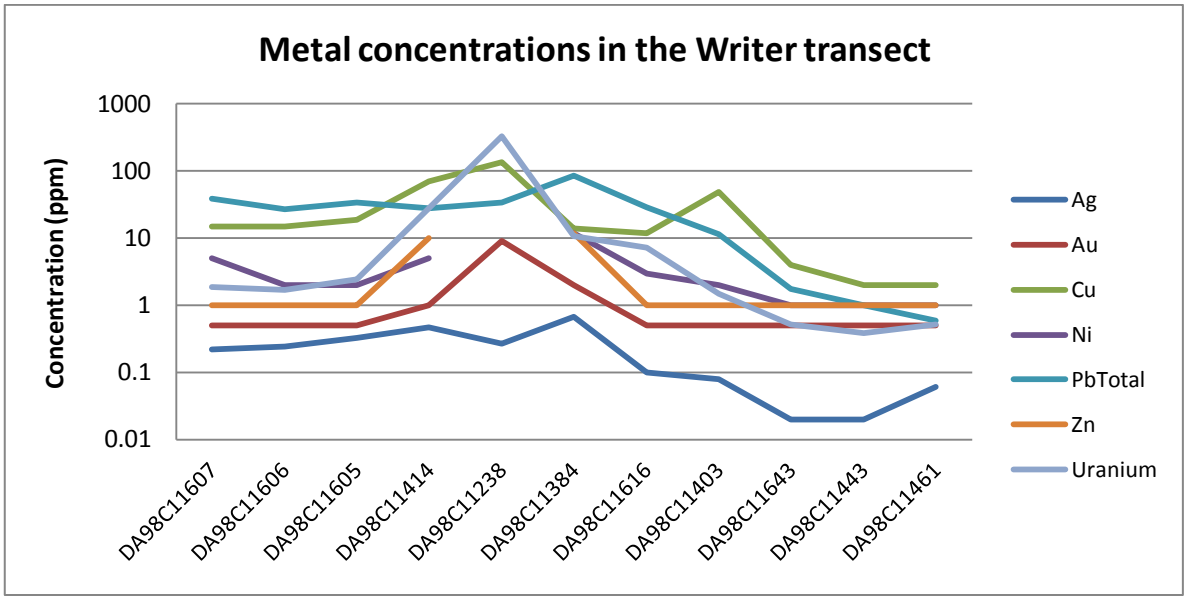
Metal concentrations in the Writer transect
Concentration (ppm)
1000
100
10
1
0.1
0.01
DA98C11607
DA98C11606
DA98C11605
DA98C11414
DA98C11238
DA98C11384
DA98C11616
DA98C11403
DA98C11643
DA98C11443
DA98C11461
Ag
Au
Cu
Ni
PbTotal
Zn
Uranium

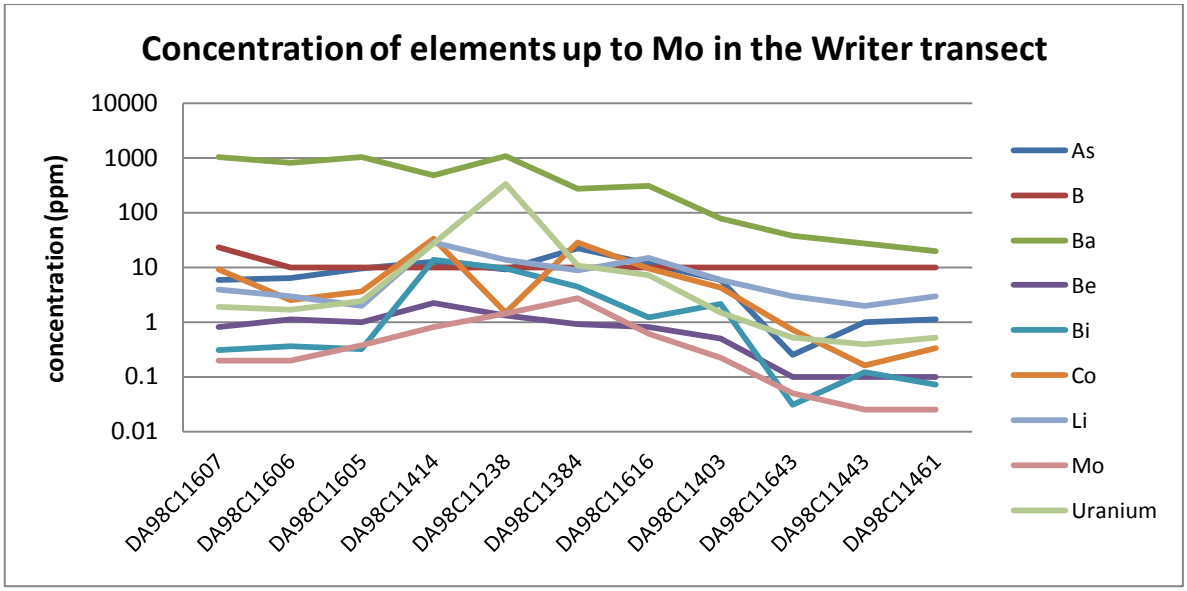
Concentration of elements up to Mo in the Writer transect
concentration (ppm)
10000
1000
100
10
1
0.1
0.01
DA98C11607
DA98C11606
DA98C11605
DA98C11414
DA98C11238
DA98C11384
DA98C11616
DA98C11403
DA98C11643
DA98C11443
DA98C11461
As
B
Ba
Be
Bi
Co
Li
Mo
Uranium

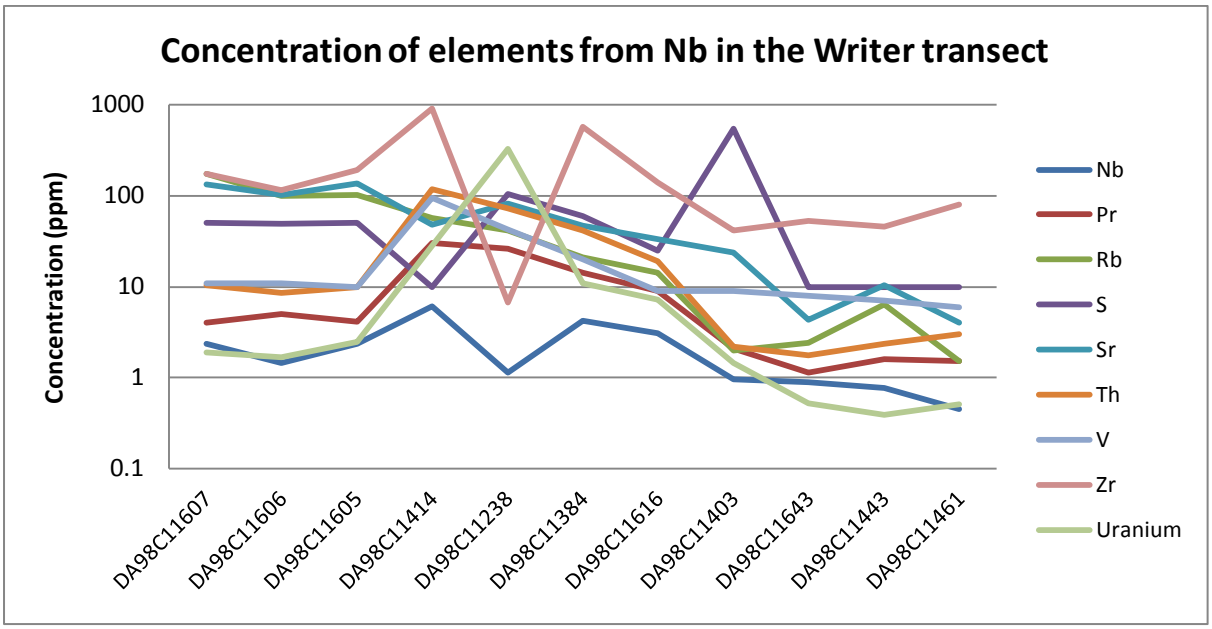
Concentration of elements from Nb in the Writer transect
Concentration (ppm)
1000
100
10
1
0.1
DA98C11607
DA98C11606
DA98C11605
DA98C11414
DA98C11238
DA98C11384
DA98C11616
DA98C11403
DA98C11643
DA98C11443
DA98C11461
Nb
Pr
Rb
S
Sr
Th
V
Zr
Uranium

Appendix 9 – Hand sample descriptions

Writer Transect

Sample DA98C11607

Hand sample description

This sample is a fine grained sandstone that is well sorted with rounded grains. It is light yellowy-brown in colour which changes to a pink colour towards the weathered surface. The layers become progressively darker towards the weathered surface. The colour of the weathered surface is generally a dark red/brown. There are what appear to be flecks of mica (possibly bleached biotite) throughout the sample with flacks ranging from 0.1 to 0.5 mm in size. The entire sample is strongly silicified.

Sample DA98C11606

Hand sample description

This sample is a fine grained, well sorted sandstone with rounded grains. It is generally light brown in colour but changes colour close to weathered surfaces. There are two weathered surfaces of different colour. One is a red-brown colour towards which the light brown sandstone becomes orange-red. The other surface is a made up of larger, medium brown quartz crystals. The light brown sandstone becomes more yellowy as it approaches this surface. As for sample DA98C11607, this sample also contains small flecks of mica and is strongly silicified.

Sample DA98C11605

Hand sample description

This is a fine grained, well sorted and rounded sandstone. It is light gray to light brown in colour and as for the samples mentioned above it becomes darker towards the weathered surface. The weathered surface is a dark orange-brown colour. There appears to be patches of iron staining in this sample which is also strongly silicified.

Sample DA98C11414

Hand sample description

This sample appears to be coarser grained than the previous samples. It is possibly a coarse grained sandstone which will be better determined with optical microscopy. The sample is generally light brown with a medium to dark brown weathered surface. It contains small holes that appear to be filled by very fine orange clay. A quartz vein cuts through the sample which is also strongly silicified.

Sample DA98C11238

Hand sample description

This sample has the highest uranium content out of the writer samples. It is a medium grey, very fine, strongly silicified sandstone with clasts or patches of a fine, light brown material and a dark brown weathered surface. There is brown staining associated with fractures through the sample that are occasionally filled with larger (up to 0.5mm) quartz crystals. There are small red-brown patches of clay like material and small patches of green that occur on the surface or surrounding the small red-brown patches.

Sample DA98C11384

Hand sample description

This sample is similar to sample DA98C11238 in that it is a medium grey sandstone with yellow-brown clasts or patches. The main difference is that the clasts or patches have been slightly dissolved and the remaining clay is a much darker yellow than in the previous sample. There are occasional black flecks and larger quartz crystals throughout the sample, the grain size of which will be determined in thin section.

Sample DA98C11616

Hand sample description

This sample is a dark pink and dark grey-black sandstone with a dark red-brown weathered surface. The different colours tend to form „layers' within the sandstone. It is fine grained, well sorted, rounded and strongly silicified and contains a small area of larger quartz grains close to the weathered surface.

Sample DA98C11403

Hand sample description

This is a very fine to medium sandstone that varies in colour, size and friability from the centre of the sample towards the weathered surface. In the centre it is medium grey, very fine, and silicified. The sandstone then becomes light brown and becomes progressively darker until it turns red at the weathered surface. The sorting of the grains becomes poorer and the sandstone becomes more friable towards the weathered surface. Unlike the other samples, the weathered surface is coated by a very fine grained brown material.

Sample DA98C11643

Hand sample description

This sample is a fine to medium grained, light pink sandstone that is well sorted, rounded and strongly silicified. The colour darkens slightly as it nears the weather surface which is light brown in colour. There are occasional patches of a red fine grained material on the weathered surface.

Sample DA98C11443

Hand sample description

This sample is a fine grained, silicified sandstone. It is light pink in colour with irregular purple patches throughout the sample. The light colour darkens towards the edge with a light stripe seen just below the weathered surface which is brown colour with occasional whitish sections. There are occasional coarser quartz lenses that appear to have no change in colour from the light pink.

Sample DA98C11461

Hand sample description

This sample is a light pink/purple sandstone with a fine brown weathered surface. There is also a possible fracture surface that is mostly white and is made up of larger quartz grains. The sandstone is fine grained and strongly silicified. There are occasional small flecks that are red, black or purple.

Casper transect

Sample DA98C11222

Hand sample description

This sample is a red orange colour with patches of purple. The colours get progressively darker towards the weathered surface which is a dark brown colour. It is a medium grained sandstone with rounded to sub-rounded grains with occasional quartz pebbles up to 5mm in size. The sample is silicified in the centre but becomes progressively crumbly towards the weathered surface.

Sample DA98C11245

Hand sample description

This is a light pink/orange sandstone whose colours get darker and patchier towards the grey weathered surface. It is fine grained with rounded, well sorted grains and appears strongly silicified. The sample contains patches of a dark red material and prismatic quartz crystals (1mm) on a fracture surface. There are occasional patches of yellow throughout the sample.

Sample DA98C11244

Hand sample description

This sample is a patchy light brown/orange/red sandstone. The colours grade into dark red near the brown/black weathered surface. It is a fine to medium sandstone with sub-angular grains and poor sorting. Pebbles occur below the weathered surface along with granules in small layers. There are occasional patches of pinky clay within the sample.

Sample DA98C11243

Hand sample description

This sample is a fine to medium grained sandstone that is patchy and light brown and orange in colour. The grains are sub-angular and moderately sorted. The orange colour fades away close to the light grey to black weathered surface. The sample is also slightly silicified away from the weathered surface. Occasional quartz filled fractures are also present.

Sample DA98C10016

Hand sample description

This sample is a dark purple/pink fine grained sandstone with a brown weathered surface. The sandstone is strongly silicified and has grains that are rounded to sub-rounded and well sorted. There are occasional quartz filled fractures in the sample as well as gaps containing red, pink or orange clay like material.

Sample DA98C11251

Hand sample description

This sample is light to dark in colour grading to dark red beneath a light brown to dark weathered surface. It is a fine grained sandstone with sub-rounded grains and moderate sorting. Occasional quartz granules occur throughout the sample. There appears to be clays cementing grains together and the sample is weakly silicified.

Sample DA97C10294

Hand sample description

This sample has the highest uranium content in the Casper transect. It is a fine grained, dark orange/brown/purple sandstone with a dark brown weathered surface that is finer grained. The grains are rounded and well sorted and the sample appears to be moderately silicified. There is a dark brown patch containing a very fine light yellow material which is thought to be the source of the uranium.

Sample DA98C11261

Hand sample description

This sample is a dark purple sandstone with red/brown clay like patches occurring throughout. It is fine grained and well sorted with sub-rounded grains. The weathered surface is light to dark brown in colour and the sample is moderately silicified.

Sample DA98C11273

Hand sample description

This sample is a fine to medium grained sandstone that is patchy light brown, pink and orange with occasional brown clasts. The grains are sub-rounded to sub-angular and the sample is fairly well sorted. There appears to be clay cementing the quartz grains together. This sample is incompetent as it has a very crumbly texture.

Sample DA98C11279

Hand sample description

This sample is a fine grained, strongly silicified sandstone. It is dark purple in colour with patches of very light brown and orange. There are small fragments of dark brown clay clasts below a dark brown weathered surface. The sample is moderately to well sorted with sub-rounded grains.

Sample DA98C11294

Hand sample description

This sample is a medium to coarse grained dark purple sandstone with occasional dark orange patches. The weathered surface is dark brown and the whole sample appears very crumbly. Clay appears to cement grains together within the sample. It is a moderately sorted sandstone with sub-rounded to sub-angular grains.

Sample DA98C11296

Hand sample description

This sample is a fine grained sandstone that is weakly silicified. It is well sorted with rounded to sub-rounded grains. It contains small patches of white clay and occasional 2mm grains of quartz. Brown staining is evident of fracture surfaces within the sample.

Flying Ghost EW transect

Sample DA97C10803

Hand sample description

This sample is a very fine sandstone with occasional 1mm grains of quartz. It is a medium purple colour but has been altered to yellow and dark orange in patches and has a dark brown weathered surface. The darker colours tend to appear in „layers' within the sample. This sample is well sorted with rounded grains.

Sample DA97C10802

Hand sample description

This sample is a very fine sandstone that is well sorted with rounded grains. It is medium pink in colour with patchy layers of dark orange/yellow and has a black weathered surface. There appears to be a faint layering in the sample along which the sample fractures.

Sample DA97C10801

Hand sample description

This sample is a fine grained, silicified sandstone that is moderately sorted with sub-rounded to sub-angular grains. It is dark purple in colour with a darker red colour in factures and on the weathered surface. There are very thin layers of very clean, medium grained sandstone that appear to be cemented by clay.

Sample DA97C10800

Hand sample description

This sample is a very fine sandstone, sandstone that is well sorted with rounded to sub-rounded grains. It is an orange colour with lighter stripes or layers. The colour becomes dark red as it nears the brown weathered surface. There are occasional 0.5 to 1 mm quartz grains throughout the sample and there appears to be clay cementing the grains together.

Sample DA97C10799

Hand sample description

This sample is a fine grained, weakly silicified sandstone that is well sorted with rounded to sub-rounded grains. It is a purple/pink colour that becomes darker towards a dark brown weathered surface. There are occasional small lithics within the sample which appears to have clay in some places cementing grains together.

Sample DA97C10798

Hand sample description

This sample is a medium grained sandstone that is well sorted with sub-rounded to sub-angular grains. The sample is generally a pink/orange colour with patches of darker orange, yellow or red. The sample also has a dark grey to black weathered surface which has occasional orange specks in places. It is incompetent as it crumbles very easily.

Sample DA97C10755

Hand sample description

This sample is a fine to medium grained sandstone that it moderately to well sorted with sub-rounded to sub-angular grains. It is a patchy light pink, orange and dark red/brown colour with a dark brown weathered surface. The darker parts of the sample appear to be slightly silicified and the lighter parts are less competent.

Sample DA97C10754

Hand sample description

This sample is a fine grained sandstone that is moderately sorted with sub rounded and sub angular grains. It is a light pink colour with patchy veins of red becoming more common towards the speckled brown/orange weathered surface. It contains occasional granules in areas close to the weathered surface.

Sample DA97C10202

Hand sample description

This sample is a medium grained sandstone with moderate sorting and sub-angular grains. It is generally patchy light pink, yellow and orange in colour with no colour change in the presence of fractures through the sample. It is very crumbly and breaks apart easily when held.

Sample DA97C10204

Hand sample description

This sample is a fine grained, competent sandstone that is well sorted with rounded grains. It is a medium pink/grey in colour with a darker pink „layer' through the middle. There are occasional patches of dark orange on the surface. This sample is much more competent than sample DA97C10202.

Sample DA97C10190

Hand sample description

This sample is very similar to sample DA97C10204. It is a fine grain, competent sandstone that is well sorted with rounded grains. It is a medium pink/grey colour with occasional clasts of clay. There are also occasional black speck throughout the sample.

Sample DA97C10191

Hand sample description

This is the sample with the highest concentration of uranium in the north-east transect of the Flying Ghost area. It is a fine grained sandstone that is moderately sorted with sub rounded grains. It is generally a light orange/pink colour with dark brown becoming more common towards the dark brown weathered surface. There are yellow clay patches on the surface and patches of dark red and black in darker parts of the sample. There is also some yellow staining on some of the lighter sections of the sample.

Sample DA97C10785

Hand sample description

This sample is a fine to medium grained sandstone that is moderately sorted with sub-rounded to sub-angular grains. The grain size is generally larger around fractures in the sandstone. It is generally light pink in colour with orange staining in the fractures and green minerals are present beneath a dark brown weathered surface. This sample is slightly incompetent as the grains tend to fall away with little effort applied.

Sample DA97C10741

Hand sample description

This sample is a medium grained sandstone that if moderately sorted with sub-angular grains. It is generally light orange in colour but changes to a dark red as it nears the medium brown weathered surface. As for sample DAD97C10785, there are small green minerals or staining beneath the weathered surface. There is a possible clay matrix and the sample is very incompetent.

Sample DA97C10742

Hand sample description

This sample is a medium sandstone that is moderately sorted with sub-angular grains in a clay matrix. It is medium purple in colour with lighter pink/orange patches that are associated with clay. The weathered surface is brown in colour with 1 to 2 mm quartz crystals common. There is an 8mm pebble in the sample.

Sample DA97C10743

Hand sample description

This sample is very similar to sample DAD97C10742. It is a medium grained, sub-angular, moderately sorted sandstone that is medium purple in colour. The main differences are that this sample has lighter patches and a black/green and red/brown weathered surface along with a reddish colour beneath the weathered surface. This sample is also cemented by clay and is slightly crumbly.

Sample DA97C10744

Hand sample description

This sample is a medium grained sandstone that is moderately sorted with sub-angular grains. It is dark purple in colour with light orange and light brown patches and a brown weathered surface. It is similar to samples DA97C10743 and DA97C10742 with the exception that this sample is less competent.

Sample DA97C10745

Hand sample description

This sample is a speckled orange colour that is lighter and darker in places with a weathered surface that is dark brown. It is a medium grained sandstone that is moderately sorted with sub-angular grains. There are rare lithics amongst the quartz grains which appear to be cemented by a clay matrix.

Sample DA97B10069

Hand sample description

This sample is a fine grained, silicified sandstone that is moderately to well sorted with sub-angular grains. It is speckled pink, red, yellow and white in colour with a patchy black weathered surface. Clay fills fractures in the sample that also had patches of yellow on the surface.

Sample DA97B10070

Hand sample description

This sample is a fine grained sandstone that is well sorted with sub-rounded grains. It is light pink/orange in colour with a darker pink layer and a brown/black weathered surface. The sandstone becomes slightly coarser and less competent towards the weathered surface with clay becoming more common. Dark red patches can be seen in fractures.

Sample DA97B10071

Hand sample description

This sample is a fine grained sandstone that is well sorted with sub-angular grains. It is light brown in colour with a dark brown weathered surface. The sample is clay rich with clay visible between grains and within fractures. It is also fairly incompetent.

Sample DA97B10072

Hand sample description

This sample is a fine grained, slightly incompetent sandstone that is well sorted with sub-rounded grains. It is light to dark orange in colour with the colours appearing as „stripes' through the sample. The weathered surface is dark brown in colour and the grains beneath the surface are crumbly and clay rich.

Appendix 10 – Correlation matrices for rare earth elements and trace elements other than REEs

Correlation Matrix for rare earth elements													
	Ce	**Dy**	**Er**	**Eu**	**Gd**	**Ho**	**La**	**Lu**	**Nd**	**Pr**	**Sm**	**Tb**	**Tm**
Ce	1.000	0.376	0.315	0.726	0.705	0.333	0.638	0.392	0.943	0.958	0.851	0.521	0.327
Dy	0.376	1.000	0.985	0.614	0.762	0.993	0.252	0.925	0.417	0.398	0.493	0.954	0.964
Er	0.315	0.985	1.000	0.531	0.681	0.996	0.211	0.947	0.339	0.327	0.408	0.900	0.986
Eu	0.726	0.614	0.531	1.000	0.925	0.563	0.467	0.584	0.831	0.792	0.911	0.782	0.537
Gd	0.705	0.762	0.681	0.925	1.000	0.712	0.447	0.714	0.801	0.758	0.903	0.909	0.674
Ho	0.333	0.993	0.996	0.563	0.712	1.000	0.225	0.941	0.364	0.349	0.436	0.923	0.982
La	0.638	0.252	0.211	0.467	0.447	0.225	1.000	0.249	0.621	0.636	0.550	0.340	0.217
Lu	0.392	0.925	0.947	0.584	0.714	0.941	0.249	1.000	0.410	0.400	0.482	0.875	0.976
Nd	0.943	0.417	0.339	0.831	0.801	0.364	0.621	0.410	1.000	0.991	0.944	0.589	0.346
Pr	0.958	0.398	0.327	0.792	0.758	0.349	0.636	0.400	0.991	1.000	0.907	0.559	0.336
Sm	0.851	0.493	0.408	0.911	0.903	0.436	0.550	0.482	0.944	0.907	1.000	0.684	0.413
Tb	0.521	0.954	0.900	0.782	0.909	0.923	0.340	0.875	0.589	0.559	0.684	1.000	0.882
Tm	0.327	0.964	0.986	0.537	0.674	0.982	0.217	0.976	0.346	0.336	0.413	0.882	1.000

Correlation Matrix for trace elements other than REE's																											
Ag	1.000	0.156	0.119	0.031	0.185	0.137	0.277	0.117	0.222	0.054	0.083	0.181	0.091	0.320	0.064	0.059	0.195	0.026	0.009	0.007	0.140	0.107	0.063	0.035	0.180
As	0.156	1.000	0.631	0.014	0.093	0.255	0.046	0.321	0.283	0.016	0.186	0.048	0.264	0.498	0.086	0.100	0.050	0.059	0.043	0.007	0.583	0.244	0.104	0.074	0.017
Au	0.119	0.631	1.000	0.095	0.080	0.123	0.010	0.173	0.032	0.019	0.052	-0.001	0.208	0.561	0.594	0.444	0.008	0.013	-0.004	-0.003	0.436	0.112	0.122	0.042	-0.015
B	0.031	0.014	0.095	1.000	0.060	0.135	-0.020	0.085	-0.017	0.150	0.025	0.143	0.168	0.010	0.085	0.068	0.126	0.024	0.019	-0.008	0.014	0.150	0.035	0.001	0.098
Ba	0.185	0.093	0.080	0.060	1.000	0.207	0.056	0.244	0.136	0.162	0.041	0.167	0.272	0.260	0.132	0.139	0.519	0.158	0.063	0.001	0.086	0.071	0.113	0.076	0.076
Be	0.137	0.255	0.123	0.135	0.207	1.000	0.043	0.453	0.696	0.218	0.281	0.328	0.308	0.099	0.165	0.119	0.248	0.020	0.010	0.005	0.030	0.307	0.110	0.109	0.146
Bi	0.277	0.046	0.010	-0.020	0.056	0.043	1.000	0.045	0.146	0.014	0.080	0.022	0.003	0.271	0.002	0.001	0.023	0.020	-0.005	0.001	0.073	0.023	0.014	-0.001	0.006
Co	0.117	0.321	0.173	0.085	0.244	0.453	0.045	1.000	0.369	0.561	0.144	0.270	0.617	0.250	0.099	0.110	0.212	0.026	0.019	0.007	0.181	0.190	0.080	0.255	0.122

	Zr	Zn	Y	V	U_t_	Th	Sr	S	Rb	Pt	Pd	PbTot	Ni	Nb	Mo	Li	Cu
Ag	0.180	0.035	0.063	0.107	0.140	0.007	0.009	0.026	0.195	0.059	0.064	0.320	0.091	0.181	0.083	0.054	0.222
As	0.017	0.074	0.104	0.244	0.583	0.007	0.043	0.059	0.050	0.100	0.086	0.498	0.264	0.048	0.186	0.016	0.283
Au	-0.015	0.042	0.122	0.112	0.436	-0.003	-0.004	0.013	0.008	0.444	0.594	0.561	0.208	-0.001	0.052	0.019	0.032
B	0.098	0.001	0.035	0.150	0.014	-0.008	0.019	0.024	0.126	0.068	0.085	0.010	0.168	0.143	0.025	0.150	-0.017
Ba	0.076	0.076	0.113	0.071	0.086	0.001	0.063	0.158	0.519	0.139	0.132	0.260	0.272	0.167	0.041	0.162	0.136
Be	0.146	0.109	0.110	0.307	0.030	0.005	0.010	0.020	0.248	0.119	0.165	0.099	0.308	0.328	0.281	0.218	0.696
Bi	0.006	-0.001	0.014	0.023	0.073	0.001	-0.005	0.020	0.023	0.001	0.002	0.271	0.003	0.022	0.080	0.014	0.146
Co	0.122	0.255	0.080	0.190	0.181	0.007	0.019	0.026	0.212	0.110	0.099	0.250	0.617	0.270	0.144	0.561	0.369
Cu	0.115	0.140	0.052	0.143	0.048	0.008	-0.002	0.019	0.131	0.020	0.013	0.153	0.155	0.128	0.374	0.018	1.000
Li	0.081	0.108	0.049	0.126	0.016	0.005	0.029	0.005	0.084	0.016	0.016	0.036	0.768	0.194	0.005	1.000	0.018
Mo	0.025	0.046	0.020	0.111	0.060	0.004	0.022	0.032	0.024	0.028	0.031	0.144	0.117	0.046	1.000	0.005	0.374
Nb	0.382	0.291	0.084	0.211	-0.004	0.003	0.020	0.049	0.260	0.007	0.007	0.059	0.188	1.000	0.046	0.194	0.128
Ni	0.081	0.208	0.078	0.243	0.214	0.003	0.022	0.011	0.108	0.145	0.145	0.238	1.000	0.188	0.117	0.768	0.155
PbTot	0.023	0.119	0.096	0.155	0.242	0.003	0.006	0.040	0.116	0.343	0.334	1.000	0.238	0.059	0.144	0.036	0.153
Pd	-0.005	0.065	0.226	0.098	0.155	-0.002	0.001	-0.001	0.005	0.861	1.000	0.334	0.145	0.007	0.031	0.016	0.013
Pt	-0.005	0.064	0.284	0.079	0.154	-0.002	0.002	-0.002	0.004	1.000	0.861	0.343	0.145	0.007	0.028	0.016	0.020
Rb	0.176	0.024	0.075	0.068	0.004	-0.001	0.028	0.030	1.000	0.004	0.005	0.116	0.108	0.260	0.024	0.084	0.131
S	-0.015	0.003	0.063	0.018	0.011	-0.003	0.671	1.000	0.030	-0.002	-0.001	0.040	0.011	0.049	0.032	0.005	0.019
Sr	-0.003	-0.001	0.092	-0.006	-0.003	-0.004	1.000	0.671	0.028	0.002	0.001	0.006	0.022	0.020	0.022	0.029	-0.002
Th	0.015	-0.001	0.001	0.015	0.000	1.000	-0.004	-0.003	-0.001	-0.002	-0.002	0.003	0.003	0.003	0.004	0.005	0.008
U_t_	-0.012	0.033	0.148	0.059	1.000	0.000	-0.003	0.011	0.004	0.154	0.155	0.242	0.214	-0.004	0.060	0.016	0.048
V	0.045	0.089	0.043	1.000	0.059	0.015	-0.006	0.018	0.068	0.079	0.098	0.155	0.243	0.211	0.111	0.126	0.143
Y	0.065	0.035	1.000	0.043	0.148	0.001	0.092	0.063	0.075	0.284	0.226	0.096	0.078	0.084	0.020	0.049	0.052
Zn	0.036	1.000	0.035	0.089	0.033	-0.001	-0.001	0.003	0.024	0.064	0.065	0.119	0.208	0.291	0.046	0.108	0.140
Zr	1.000	0.036	0.065	0.045	-0.012	0.015	-0.003	-0.015	0.176	-0.005	-0.005	0.023	0.081	0.382	0.025	0.081	0.115

Appendix 11 – Drill core geochemistry data

See attached CD

Appendix 12 – Graphs for elements in each drill core

DAD-0001

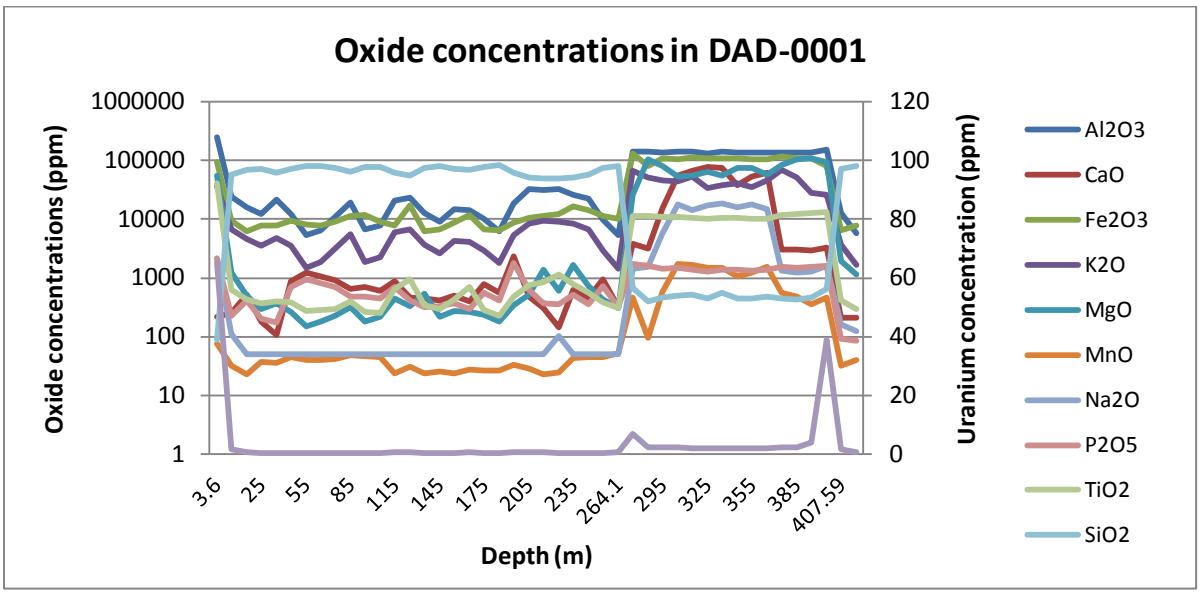

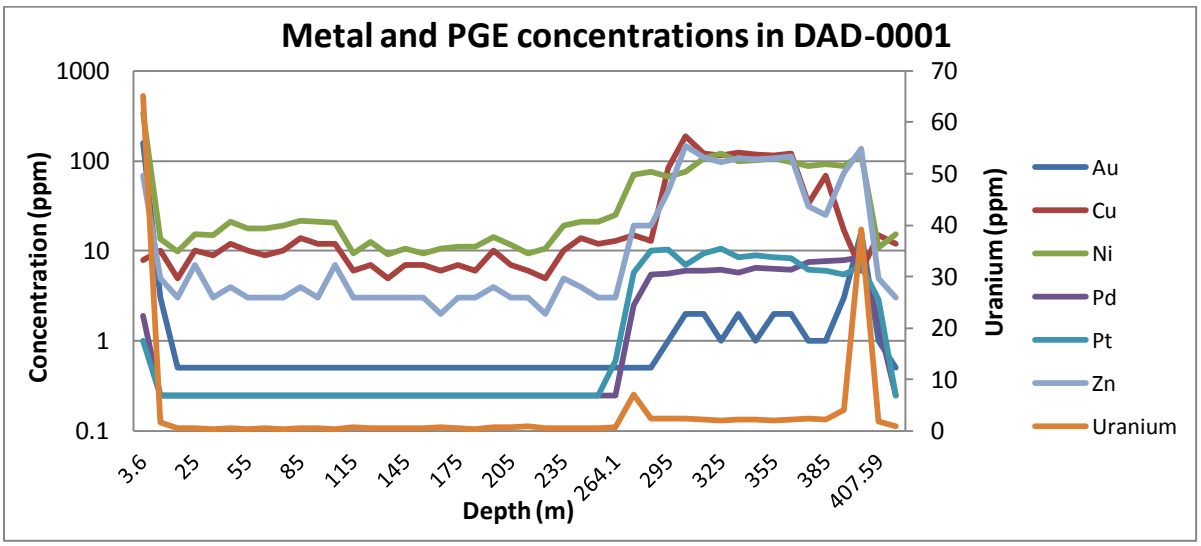

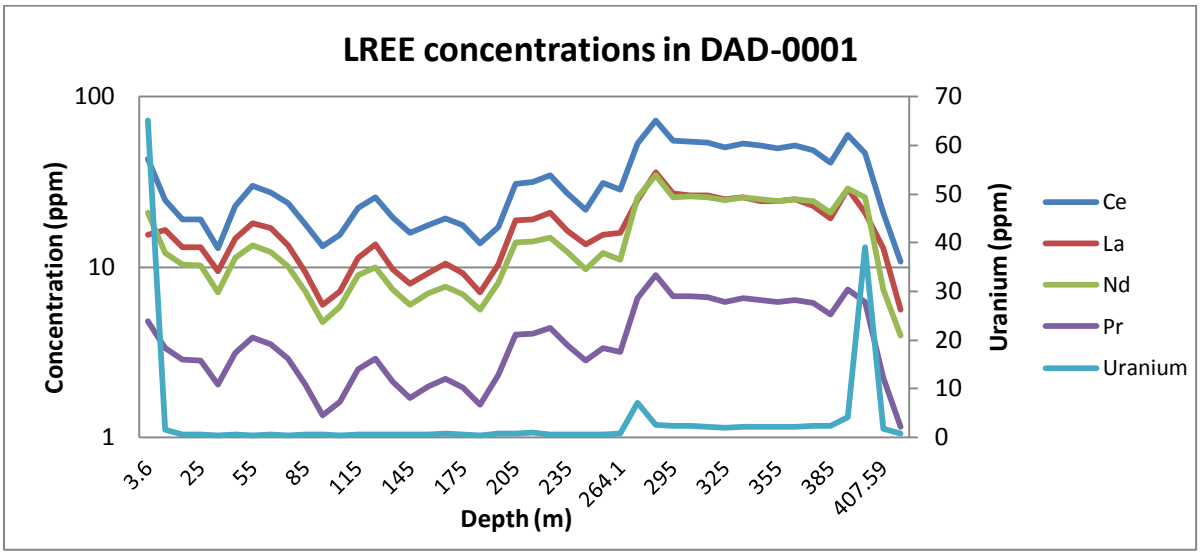
LREE concentrations in DAD-0001
Concentration (ppm)
100
10
1
Uranium (ppm)
70
60
50
40
30
20
10
0
3.6
25
55
85
115
145
175
205
235
264.1
295
325
355
385
407.59
Depth (m)
Ce
La
Nd
Pr
Uranium

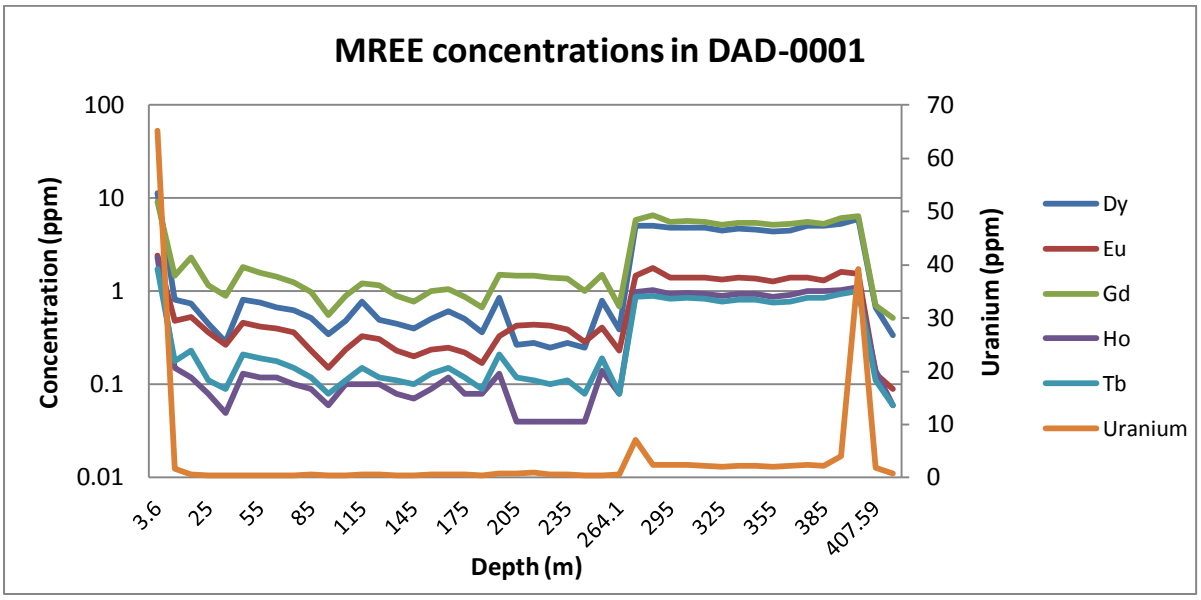
MREE concentrations in DAD-0001
Concentration (ppm)
100
10
1
0.1
0.01
Uranium (ppm)
70
60
50
40
30
20
10
0
3.6
25
55
85
115
145
175
205
235
264.1
295
325
355
385
407.59
Depth (m)
Dy
Eu
Gd
Ho
Tb
Uranium

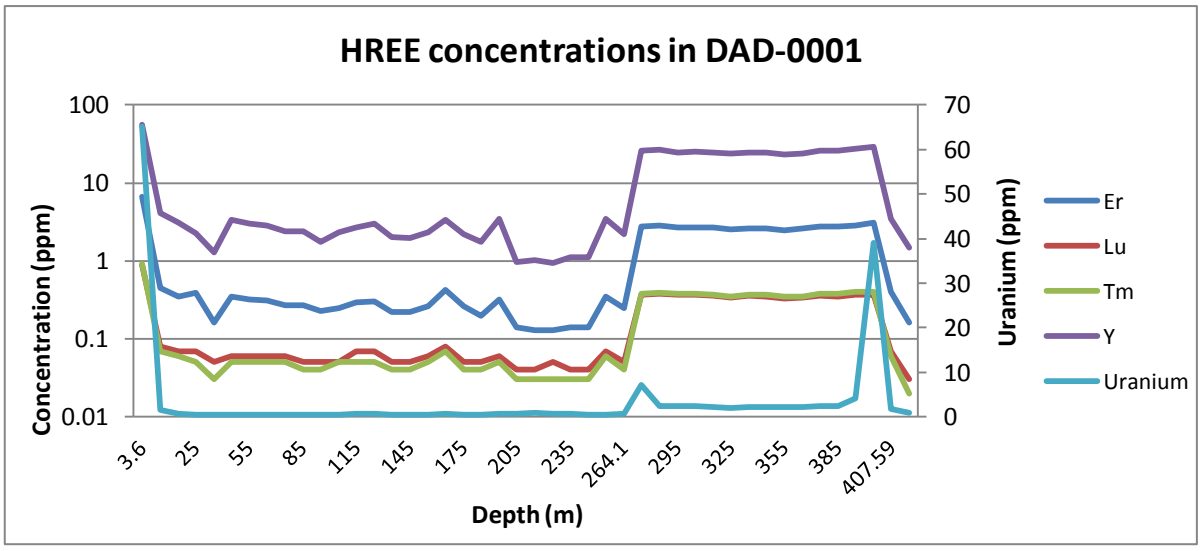
HREE concentrations in DAD-0001
Concentration (ppm)
100
10
1
0.1
0.01
Uranium (ppm)
70
60
50
40
30
20
10
0
3.6
25
55
85
115
145
175
205
235
264.1
295
325
355
385
407.59
Depth (m)
Er
Lu
Tm
Y
Uranium

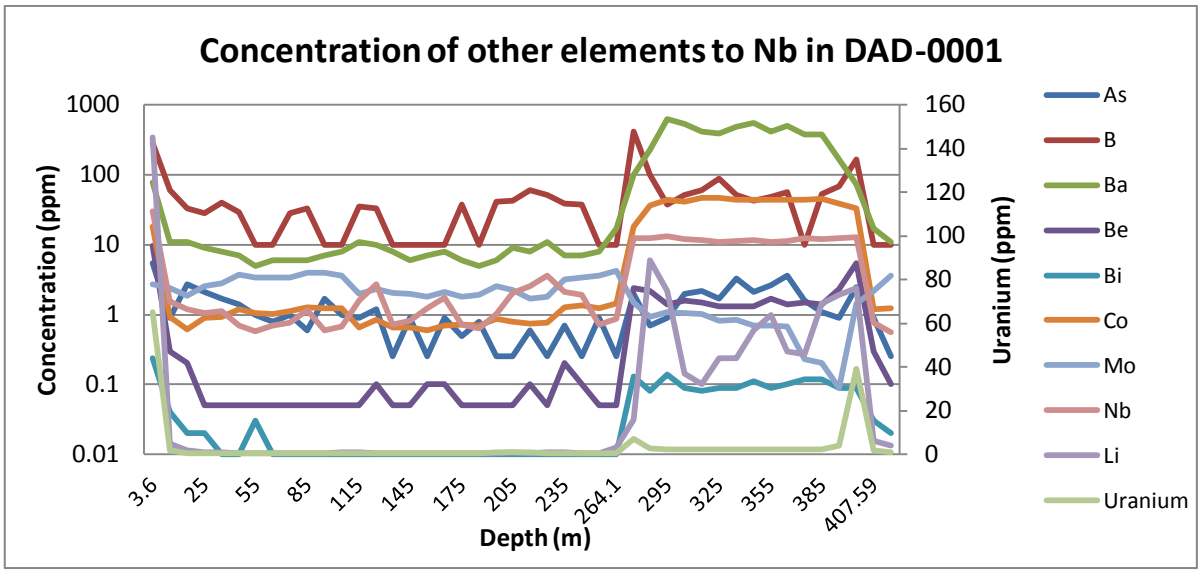
Concentration of other elements to Nb in DAD-0001
Concentration (ppm)
1000
100
10
1
0.1
0.01
Uranium (ppm)
160
140
120
100
80
60
40
20
0
3.6
25
55
85
115
145
175
205
235
264.1
295
325
355
385
407.59
Depth (m)
As
B
Ba
Be
Bi
Co
Mo
Nb
Li
Uranium

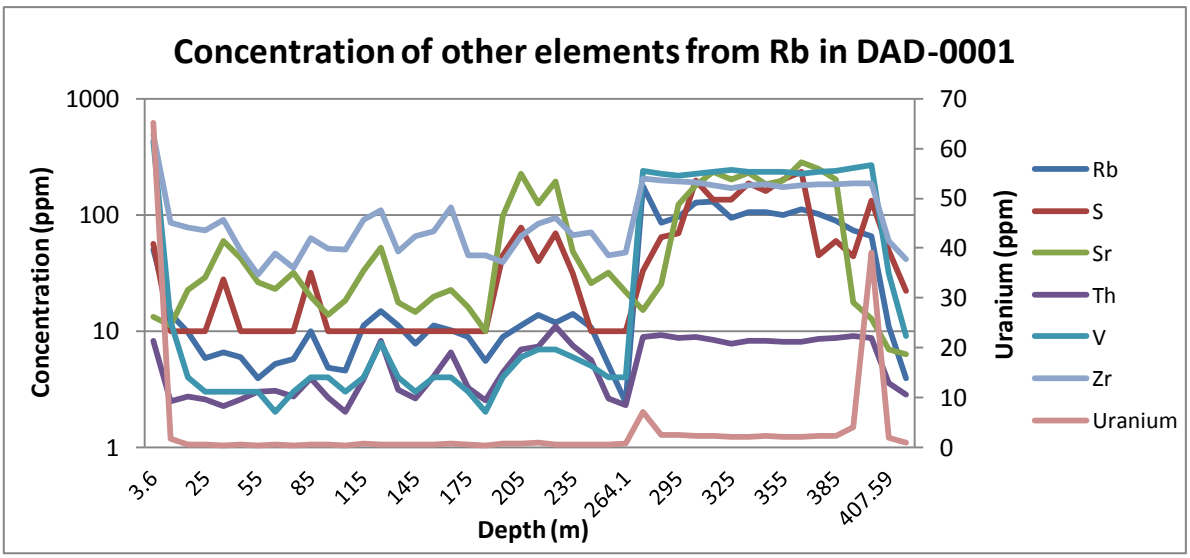
Concentration of other elements from Rb in DAD-0001
Concentration (ppm)
1000
100
10
1
Uranium (ppm)
70
60
50
40
30
20
10
0
3.6
25
55
85
115
145
175
205
235
264.1
295
325
355
385
407.59
Depth (m)
Rb
S
Sr
Th
V
Zr
Uranium

DAD-0002

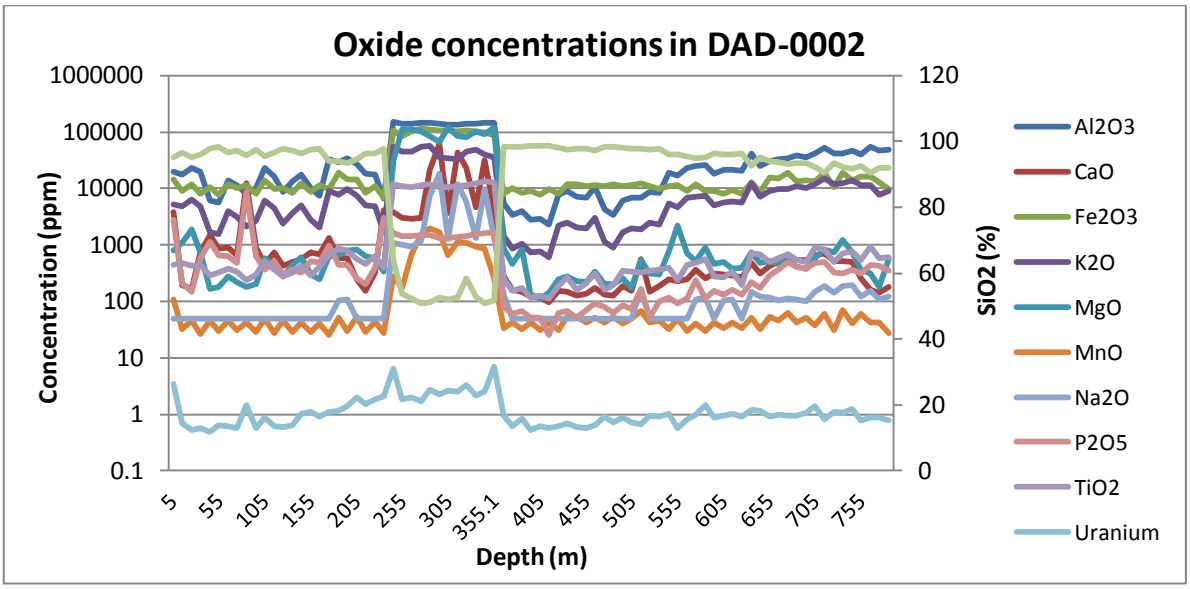
Oxide concentrations in DAD-0002
Concentration (ppm)
1000000
100000
10000
1000
100
10
1
0.1
SiO2 (%)
120
100
80
60
40
20
0
5
55
105
155
205
255
305
355.1
405
455
505
555
605
655
705
755
Depth (m)
Al2O3
CaO
Fe2O3
K2O
MgO
MnO
Na2O
P2O5
TiO2
Uranium

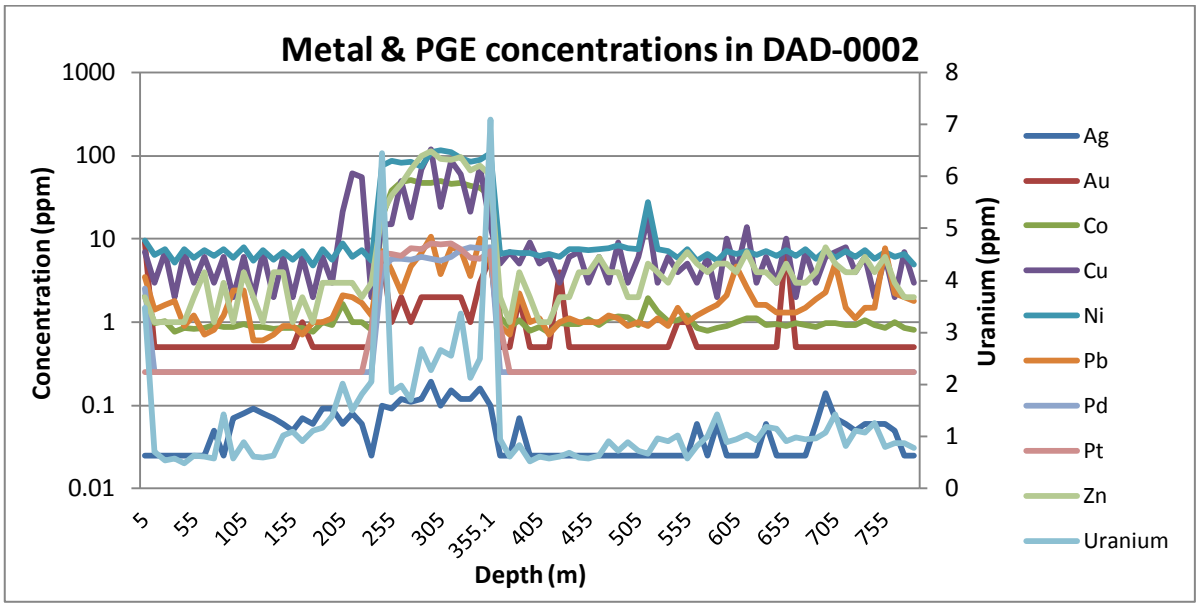
Metal & PGE concentrations in DAD-0002
Concentration (ppm)
Uranium (ppm)
Depth (m)
1000
100
10
1
0.1
0.01
8
7
6
5
4
3
2
1
0
5
55
105
155
205
255
305
355.1
405
455
505
555
605
655
705
755
Ag
Au
Co
Cu
Ni
Pb
Pd
Pt
Zn
Uranium

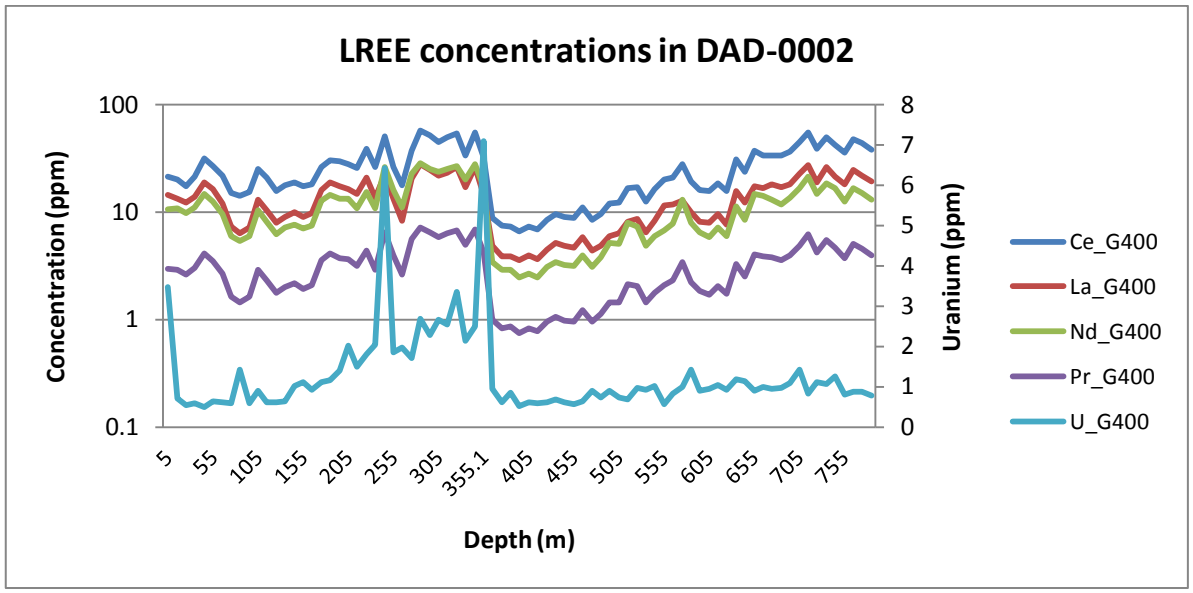
LREE concentrations in DAD-0002
Concentration (ppm)
Uranium (ppm)
Depth (m)
100
10
1
0.1
8
7
6
5
4
3
2
1
0
5
55
105
155
205
255
305
355.1
405
455
505
555
605
655
705
755
Ce_G400
La_G400
Nd_G400
Pr_G400
U_G400

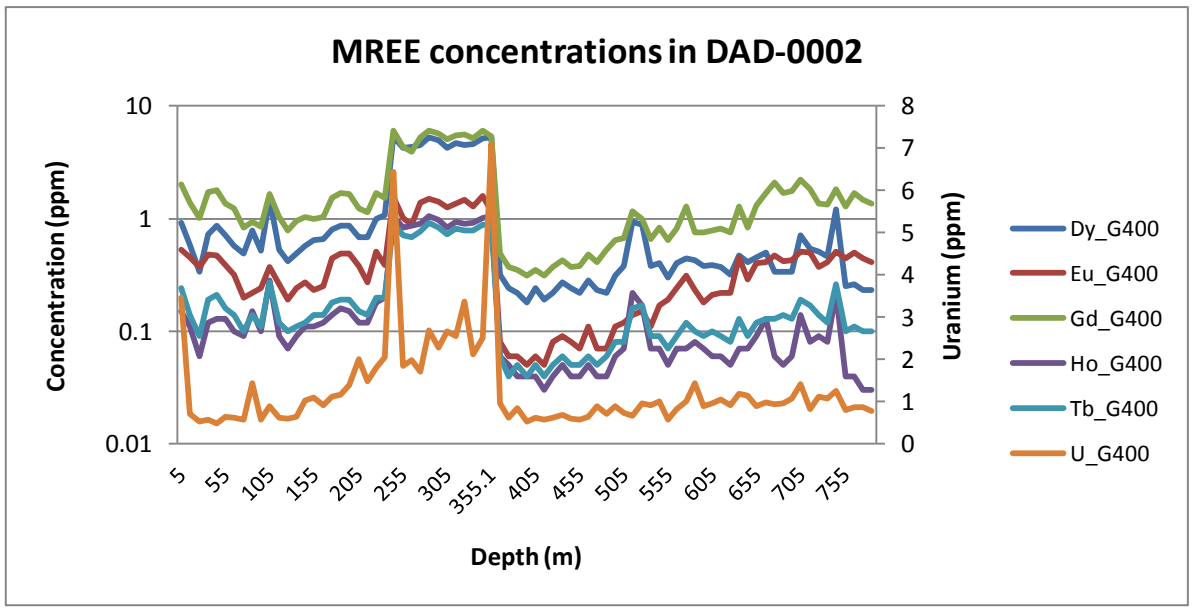
MREE concentrations in DAD-0002
Concentration (ppm)
Uranium (ppm)
Depth (m)
10
1
0.1
0.01
8
7
6
5
4
3
2
1
0
5
55
105
155
205
255
305
355.1
405
455
505
555
605
655
705
755
Dy_G400
Eu_G400
Gd_G400
Ho_G400
Tb_G400
U_G400

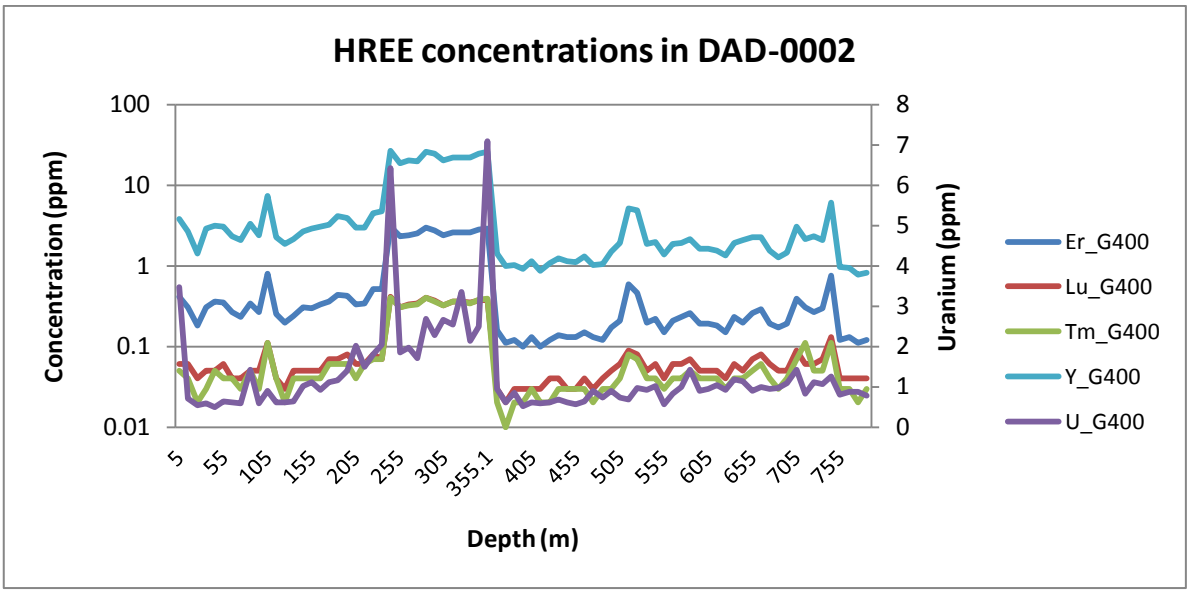
HREE concentrations in DAD-0002
Concentration (ppm)
Uranium (ppm)
Depth (m)
Er_G400
Lu_G400
Tm_G400
Y_G400
U_G400

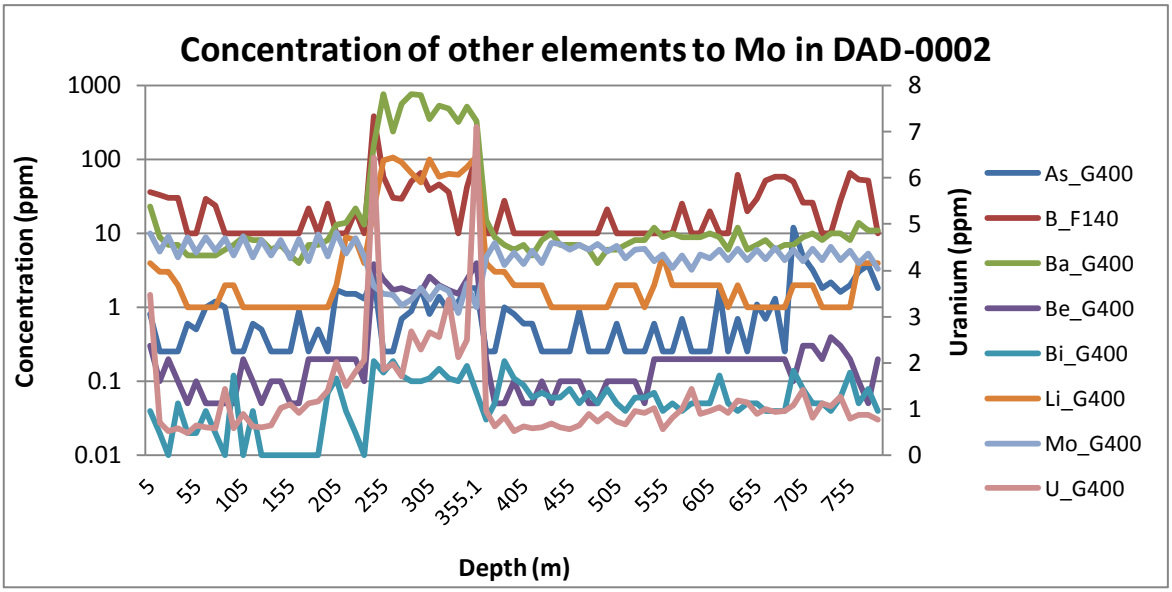
Concentration of other elements to Mo in DAD-0002
Concentration (ppm)
Uranium (ppm)
Depth (m)
As_G400
B_F140
Ba_G400
Be_G400
Bi_G400
Li_G400
Mo_G400
U_G400

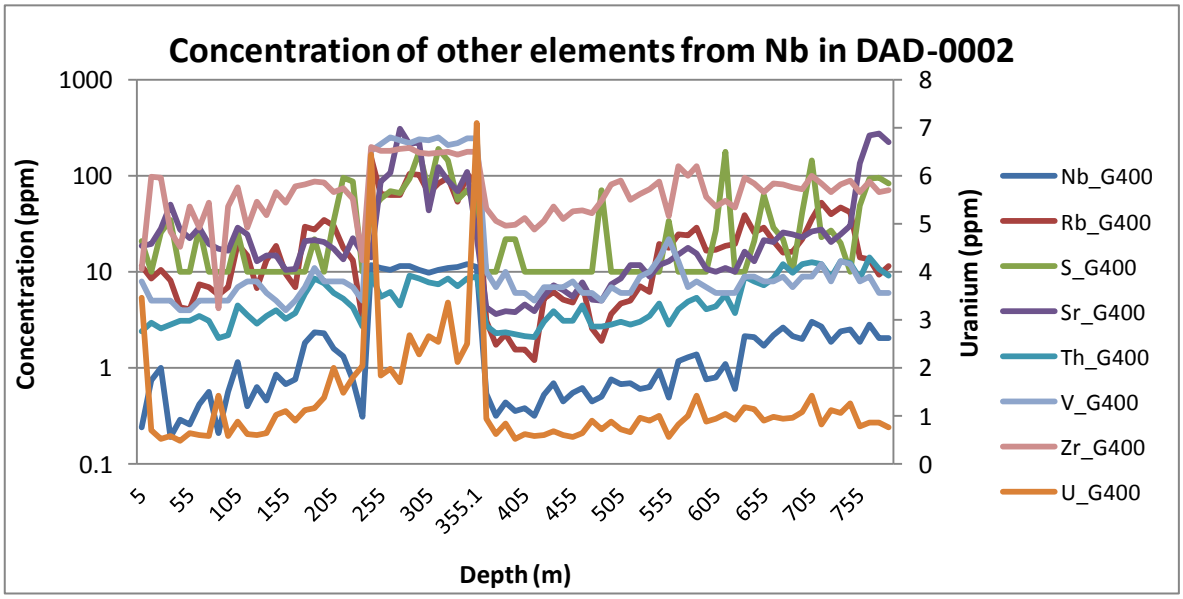
Concentration of other elements from Nb in DAD-0002
Concentration (ppm)
Uranium (ppm)
Depth (m)
Nb_G400
Rb_G400
S_G400
Sr_G400
Th_G400
V_G400
Zr_G400
U_G400

DAD-0003

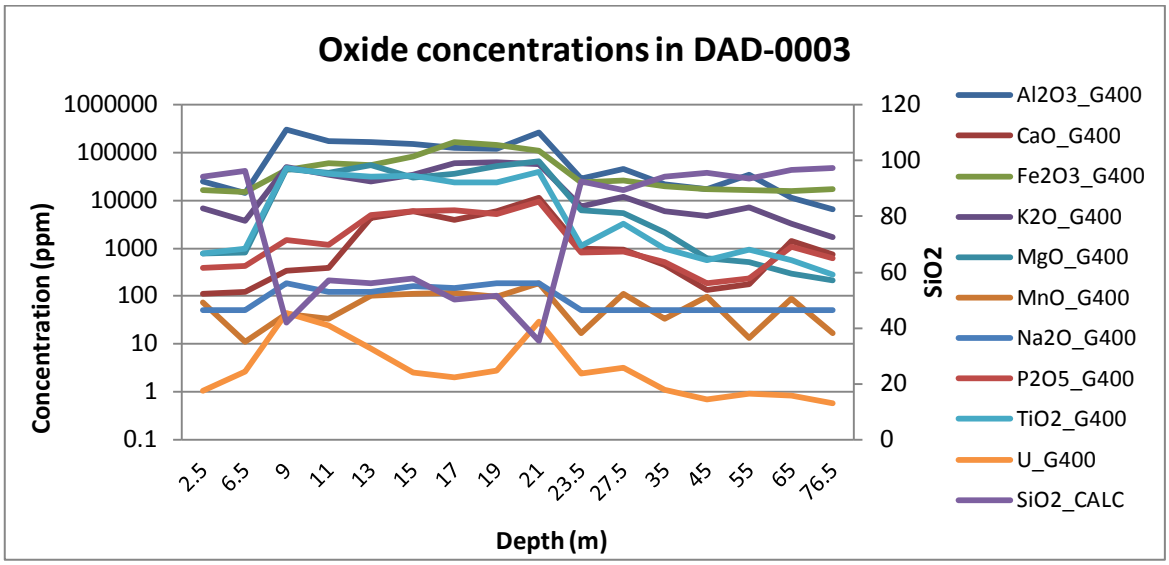
Oxide concentrations in DAD-0003
Concentration (ppm)
1000000
100000
10000
1000
100
10
1
0.1
120
100
80
60
40
20
0
SiO2
2.5
6.5
9
11
13
15
17
19
21
23.5
27.5
35
45
55
65
76.5
Depth (m)
Al2O3_G400
CaO_G400
Fe2O3_G400
K2O_G400
MgO_G400
MnO_G400
Na2O_G400
P2O5_G400
TiO2_G400
U_G400
SiO2_CALC

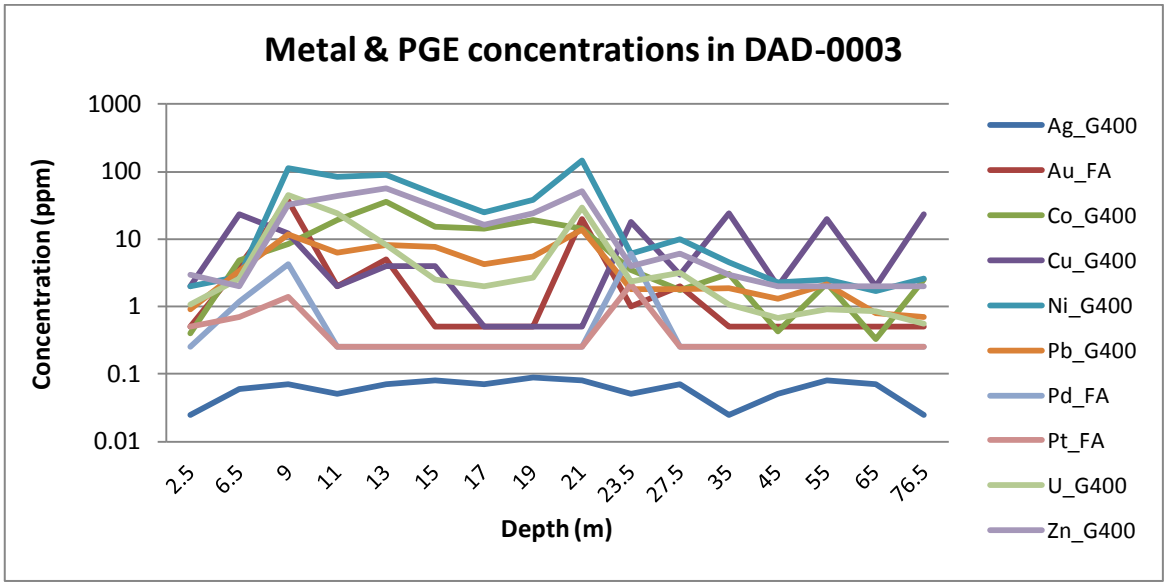
Metal & PGE concentrations in DAD-0003
Concentration (ppm)
1000
100
10
1
0.1
0.01
2.5
6.5
9
11
13
15
17
19
21
23.5
27.5
35
45
55
65
76.5
Depth (m)
Ag_G400
Au_FA
Co_G400
Cu_G400
Ni_G400
Pb_G400
Pd_FA
Pt_FA
U_G400
Zn_G400

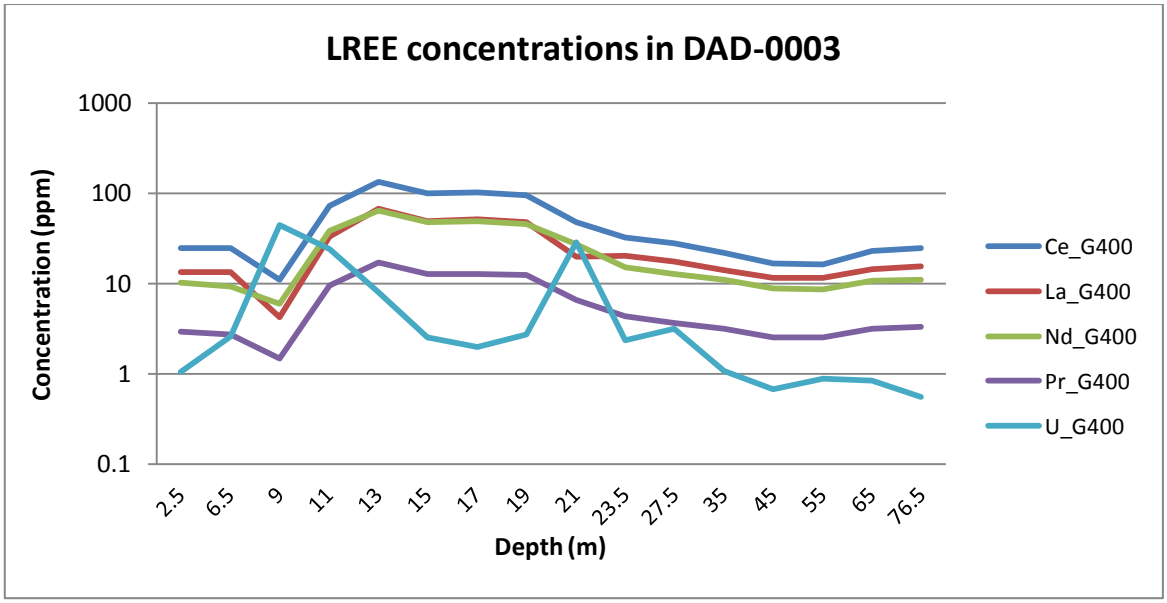
LREE concentrations in DAD-0003
Concentration (ppm)
1000
100
10
1
0.1
2.5
6.5
9
11
13
15
17
19
21
23.5
27.5
35
45
55
65
76.5
Depth (m)
Ce_G400
La_G400
Nd_G400
Pr_G400
U_G400

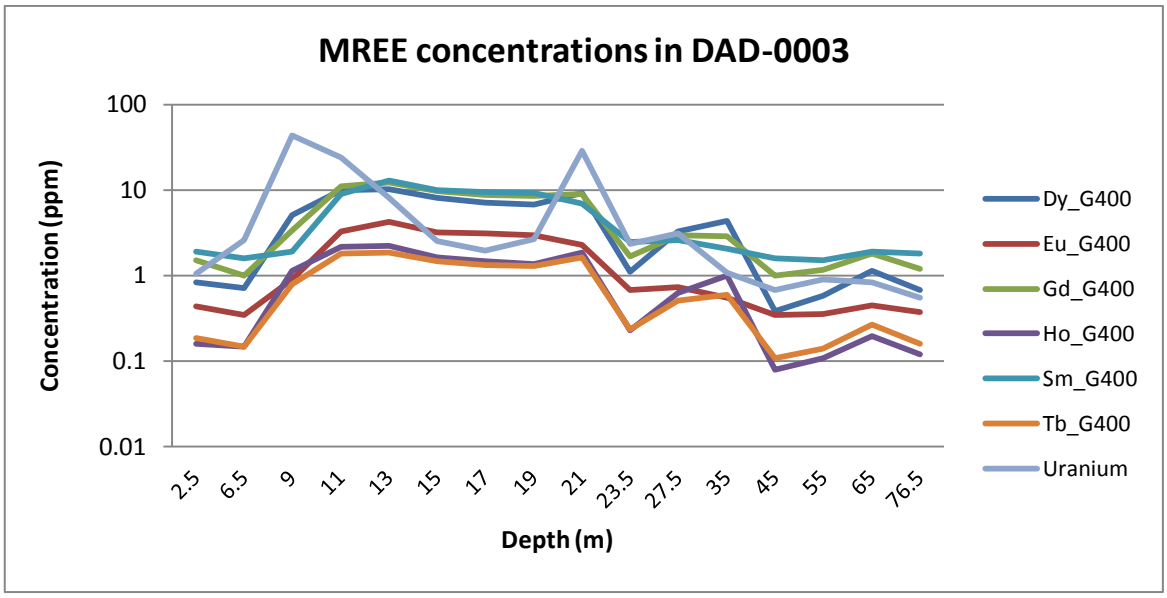
MREE concentrations in DAD-0003
Concentration (ppm)
100
10
1
0.1
0.01
2.5
6.5
9
11
13
15
17
19
21
23.5
27.5
35
45
55
65
76.5
Depth (m)
Dy_G400
Eu_G400
Gd_G400
Ho_G400
Sm_G400
Tb_G400
Uranium

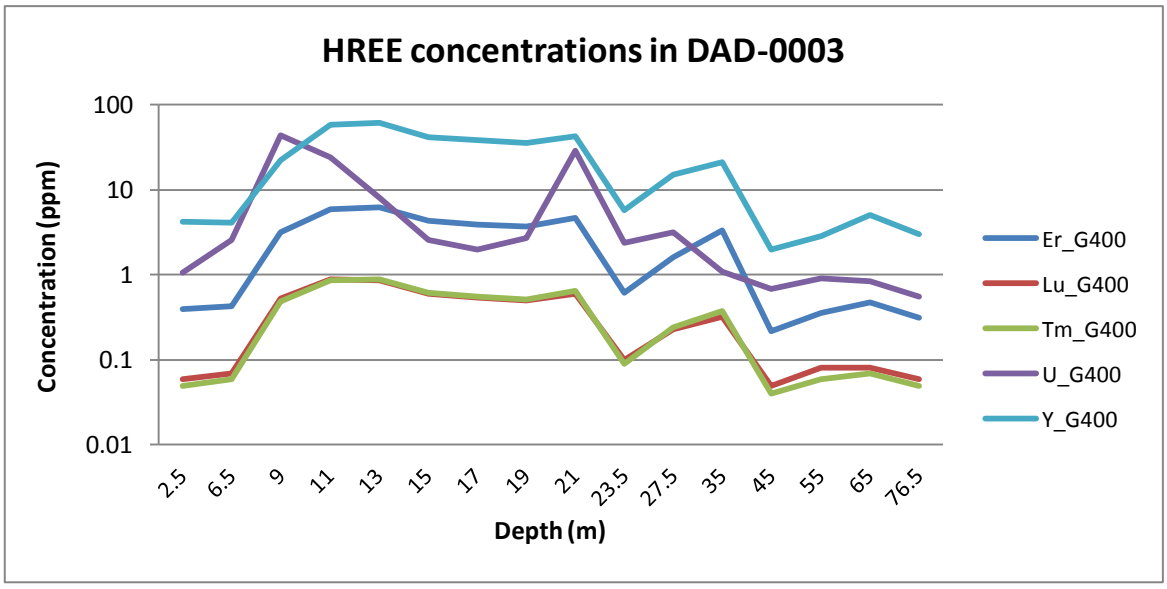
HREE concentrations in DAD-0003
Concentration (ppm)
100
10
1
0.1
0.01
2.5
6.5
9
11
13
15
17
19
21
23.5
27.5
35
45
55
65
76.5
Depth (m)
Er_G400
Lu_G400
Tm_G400
U_G400
Y_G400

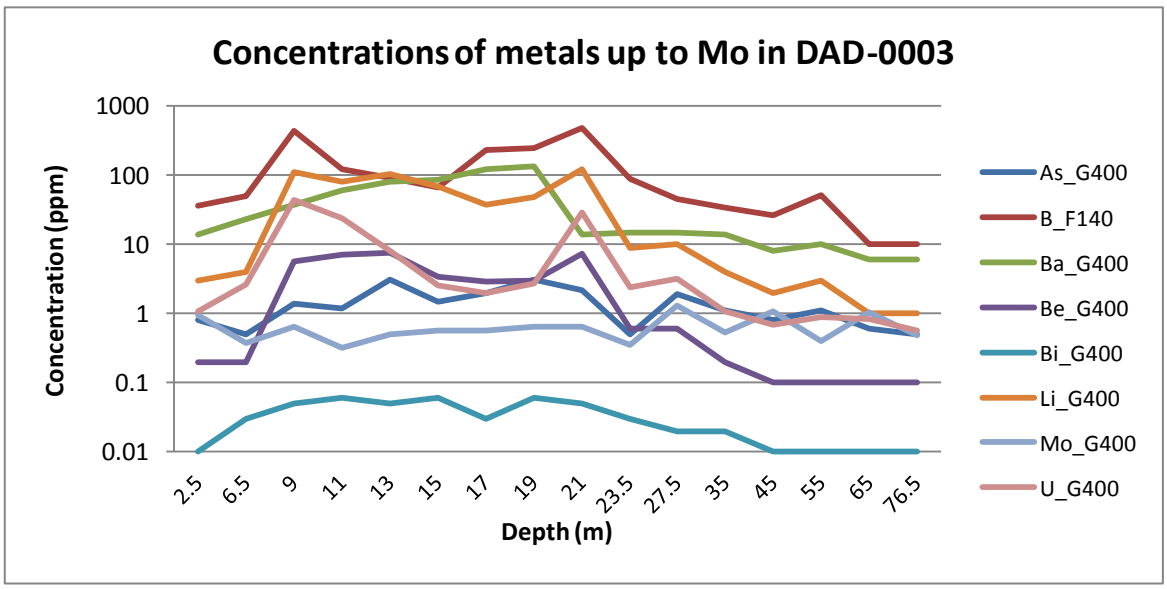
Concentrations of metals up to Mo in DAD-0003
Concentration (ppm)
1000
100
10
1
0.1
0.01
2.5
6.5
9
11
13
15
17
19
21
23.5
27.5
35
45
55
65
76.5
Depth (m)
As_G400
B_F140
Ba_G400
Be_G400
Bi_G400
Li_G400
Mo_G400
U_G400

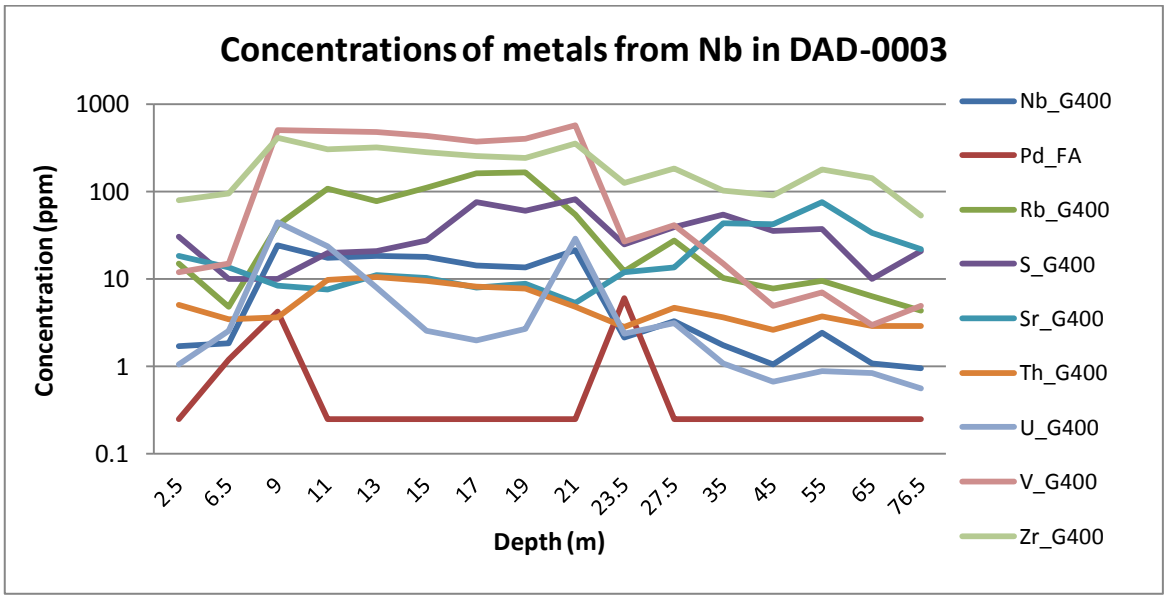
Concentrations of metals from Nb in DAD-0003
Concentration (ppm)
1000
100
10
1
0.1
2.5
6.5
9
11
13
15
17
19
21
23.5
27.5
35
45
55
65
76.5
Depth (m)
Nb_G400
Pd_FA
Rb_G400
S_G400
Sr_G400
Th_G400
U_G400
V_G400
Zr_G400

DAD-0004

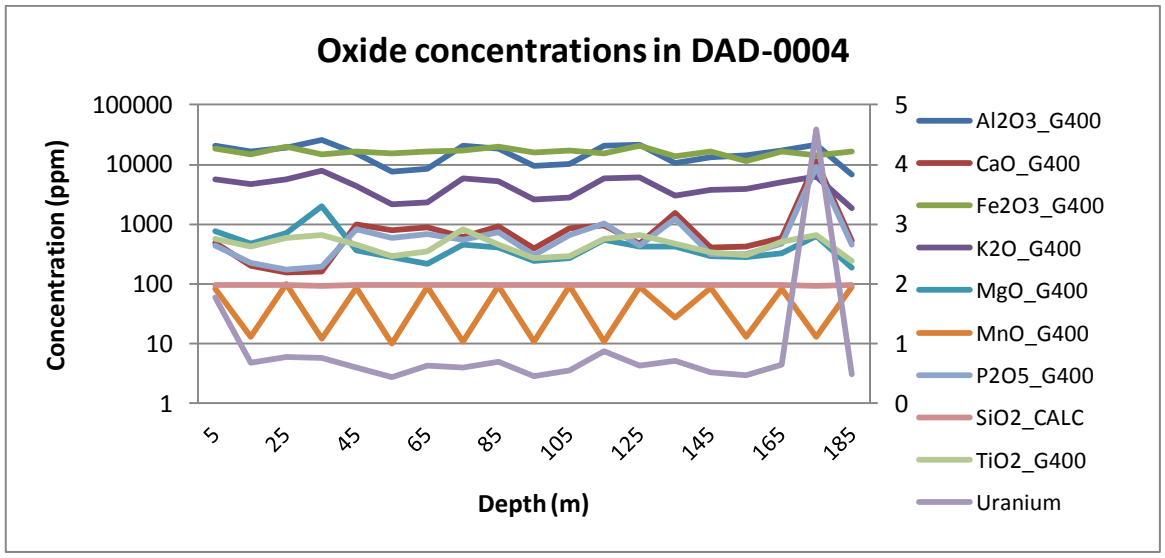
Oxide concentrations in DAD-0004
Concentration (ppm)
100000
10000
1000
100
10
1
5
4
3
2
1
0
5
25
45
65
85
105
125
145
165
185
Depth (m)
Al2O3_G400
CaO_G400
Fe2O3_G400
K2O_G400
MgO_G400
MnO_G400
P2O5_G400
SiO2_CALC
TiO2_G400
Uranium

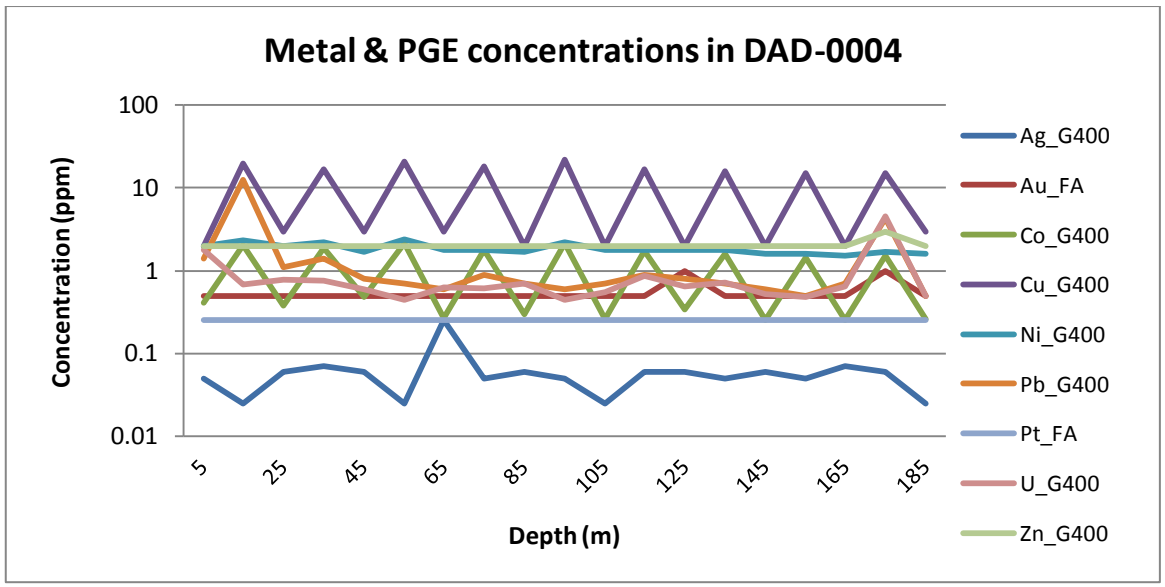
Metal & PGE concentrations in DAD-0004
Concentration (ppm)
100
10
1
0.1
0.01
5
25
45
65
85
105
125
145
165
185
Depth (m)
Ag_G400
Au_FA
Co_G400
Cu_G400
Ni_G400
Pb_G400
Pt_FA
U_G400
Zn_G400

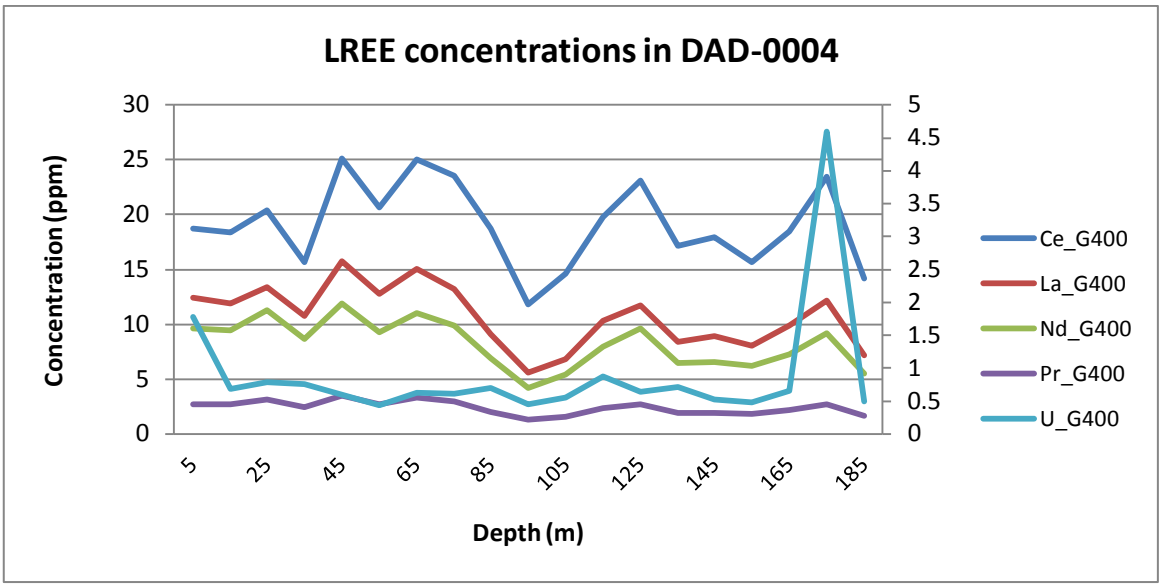
LREE concentrations in DAD-0004
Concentration (ppm)
30
25
20
15
10
5
0
5
4.5
4
3.5
3
2.5
2
1.5
1
0.5
0
5
25
45
65
85
105
125
145
165
185
Depth (m)
Ce_G400
La_G400
Nd_G400
Pr_G400
U_G400

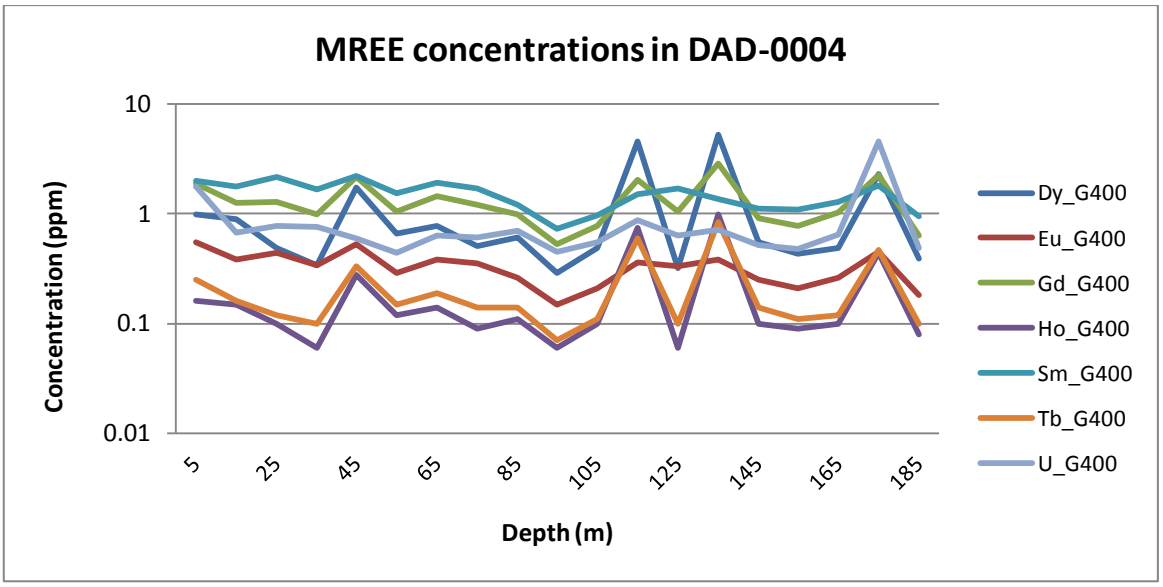
MREE concentrations in DAD-0004
Concentration (ppm)
10
1
0.1
0.01
5
25
45
65
85
105
125
145
165
185
Depth (m)
Dy_G400
Eu_G400
Gd_G400
Ho_G400
Sm_G400
Tb_G400
U_G400

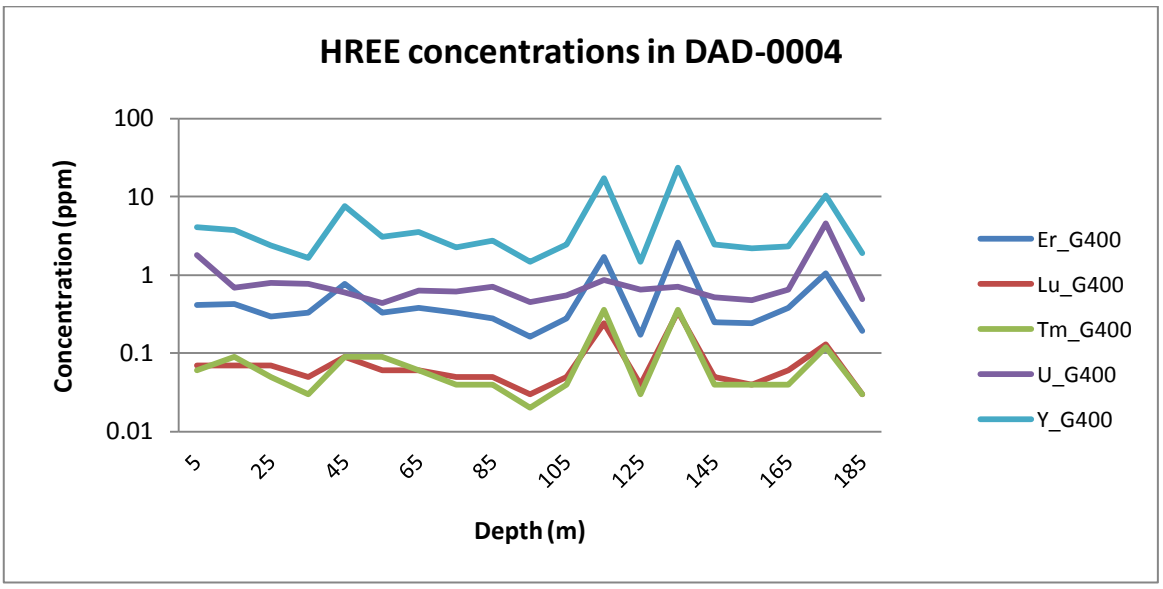
HREE concentrations in DAD-0004
Concentration (ppm)
100
10
1
0.1
0.01
5
25
45
65
85
105
125
145
165
185
Depth (m)
Er_G400
Lu_G400
Tm_G400
U_G400
Y_G400

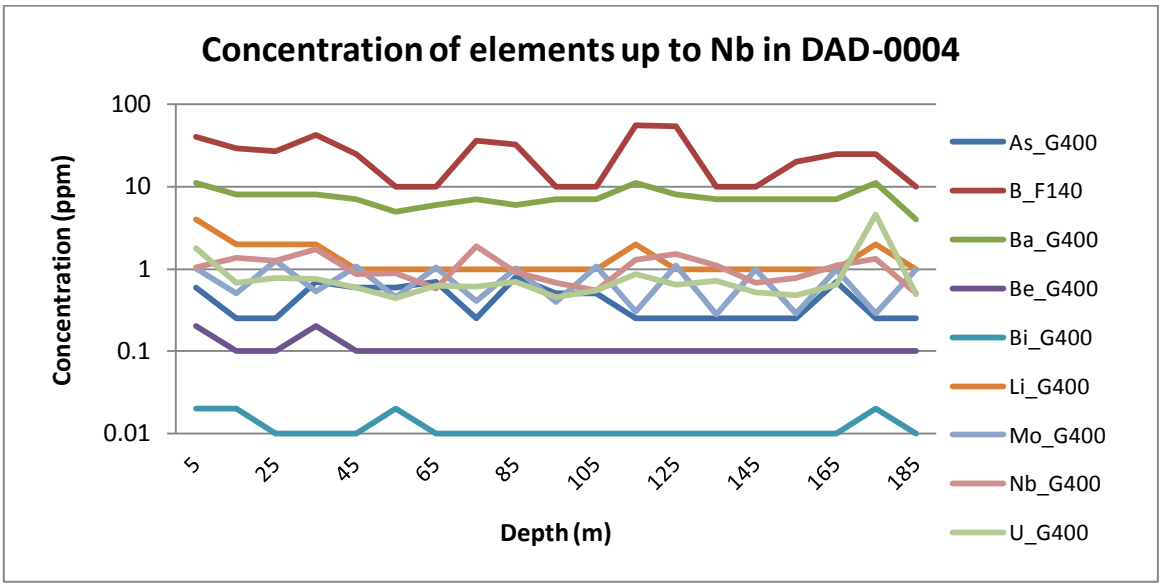
Concentration of elements up to Nb in DAD-0004
Concentration (ppm)
100
10
1
0.1
0.01
5
25
45
65
85
105
125
145
165
185
Depth (m)
As_G400
B_F140
Ba_G400
Be_G400
Bi_G400
Li_G400
Mo_G400
Nb_G400
U_G400

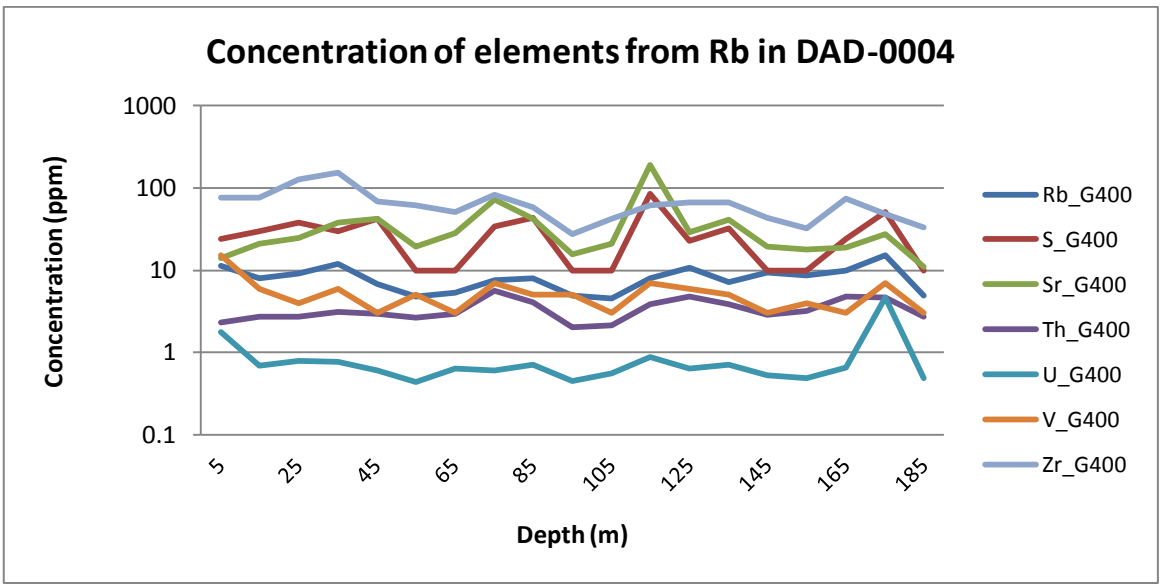
Concentration of elements from Rb in DAD-0004
Concentration (ppm)
1000
100
10
1
0.1
5
25
45
65
85
105
125
145
165
185
Depth (m)
Rb_G400
S_G400
Sr_G400
Th_G400
U_G400
V_G400
Zr_G400